Durham E-Theses

Oxidative modifications of polymer surfaces

Boyd, Robert Deric

How to cite:

Boyd, Robert Deric (1996) *Oxidative modifications of polymer surfaces*, Durham theses, Durham University. Available at Durham E-Theses Online: http://etheses.dur.ac.uk/5180/

OXIDATIVE MODIFICATIONS OF POLYMER SURFACES

Robert Deric Boyd BSc. (Hons.) (Dunelm)

Ph.D. Thesis

Department of Chemistry

University of Durham

September 1996

1 0 MAR 1997

For Mum and Dad

DECLARATION

STATEMENT OF COPYRIGHT

The work described in this thesis was carried out in the Department of Chemistry at the University of Durham between October 1993 and September 1996. It is the original work of the author except where otherwise acknowledged.

Solution state NMR analysis (chapters 3 and 4) was performed by Dr A. M. Kenwright. Static secondary ion mass spectrometry (chapter 3) was provided by Prof. D. Briggs.

Work in this thesis has formed all or part of the following publications:-

'Silent Discharge Treatment of Biaxially Orientated Polypropylene';
R. D. Boyd, O. D. Greenwood, J. Hopkins and J. P. S. Badyal. *Proceedings of the 12th International Symposium on Plasma Chemistry*. **1995**, *1*, p239-244.

'Plasma Fluorination Versus Oxygenation of Polypropylene';
J. Hopkins, R. D. Boyd and J. P. S. Badyal. *Journal of Physical Chemistry*. **1996**. *100*. p6755-6759.

'Atmospheric Non-Equilibrium Plasma Treatment of Biaxially Oriented Polypropylene';
R. D. Boyd, A. M. Kenwright and J. P. S. Badyal. Submitted for publication.

'Non-Equilibrium Plasma Treatment of Miscible Polystyrene / Polyphenylene Oxide Blends'; R. D. Boyd and J. P. S. Badyal. Submitted for publication.

ACKNOWLEDGEMENTS

ABSTRACT

Non-equilibrium plasma modification of polymer surfaces in an oxygen atmosphere provides a highly efficient, solventless method of raising the surface energy. The chemical and physical effects of non-equilibrium plasma treatment on polymer surfaces have been investigated.

Oxygen glow discharge and silent discharge treatment of several polymers (polypropylene, polystyrene, polyphenylene oxide and polycarbonate) has been shown to cause both surface oxidation and chain scission at the polymer surface. This generates low molecular weight oxidised material on the polymer surface which conglomerates into globular features due to the difference in surface energy between the oxidised material and the untreated polymer. These features can be removed by solvent washing. Generally silent discharge treatment generates more low molecular weight oxidised material whereas oxygen glow discharge treatment generates more non-soluble oxidised material.

Crystalline polymers react at a slower rate than amorphous material. During the treatment of a model crystalline polymer (hexatriacontane) the plasma attacks the edges of the crystal, rather than the surface, due to the greater chain mobility at the edge.

Non-equilibrium plasma treatment of both miscible and immiscible polymer blends were investigated. The size and distribution of the globular features formed were found to be dependent on the blend composition. For the immicible polymer blend, non-equilibrium plasma treatment reveals the blend morphology arising from the difference in reaction rates of the parent polymers.

TABLE OF CONTENTS

CHAPTER 3: ATMOSPHERIC SILENT DISCHARGE TREATMENT OF BIAXIALLY ORIENTED POLYPROPYLENE

CHAPTER 4: STRUCTURE AND OXIDATIVE PLASMA DEGRADATION OF HEXATRIACONTANE CRYSTALS

CHAPTER 6: OXYGEN GLOW DISCHARGE AND SILENT DISCHARGE TREATMENT OF IMMISCIBLE POLYSTYRENE / POLYCARBONATE BLEND SURFACES

CHAPTER 7: ATOMIC FORCE MICROSCOPY INVESTIGATIONS INTO SINGLE CRYSTALS OF POLY (DIMETHYL SILANE).

CHAPTER 8: CONCLUSIONS

CHAPTER 1:

INTRODUCTION TO POLYMER SURFACES, NON - EQUILIBRIUM PLASMAS AND CHARACTERISATION TECHNIQUES.

It was not until the third decade of this century that the science of polymers began to emerge. Since then of course, the science and technology of polymers has grown into a vast area and world wide industrial production now runs to billions of tonnes per year.[1] In spite of this many aspects of polymer science are not yet fully understood. One of these aspects is polymer surfaces. Indeed fundamental questions of polymer surface science, such as 'what do polymer surfaces look like?' and 'how do they behave?' have yet to be completely answered. It is the aim of this thesis to investigate both the chemical and physical properties of polymers and polymer composites both before treatment and following oxidative treatment using non-equilibrium plasmas. This chapter will introduce polymer surfaces, why they need to be modified and other methods of modifying polymer surfaces, before going on to describe non-equilibrium plasmas.

1.1 THE SURFACE PROPERTIES OF POLYMERS.

The properties at the surface are very different from those in the bulk,[2-4] where the molecules are subject to a different environment. The surface molecules will be subject to intermolecular forces from one side only, meaning that the packing at least will differ from the bulk.[4] In addition there may be both chemical and physical changes at the polymer surface. The orientation of polymer chains is almost always different from that of the bulk.[5] The polymer chains may be lying flat, orientated in the surface plane or, if some special group is attached, the orientation may be normal to the plane of the surface. The surface region is generally thought to be 50-100 Å thick,[5] but the depth of interest depends on the nature of what is being studied and the limitations of the instrument being used.

1.1.1 The Surface Energy

An important property of a surface is surface energy. This is also called the surface tension and is usually given the symbol γ. The surface energy is defined as the energy required to generate a unit area of a polymer surface[3-5] and is usually measured in dyns cm^{-1} or mJ m^{-2}. The usual method for determining the surface energy is to measure the contact angle between a liquid, of known surface energy, and the surface to be analysed, as shown in figure 1. The surface energy can then be determined using the following equation:[6]

$$\gamma_{LS} - \gamma_S + \gamma_L (\cos \theta) = 0 \qquad (1.1)$$

Where γ_S is the surface energy of the polymer, γ_L is the surface energy of the liquid, γ_{LS} is the surface energy of the liquid surface interface and θ is the contact angle. γ_{LS} can be described in term of γ_L and γ_S be the following equation:[4]

$$\gamma_{LS} = \gamma_S + \gamma_L - 2(\gamma_S \gamma_L)^{1/2} \qquad (1.2)$$

Combining equations (1.1) and (1.2) gives:

$$\gamma_L (1-\cos\theta) - 2(\gamma_S \gamma_L)^{1/2} = 0 \qquad (1.3)$$

The surface energy of the polymer surface can be determined by knowing both θ and γ_L. There are various methods for determining the contact angle. The simplest is the sessile drop method[7] which measures the angle between a drop of liquid and the surface directly. However more advanced methods exist, such as the Wilhemly plate method[8] which can give the accuracy of a contact angle to 0.1°, compared to 2° for the sessile drop method. Table I shows typical surface energy measurements for some common polymers and Figure 2 compares the surface energy of polymers with those of other materials. Typically polymers have a low surface energy. We shall see that the surface energy dictates many properties of a surface, such as adhesion and composition.

Figure 1: Showing the surface energies acting on a drop of liquid on a polymer surface.
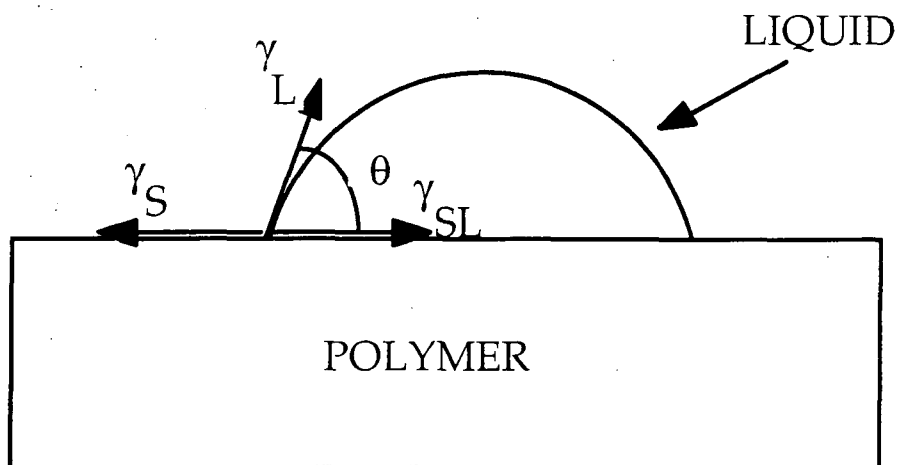
Table I: Examples of Surface energies.

Material	Surface Energy / dyn cm^{-1}	Reference
Polypropylene	29	9
Polyethylene	31	4
PET	43	4

Figure 2: The Surface Energy of Materials.
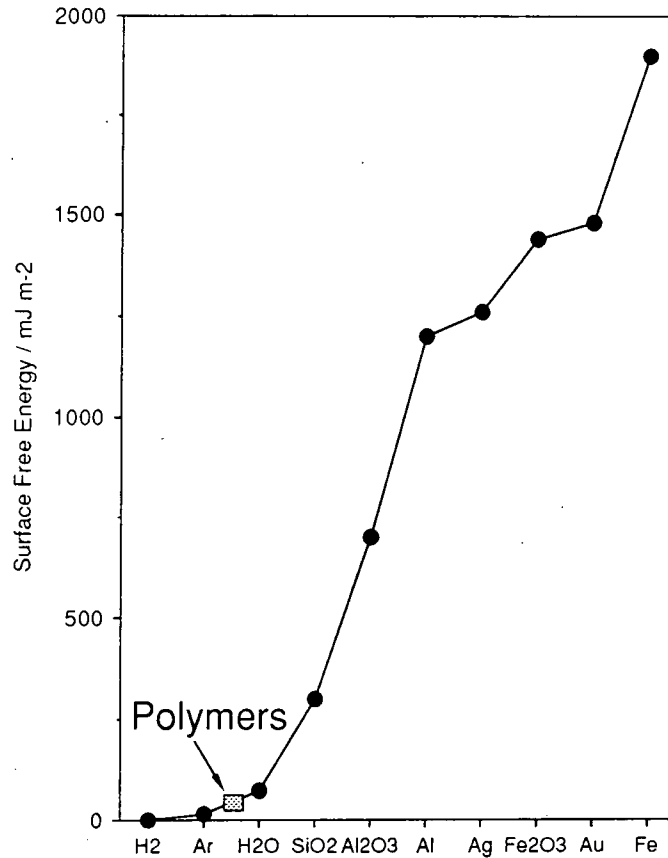
1.1.2 Polymer Surface Dynamics

The dynamic properties of polymers have been known since 1938[10] and have been widely reported.[11 -13] This behaviour arises from the large size and molecular weight of polymers which cause the polymer surface to rarely be in equlibrium,[12] due to molecular entanglements. The driving force of polymer dynamics is surface energy. A system will always try and match its surface energy with its environment, minimising the interfacial energy. This means that the surface properties of polymers are dependant on time, temperature and environment as the surface moves towards a more equilibrated state. A good example of this is when a polymer contains highly polar phases, blocks, segments or side chains. When in contact with a low energy environment, such as air or a vacuum, the polar components orient themselves towards the bulk, minimising the surface energy. Whereas, when the sample is in contact with a high energy environment,

4

such as water, the polar groups re-orient themselves towards the surface, reducing the interfacial energy.[12,14,15]

1.1.3 The Adhesion Properties of Polymers

Adhesion is of critical importance for industrial applications of polymers. Adhesion controls the coating, printing and bonding of a polymer surface[4,16-18] Generally the adhesion properties are controlled by the surface energy of the polymer substrate. Consider a polymer substrate of surface energy γ_S and an adhesive of surface energy γ_L, then the work of adhesion W_L, can be defined as the energy required to separate a unit area of a liquid and a solid:

$$W_L = \gamma_S + \gamma_L - \gamma_{SL} \qquad (1.4)$$

Rewriting equation (1.1) gives:

$$\gamma_{SL} = \gamma_S - \gamma_L(\cos\theta) \qquad (1.5)$$

Combining equations (1.4) and (1.5) gives:

$$W_L = \gamma_L(1 + \cos\theta) \qquad (1.6)$$

This argument also represents two surfaces meeting together. For good adhesive properties one needs a high work of adhesion and for this you need a low contact angle. Which means that you need the surface energy of the two substrates to be a close as possible. It has been mentioned previously that polymers tend to have a low surface energy, which means that polymers bond well to low surface energy materials. However virtually all metals (>100 mJ m^{-2}), solvents (for printing and coating applications) and resins for adhesives[19] ($40 - 100$ mJ m^{-2}) tend to have higher surface energies compared to polymers. For metallisation,[20,21] coating[22] or printing[23] of polymers and polymer films it is necessary to surface treat them in order to raise their surface energies.

1.2 SURFACE MODIFICATION OF POLYMERS

1.2.1 Physical Abrasion

One of the simplest methods of modifying a polymer surface is by physically roughening the surface. Wenzel[24] first noticed that roughing a polymer surface decreases the contact angle and promotes adhesion. This arises from the increased polymer surface

area for contact.[25] However an alternative theory states that surface roughing also breaks chemical bonds which creates radicals on the surface which then react with molecular oxygen or water in the atmosphere to create a polar surface, which increases the surface energy.[26] Physical abrasion is easy to perform however it is a non-specific technique.

1.2.2 Additives

Additives are often used to modify the friction, adhesion and electrical properties of polymer surfaces.[27] Introduction of an additive that will increase the surface roughness of the polymer surface will improve its adhesion properties.[24] Alternatively introducing compatible polar additives (containing carboxylic acid, amine or urethane groups) can raise the surface energy. However, these polar additives need to have a high diffusibility and be able to readily migrate to the surface and not remain in the bulk. They should also be easily deformable, to promote bonding and have a low conformational energy to allow the polar groups to align with the surface. This suggests that low molecular weight additives are preferred. These can, however, form a weak boundary layer at the surface which will have a low bond strength with the polymer.[27] Other disadvantages in using additives is that they may require large quantities to be effective, the surface effects may be non-specific and they might alter the bulk properties of the polymer.

1.2.3 Wet Chemical Treatment.

This technique involves altering the chemical composition of the polymer surface via the chemical reaction with a given solution. The most common method of improving the adhesive properties of a polymer surface is to either react with an oxidising solution or to hydrolysese the surface. The most common solvents for oxidising polymer surfaces are chromic acid solutions.[28] A good example of this is the treatment of ABS (a rubber modified two phase plastic made from acrylonitrile, butadiene and styrene) with sulphuric acid saturated with chromium trioxide[29,30] to produce a highly adhesive surface, which is widely used in the electroplating industry. However treatment with chromic acid solutions also causes physical as well as chemical changes at the surface. In the case of ABS, the surface becomes very rough after treatment, caused by preferential attack of

6

the rubber phase and in the case of treatment of polypropylene the surface also becomes very rough due to the amorphous polymer reacting much more readily than the spherulitic crystallites of the polymer.[28,31] Reaction with chromic acid solution also causes etching of the polymer.[28] Hydrolysis of a polymer surface involves attack of a nucleophilic agent, such as a base, on electron deficient carbon atoms. The most widely used application of hydrolysis is the reaction of PET by hot sodium hydroxide. Again the increase in the surface energy of the polymer is caused by the introduction of polar groups at the surface and increasing the surface roughness.[28]

There are many disadvantages in using wet chemical treatments. The depth of modification is very large, usually 300 Å.[32] Care must be taken that the solvent does not penetrate into the bulk to cause bulk modification. The solvents are usually polymer specific making the process inflexible. Finally wet chemical treatment usually requires large quantities of toxic solvents, which are environmentally damaging and the cost of solvent disposal or re-purification makes wet chemical modification very unattractive for industrial applications.

1.2.4 Surface Grafting

In surface grafting the modification is achieved by the covalent bonding of new macromolecules onto the surface. The fundamental step in surface grafting is the creation of reactive sites on the substrate surface. This is achieved by either wet chemistry or by irradiation with ionising radiation or UV light. These reactive sites are coupled to preformed macromolecular chains, or more common, the activated sites are placed in contact with a suitable monomer so that chains start to grow from the activated site.[28] This is a highly specific method for modifying the surface properties. An example of this is the UV irradiation of polyethylene through a solution of 2 hydroxyethyl methacrylate (and benzophenone in acetone) resulting in a surface with poly (2 hydroxyethymethacrylate) grafted upon it. This results in an increase in the surface energy.[33]

1.2.5 Ultra-Violet Irradiation

Polymer surface modification initiated by ultra-violet (UV) irradiation has been performed using either a standard UV source or a laser. The type of modification depends on the UV source and the presence of reactive species.[34] Bombardment with UV photons leads to the breaking of C-C and C-H bonds via a free radical mechanism. In a vacuum or in the absence of oxygen this can led to chain scission, crosslinking or the formation of unsaturated units.[34] However when UV irradiation occurs in a oxygen rich environment it can led to the generation of oxygen containing carbon moieties, such as alcohol, hydroperoxide, ketone and acid groups.[35] This is called photo-oxidation. This has been exploited to enhance wettability and adhesion properties of polymers.[36] Photo-oxidation is limited by the range of surface modification that can be achieved and vacuum systems sometimes have to be employed to optimise the treatment.

1.2.6 Flame Treatments

Flame treatment involves burning a air and methane mixture in a controlled manner so that the richness of the flame is kept constant. The polymer is then positioned a fixed distance from the flame.[28] The active species produced by the flame include radicals, ions and molecules in excited states, which produce a plethora of reactive products at the surface. Analysis of flame treated polyethylene[37] shows that flame treatment causes the generation of oxygen containing carbon groups at the surface. Flame treatments are simple to perform at atmospheric pressure, and are now widely used to improve the adhesive properties of polymers.[38] However flame treatment is a very harsh treatment and it is difficult to control the depth of modification.[37] For very rough surfaces inaccessible nooks and crannies may not get treated.[39]

1.3 PLASMAS

The term 'plasma' was first used by Langmuir[40] in 1929 in order to describe the ionised gases he was studying. Plasmas are often referred to as the fourth state of matter[41] consisting of electrons, ions and neutrals, with the number of electrons roughly equal to the number of ions so that the system has overall neutrality.[42] This criterion can

only be satisfied if the Debye length, λ_D, the distance over which a charge imbalance can exist, is small compared with the physical dimensions of the plasma.[43,44] The Debye length is defined by equation (1.7).

$$\lambda_D = (\varepsilon_o kT_e/ne^2)^{1/2} \qquad (1.7)$$

Where ε_o is the permittivity of free space, k is the Boltzman constant, T_e is the electron temperature, n is the electron density and e is the charge on an electron.

1.3.1 Types of Plasma

There are two main types of plasma. The first are equilibrium plasmas, where the gas temperature and the electron temperature are approximately equal.[45] Examples of such plasmas are plasma arcs and plasma jets.[46] However the very high gas temperatures required for such plasmas (up to 30 000 K) make equilibrium plasmas extremely impractical for polymer modification. Therefore equilibrium plasmas will not be considered further.

The second type of plasma are non-equilibrium plasmas or cold plasmas. Here the electron temperature is very much greater than the gas temperature.[45,47] Typically in non-equilibrium plasmas the electron temperature reaches $10^4 - 10^5$ K (1-10 eV) whist the gas temperature can be as low as room temperature.[47] Two types of non-equilibrium plasma will be covered in this thesis; the glow discharge and the silent discharge.

1.3.2 The Glow Discharge

1.3.2.1 The Origin of a Glow Discharge

A glow discharge plasma is produced by applying a electric field to a gas at low pressure. A small amount of free electrons are always present in such a gas as a result of ionisation from naturally occurring radioactivity or cosmic rays. Free electrons can also be produced by photoionisation or field emmission.[47] These electrons are accelerated by the electric field and gain kinetic energy. The electrons lose kinetic energy by bombarding gas atoms or molecules. If the kinetic energy of the electrons is too low to excite or ionise the atoms and/or molecules then the collisions will be elastic, with the

atoms or molecules gaining kinetic energy and the electrons losing it. The fraction of kinetic energy lost by the electrons during a elastic collision is given by:

$$\Delta E/E = -2M_e/M \qquad (1.8)$$

Where M is the mass of the target atom and M_e is the mass of the electron. For an electron only a small amount of its kinetic energy is lost (approximately 10^{-5}) during an elastic collision. The electron will continue to gain kinetic energy between collisions, until it attains enough kinetic energy to ionise or excite the target atom or molecule. In the former case this leads to the generation of more free electrons, which in turn are accelerated by the electric field and ionise further atoms or molecules.[43-47] An electron multiplication process then takes place.

The number of free electrons will depend on the applied voltage of the electric field, V, and can be followed by measuring the discharge current, I. A typical DC glow discharge I-V curve is shown in Figure 3.[47] For a low voltage the number of free electrons is small. Increasing the voltage increases the number of charged species generated by the plasma. At a critical voltage there is an abrupt rise in the current, which is known as the breakdown voltage, V_b. At this voltage the number of free electrons generated is sufficient to replace the electrons lost to recombination, diffusion, drift to the boundary surrounding the plasma or attachment to neutrals to form negative ions. At this point the plasma is self-sustaining,[48] and the glow discharge is established.

Within the bulk of the glow discharge the electron temperature, T_e, is much greater than the ion temperature, T_i. This arises from the vast difference in the mass of the electron compared to that of the ions, and then can attain much more kinetic energy from the applied field. This is shown by equation (1.9):[43]

$$\text{Work Done by Electric Field} = Eed = (Eet)^2/2M_e \qquad (1.9)$$

Where E is the electric field, d is the distance travelled and t is the time of travel. All other symbols are as described previously.

Figure 3: The I-V characteristics of a DC glow discharge
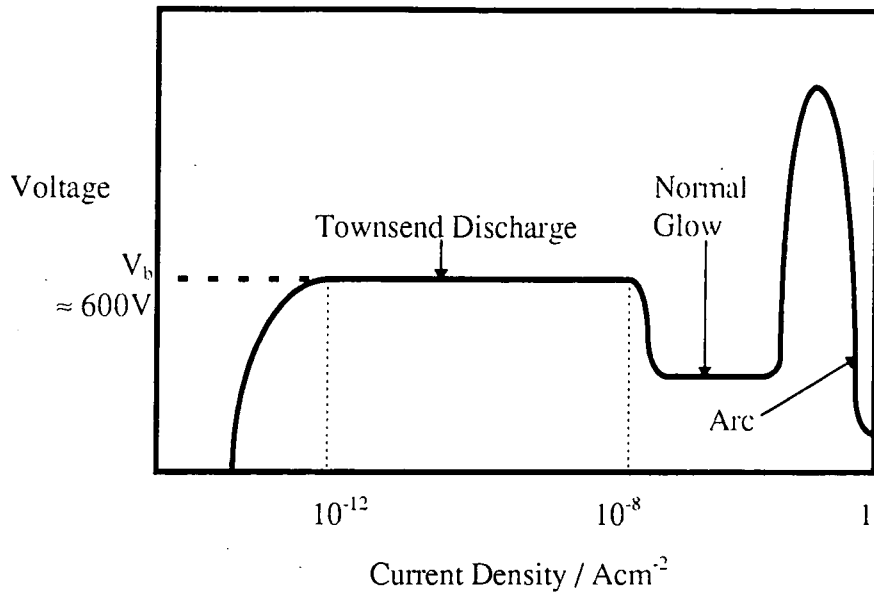
The characteristic glow of a glow discharge arises from relaxation of excited species. The range of electromagnetic radiation emitted by a glow discharge plasma ranges from the infra-red through the visible and ultra-violet through to the vacuum ultra-violet.

1.3.2.2 Radio Frequency Glow Discharges

The simplest form of a glow discharge is a direct current (DC) glow discharge,[49] which requires the electrodes generating the electric field to be in contact with the plasma. This suffers from degradation of the electrodes by the plasma, especially when using a organic material which can be ionised by the plasma and deposited on the electrodes.[48] This can cause the glow discharge to be short lived.

In order to overcome this problem Anderson[50] proposed using a radio frequency (R.F.) potential to power the plasma. Rapidly changing the electric field means that the electrodes can now be placed remote from the plasma.[48] Although a R.F. glow discharge plasma can be run at any frequency from 1 megahertz to the gigahertz range it is usual to run at 13.56 MHz in order to comply with the government communication regulations. It is common practice to inductively or capacitivity couple the R.F. generator to the

11

plasma via a matching unit. The purpose of this unit is to match the impedance of the plasma to the output impedance of the R.F. generator, so that the power dissipation in the discharge is maximised and to protect the generator.[43] R.F. generated glow discharges are very homogenous as the wavelength of the R.F. is much greater than the dimensions of the plasma reactor.

1.3.2.3 Plasma Potential

It has been previously mentioned that the kinetic energy, and hence the velocity of electrons, is much greater than that of the ions. The electrons will escape from the plasma at a higher rate than the ions and end up at the reactor walls, causing the plasma will build up a net positive charge relative to the reactor walls. This positive charge will then attract the electrons towards the plasma, making it more difficult for the electrons to escape. Eventually a steady sate situation will arise where the loss of electrons equal those of the ions. When this occurs the plasma potential is roughly several volts more positive than the reactor wall potential.

1.3.2.4 Floating Potential

Consider a electrically isolated substrate placed into a plasma. This substrate will rapidly gain a negative charge because of the greater flux of electrons relative to ions.[43,49] Eventually the substrate will be sufficiently negative to repel the electrons so that there is a equal flux of electrons and ions. The potential on the substrate surface is called the floating potential and is typically negative of the plasma potential.

1.3.2.5 Plasma Sheath.

A dark space or sheath is usually observed adjacent to all surfaces in contact with the glow discharge.[49] It has been mentioned above that a surface in contact with a plasma will be at a more negative potential than the plasma. The plasma however is a region of uniform potential. The voltage change from the plasma to the surface occurs in the sheath. The sheath has a negative voltage compared to the plasma, so electrons are repelled away from the sheath region. This lack of electrons results in low levels of

excitation of the gas species, so that the region appears dark. Positive ions leaving the plasma are accelerated by the sheath as they bombard the surface.

1.3.2.6 Plasma Chemistry

A very broad spectrum of chemical reactions are observed to occur within a plasma. These include reactions between electrons and molecules, ions and molecules and electrons and ions.[45] The chemistry of the glow discharge is controlled by the electron energy distribution. In a glow discharge plasma it is best described by the Druyvesteyn distribution.[45,47] The major characteristics of this distribution function are shown in Figure 4, namely that the distribution function peaks at around 1 to 2 eV and has a high energy tail, with electron energy reaching up to 25 eV and beyond.[48] This high energy tail has a significant impact on the overall plasma chemistry. In this section the major processes occurring within a glow discharge plasma are described.[47, 51]

1.3.2.6.1 Electron - Molecule Reactions

The bombardment of molecules with electrons of sufficient kinetic energy leads to a transfer of energy between the electrons to the molecules. This causes many reactions summarised below:

Excitation: Production of an excited vibrational, rotational or electronic state of the molecule.

$$e + A \rightarrow e + A^*$$
$$e + A_2 \rightarrow e + A_2^*$$
$$e + AB \rightarrow e + AB^*$$
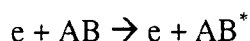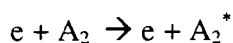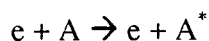
These excited states very quickly decay back to ground states emitting electromagnetic radiation. Excited species tend to decay so quickly that they do not participate in chemical reactions.

Dissociative Attachment or Dissociative Capture: If a highly electronegative gas is used then a low energy electron (< 1 eV) can attach itself to a molecule.

$$e + AB \rightarrow A + B^-$$

13
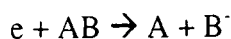
Figure 4: Example of a Druyvesteyn distribution.
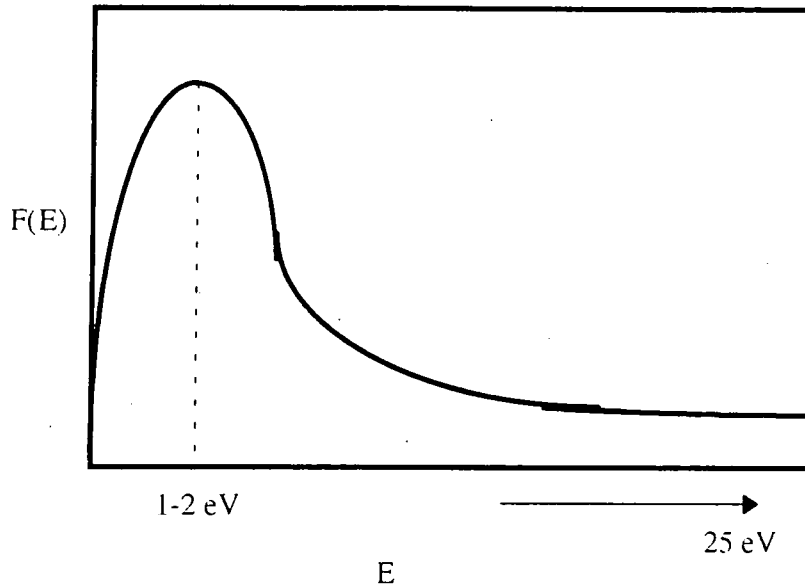
Dissociative Ionisation or Ion Pair Formation: This occurs with electrons of much higher energy (> 20 eV), in order to generate a positive ion.

$$e + AB \rightarrow A^+ + B^- + e$$
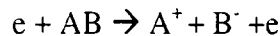
Dissociation: A inelastic collision between a electron and a molecule leading to dissociation without the formation of ions.

$$e + AB \rightarrow e + A + B$$
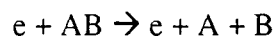
Most dissociation reactions involve slow electrons exciting a molecule above a threshold electronic level (usual several eV). This decays to a lower energy state involving dissociation of the excited molecule into neutral fragment, or radicals. This occurs much faster than (10^{-13} s) than radiative decay (10^{-7} to 10^{-8} s). It is much more probable that dissociation occurs and not radiative decay.[47]

Ionisation: Electron impact leading to the production of positive, negative, atomic or molecular ions.

$$e + A_2 \rightarrow A_2^-$$

$$e + AB \rightarrow e + A^+ + B^-$$
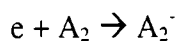
This requires electrons in the 10 - 30 eV range, which occur in the high energy tail of the electron distribution.

Recombination: Leading to the emission of electromagnetic radiation.

$$e + A^+ \rightarrow A + h\upsilon$$
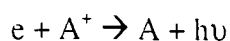
Alternatively the energy released can lead to a *dissociative recombination* reaction.

$$AB^+ + e \rightarrow AB^* \rightarrow A^* + B$$

1.3.2.6.2 Ion - Ion Reactions

When two ions collide several possible reactions can occur.

Recombination:

$$A^+ + B^- \rightarrow AB + h\upsilon$$

Neutralisation:

$$A^+ + B^- \rightarrow A^* + B^* + h\upsilon$$
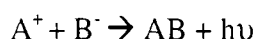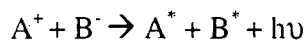
Recombination via a three body collision, which occurs at pressures above 0.1 mtorr:

$$M + A^+ + B^- \rightarrow AB + M$$
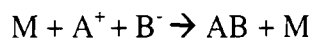
1.3.2.6.3 Ion - Molecule Reactions

The following reactions can occur during a collision between a ion and a neutral particle.

Charge Transfer:

$$A^+ + BC \rightarrow A + BC^+$$
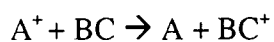
Charge Transfer leading to dissociation:

$$A^+ + BC \rightarrow A + B^+ + C$$
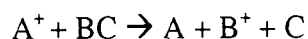
Formation of new species:

$$A^+ + BC \rightarrow AB^+ + C$$
$$\rightarrow AB + C^+$$
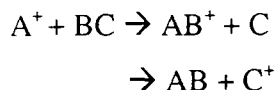
Associative detachment:

$$A^- + BC \rightarrow ABC + e$$

1.3.2.6.4 Radical - Molecule Reactions

Radicals can be single atoms or multi-atomic. They are unstable and very reactive. Radical reactions are summarised below.

Electron Transfer:

$$A + B \rightarrow A^+ + B^-$$

Ionisation:

$$A + B \rightarrow A^+ + B + e$$

Attachment of Atoms:

$$A + BC + M \rightarrow ABC + M$$

Disproportionation:

$$A + BC \rightarrow AB + C$$
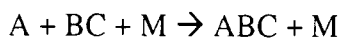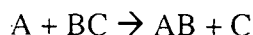
Recombination via disproportionation:

$$2A \rightarrow B + C$$
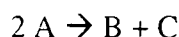
Recombination via combination:

$$2A \rightarrow A\text{-}A$$

1.3.2.6.5 Summary

The reactions occurring in a plasma are summarised in Figure 5. The three major reactive species produced are electromagnetic radiation, free radicals and ions. Typically in a glow discharge plasma the free radical concentration can estimated to be 10^{14} cm^{-3}. This compares with a ion and electron concentration of 10^9 to 10^{11} cm^{-3}.

1.3.2.7 Plasma - Polymer Surface Interactions in the Glow Discharge

Many species are generated in a plasma. These can then bombard any surface in contact with the plasma, as summarised in Figure 6. Electrons and negative ions tend to be repelled by the plasma sheath away from the surface. Generally, energy is transferred to a solid surface by electromagnetic radiation, radical bombardment and ionic particle bombardment.[52] Although infra-red, visible and ultra-violet radiation is produced by the plasma. Infra-red radiation is absorbed by the polymer surface but is quickly dissipated through thermal reactions and visible radiation is not strongly absorbed. Only UV and VUV radiation is strongly absorbed and is able to react with the surface creating free radical sites on the surface.

Free radical bombardment modifies the polymer surface by abstraction or addition reactions. Ionic bombardment leads to the production of free radicals at the surface and the removal of material by sputtering.[43] However the concentration of ions is much smaller than that of free radicals. For polymer modification by plasmas the major reactive species generated by the plasma are free radicals and UV and VUV photons

1.3.3 The Silent Discharge

1.3.3.1 The Origins of the Silent Discharge

Like the glow discharge the silent discharge is a non-equilibrium plasma. However unlike the glow discharge the silent discharge can be operated at pressures up to and beyond atmospheric pressure. The silent discharge was first proposed by Siemen[53] in 1857 in order to generate ozone. Although silent discharge reactors can have many possible configurations, they have the same basic component, namely a set of parallel electrodes and a dielectric barrier layer between the discharge gap and at least one of the electrodes. As with the glow discharge, a silent discharge is generated by producing an electric field between the electrode plates. When the electric field exceeds the electric breakdown field of the discharge gas, a large number of distributed microdischarges are generated between the plates.[54-58] The characteristics of these microdischarges are that they are short lived (typical lifetime of 100 ns), consisting of a cylindrical plasma channel (typical radius of 100 μm) which spreads into a larger surface discharge at the dielectric surface. Reducing the pressure of the silent discharge causes the radius of the microdischarge to increase, until a homogenous glow discharge, as described above, is produced. The major differences between a silent and a glow discharge are that a silent discharge is run at atmospheric pressure and the presence of a dielectric.

17

Figure 5: Schematic diagram of reactions occurring in a plasma reactor.
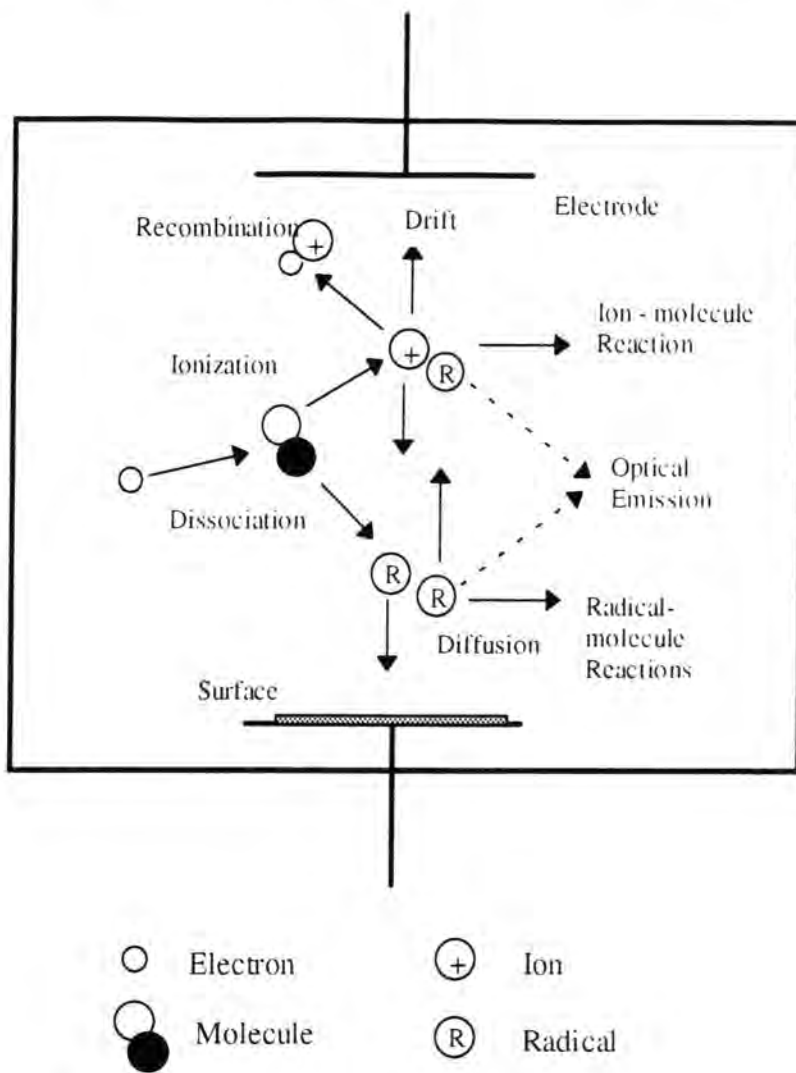
Figure 6: Plasma particles interacting with a surface
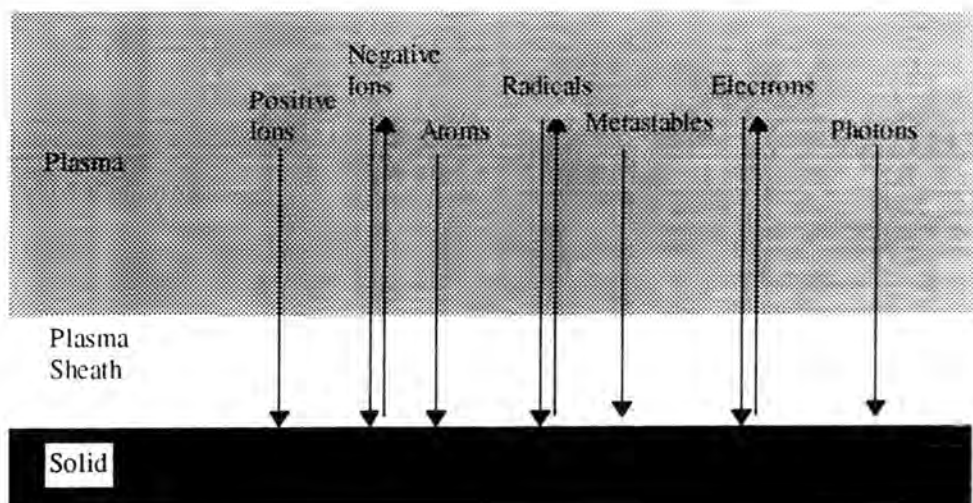
Understanding the microdischarges is the key to understanding the silent discharge. The microdischarges are caused by electrons being emitted from the cathode. These electrons bombard the gas molecules between the discharge gap causing ionisation and excitation. An electron avalanche is formed which moves towards the anode. This generates a local field enhancement in the region of the avalanche. When this electron avalanche reaches the opposite electrode this field enhancement, which travels much faster than the drift velocity of the electrons, is reflected back towards the cathode ionising atoms and molecules in its way. This leads to, within 1 ns, the formation of an extremely thin conductive channel[54,59,60] or microdischarge. This channel spreads out when it hits the dielectric surface. This conductive channel has many of the properties of a glow discharge plasma. Electrons and ions are formed within the microdischarge with a typical electron density of 10^{14} to 10^{15} cm^{-3}.[56] UV radiation is also produced within the silent discharge, caused by the relaxation of excited molecules and atoms.[54] Current flow through the microdischarge has to also flow through the dielectric via charge displacement. Therefore, by its nature, the silent discharge has to be an AC plasma with a frequency ranging from the Hz to the MHz region.

Immediately after the current flow of the microdischarge is initiated, charge will start to accumulate in the area where the microdischarge hits the dielectric. This reduces the electric field in the area of the microdischarge. Approximately 100 ns after the microdischarge is initiated this build up of charge will choke the current flow and extinguish the microdischarge. Because the lifetime of the microdischarge is so short, the microdischarge will see a constant electric field, although the electric field is oscillating with time. If the external voltage is still increasing then other microdischarges can form where there is no charge build up on the dielectric. The dielectric has a two-fold purpose; to limit the charge and energy of any single microdischarge and to distribute the microdischarges over the entire discharge gap.

1.3.3.2 The Chemistry of the Silent Discharge

In order to describe the chemistry of the silent discharge one must first consider the nature of the microdischarge. Most of the reactions that occur within the glow discharge (see section 1.3.2.6) also occur within the microdischarge.[56] This generates electrons, ions, neutral radicals and UV radiation. However once the microdischarge is

19

extinguished the vast majority of the charged species (i.e. ions and electrons) decay before they have time react.[54] Therefore the chemistry of the silent discharge is dominated by neutral species like atoms, excited molecules and molecular fragments.

Dissociation of molecules to produce radicals is the major source of reactive species in a microdischarge. Indeed the efficiency of the dissociation process in a silent discharge can be up to 80 %. After the microdischarge in extinguished these free radicals can then react with gas molecules to form new chemical species, that are not normally formed under ambient conditions. The spatial generation of these species radiates out from the initial microdischarge position, as shown in Figure 6.

A good example of this is the action of the silent discharge on air. Figure 7 shows the action of a single microdischarge in air.[54] As with the glow discharge the microdischarge creates positive ions, negative ions, electrons and free radials. Once the microdischarges is extinguished the electrons and ions decay away very quickly. This generates free radical atomic oxygen and nitrogen. These free radicals can then react with the nitrogen and oxygen gas molecules creating ozone and nitrous oxides.

$$O + O_2 + M \rightarrow O_3^* + M \rightarrow O_3 + M$$

$$N + O_2 \rightarrow NO + O$$

$$NO + O_3 \rightarrow NO_2 + O_2$$
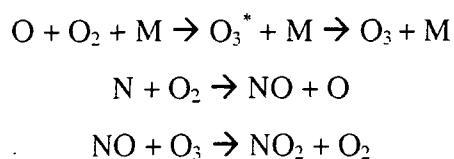
Where M is a third collision partner.

1.3.3.3 Plasma - Polymer Surface Interactions in the Silent Discharge

Energy transfer from the silent discharge to a solid surface placed between the discharge gap occurs by several different processes. Electromagnetic radiation is generated in the microdischarges, as with the glow discharge. However the VUV component is removed by the discharge gap, leaving primarily UV as the surface activating component of the electromagnetic radiation (see section 1.3.2.7). Radical and ion concentrations in the silent discharge tend to remain small, due to their fast reaction rates. The new reactive species (such as ozone in air) play a more significant role in the modification of polymer surfaces, with bombardment on the polymer surface causing addition and abstraction reactions. If the solid sample forms part of the dielectric then

electron bombardment will occur, arising from the surface discharge at the dielectric surface.

Figure 6: The generation of new species in a glow discharge. t_1 initiation of the microdischarge with the creation of electrons. t_2 the electrons cause the production of excited species (A^*). t_3 after the microdischarge has been extinguished, when the excited species reacts to form new species (B). With $t_1 < t_2 < t_3$.

Electrons
Neutral Species A

t_1

Neutral Species A
Excited Species A^*
Ions   I

t_2

Neutral Species A
New Species   B

t_3
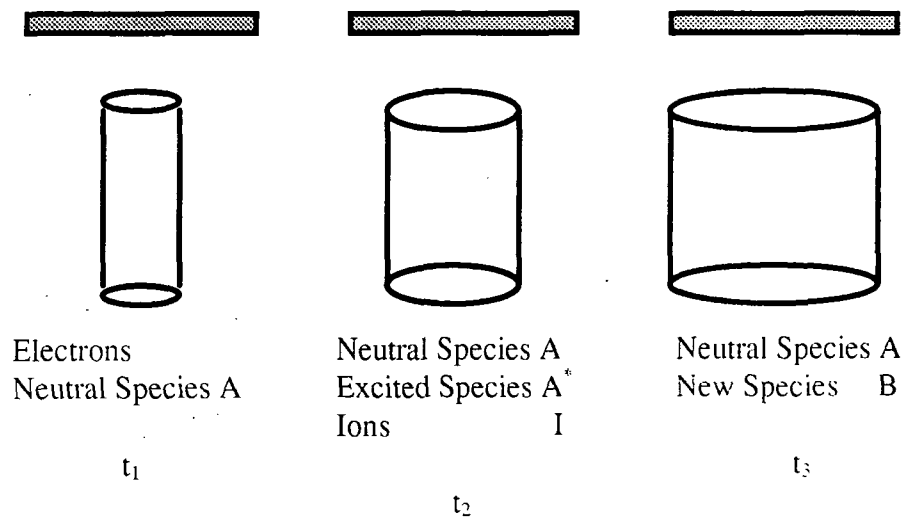
Figure 7: Chemical species generated by a microdischarge in air.
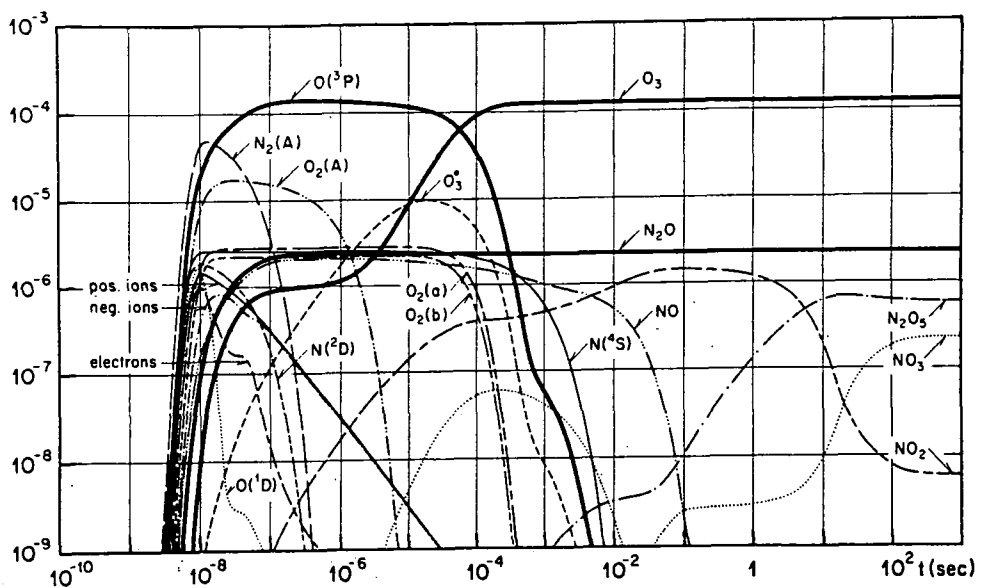
1.3.4 Summary

The surface properties of polymers play an important role in determining the end uses of a polymer. We have seen that in order to fully exploit the properties of polymers the surface energy of the polymer needs to be modified.

Although many methods exist for modifying the surface energy, most methods are very crude in their application. They are usually difficult to control, lead to non-specific results and can easily cause bulk modification. Non-equilibrium plasma treatment of polymers and polymer composites have gained great scientific and industrial interest in modifying polymer surfaces.[61] The great advantage of using plasma are that they produce reactive species that can be used to modify a polymer surface and which are not normally present at ambient conditions.

It is the aim of this thesis to show and investigate how these new reactive species, generated by non-equilibrium plasmas, can be used to modify the surface properties of a variety of polymer systems. The effects of two non-equilibrium plasmas will be investigated; the glow discharge (operated under oxygen) and the silent discharge (operated in air). Both the chemical and physical effects of plasma treatment have been investigated. The characterisation techniques that have been used are X-ray photoelectron spectroscopy, atomic force microscopy, nuclear magnetic resonance and static secondary ion mass spectrometry.

1.4 ANALYTICAL TECHNIQUES

1.4.1 X-ray Photoelectron Spectroscopy

The basic technique of x-ray photoelectron spectroscopy (XPS) is very simple. It involves irradiating a surface with high energy photons and measuring the energy of the emitted electrons.[62] Electrons are emitted from the surface via the photoelectron effect,[63] which is shown in Figure 8.[64] A photon, with energy $h\nu$, interacts with a core electron energy level of an atom causing the emission of a photoelectron with kinetic energy given by:[65]

$$E_{KE} = h\nu - E_b - \phi - S \qquad (1.10)$$

Where E_b is the binding energy of the photoelectron, ϕ is the work function of the surface and S is a term to account for surface charging. Normally S is ignored and included with ϕ. Therefore by knowing both $h\nu$ and E_{KE} the binding energy can be determined, which is unique for a given element. ϕ is normally determined by referencing the experimentally determined E_b with the known E_b for a given element. Any photon source with energy greater than ϕ can be used for XPS. This excludes ultra-violet and longer wavelength radiation. The most common source of radiation are narrow wavelength x-ray sources.[62]

The surface sensitivity of XPS arises not from the penetration depth of the x-rays but from the escape depth of the photoelectrons. The variation in escape depth with electron kinetic energy is shown in Figure 9. An electron in a solid can lose energy by three main processes.[66] Excitation of lattice vibrations (phonons), excitation of collective density fluctuations in the electron gas (plasmons) and excitation of particles. For low electron energies the electron is unable to cause any of the above excitations and the escape depth is large.[66] For higher kinetic energies the cross-section of exciting these transitions is low and the escape depths are again large. Therefore the escape depth goes through a minimum of 1 nm near 100 eV. The kinetic energy of photoelectrons emitted using a x-ray source is in the range 100 eV to 1000 eV, which corresponds with electrons having an escape depth ranging from 1 nm to 3 nm.

Figure 8: The process of photoionisation.
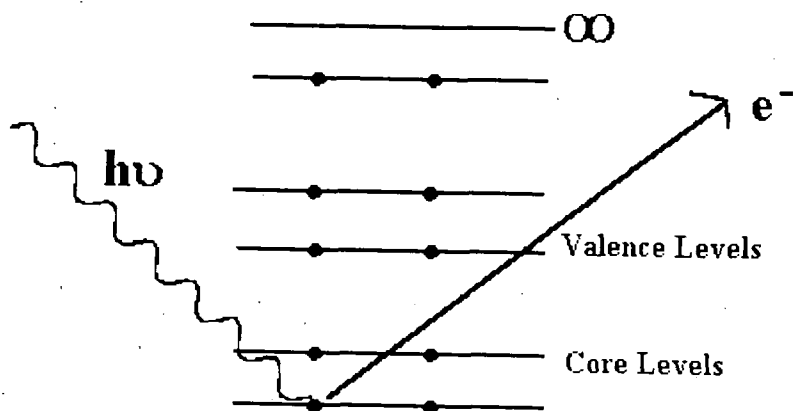
Figure 9: Graph showing the variation of escape depth with electron kinetic energy.
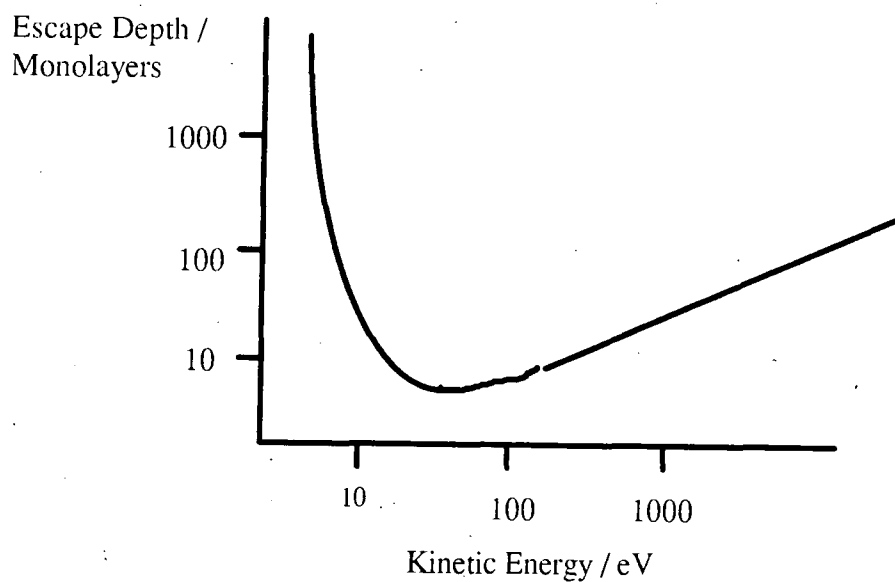
1.4.1.1 Instrumentation

XPS requires a UHV system (better than 10^{-6} torr).[67] The typically layout of a XPS spectrometer is shown in Figure 10.[65] The three basic components are a x-ray source, an electron energy analyser and an electron detector. One of two x-ray sources are normally used; Mg Kα source (1253.6 eV) and Al Kα source (1486.6 eV).[62] A very thin aluminium window is usually placed after the x-ray source in order to eliminate the bremsstrahlung or background radiation. The emitted electrons from the surface are collected by the electron lens array, in front of the electron detector, and slowed down before they enter the analyser in order to reduce the size of the analyser.[67] The most common electron analyser in use with XPS spectrometers is the concentric hemispherical analyser (CHA). The CHA consists of two hemispheres that are positioned concentricity and the voltage between the hemispheres is set so that only electrons of a known energy can pass through the analyser and reach the detector.[67] The XPS spectrometer can be operated in two modes. The first is to scan by varying the voltage on the analyser, keeping the voltages on the lenses constant (called fixed retard ratio or FRR mode) or keeping the voltage on the analyser constant and varying the voltage on the lens array (fixed analyser transmission or FAT mode).[65]

1.4.1.2 Spectral Interpretation

XPS spectra are displayed as a function of electron counts per second versus electron binding energy. The intensity of the photoelectron peaks from an atom's core energy level indicates the abundance of that element. Care must be taken when comparing the intensity from different element due to their different ionisation cross sections. Experimentally determined sensitivity factors can be used to relate the intensity from one element with another.[68]

Figure 10: Schematic representation of an x-ray photoelectron spectrometer.

Electron Analyser

X-ray Source

Lens Array

Electron Detector

Sample
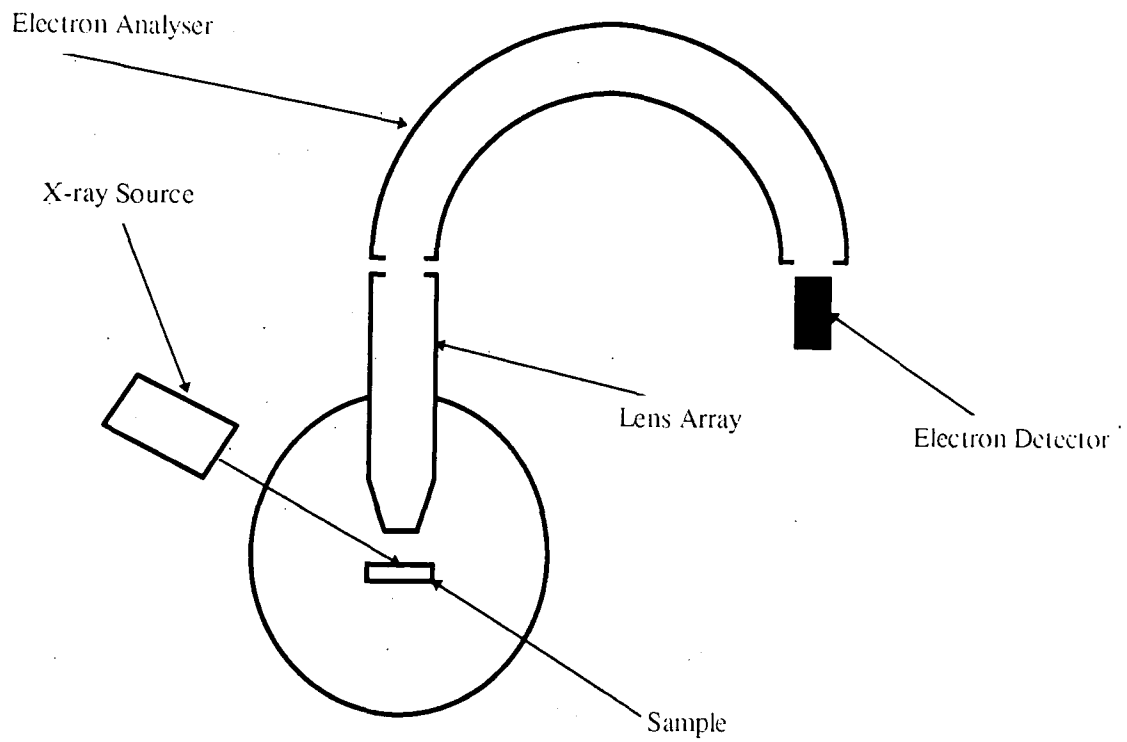
XPS spectra show that non-equivalent atoms of the same element have different binding energies. This effect is called the chemical shift.[69,70] The binding energy of an electron is determined by the shielding of the nucleus by the outer electrons. If an atom is surrounded by highly electronegative atoms this will cause the outer electron density to drop, reducing the shielding of the nucleus. Causing the electrons binding energy to increase.[62,69,70]

Interpretation of the XPS spectrum is complicated by several effects. The x-ray emission from Al and Mg x-ray sources not only consists of a $K\alpha_{1,2}$ doublet, associated with $2P_{1/2}$ to $1S$ and $2P_{3/2}$ to $1S$ transitions but also of the doubly ionised $(K\alpha_{3,4})$ transition. This leads to a photoelectron peak at about 8 % of the main intensity at approximately 10 eV lower binding energy. This peak is called a x-ray satellite.[71] Another complication is shake-up.[69] This occurs when the kinetic energy of an emitted photoelectron is reduced by the excitation of an valence electron. This results in satellite peaks a few eV higher in binding energy than the main photoelectron peak. In organic compounds the presence of shake-up peaks is indicative of aromatic species (π to π^* transitions).[72]

1.4.2 Atomic Force Microscopy

The atomic force microscope (AFM) was invented in 1986 by Binning.[73] At the heart of the AFM is a very sharp tip which is attached to a cantilever. The AFM measures the forces between the tip and a surface. The forces curve that exists between the tip and a surface as shown in Figure 11, can be described by a Lennard-Jones potential:[74]

$$U(r) = -U_0[(r_0/z)^{12} - (r_0/z)^6] \qquad (1.11)$$

When the tip and the surface are far apart, long range (Van der Waals) forces dominate and the net force between the tip and the surface is attractive. As the tip is moved closer to the surface the outermost atoms of the probing tip begin to come into contact with the surface atoms. The electron-electron interactions leads to strong repulsive forces between the tip and the sample.[75,76] Measurement of the forces between the tip and the sample reveals information about the surface, such as topography[77] and magnetic domain structure.[78]

Figure 11: Typical force curve for AFM experiments in air. The dip just before the contact portion is caused by the tip being sucked down to the surface, usually due to the surface tension of the water layer. As the tip retracts, the tip continues to stick to the surface until it is pulled clear.
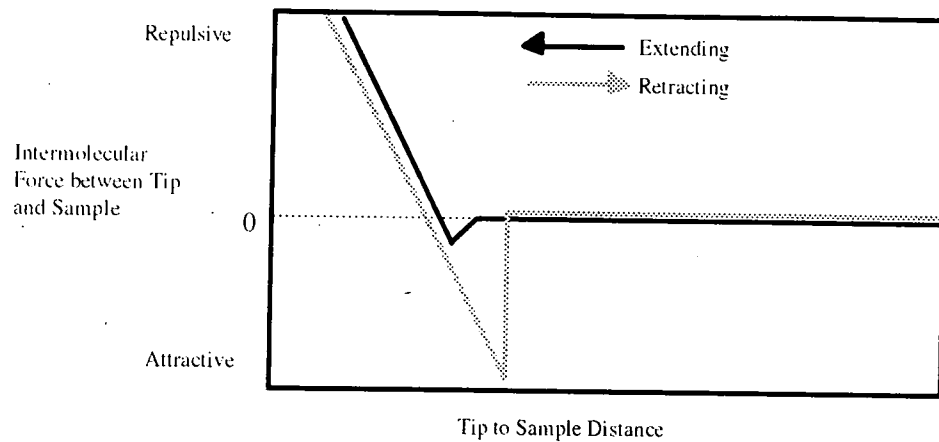
Figure 12: A schematic of the atomic force microscope.
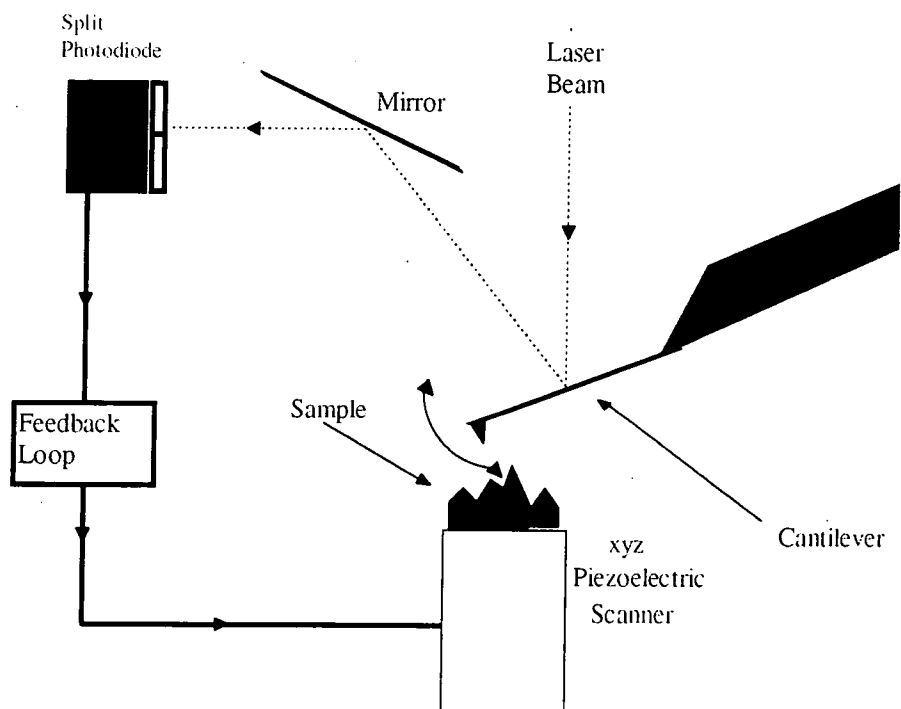
A schematic of the AFM is shown in Figure 12. The AFM can be operated in various modes in order to measure the surface forces. The two most common operating modes, contact mode and tapping mode, used to determine topography are described below.

1.4.2.1 Contact Mode AFM

In contact mode AFM[79,80] the tip is held very close to the sample so that the force between the tip and the sample is repulsive. When the tip is subjected to a force it will move in response to the force. This causes the cantilever to bend which sets up an opposing bending moment. The bending of the cantilever, dz, which is much smaller than the cantilever length (usually 100 μm or 200 μm) can be obtained from:[75]

$$EI(x)d^2z/dx^2 = M(x) \qquad (1.12)$$

Where E is the modulus of elasticity, $I(x)$ is the moment of inertia and $M(x)$ is the bending moment. This describes the equilibrium case where the external force is balanced by the internal bending moment of the cantilever. Practically $M(x)$ is given by:

$$M(x) = F_z(x - l_c) \qquad (1.13)$$

where F_z is the external force and l_c is the cantilever length. By determining the deflection of the cantilever the forces between the tip and the surface can be determined.

The most common method of determining cantilever deflection is to use a laser diode focused onto the back of the cantilever,[81] as shown in Figure 12. The position of the reflected laser beam is determined using a two or four segmented photodiode. The difference in intensity between the top half and bottom half of the photodiode, divided by the total intensity of the light hitting the photodiode gives the position of the reflected laser beam and hence the deflection of the cantilever.

Scanning the sample beneath the tip and studying the deflection of the cantilever as the repulsive forces between the tip and the surface change, as a result of changes in topography, builds up an image of the surface. Normally a feedback loop is employed varying the height of the sample so that the deflection of the cantilever is kept constant.[82] This ensures a constant tip to surface force. The image of the surface is obtained by recording the height of the sample with tip position. In order to minimise the possibility of deformation at the surface by the tip, the cantilever must have a very

small spring constant. Commercial cantilevers tend to have spring constants in the range 0.06 to 0.2 Nm^{-1} which leads to forces between the tip and the sample in the region of 10^{-11} to 10^{-7} N.

Contact mode suffers from several severe limitations, which arise from the fact that it is often difficult to limit the surface-tip forces. Surfaces in air are typically covered with a layer of water containing unknown contaminants. When a tip covered with a layer of contaminants comes near a sample that is also covered then there is an adhesion force (of the order 10^{-7} N) that drives the tip toward the sample.[83] Performing contact mode AFM in UHV[84] and in a liquid[83] have been proposed in order to overcome this problem. The sample in contact mode AFM will also experience shear forces from the tip due to the scanning motion which could lead to deformation of the surface and poor resolution due to stick-slip motions of the tip.[85]

1.4.2.2 Tapping Mode AFM

Tapping mode AFM[86,87] was invented to overcome the limitations of contact mode AFM. The set-up is the same as for contact mode AFM as shown in Figure 12. In tapping mode the cantilever is vibrated close to its resonance frequency[87] (approximately 300 kHz) with an oscillation amplitude ranging from, typically, 20 to 100 nm. The tip is made to strike the surface on each oscillation, at the downward apex of each cycle. Due to the large oscillations of the cantilever, the tip is able to overcome the stickiness of the absorbed water layer. The oscillation amplitude is measured as a RMS value of the deflection detector signal. Again a feedback system is employed to keep the RMS amplitude of the cantilever constant, with the topography determined by recording the variation of the height of the sample with tip position. The tip striking the surface at the downward apex of a cycle means that the force imparted to the surface is very small, 10^{-10} to 10^{-9} N,[88] generally lower than for contact mode AFM. In addition since the tip is no longer dragged along the surface there are virtually no shear forces and this technique can achieve very high resolution since the tip strikes the surface many times before it is displaced laterally by a tip diameter.

Phase imaging is a very recent variation on tapping mode AFM.[89,90] Tapping mode AFM changes in the oscillation amplitude of the cantilever are recorded to determine topography. For phase imaging AFM the phase of the oscillation is recorded with respect to the piezoelectric driving oscillations of the cantilever. The phase shift is very sensitive to variations in material properties, such as adhesion and viscoelasticity, and change when the tip encounters surface regions of different compositions.

1.4.3 Nuclear Magnetic Resonance Spectroscopy

Nuclear magnetic resonance (NMR) spectroscopy was invented over 40 years ago and is now routinely used to determine molecular structure and stereochemistry of organic molecules.[91] The fundamental property that is studied is the nuclear spin (I) of the atomic nucleus[92] which can have values of 0, $^1/_2$, 1, $1^1/_2$ etc. in units of $h/2\pi$. Here we shall consider the simplest case when I= $^1/_2$. The nuclear magnetic moment (μ) of a nucleus is directly proportional to the nuclear spin:[92]

$$\mu = \gamma Ih/2\pi \qquad (1.14)$$

Where γ is the magnetogyric ratio. When a magnetic field is applied the magnetic moments orient themselves with only certain allowed orientations. For a spin $I = ^1/_2$ there are two possible orientations of the nuclear spin, $m_I = \pm \, ^1/_2$, both with different energies as shown in Figure 13. The energy between the energy levels is given by:

$$\Delta E = \gamma Bh/2\pi \qquad (1.15)$$

or $$\nu = \gamma B/2\pi \qquad (1.16)$$

Where B is the strength of the magnetic field and ν is the resonant frequency. NMR works by the detection of this transition energy. It should be noted that the transition energy is dependent on the applied magnetic field. The greater the strength of the field the bigger the transition energy. With magnetic field currently available in the laboratory (1 - 15 T) the resonant frequency of most atoms is in the radio frequency of the electromagnetic spectrum.

Figure 13: Energy levels for a nucleus $I = \frac{1}{2}$.
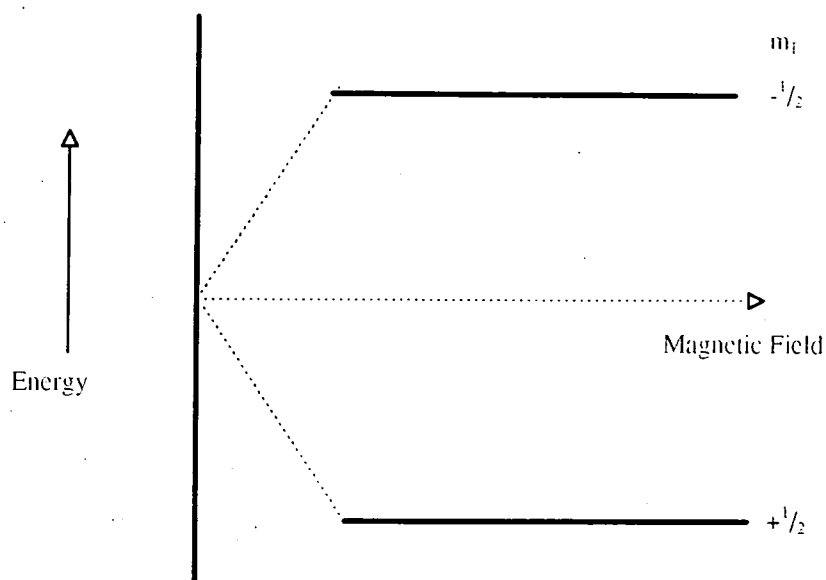
1.4.3.1 The Chemical Shift

The resonant frequency of a given nucleus is dependant, to a very small but measurable extent, on the chemical environment. The field at the nucleus is not equal to the applied field. The electrons in the molecule shielding the nucleus from the external applied field by setting up opposing magnetic fields.[93] Any change in the electron density will change the magnetic field at the nucleus and the resonant frequency. For example in the substituted methane's CH_3X, as X becomes more electronegative the electron density around the protons decreases and the y resonate at lower fields.[92]

The chemical shift, δ, is defined as the nuclear shielding divided by the applied field.[92] The chemical shift is a function of the nucleus and its environment. It is normally measured from a suitable reference compound (normally tetra methyl silane ($Si(CH_3)_4$) which can either be external or internal. The chemical shift is determined from the following equation:

$$\delta = (\nu_{sample} - \nu_{reference}) / \text{Oscillator frequency} \times 10^6 \quad (1.17)$$

The chemical shift (in units of ppm) is dependent on the sample and not the spectrometer.

NMR spectrometers can be operated in two modes. Continuous wave involves scanning across either the resonant frequency or the magnetic field strength.[94] This is very time consuming with the spectra having a low signal to noise ratio. In order to overcome this pulsed Fourier transform (PFT) NMR was developed. This involves hitting the sample, with the magnetic field applied, with a short high intensity radio frequency pulse. This then excites the nuclei to the higher energy state. These nuclei will then relax back to the thermal distribution at a rate that depends on the magnetic field at the nucleus. Measuring the free-inductive decay (FID) for the nucleus gives the time domain NMR spectrum which is converted into the frequency domain by Fourier transform of the FID.[95] Since the R.F. pulse need only be very short (region of μs) many spectra can recorded of the same sample in a short space of time. Combination of these spectra give an overall spectrum with a very low signal to noise ratio. Today virtually all NMR spectrometers using PFT-NMR.

1.4.4 Static Secondary Ion Mass Spectrometry

The basic process involved with static secondary ion mass spectrometry (SSIMS) is the bombardment of a surface with low energy and low density ions giving rise to the emission of secondary ions.[96] This is caused by sputtering from the surface. The general outline of this process is widely accepted. The primary particle impacts with the surface atoms transferring energy to the surface and causing collision sequences between atoms in the near surface region. Some energy will be dissipated into the bulk of the solid whist some collision sequences or cascades return to the surface causing the emission of secondary ions or atoms.[96] In general this emitted particle will be released at a point remote from the initial impact. The extension of the model after this point is the subject of considerable debate[97,98] and will not be considered further.

The great advantage of is that fragment or cluster ions are emitted from the surface. All the chemical characterisation facilities associated with organic mass spectrometry should enable the determination of the chemical structure of the fragment, which gives information of the chemical structure at the surface.

33

1.4.4.1 Instrumentation

Like XPS, SSIMS has to be performed under UHV.[99] There are two main components to the experiment; the primary particle beam and the mass spectrometer.[100] In order to prevent extensive surface damage of the sample low ion beam currents (10^{-10} to 10^{-8} A cm^{-2}) normally have to be used.[100] Most SSIMS systems use electron bombardment of gaseous molecules (usually argon or xenon) to produce the ion beam which is then accelerated to energies between 0.5 and 4 KeV before they bombard the surface. Particle bombardment always leads to the emission of vast numbers of secondary electrons as well as ions. Hence positive charging of the surface nearly always occurs. In order to overcome this an electron gun is used in order to flood the surface with electrons. Most modern SSIMS spectrometers use one of two mass spectrometers; the quadrupole mass spectrometer or the more advanced time of flight mass spectrometer.[99,100]

1.4.4.2 Spectral Interpretation

SSIMS spectra are displaced as a function of signal counts versus the mass / charge ratio. In common with conventional mass spectrometry, SSIMS spectra can be 'interpreted' in two ways. Either by matching spectra with fingerprint spectra of standard samples or by logical determination of structure from the form of the fragmentation pattern and a knowledge of the fragmentation pathways.[101,102] A unique molecular formula can often be derived from a sufficiently accurate mass measurement alone, as the atomic masses are not integers,[101] the molecular structure can then be determined by considering factors such as the parent structure or the degree of unsaturation.

In addition once a fragment has been identified the spatial distribution of that fragment can be determined by focusing the ion beam and rastering the beam across the sample whist only detecting for that fragment.[102] The spatial resolution of this technique is now better than 1 μm.

REFERENCES

1 . McMurry, J. *Organic Chemistry*; Brooks/Cole: California, 1988; 2nd ed.

2 . Garbassi, F.; Morra, M.; Occhiello, E. *Polymer Surfaces: From Physics to Technology*; Wiley: Chichester, 1994; Chapter 1.

3 . Adamson, A. W. *Physical Chemistry of Surfaces*; Wiley: Chichester. 1991: 5th edn.

4 . Cherry, B. W. *Polymer Surfaces*; Cambridge University: Cambridge. 1981.

5 . Sperling, L. H. *Introduction to Physical Polymer Science*; Wiley: Chichester, 1992; 2nd edn.

6 . Young, T. *Miscellaneous Works*; Peakcock, G., Ed.; Murray: London. 1855: Vol . 1.

7 . Bigelow, W. C.; Pickett, D. L.; Zisman, W. A. *J. Colloid Sci.* **1946**, *1*, 513.

8 . Newmann, A. W.; Ranszow, D. *Z. Phys. Chemie. Neue Folge* **1969**, *68*, 11.

9 . Lee, L.-H. *J. Polym. Sci., A-2* **1967**, *5*, 1103.

10 . Langmuir, I. *Science* **1938**, *87*, 493.

11 . Fedotov, V. D.; Schneider, H. *Structure and Dynamics of Bulk Polymer by NMR Methods*; Springer-Verlag:1989; Chapter 4.

12 . Andrade, J. D. In *Polymer Surface Dynamics*; Andrade, J. D., Ed.; Plenum: New York, 1988, Chapter 1.

13 . Yasuda, T.; Okuno, T.; Yoshida, K.; Yasuda, H. *J. Polym. Sci., Polym. Phys. Ed.* **1988**, *26*, 1781.

14 . Yasuda, H.; Sharma, A. K.; Yasuda, T. *J. Polym. Sci., Polym. Phys. Ed.* **1981**, *19*, 1285.

15 . Ratner, B. D.; Weathersby, P. K.; Hoffman, A. S.; Kelly, M. A.; Scharpen, L. H. *J. Appl. Polym. Sci.* **1978**, *22*, 643.

16 . Brewis, D. M. In *Polymer Science*; Jenkins, A. D., Ed.; North-Holland: Amsterdam, 1972; Vol.2, Chapter 13.

17 . Andrews, E. H.; King, N. E. In *Polymer Surfaces*; Clark, D. T.; Feast, W. J., Eds.; Wiley: Chichester, 1978; Chapter 3.

18 . Houwink, R.; Salomon G., Eds. *Adhesion and Adhesives*; Elsevier: Amsterdam, 1965.

19 . Levine, M.; Ilkka, G.; Weiss, P. *J. Polym. Sci., B* **1964**, *2*, 915.

20 . Weiss, J.; Leppin, C.; Mader, W.; Salzberger, U. *Thin Solid Films* **1989**, *174*, 155.

21 . Jamieson, E. H.; Windle, A. H. *J. Mat. Sci.* **1983**, *18*, 64.

22 . Garbassi, F.; Morra, M.; Occhiello, E. *Polymer Surfaces: From Physics to Technology*; Wiley: Chichester, 1994; Chapter 11.

23 . Karttunen, S.; Oittnen, R. In *Science and Technology of Surface Coatings*; Chapman, B. N.; Anderson, J. C. Eds., Academic: London; 1974, Chapter 24.

24 . Wenzel, R. N. *Ind. Eng. Chem.* **1936**, *28*, 988.

25 . Leclerq, B.; Sotton, M. *Polymer* **1977**, *18*, 675.

26 . Lerchenthal, C. H.; Brenman, M.; Yits`hag, N. *J. Polym. Sci., Polym. Chem. Ed.* **1975**, *13*, 737.

27 . Mascia, L. *The Role of Additives in Plastics*; Arnold: London, 1974; Chapter 4.

28 . Garbassi, F.; Morra, M.; Occhiello, E. *Polymer Surfaces: From Physics to Technology*; Wiley: Chichester, 1994; Chapter 7.

29 . Kato, K. *Polymer* **1967**, *8*, 33.

30 . Kato, K. *Polymer* **1968**, *9*, 419.

31 . Armond, V. J.; Atkinson, J. R. *J. Mater. Sci.* **1968**, *3*, 332.

32 . Briggs, D.; Brewis, D. M.; Konieczo, M. B. *J. Mat. Sci.* **1976**, *11*, 1270.

33 . Edge, S.; Walker, S.; Feast, W. J.; Pacynko, W. F. *J. Appl. Polym. Sci.* **1993**, *47*, 1075.

34 . Wells, R. K. Ph. D. Thesis, University of Durham, 1994.

35 . Adams, J. H. *J. Polym. Sci., A-1* **1970**, *8*, 1279.

36 . Imada, K.; Nishina, Y.; Norma, H. U. S. Patent 4307045, 1981.

37 . Sheng, E.; Sutherland, I.; Brewis, D. M.; Heath, R. J.; Bradley, R. H. *J. Mat. Chem.* **1994**, *4*, 487.

38 . Sutherland, I.; Brewis, D. M.; Heath, R. J.; Sheng, E. *Surf. Inter. Anal.* **1991**, *17*, 507.

39 . Mohl., W. *Adv. Mater.* **1990**, *2*, 57.

40 . Tanks, L.; Langmuir, I. *Phys. Rev.* **1929**, *33*, 195.

41 . Lord Rayleigh *Phil Mag.* **1906.** *11*, 117.

42 . Warson, C. J. H. In *Plasma Physics*: Kenn, B. E. Ed.; Institute of Physics: London, 1974; Chapter 1.

43 . Chapman, B. *Glow Discharge Processes*: Wiley: New York, 1980.

44 . Uman, M. A. *Introduction to Plasma Physics*; McGraw-Hill: New York, 1964.

45 . Bell, A. T. In *Techniques and Applications of Plasma Chemistry*: Hollahan, J. R.; Bell, A. T. Eds.; Wiley: New York, 1974; Chapter 1.

46 . Krall, N. A.; Trivelpiece, A.W. *Prinicples of Plasma Physics*: Mcgraw-Hill: New York, 1973.

47 . Grill, A. *Cold Plasma in Materials Fabrication*; IEEE: New York, 1994.

48 . Fang, D.; Marus, R. K. In *Glow Discharge Spectroscopies*: Marus, R. K. Ed.; Plenum: New York, 1993; Chapter 2.

49 . Rossnagel, S. M. In *Thin Film Processes II*; Vossen, J. L.; Kern, W. Eds.; Academic: Boston, 1991; Chapter 1.

50 . Anderson, G. S.; Meyer, W. N.; Wehner, G. K. *J. Appl. Phys.* **1962.** *33*, 2991.

51 . McTaggart, F. K. *Plasma Chemistry in Electrical Discharges*: Elsevier: Amsterdam, 1967.

52 . Hudis, M. In *Techniques and Applications of Plasma Chemistry*: Hollahan, J. R.; Bell, A. T. Eds.; Wiley: New York, 1974; Chapter 3.

53 . Siemen, W *Ann. Phys. Chem.* **1857**, *102*, 66.

54 . Eliasson, B.; Kogelschatz, U. *IEEE Trans. Plasma Sci.* **1991**, *19*, 309.

55 . Eliasson, B.; Egli, W.; Kogelschatz, U. *Pure Appl. Chem.* **1994**, *66*, 1766.

56 . Eliasson, B.; Hirth, M.; Kogelschatz, U. *J. Phys. D., Appl. Phys.* **1987**, *20*, 1421.

57 . Kogelschatz, U.; Eliasson, B. *Proceedings. Symp. High Presure Low Tepmerature Plasma Chem.* **1987**, 1.

58 . Kogelschatz, U. *Proceedings XVI Int. Conf. Phen. Ionized Gases* **1983**, 240.

59 . Braun, D.; Kuchler, U.; Pietsch, G. *J. Phys. D., Appl. Phys.* **1991**, *24*, 564.

60 . Braun, D.; Gibalov, V.; Pietsh, G. *Plasma Source Sci. Technol.* **1992**, *1*, 166.

61 . Clark, D. T.; Dilks, A. *J. Polym. Sci., Polym. Chem. Ed.* **1979**, *17*, 957.

62 . Woodruff, D. P.; Delchar, T. A. *Modern Techniques of Surfcae Science*; Cambridge University: Cambridge, 1986.

63 . Sherwood, P. M. A. In *Spectroscopy*; Straughan, B. P.; Walker, S. Eds.; Chapman and Hall: London, 1976; Vol. 3, Chapter 7.

64 . Hollas, J. M. *Modern Spectroscopy*; Wiley: Chichester, 1987.

65 . Desimioni, E.; Zambonin, P. G. *Surface Characterization of Advanced Polymers*; Sabbatini, L.; Zambonin, P. G. Eds.; VCH: Weinheim, 1993; Chapter 1.

66 . Prutton, M. *Surface Physics*; Clarendon: Oxford, 1983.

67 . Riviere, J. C. In *Practical Surface Analysis*; Briggs, D.; Seah, M. P. Eds.; Wiley: Chichester, 1983; 2nd ed., Vol. 1, Chapter 2.

68 . Seah, M. P. In *Practical Surface Analysis*; Briggs, D.; Seah, M. P. Eds.; Wiley: Chichester, 1983; 2nd ed., Vol. 1, Chapter 5.

69 . Briggs,D.; Riviere, J. C. In *Practical Surface Analysis*; Briggs, D.; Seah, M. P. Eds.; Wiley: Chichester, 1983; 2nd ed., Vol. 1, Chapter 3.

70 . Nelson, A. J. In *Microanalysis of Solids*; Yacobi, B. G.; Holt, D. B.; Kazmerski, L. L. Eds.; Plenum: New York, 1994; Chapter 9.

71 . Riviere, J. C. *Surface Analytical Techniques*; Clarendon: Oxford, 1990.

72 . Clark, D. T.; Dilks, A. *J. Polym. Sci., Polym. Chem. Ed.* **1976**, *14*, 533.

73 . Binning, G.; Quate, C. F.; Gerber, Ch. *Phys. Rev. Lett.* **1986**, *56*, 930.

74 . Burnham, N. A.; Colton, R. J. In *Scanning Tunneling Microscopy and Spectroscopy: Theory, Techniques and Applications*; Bonnell, D. Ed.; VCH:New York, 1993; Chapter 7.

75 . Magonov, S. N. *Applied Spectroscopy Reviews* **1993**, *28*, 1.

76 . Quate, C. F. *Surface Sci.* **1994**, *299/300*, 980.

77 . Albrecht, T. R.; Dovek, M. M.; Grutter, L. P.; Quate, C. F.; Kuan, S. W. J.; Frank. C. W.; Pease, R. F. W. *J. Appl. Phys.* **1988**, *64*, 1178.

78 . Rugar, D.; Mannin, H. J.; Erlandson, R.; Stern, J. E.; Terris, B. D. *Rev. Sci. Instrum.* **1988**, *53*, 1563.

79 . Meyer, E. *Progress in Surface Science* **1992**, *41*, 3.

80 . Sarid, D. *Scanning Force Microscopy: With Applications to Electric, Magnetic, and Atomic Forces*; Oxford University: Oxford, 1991.

81 . Hues, S.; Colton, R.; Meyer, E.; Guntherodt, H. J. *MRS Bulletin;* January 1993, 41.

82 . Joyce, S. A.; Houston, J. E. *Rev. Sci. Instrum.* **1991**, *62*, 710.

83 . Drake, B.; Prater, C. B.; Weisenhorn, A. C.; Gould, S. A. C.; Albrecht, T. R.; Quate, C.F.; Cannell, D. S.; Hansma, H. G.; Hansma, P. K. *Science* **1989**, *243*, 1586.

84 . Howald, L.; Meyer, E.; Luthi, R.; Haefke, H.; Overney, R.; Rudin, H.; Guntherodt, H.-J. *Appl. Phys. Lett.* **1993**, *63*, 117.

85 . Oshea, S. J.; Weland, M. E.; Wong, J. M. H. *Ultramicroscopy* **1993**, *52*, 55.

86 . Elings, V.; Gurley, J. U.S. Patent 5266801, 1993.

87 . Zhong, Q.; Inniss, D.; Kjoller, K.; Elings, V. B. *Surf. Sci. Lett.* **1993**, *290*, 688.

88 . Nanoscope III Operating Manual; Digital Instruments Inc: California.

89 . Babcock, K. L.; Prater, C. B. *Phase Imaging: Beyond Topography;* Technical Support Note, Digital Instruments: California; 1995.

90 . Chernoff, D. A. *Phase Imaging: What, How and Why;* Applications Note, Digital Instruments: California; 1995.

91 . Brown, D. W.; Floyd, A. J.; Sainsbury, M. *Organic Spectroscopy;* Wiley: Chichester, 1988.

92 . Abraham, R. J.; Fisher, J.; Loftus, P. *Introduction to NMR Spectroscopy;* Wiley: Chichester, 1988.

93 . Bovey, F. A. *Nuclear Magnetic Resonance Spectroscopy;* Academic: San Diego, 1988.

94 . Martin, M. L.; Delpuech, J.-J.; Martin, G. J. *Practical NMR Spectroscopy*; Heyden: London, 1980.

95 . Farrar, T. C.; Becker, E. D. *Pulse and Fourier Transform NMR spectrscopy: Introduction to Theory and Methods*; Academic: New York, 1971.

96 . Vickermann, J. C. In *Methods of Surface Analysis: Techniques and Applications*; Wallis, J. M. Ed.; Cambridge University: Cambridge, 1989; Chapter 6.

97 . Williams, P. *Surface Sci.* **1979**, *90*, 588.

98 . Williams, P. *Appl. Surf. Sci.* **1982**, *13*, 241.

99 . Jede, R.; Gunshow, O.; Kaiser, U. In *Practical Surface Analysis*; Briggs, D.; Seah, M. P. Eds.; Wiley: Chichester, 1983; 2nd ed., Vol. 2, Chapter 2.

100 . Briggs, D.; Brown, A.; Vickerman, J. C. *Handbook of Static Secondary Ion Mass Spectrometry*; Wiley: Chichester, 1984.

101 . Silverstein, R. M.; Bassler, G. C.; Morrill, T. C. *Spectrometric Indentification of Organic Compounds*; Wiley: New York, 1991; 5th ed.

102 . Briggs, D. In *Practical Surface Analysis*; Briggs, D.; Seah, M. P. Eds.; Wiley: Chichester, 1983; 2nd ed., Vol. 2, Chapter 7.

CHAPTER 2:

OXYGEN GLOW DISCHARGE PLASMA TREATMENT OF BIAXIALLY ORIENTED POLYPROPYLENE.

2.1 INTRODUCTION

Non-equilibrium plasmas are widely used to modify the surface properties of polymers, plastics and rubbers. For instance, noble gas plasmas are effective at etching polymer surfaces,[1] CF$_4$ plasmas can lead to surface fluorination,[2,3] and oxygen plasma treatment can enhance polymer wettability and adhesion via surface oxidation.[4] Both the chemical and physical changes taking place at the electrical discharge / substrate interface can influence the performance of the resulting surface.

The chemical nature of plasma treated polymers has been extensively examined by surface sensitive analytical techniques, these include: X-ray photoelectron spectroscopy (XPS),[5-8] secondary ion mass spectrometry (SIMS),[9] and contact angle measurements.[10] Investigation of the physical changes imparted during plasma treatment has in the past been mainly restricted to scanning electron microscopy (SEM) studies.[11,12] One of the major drawbacks of SEM is that it usually requires insulating samples to be coated with a conductive layer which can lead to the deformation of soft samples (e.g. polymers), this can also mask any plasma induced surface modification. Furthermore, SEM probes the specimen with a high energy electron beam, which can damage the polymer surface during analysis. The relatively recent invention of atomic force microscopy (AFM) overcomes the aforementioned limitations of SEM.[13] AFM works by scanning a very sharp tip attached to a lightly sprung cantilever, across the sample surface whilst keeping the repulsive force between the probe and surface constant. Nanometer resolution of non-conducting substrates can routinely be achieved using AFM without the need for any additional sample preparation. Although the morphology of untreated polymer samples has been widely studied by AFM,[14-16] not much attention has been paid to the topography of plasma treated polymers.[17-19]

2.1.1 Review of Oxygen Glow Discharge Treatment of Polypropylene.

2.1.1.1 Species Generated by an Oxygen Plasma

Previous studies have shown that many chemical reactions occur within a oxygen glow discharge plasma.[20] Electrons colliding with molecules of oxygen lead to the transfer of energy, which causes the molecule to be excited to a higher electronic state, many of which dissociate into ground state atoms. Other reactions that can occur within the plasma include dissociation with the production of both negative (O^-) and positive (O^+) ions. Both atomic oxygen and ionic oxygen can lead to the production of ozone and molecular ions (such as O_2^-, O_3^- etc.). Also produced are large amounts of vacuum ultra-violet (VUV) radiation.[21] Oxygen atoms and VUV are generally regarded as begin the primary reactive species involved with surface activation.[8,22]

2.1.1.2 Surface Oxidation by an Oxygen Plasma

The rate determining step for plasma oxidation is the initiation step. Which occurs via several mechanisms, all of which are free radical based reactions, such a mechanism is an oxygen abstraction:
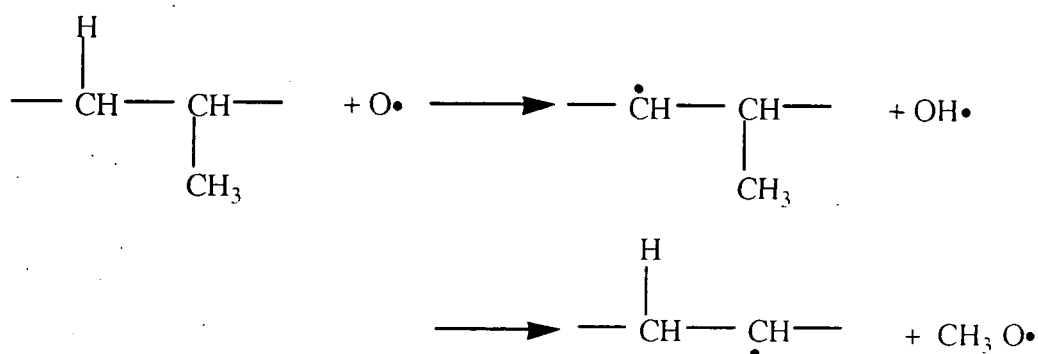
The other mechanisms are dissociation reactions driven either by the dissociation energy of molecular oxygen or by the absorption of VUV radiation causing C-H bond rupture.[23] leading to the production of carbon radicals and possibly causing chain scission.

i)

$$\overset{\displaystyle H}{\underset{\displaystyle CH_3}{—CH—\overset{|}{CH}—}} \quad + 2O\bullet \quad \longrightarrow \quad —\overset{\bullet}{CH}—\underset{\displaystyle CH_3}{\overset{|}{CH}}— \quad + O_2 \; + \; H\bullet$$

ii)

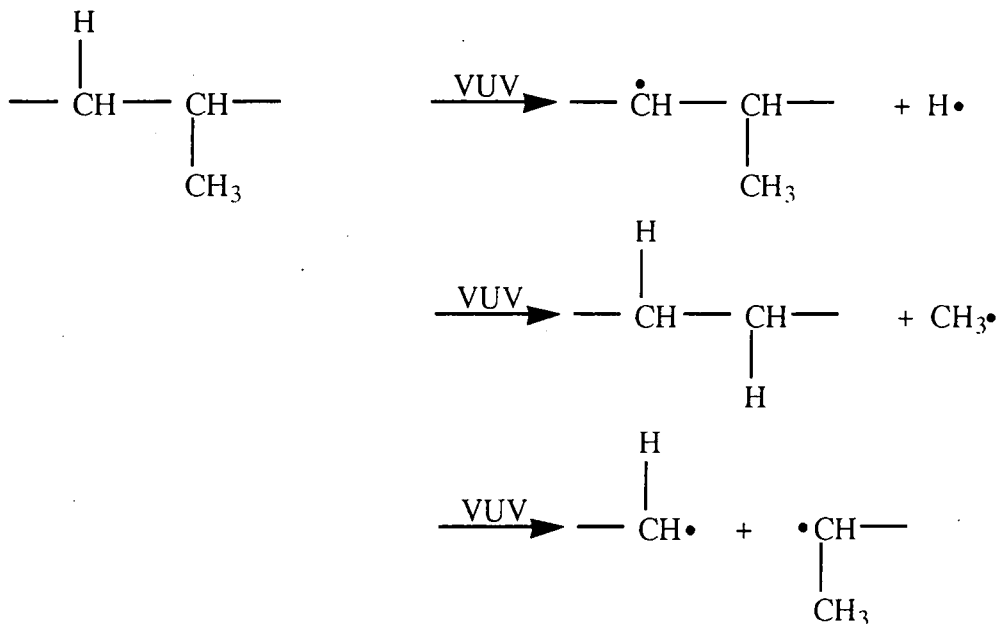$$\overset{\displaystyle H}{\underset{\displaystyle CH_3}{—CH—\overset{|}{CH}—}} \quad \xrightarrow{\;VUV\;} \quad —\overset{\bullet}{CH}—\underset{\displaystyle CH_3}{\overset{|}{CH}}— \quad + \; H\bullet$$

$$\xrightarrow{\;VUV\;} \quad \overset{\displaystyle H}{\underset{\displaystyle H}{—CH—\overset{|}{CH}—}} \quad + \; CH_3\bullet$$

$$\xrightarrow{\;VUV\;} \quad \overset{\displaystyle H}{—CH\bullet} \quad + \quad \bullet\underset{\displaystyle CH_3}{\overset{|}{CH}}—$$
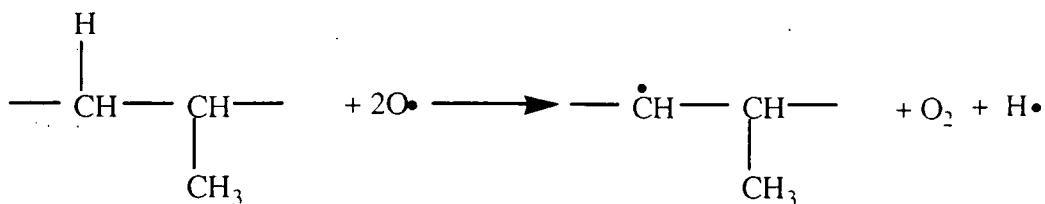
These newly created radical sites can then either react with atomic or molecular oxygen to create hydroperoxide and hydroxyl radicals, which combine with hydrogen radicals or abstract hydrogen from the same or a nearby polymer chain, creating another carbon radical in doing so this is called 'auto oxidation',[24] to form their respective groups. These groups can then undergo further oxidation to form the more highly oxidized carbon species, such as acid groups. Alternatively the carbon radicals can decompose leading to chain scission. This occurs by two main reactions. β-scission[25] and a disportionation reaction.[26] Molecular orbital analysis has shown that addition of oxygen onto the backbone of a hydrogen carbon polymer severely weakens the adjacent carbon-carbon bond, which will increase the rate of chain scission occurring.[27] It is possible that oxygen plasma treatment can cause cross-linking however the extent of cross-linking is negligible due to the high rate of oxidation occurring.[28]

2.1.1.3 Ion Sputtering

Although atomic oxygen is the primary force for surface modification in a oxygen plasma,[29] the role of ion bombardment has to be considered. Negative molecular oxygen ions are held within the plasma by the plasma sheath, whereas positive molecular oxygen ions are accelerated by the sheath then bombard the surface with up to 2 eV of energy.[30] This energy is sufficient to cause sputtering from the surface and surface activation.[22] Mayoux[31,32] bombarded a polymer surface with ions, in an oxygen environment, and detected the generation of alcohol and ketone groups following bombardment with inert gas ions as well as positive oxygen ions.

2.1.1.4 Ablation from the Polymer Surface.

Hansen[4] presented the first mass loss rate data of polymers exposed to an oxygen plasma. He found a linear mass loss rate with time for all of the polymers he tested and the process started virtually immediately with treatment. This mass loss is due to ablation of material from the polymer surface and is caused by two effects. The first is sputtering caused by ion bombardment and the second is chemical reactions of the polymer with the atomic oxygen producing volatile material which then ablates from the surface.[22,33] Various techniques have been used to investigate the nature of the gaseous products ablated from the plasma exposed polymers. Hansen[4] examined the spectra from the emitted light for oxygen plasma containing polymer samples and found bands corresponding to carbon dioxide and OH groups. MacCallum[34] performed mass spectrometry of the volatile products to reveal carbon dioxide and water vapor. Whitaker[35] performed residual gas analysis of the gaseous products evolved from the polymer sample and found evidence for water vapour, carbon dioxide and carbon monoxide being produced.

2.2 EXPERIMENTAL

2.2.1 Sample Preparation

An industrially produced sample of tubular blown biaxially oriented polypropylene (ICI D509) was obtained. Small strips of which were washed in a 50/50

mixture of isopropyl alcohol (BDH) / cyclohexane (BDH) prior to treatment for 5 seconds.

2.2.2 Oxygen Glow Discharge Plasma Treatment

All oxygen plasma treatments were carried out in a electrodeless cylindrical glass reactor (5 cm diameter, 25 cm long), which was enclosed in a Faraday cage. The reactor had a base pressure of 5×10^{-3} torr and a leak rate of better than 10^{-4} torr l s^{-1}. The reactor was fitted with a needle value (Edwards FCV10K), a pirani pressure gauge (Edwards PR10-k) and a Fomblin oil, two stage rotary pump (Edwards E2M2) attached to a liquid nitrogen cold trap. A home made L-C matching network was used to inductively couple a copper coil (4 mm diameter copper with 11 coils wrapped around the reactor) to a 13.56 MHz radio frequency source. The matching network matched the output impedance of the frequency source to that of the partially ionized gas load by minimizing the standing wave ratio (SWR). A schematic diagram of the setup used is shown in Figure 1. A typical experimental run comprised of initially scrubbing the reactor with detergent, rinsing in isopropyl alcohol, then oven drying. The reactor was then cleaned with a 40 W air plasma for at least 30 minutes, after which the reactor was opened and the polymer sample was inserted into the reactor. A small strip of the polymer was placed in the centre of the reactor, which is also at the center of the copper coils. The reactor was closed and pumped down to its base pressure. Oxygen was then introduced into the reactor to a pressure of 2×10^{-1} torr. The reactor was purged for 600 s, after which the glow discharge plasma was ignited at 10 W. After treatment the sample was purged for 120 s. Each sample was characterized immediately after treatment.

2.2.3 Sample Analysis

A Kratos ES300 electron spectrometer equipped with a MgKα X-ray source (1253.6 eV) and a concentric hemispherical analyser was used for XPS analysis. Photoemitted electrons were collected at a take-off angle of 30° from the substrate normal, with electron detection in the fixed retard ratio (FRR, 22:1) mode. XPS spectra were accumulated on an interfaced IBM PC computer. Instrumentally

47

determined sensitivity factors for unit stoichiometry of C(1s) : O(1s) were taken as equaling 1.00 : 0.62.

A Digital Instruments Nanoscope III atomic force microscope was used to examine the topographical nature of the polypropylene surface prior to and immediately after electrical discharge exposure. All of the AFM images were acquired in air using the Tapping mode,[36] and are presented as unfiltered data.

Figure 1: A schematic of the plasma reactor set-up.
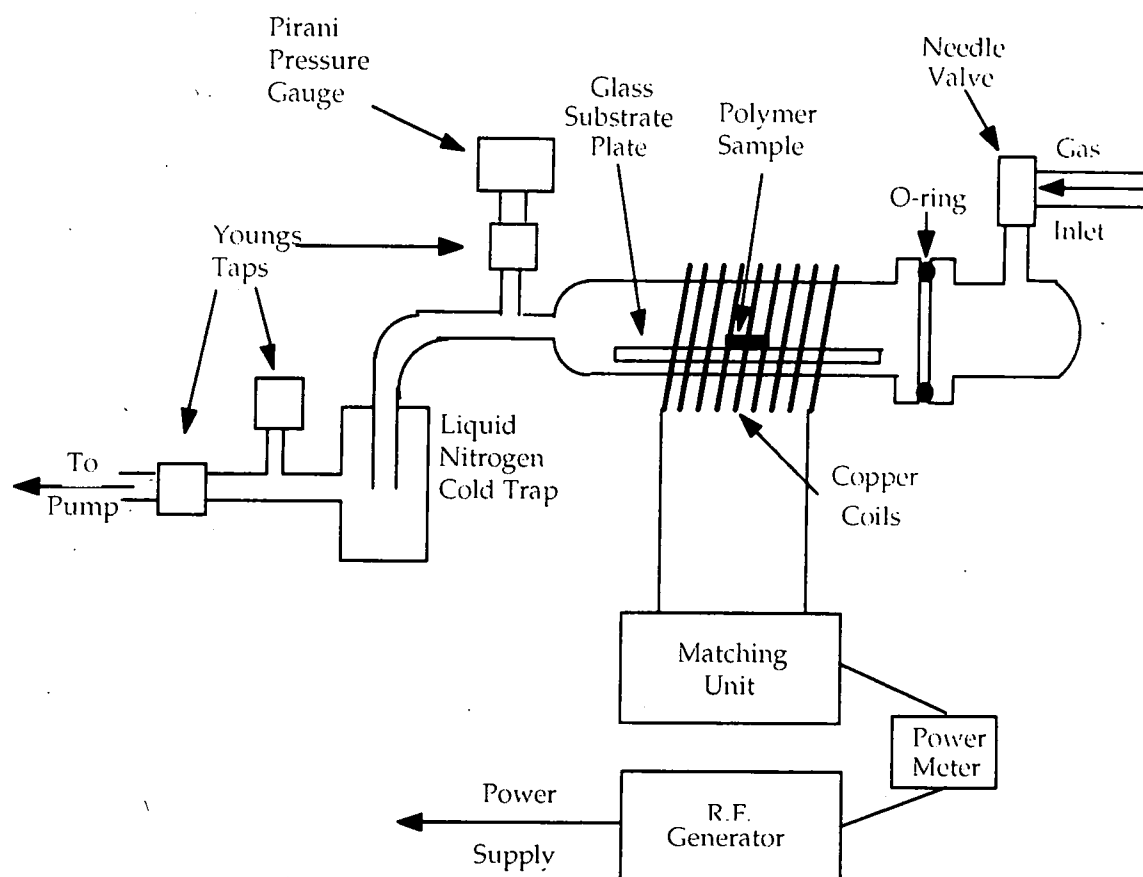
2.3 RESULTS

2.3.1 X-ray Photoelectron Spectroscopy Results

XPS was used to determine the surface composition of the treated polymer. Only oxygen and carbon were detected. The XPS experimentally determined oxygen to carbon (O/C) ratios for oxygen plasma treated polymers, using a variety of treatment times, are shown in Figure 2(a). From the O/C ratios it can be seen that the maximum rate of oxidation of the surface by the plasma occurs within the first 30 seconds of treatment. After which the rate of oxidation rapidly drops and the O/C ratio saturates out after 2 minutes of treatment. C(1s) XPS spectra were fitted with Gaussian peaks of equal full width at half maximum (FWHM),[37] using a Marquardt minimisation computer program. Energies distinctive of different types of oxidised carbon moieties[38] were referenced to the hydrocarbon peak ($-\underline{C}_xH_y-$) at 285.0 eV: carbon adjacent to a carboxylate group ($>\underline{C}-CO_2-$) at 285.7 eV, carbon singly bonded to one oxygen atom ($>\underline{C}-O-$) at 286.6 eV, carbon singly bonded to two oxygen atoms or carbon doubly bonded to one oxygen atom ($-O-\underline{C}-O- / >\underline{C}=O$) at 287.9 eV, carboxylate groups ($-O-\underline{C}=O$) at 289.0 eV, and carbonate carbons ($-O-\underline{C}O-O-$) at 290.4 eV. Untreated polymer exhibits a single C(1s) peak which corresponds to C_xH_y functionalities (i.e. -CH, -CH$_2$, and -CH$_3$ groups). Peak fitted C(1s) XPS spectra of untreated and oxygen plasma treated polypropylene surfaces are shown in Figure 2(b). The untreated polypropylene C(1s) spectrum shows a single peak corresponding to carbon bonded to hydrogen. Oxygen plasma treatment of the polypropylene surface introduces -C-O, O-C-O, C=O, and -CO-O groups onto the surface. A plot of the relative intensities of the oxidized carbon peaks with respect to the total intensity of the oxidized carbon peaks is shown in Figure 2(c). The relative intensity of the -C-O peak is seen to peak at 30s treatment and then to decrease with treatment time, which corresponds to -C-O groups undergoing further oxidation with treatment.

Washing of the oxygen plasma modified surface causes the XPS O/C ratio to drop from 0.27 to 0.12, which indicates that the majority of the plasma modified material is removed on washing. From the peak fitted C(1s) XPS spectrum of the washed modified surface, shown in Figure 3, the relative intensities of the oxidized

carbon peaks were determined and compared to the relative intensities of the unwashed oxygen plasma treated polypropylene, as shown in Table 1. From which it can be seen that the more highly oxidized species are preferentially removed on washing.

Table 1: Relative concentrations of oxidized carbon moieties for oxygen plasma treated and oxygen plasma treated then washed polypropylene.

	O-C	O-C-O / C=O	CO-O
Unwashed	0.47	0.26	0.27
washed	0.55	0.28	0.17

Figure 2(a):

Influence of oxygen plasma treatment time on O/C ratio.
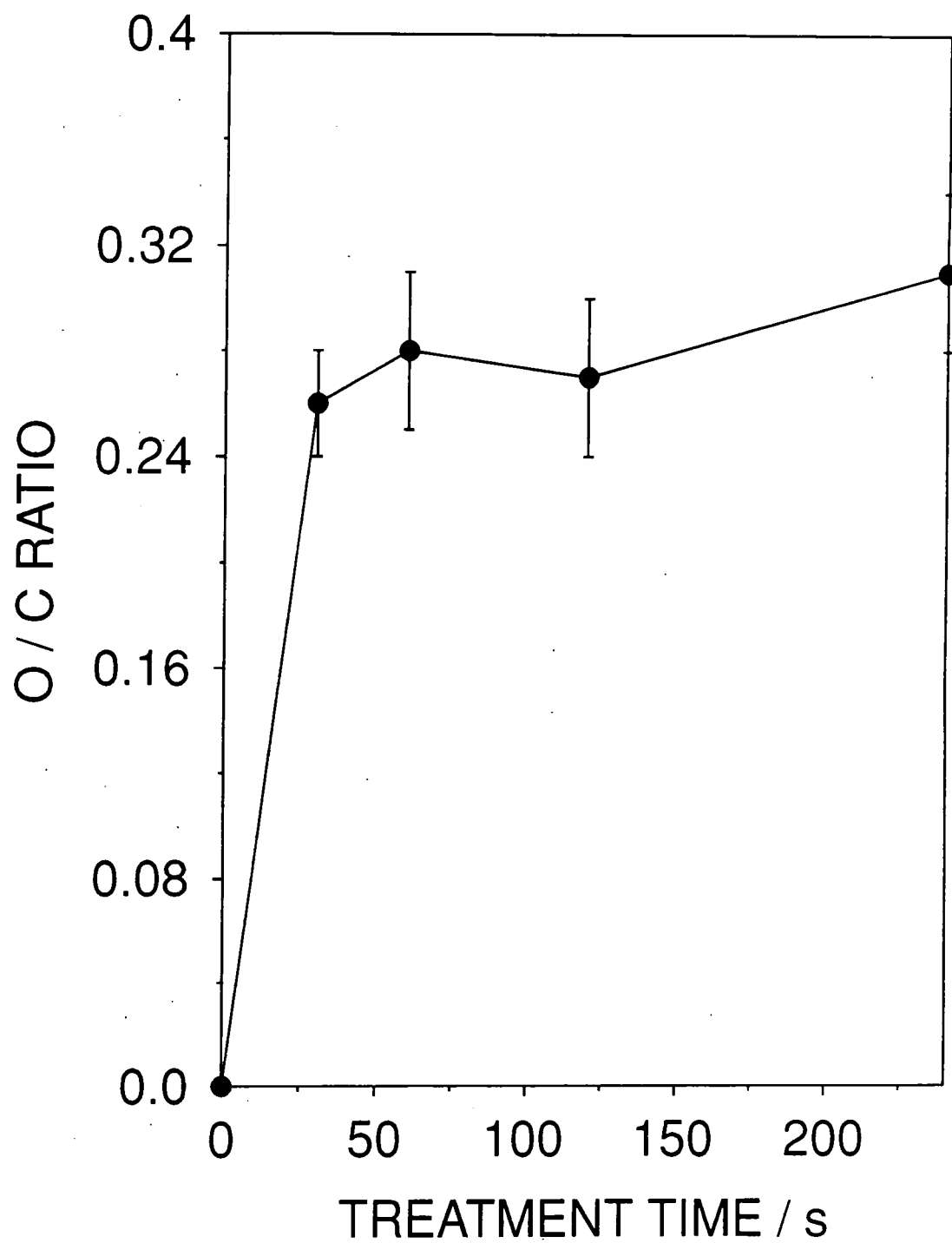
Figure 2(b):

Influence of oxygen plasma treatment time on C(1s) spectra.
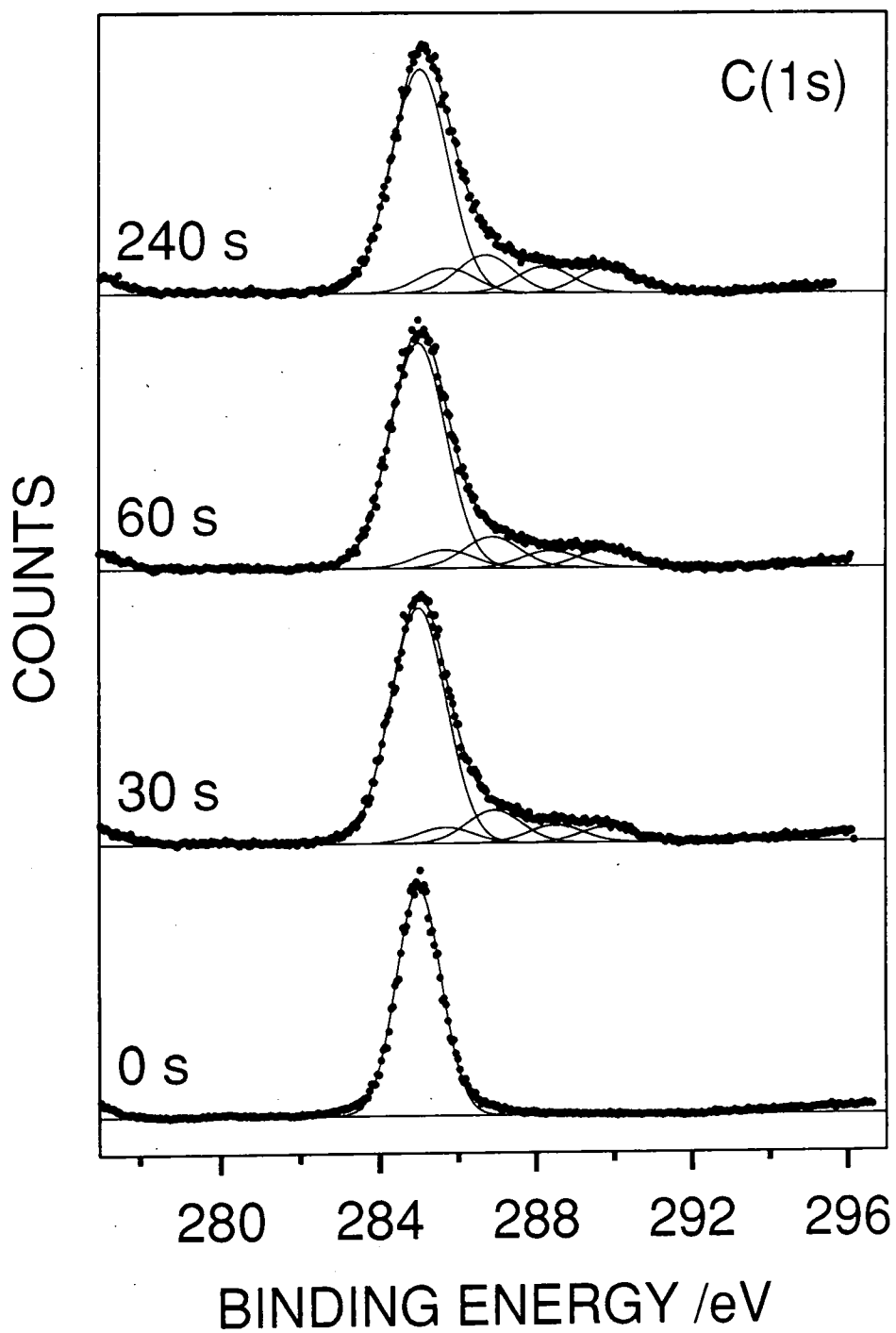
Figure 2(c):

Influence of oxygen plasma treatment time on relative concentration of oxidized carbon moieties ($\Sigma = 100\ \%$).
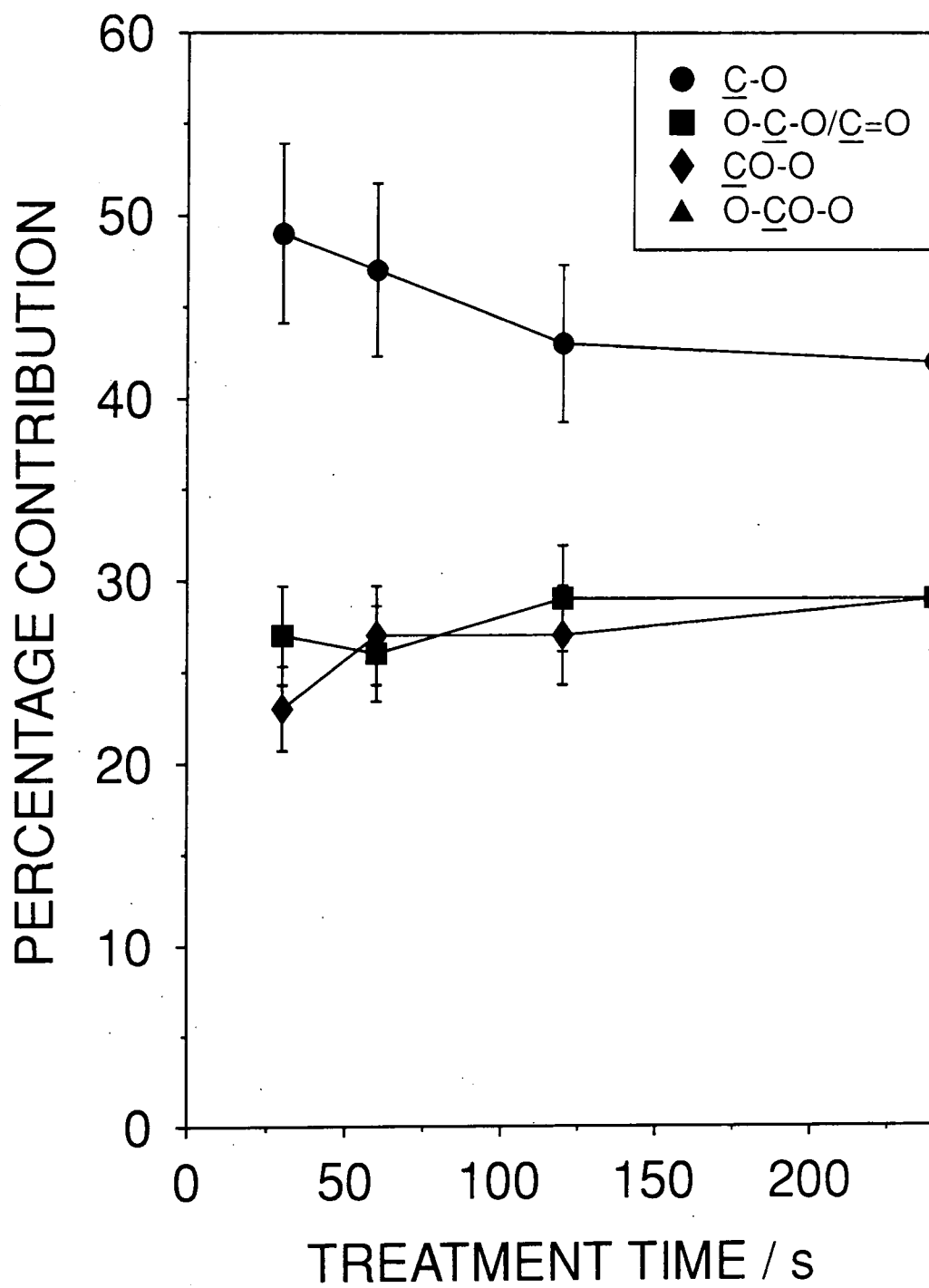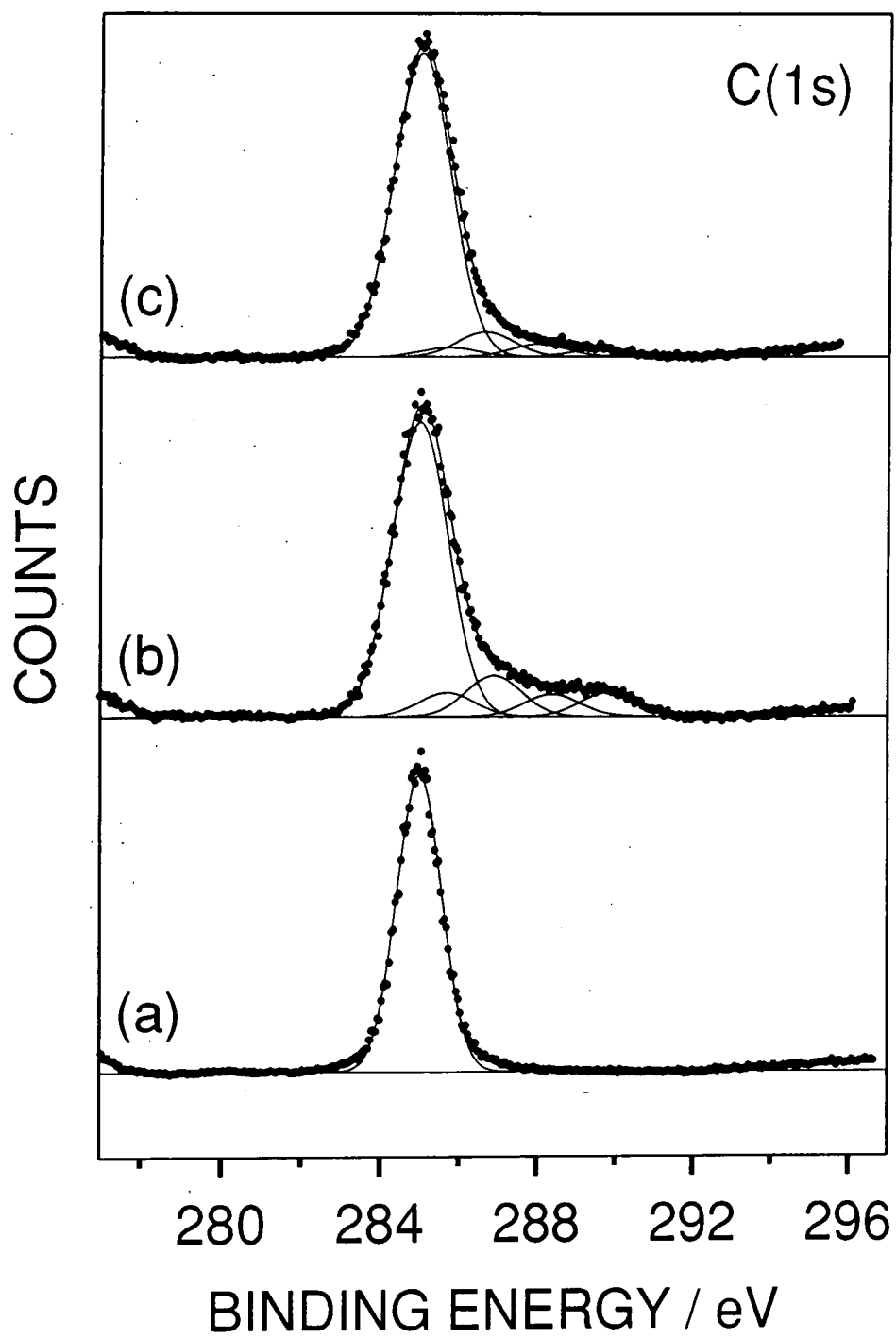
Figure 3:

C(1s) XPS spectra of polypropylene: (a) untreated; (b) 60 s oxygen plasma treated; and (c) oxygen plasma treated followed by washing.

2.3.2 Atomic Force Microscopy Results

The untreated biaxially oriented polypropylene and oxygen plasma treated polypropylene were scanned using AFM at two different resolutions. A low resolution 10 μm wide scan (Figure 4(a)) and a higher resolution 2 μm wide scan (Figure 4(b)). AFM analysis of untreated polymer shows evidence of two topographical features. The first are micro-fibrils of the polymer, which are more clearly seen in the 2 μm wide scan. These micro-fibrils of the polymer are formed during the film's manufacture. In the production of blown polypropylene film the biaxial orientation is achieved by first drawing the film into a tube. The fibrils are generally formed at this stage.[39] The film is then re-heated and then blown outward, causing the film to be oriented along the diameter of the bubble.[40] The fibrils are predominately oriented in the parallel to the drawing direction of the film, in which direction they are first formed. The fibrils are then seen to be pulled apart by the formation of the bubble. Polypropylene films prepared by this method tend to be highly crystalline,[41] however the AFM micrographs do not reveal any spherulitic structure (Figure 4); this suggests that the crystalline spherulites are situated beneath the surface of the polymer film, as reported previously.[42,43] Large scale features are seen which forms a curve across the scan approximately 0.25 μm high. This is in fact part of a much larger ring type structure on the surface of the polymer,[44] called 'haze rings', so called because in extreme cases they can make the film appear hazy or cloudy. These haze rings are caused by β-crystallites of polypropylene.[45] These β- crystallites are formed in the initial drawing process, and melt at a much lower temperature than α-crystallites. During the re-heating and orientation of the film, when the film is blown into a bubble causing the biaxial orientation of the film, the film's temperature is between the melting temperature of the α-crystallites and the β-crystallites, the β-crystallites melt and collapse forming the crater like features seen.

AFM analysis of the oxygen glow discharge plasma treated surface shows, at 10 μm wide scan (Figure 5(a)), that the larger topographical features on the sample surface, such as haze rings, remain intact after plasma treatment. The 10 μm wide scan also shows the presence of small circular features on the surface. The 2 μm wide scan (Figure 5(b)), however, shows that the plasma treatment effectively destroys the fine fibrillar structure seen on untreated polypropylene. This is contrary to previous electron

microscopy studies.[9] The original structure is replaced by small globular features. hundreds of nanometers in diameter.

AFM images of washed oxygen plasma treated polypropylene are shown in Figures 6(a) and 6(b). Washing reveals 30 roughly circular features, approximately 0.25 μm high, the tops of which are just visible in the images of unwashed oxygen plasma treated polypropylene, which are obviously obscured by the plasma modified polymer. Removal of the plasma modified material by washing reveals these insoluble particles. A curved ridge of these particles is seen at the bottom right of the image. The shape of this ridge indicates that it is likely to originate from a haze ring. The 2 μm wide scan reveals the small globular morphology seen with the unwashed sample. The globular size has slightly decreased on washing.

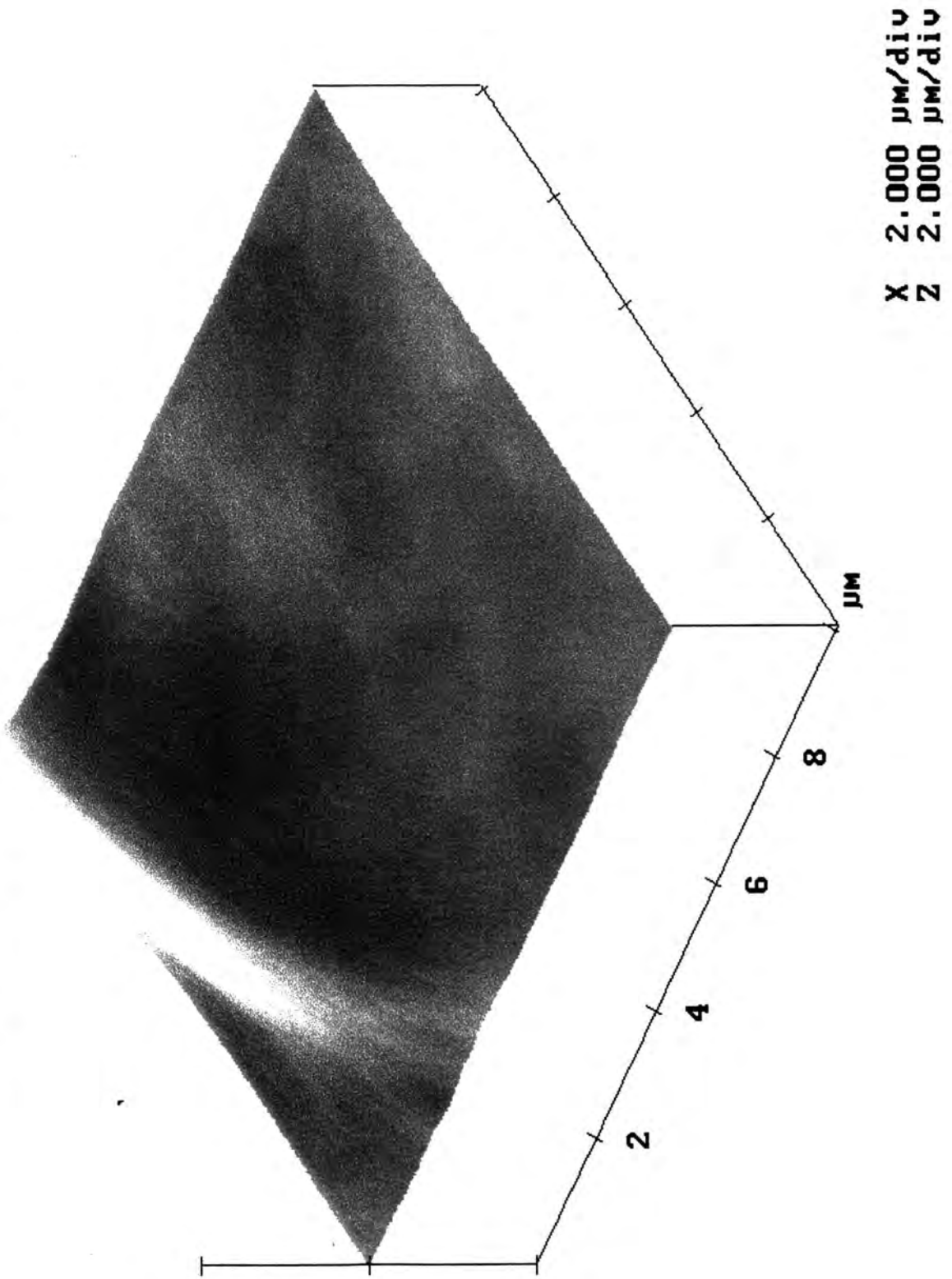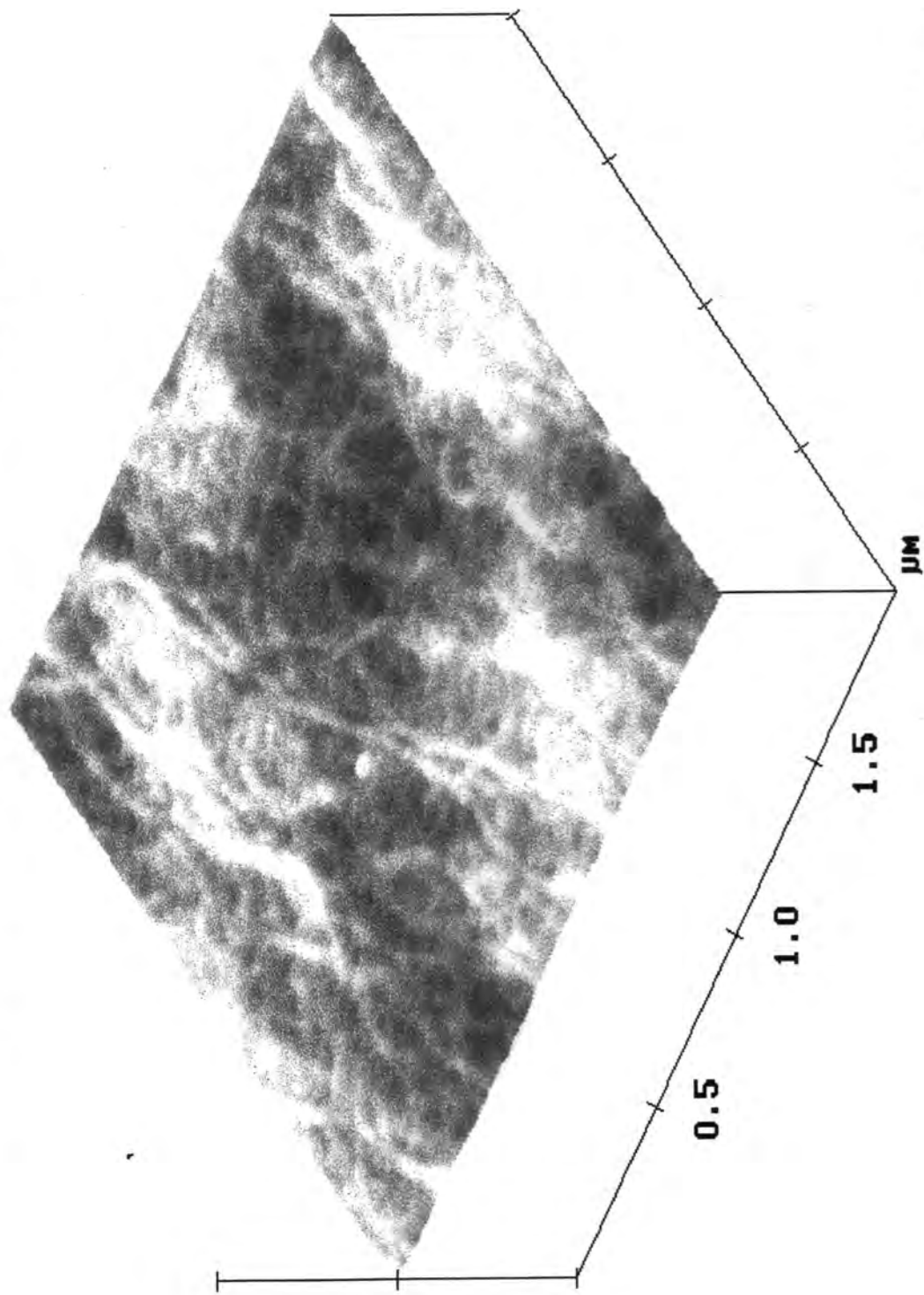Figure 4(a): 10 μm AFM image of untreated biaxial orientated polypropylene.

X 2.000 μm/div
Z 2.000 μm/div

57

Figure 4(b): 2 µm AFM image of untreated biaxial orientated polypropylene.

X   0.500 µm/div
Z   500.000 nm/div

µm

0.5   1.0   1.5

58

Figure 5(a): 10 µm AFM image of biaxial orientated polypropylene oxygen plasma treated for 60 s.

X 2.000 µm/div
Z 2.000 µm/div

59

Figure 5(b): 2 μm AFM image of biaxial orientated polypropylene oxygen plasma treated for 60 s.

μm

X   0.500 μm/div
Z   500.000 nm/div

60
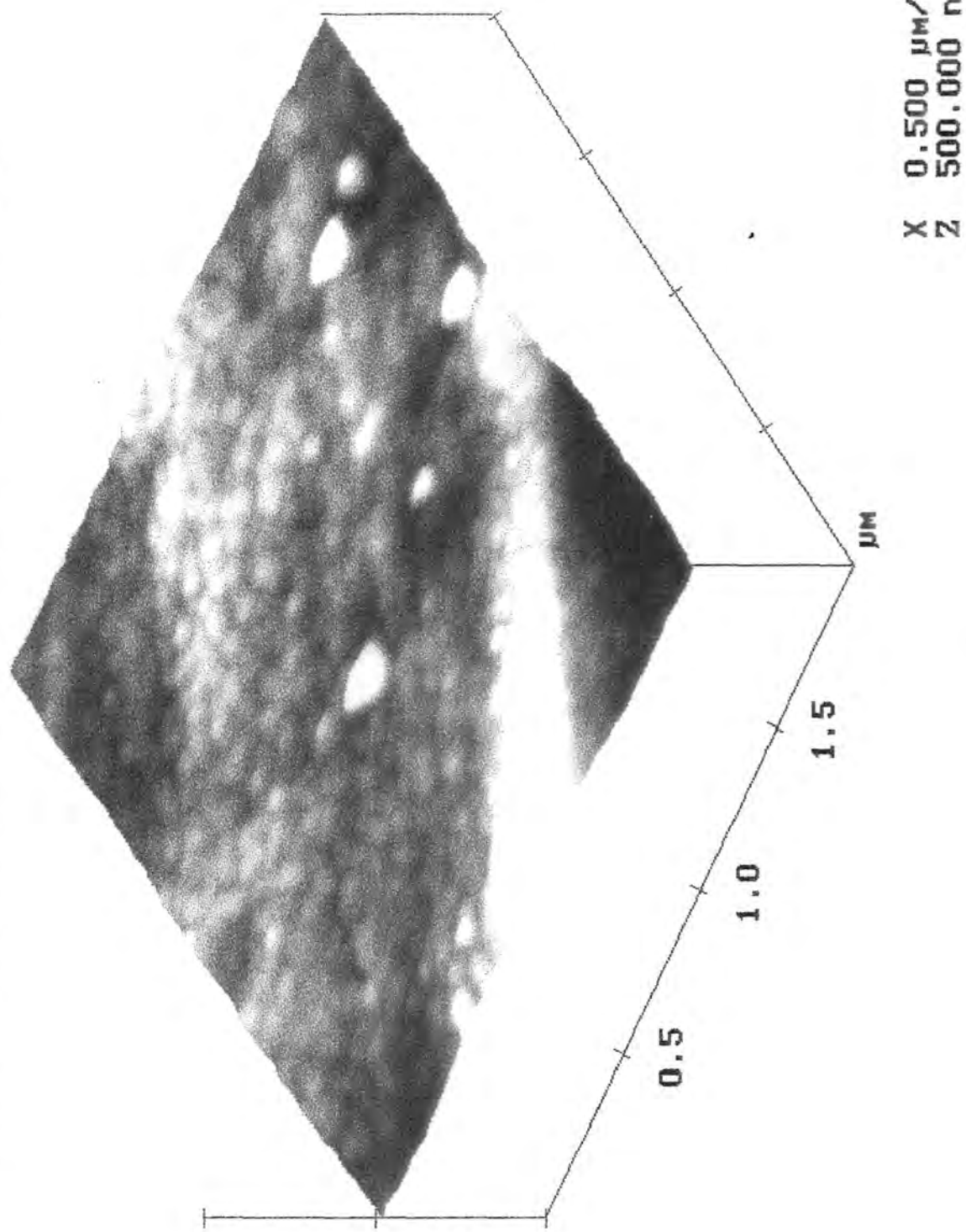
Figure 6(a) 10 μm AFM image of biaxial orientated polypropylene oxygen plasma treated for 60 s followed by solvent washing.

X   2.000 μM/div
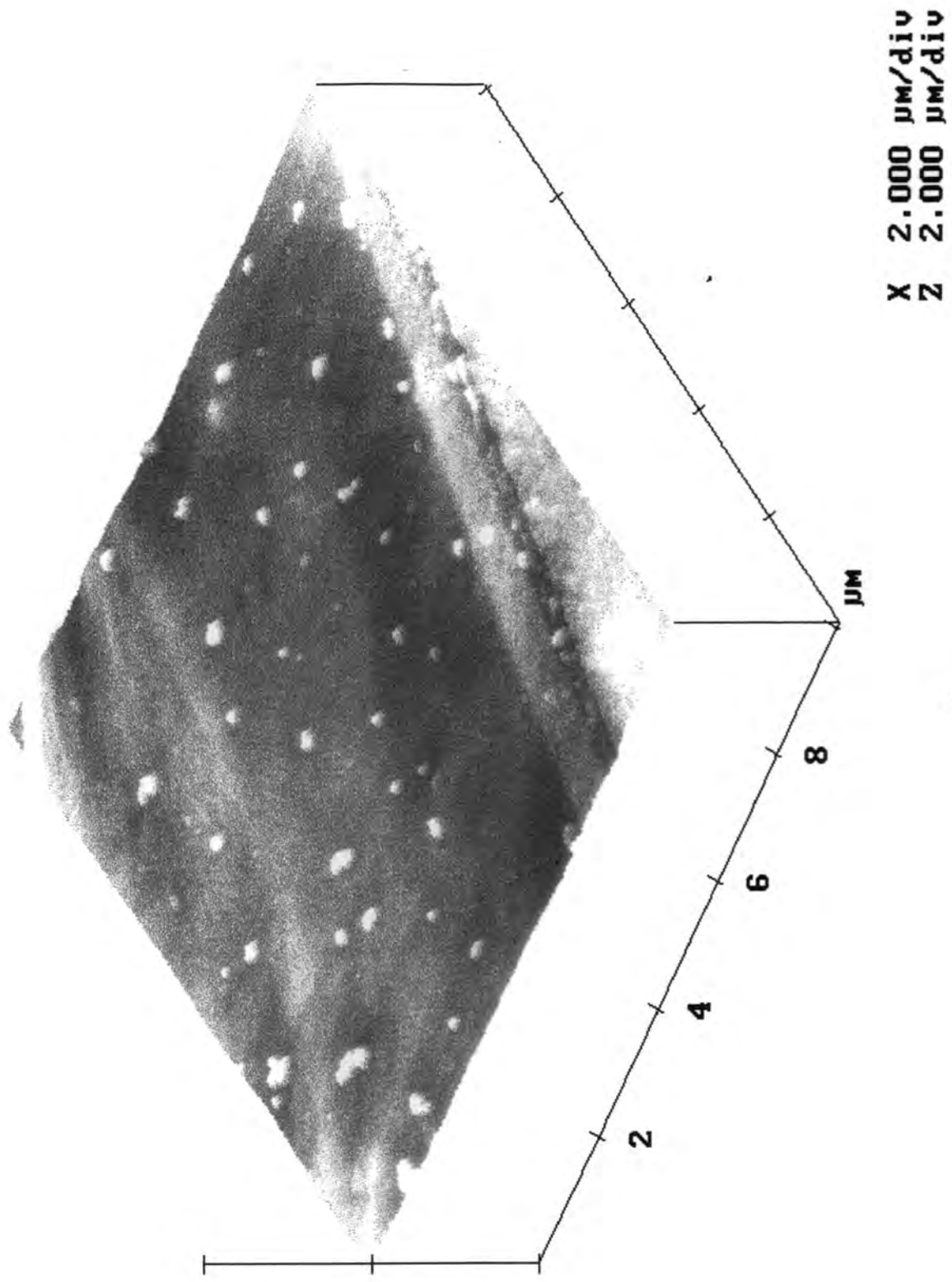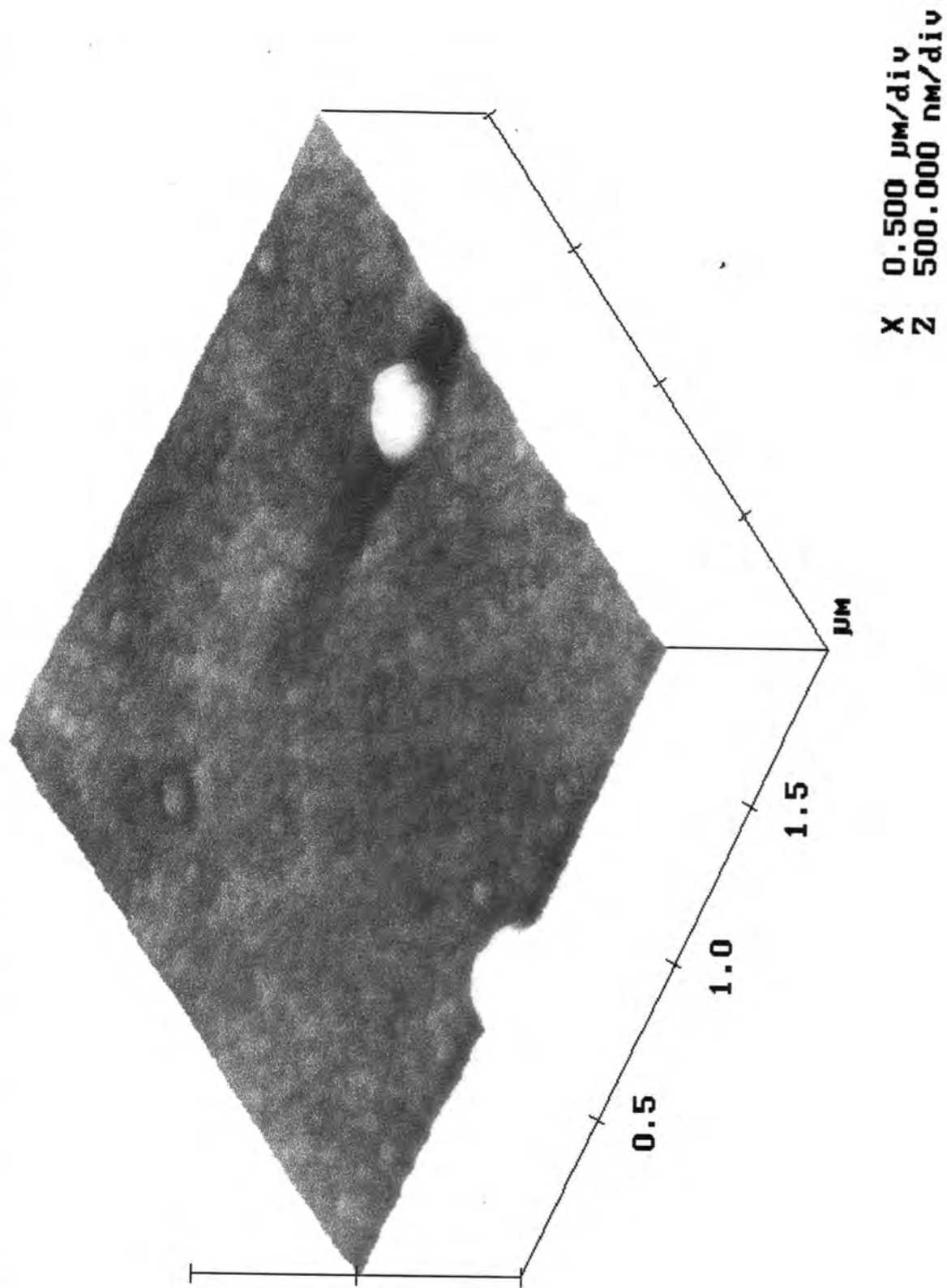Z   2.000 μM/div

61

Figure 6(b): 2 μm AFM image of biaxial orientated polypropylene oxygen plasma treated for 60 s followed by solvent washing.

X   0.500 μM/div
Z   500.000 nM/div

μM

0.5   1.0   1.5

62

2.4 DISCUSSION
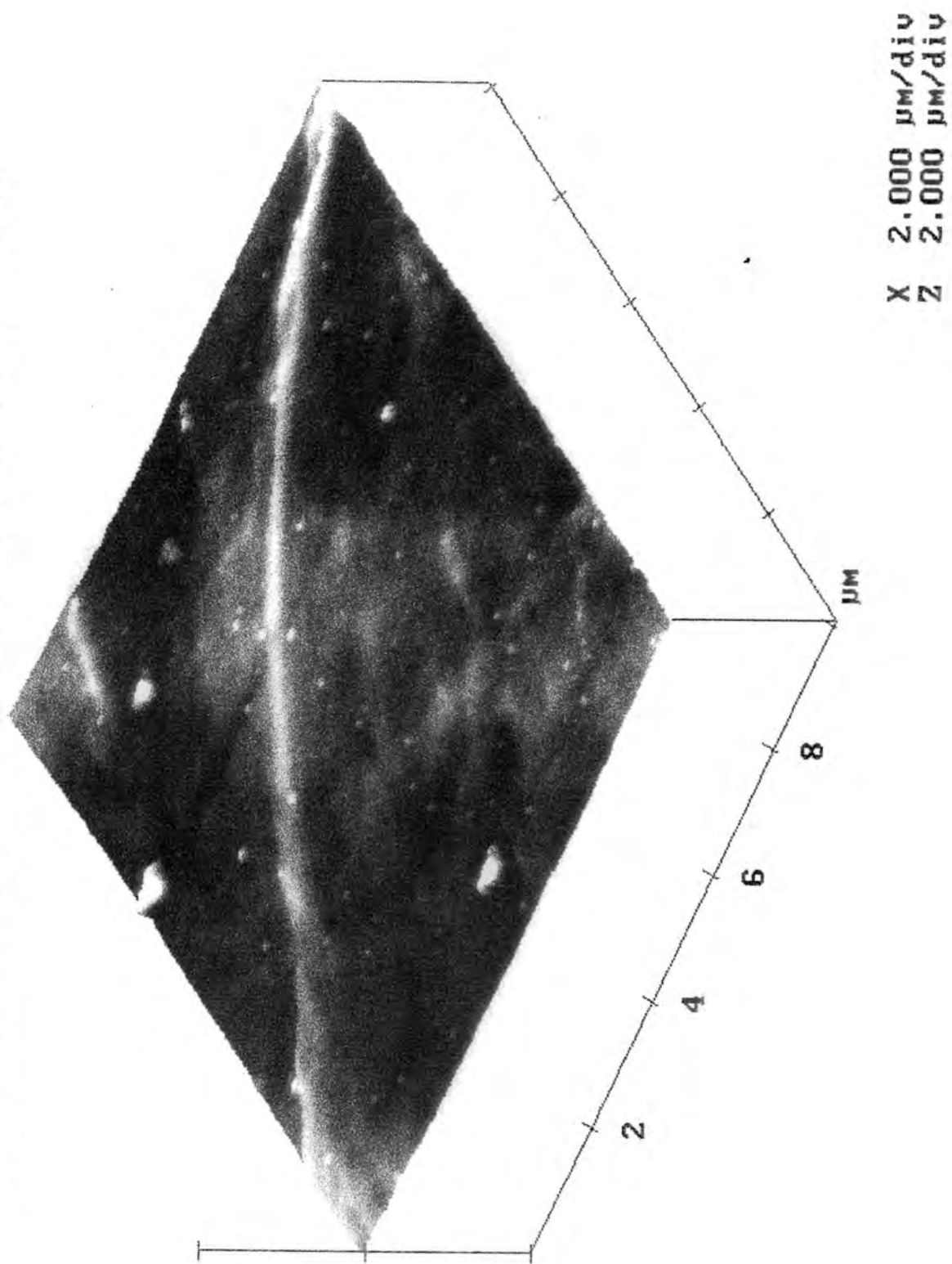
A oxygen plasma produces a large quantity of reactive species which can interact with a polymer surface. These include atomic oxygen, ions and VUV radiation, as discussed previously. These cause three main effects at the polymer surface; oxidation, chain scission and ablation. The almost complete saturation of surface oxidation by the plasma after 30 seconds of treatment indicates that an equilibrium is soon reached between the ablation from the surface of volatile material and the generation of new oxidized material. The dual effect of surface oxidation and chain scission generates a large amount of low molecular weight oxidized material (LMWOM),[46] which can then be removed from the surface by washing.[17] Due to the high amount of oxygen incorporated into the LMWOM, it tends to have a much higher surface energy than the untreated polymer. The LMWOM then will tend to conglomerate together into globules, rather than interacting with the untreated polymer, which is energetically unfavorable.

Washing of oxygen plasma treated polypropylene shows the presence of small globular features and not the original biaxial orientation. This indicates that a significant proportion of plasma modified material remains on the surface, as also shown by XPS analysis. This material is either oxidized material that is of too high molecular weight to be soluble or material that has been lightly oxidized, but its molecular weight has been modified by VUV component of the electrical glow discharge, since it is known that VUV radiation can penetrate into the sub-surface of polymers to cause chain scission and cross-linking.[43,47] Polypropylene is known to form spherulitic crystallites beneath the surface.[42] Crystallites of polymer are known to react at a lower rate than amorphous polymer,[48] Crystalline polymers are known to be more closely packed than amorphous polymer,[49] so that less material is exposed to the plasma. Washing of the plasma treated polymer reveals the core of the spherulitic crystallites, which remain unoxidised. Therefore the insoluble lumps seen with plasma treatment are likely to consist of the untreated core of spherulitic crystallites of the polymer.

2.5 CONCLUSIONS

Here we have examined both the chemical and physical effects of oxygen plasma treatment on the surface of polypropylene. It has been shown that oxygen plasma treatment causes surface oxidation and chain scission, producing low molecular weight oxidized material. This material conglomerates into small globular features on the surface and can be removed by washing. Crystallites of polypropylene react at a slower rate than amorphous polypropylene and core residues of crystalline polypropylene are seen after plasma treatment.

REFERENCES

1 . d'Agostino, R.; Cramarossa, F.; and Illuzzi, F. *J. Appl. Phys.* **1987,** *61,* 2754.

2 . Strobel, M.; Corn, S.; Lyons, C. S.; Korba, G. A. *J. Polym. Sci., Polym Chem. Ed.* **1985,** *23,* 1125.

3 . McCaulley, J. A.; Goldberg H. A. *J. Appl. Polym. Sci.* **1994,** *53,* 543.

4 . Hansen, R. H.; Pascale J. V.; DeBenedictics, T.; Rentzepis P. M. *J. Polym. Sci. A* **1965,** *3,* 2205.

5 . Morra, M.; Occhiello, E.; Garbassi, F. *Metallized Plastics* **1991,** *2,* 363.

6 . Strobel, J. M.; Strobel, M.; Lyons, C. S.; Dunatov, C.; Perron, S. J. *J. Adhesion. Sci. Techol* **1991,** *5,* 119.

7 . Hopkins, J.; Badyal, J. P. S. *J. Phys. Chem.* **1995,** 99, 4261.

8 . Shard, A. G.; Badyal, J. P. S. *J. Phys. Chem.* **1991,** 95, 9436.

9 . Occhiello, E.; Morra, M.; Morini, G.; Garbassi, F.; Humphrey, P.; *J. Appl. Polym. Sci* **1991,** *42,* 551.

10 . Adamson, A. W. *Physical Chemistry of Surfaces*; Wiley: New York, 1960.

11 . Strobel, M.; Dunatov, C.; Strobel, J. M.; Lyons, C. S.; Perron, S. J.; Morgen, M. C. J. *Adhesion. Sci. Techol.* **1989,** *3,* 321.

12 . Gerenser. L. J. *J. Adhesion. Sci. Technol.* **1987,** *1,* 303.

13 . Binnig, G.; Quate, C. F.; Gerber, Ch. *Phys. Rev. Lett.* **1986,** *56,* 930.

14 . Magonov, S. N.; Sheiko, S. S.; Deblieck, R. A. C.; Moller, M. *Macromolecules* **1993**, *26*, 1380.

15 . Snetivy, D.; Vancso, G. J. *Polymer* **1994**, *35*, 461.

16 . Jandt, K. D.; Buhk, M.; Miles, M. J.; Petermann, J. *Polymer* **1994**, *35*, 2458.

17 . Hopkins, J.; Boyd, R. D.; Badyal, J. P. S. *J. Phys. Chem.* **1996**, *100*, 6755.

18 . Greenwood, O. G.; Boyd, R. D.; Hopkins, J.; Badyal, J. P. S. *J. Adhesion. Sci. Technol.* **1995**, *9*, 311.

19 . Hopkins, J.; Badyal, J. P. S. *Macromolecules* **1994**, *27*, 5498.

20 . Bell, A. T. In *Techniques and Applications of Plasma Chemistry*; Hollahan, J. R.; Bell, A. T., Eds.; .Wiley: London, 1974; Chapter 1.

21 . Hopkins, J. Ph. D. Thesis, University of Durham, 1995.

22 . Hudis, M. In *Techniques and Applications of Plasma Chemistry*; Hollahan, J. R.; Bell, A. T., Eds.; .Wiley: London, 1974; Chapter 3.

23 . Hollander, A.; Klemberg-Sapieha, J. E. *Macromolecules*, **1994**, *27*, 2893.

24 . Adams, J. H. *J. Polym. Sci. A* **1970**, *8*, 1279.

25 . Carlsson, D. J.; Wiles, D. M. *Macromolecules* **1969**, *2*, 587, 597.

26 . uErshov; Yu. A.; Gale, Yu. V. *Izu. Aked. Nauk. SSSR Ser Khim.* **1967**, *4*, 778.

27 . Cain, S. R.; Egittio, F. D.; Emmi, F. *J. Vac. Sci. Technol.* **1987**, *A5*, 1578.

28 . Yasuda, H.; Lanage, C. E.; Sakaouka, K. *J. Appl. Polym. Sci.* **1973**, *17*, 137.

29 . Grill, A. In *Cold Plasma in Materials Fabrication*; IEEE: New York, 1993; Chapter 6.

30 . Clark, D. T.; Dilks, A.; Shuttleworth, D. In *Polymer Surfaces*; Clark, D. T.; Feast, W. J.; Eds. Wiley: Chichester, 1978; Chapter 9.

31 . Mayoux, C. J. *IEEE Trans. Elect. Insul.* **1976**, *11*, 139.

32 . Mayoux, C.; Antoniou, A.; Bui, A; Lacoste, R. *Europ. Polym. J.* **1973**, *9*, 1069.

33 . Yasuda, H. *Plasma Polymerization*; Academic: Orlando, Florida, 1985; Chapter 7.

34 . MacCallum, J. R.; Rankin, C. T. *Die Makromolek. Chemie* **1974**, *175*, 2477.

35 . Whitaker, A. F.; Jang, B. Z. *J. Appl. Polym. Sci.* **1993**, *48*, 1341.

36 . Zhong, Q.; Inniss, D.; Kjoller, K.; Elings, V. B. *Surf. Sci.* **1993**, *290*, L688.

37 . Evans, J. F.; Gibson, J.H.; Moulder, J. F.; Hammond, J. S.; Goretzki, H. *Fresenius Z. Anal. Chem.* **1984**, *319*, 841.

38 . Beamson, G.; Briggs, D. *High Resolution XPS of Organic Polymers. The Scienta ESCA300 Database*; Wiley: Chichester, 1992.

39 . Bottin, M. F.; Boudulle, M.; Gullet, J. *J. Polym. Sci., Polym. Phys. Ed.* **1983** *21*, 401.

40 . Savolainen, A. *Polym. Eng. Sci.* **1990**, *30*, 1258.

41 . Paulos, J. P.; Thomas E. L. *J. Appl. Polym. Sci.* **1980**, *25*, 15.

42 . Norton, D. R.; Keller A.; *Polymer* **1985**, *26*, 704.

43 . Aboulfaraj. M.; Ulrich, B.; Dahoun, A.; G'Sell. C. *Polymer* **1993**, *34*, 4817.

44 . Olley, R. H.; Bassett, D. C. *J. Macromol. Sci. Phys.* **1994**, *B 33*, 209.

45 . Fujiyama, M.; Kawamura, Y.; Wakino, T.; Okamoto, T. *J. Appl. Polym. Sci.* **1988**, *36*, 995.

46 . Garbassi, F.; Morra, M.; Occhiello, E.; Barino, L.; Scordamaglia, R.; *Surf. Interface Sci.* **1989**, *14*, 585.

47 . Clark, D. T.; Dilks, A. *J. Polym. Sci., Chem. Ed.* **1977**, *15*, 2321.

48 . Brennen, W. J.; Feast, W. J.; Munnon, H. S.; Walker, S. A. *Polymer* **1991**, *32*, 1527.

49 . Sharples, A. In *Polymer Science*; Jenkins, A. D., Ed.; North-Holland: Amsterdam. 1972; Vol. 1, Chapter 4.

CHAPTER 3:
ATMOSPHERIC SILENT DISCHARGE TREATMENT OF BIAXIALLY ORIENTED POLYPROPYLENE

3.1 INTRODUCTION

Although oxygen glow discharge treatment of polymers is growing as an industrial method of modifing polymer surfaces, it requires a low pressure system. This is very expensive and unattractive for industrial mass production applications.[1] An alternative to low pressure plasma treatment is to use an atmospheric non-equlbrium plasma, such as the dielectric barrier (silent) discharge and the corona discharge.[2] The chemical and physical properties of silent discharge treated polypropylene, analogous to chapter 2, will be studied to compare atomspheric and low pressure plasma treatment.

The chemical nature of plasma treated polymers has been extensively examined by surface sensitive analytical techniques (XPS, SSIMS, etc.). However, plasma modification can penetrate to several microns below the polymer surface,[3] and therefore the sampling depth of such surface sensitive techniques (which is typically of the order of nanometers)[4] may not necessarily be representative of the whole plasma modified layer. Here we combine XPS, SSIMS and solution state NMR analysis in order to attain a better insight into the chemical composition of the treated surface layer produced during atmospheric dielectric barrier (silent) discharge modification of biaxially oriented polypropylene.

The chemical effects of plasma treatment have long been known to be time dependant with the plasma effect diminishing with time after treatment.[5,6] The physical effects of ageing will also be studied here.

3.1.1 Background to the Modification of Polypropylene using the Silent Discharge.

The silent discharge reactor was invented over a hundred years ago[7] and both the physics and chemistry of the discharge have been widely studied. It has long been known that a silent discharge reactor operating in air will produce a large quantity of reactive
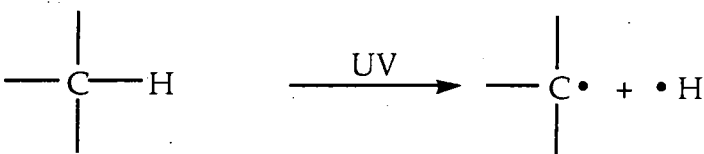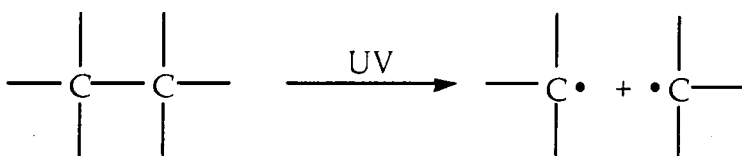
species including ozone, atomic oxygen, ultra violet radiation and electrons.[8,9] Ozone and ultra-voilet radiation are generated throughout the reactor, whilst electrons are restricted to microdischarges and a thin layer close to the dielectric polymers surface.[9] All of these species, when bombarding a polymer surface in air, led to surface activation and modification.

3.1.1.1 Surface Oxidation

The rate determining step for the oxidation of polymers is usually the initiation step. For ozone, ultra-violet radiation or electron activation this occurs by a free radical reaction. In the case of ozone bombardment activation occurs via a hydrogen abstraction reaction:[10]

$$-\overset{|}{\underset{|}{C}}-H \ + \ O_3 \quad \longrightarrow \quad -\overset{|}{\underset{|}{C}}\bullet + \ \bullet OH \ + O_2$$
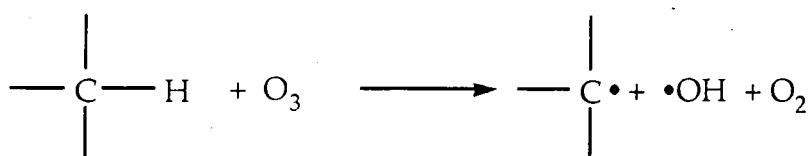
Electron and ultra-violet radiation both act in a similar way in cleaving either C-H or C-C bonds[11,12] leading to the formation of carbon radicals and chain scission.

$$-\overset{|}{\underset{|}{C}}-\overset{|}{\underset{|}{C}}- \quad \xrightarrow{\text{UV}} \quad -\overset{|}{\underset{|}{C}}\bullet \ + \ \bullet\overset{|}{\underset{|}{C}}-$$

$$-\overset{|}{\underset{|}{C}}-H \quad \xrightarrow{\text{UV}} \quad -\overset{|}{\underset{|}{C}}\bullet \ + \ \bullet H$$

The generated carbon radicals on the surface can then either react with molecular oxygen or ozone or decompose leading to chain scission. Reaction of carbon radicals with molecular oxygen then leads to the formation of a hydroperoxide group, which is unstable and either decomposes or reacts with another hydrocarbon group forming, in both cases, an alcohol radical:

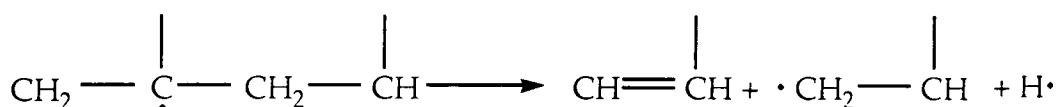$$-\overset{|}{\underset{|}{C}}-O\bullet$$
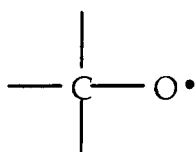
Reaction with ozone again leads to the formation of an alcohol radical and oxygen. The alcohol radical can either abstract a hydrogen from a nearby polymer chain or decompose

forming a ketone group and chain scission, via β-scission.[13] In both cases more carbon radicals are created which can react with molecular oxygen or ozone continuing the reaction ('auto-oxidation'). The generated alcohol and ketone groups can undergo further oxidation, by ozone or molecular oxygen, to form the more highly oxidised carbon species. Although atomic oxygen is generated within the silent discharge it very quickly recombines and reacts with oxygen to form ozone and does not significantly affect the modification of polymers.

3.1.1.2 Molecular Weight Changes

Electron and ultra-violet radiation bombardment can lead to chain scission directly along the polymer backbone.[14][15] However the formation of carbon radicals at the surface can also lead to chain scission along the polymer backbone. If the generated carbon radicals cannot combine with a molecule of oxygen or ozone then the radical will disproportionate forming a carbon-carbon double bond and a chain end radical:[16]

$$CH_2 \!-\! \overset{|}{\underset{\cdot}{C}} \!-\! CH_2 \!-\! \overset{|}{CH} \longrightarrow \quad \overset{|}{CH} \!=\! \overset{|}{CH} + \cdot CH_2 \!-\! \overset{|}{CH} + H\cdot$$

This chain end radical will undergo oxidation, abstract a hydrogen or decompose to form a carbon-carbon double and lose a hydrogen radical. However carbon-carbon double bonds are chemically active sites and chromphoric. The generation of these carbon-carbon double bonds will then increase the rate of activation and oxidation of the polymer.[11] If two carbon radicals are formed on different polymer chains but in the same region of space then the radicals can combine to form a cross-linking bond.[11] However it is much more probable that the carbon radical will react with oxygen or disportionartre before the second radical is formed.[17]

3.1.1.3 Low Molecular Weight Oxidised Material

There are two effects caused by the silent discharge plasma on the polymer surface. The first is the generation of oxygen containing carbon moieties, such as alcohol and ketone groups. The second is chain scission, leading to the decrease in the average molecular weight of the polymer at the surface. This dual effect leads to the formation of low molecular weight oxidised material (LMWOM) at the surface.[18][19] The high oxygen

content of LMWOM combined with its low molecular weight causes it to be, unlike the original polymer, soluble in most common solvents.

3.2 EXPERIMENTAL

3.2.1 Dielectric Barrier Discharge Treatments

Atmospheric silent discharge treatments were carried out using a home built parallel plate dielectric barrier discharge reactor operating at 3 kHz, 11 kV, with an electrode gap of 3.00 ± 0.05 mm, as shown in Figure 1. Small strips of biaxially oriented polypropylene film (ICI) were washed in a 50/50 mixture of isopropyl alcohol and cyclohexane and dried in air prior to electrical discharge treatment for times ranging from 1 to 300 s.

3.2.2 Sample Analysis

A Kratos ES300 electron spectrometer equipped with a MgKα X-ray source (1253.6 eV) and a concentric hemispherical analyser was used for XPS analysis, as described in chapter 2. Instrumentally determined sensitivity factors for unit stoichiometry of C(1s) : O(1s) were taken as equalling 1.00 : 0.62.

Solution state ^{1}H NMR spectroscopy was used to characterise the soluble component of the plasma modified polymer surface. Approximately 120 cm^2 of polypropylene film was exposed to the dielectric barrier discharge for 120 s in order to generate sufficient soluble material for NMR analysis. Next, the treated layer was extracted from the polypropylene substrate by washing in chloroform solution for a duration of 30 s. Then the chloroform solvent was allowed to evaporate and replenished with deuterated chloroform prior to analysis by solution state proton NMR spectroscopy on a Varian VXR-400s spectrometer.

TOFSIMS analysis was carried out with a Physical Electronics 7200 instrument.[20] The primary ion beam (8 keV Cs$^+$) with a spot size of ~ 50 μm^2 was rastered over an area of 100 x 100 μm keeping the total dose well under 10^{13} ions cm^{-2}

(static conditions). In addition to studying the treated film for comparison with XPS data, the material washed from the surface of a few cm^2 of this film was also studied, by deposition onto a substrate, for comparison with NMR data. The chloroform extract was sufficiently concentrated to deposit several monolayers onto silicon wafer (spin coating) or a submonolayer on nitric acid - etched silver foil in order to generate Ag+ cationized secondary ions.

A Digital Instruments Nanoscope III atomic force microscope was used to examine the topographical nature of the polypropylene surface prior to and after electrical discharge exposure. All of the AFM images were acquired in air using the Tapping mode, and are presented as unfiltered data.

Figure 1: Apparatus used for atmospheric silent discharge treatment of polymer films.

Insulation Box

High Voltage R.F. Supply

Height Adjuster

Dielectric Covering

Polymer Film

Earthed Electrode
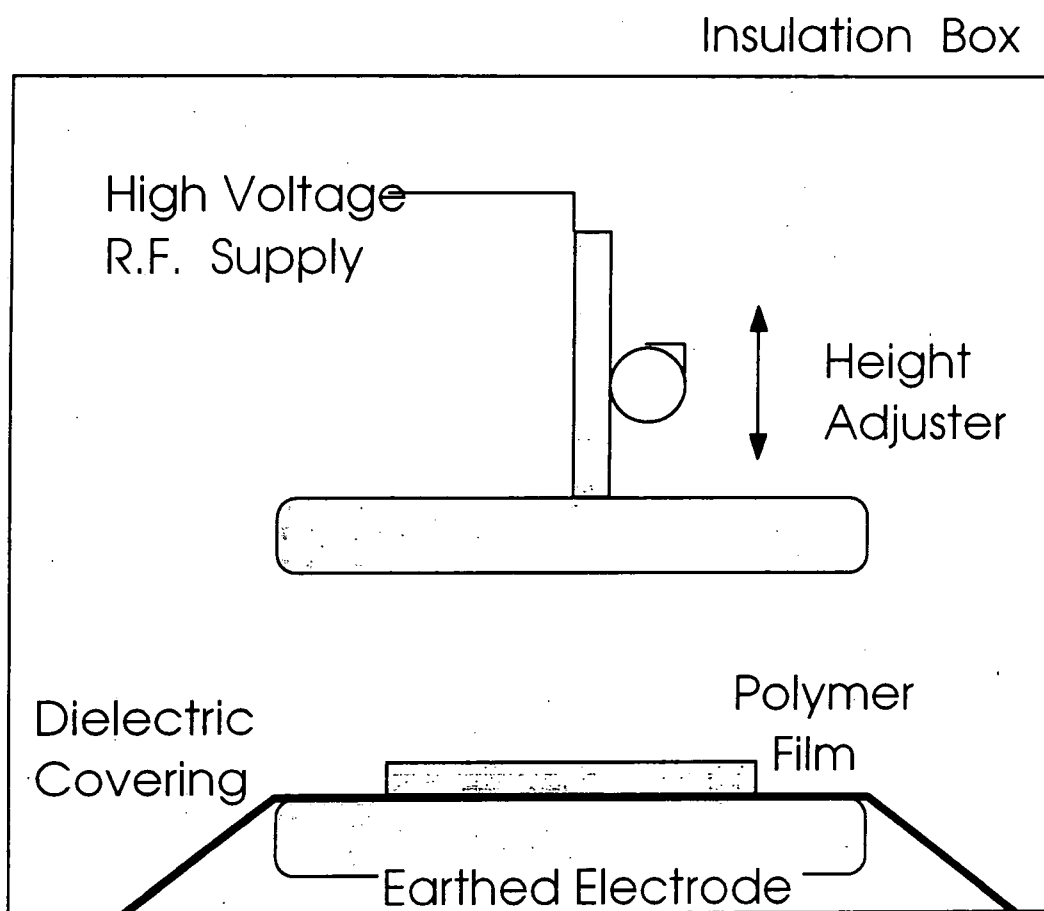
3.3 RESULTS

3.3.1 X-ray Photoelectron Spectroscopy

XPS was used to follow the rise in O/C ratio at the polymer surface with increasing silent discharge treatment duration, Figure 2(a). A gradual levelling off was evident after 120 s plasma exposure. C(1s) XPS spectra were fitted with Gaussian peaks of equal full width at half maximum (FWHM) as described in chapter 2, Figure 2(b). Untreated polymer exhibits a single C(1s) peak which corresponds to C_xH_y functionalities (i.e. -CH, -CH$_2$, and -CH$_3$ groups). Silent discharge modification led to the appearance of a shoulder at higher binding energies which was taken as being indicative of the build-up of oxygenated carbon centres, this is consistent with the observed variation in O/C ratio. The relative concentration of the >$\underline{C}$-O- component passes through a maximum following 30 s treatment, Figure 2(c); the subsequent fall in intensity can be attributed to >$\underline{C}$-O- groups undergoing further oxidation following the initial stages of reaction to form the more highly oxidised species.[21]

Washing a 30 s silent discharge treated polypropylene sample for 5 s in a 50/50 mixture of isopropyl alcohol / cyclohexane resulted in a drop in the O/C ratio from 0.31 $\pm$ 0.03 to 0.09 $\pm$ 0.01, Figure 3, thereby showing that a large proportion of the modified polymer is weakly bound to the surface. However, it is interesting to note that the relative distribution amongst the oxidised moieties does not differ significantly between the washed and unwashed plasma treated samples, Table 1.

Ageing studies showed that the oxidised layer gradually disappears with time. This is evident from the fall in O/C ratio and the corresponding attenuation of the high binding energy shoulder in the C(1s) envelope with ageing time, Figure 4. Carbonate species are lost from the surface at a much faster rate in comparison to the other types of oxidised carbon functionalities.

Figure 2(a):

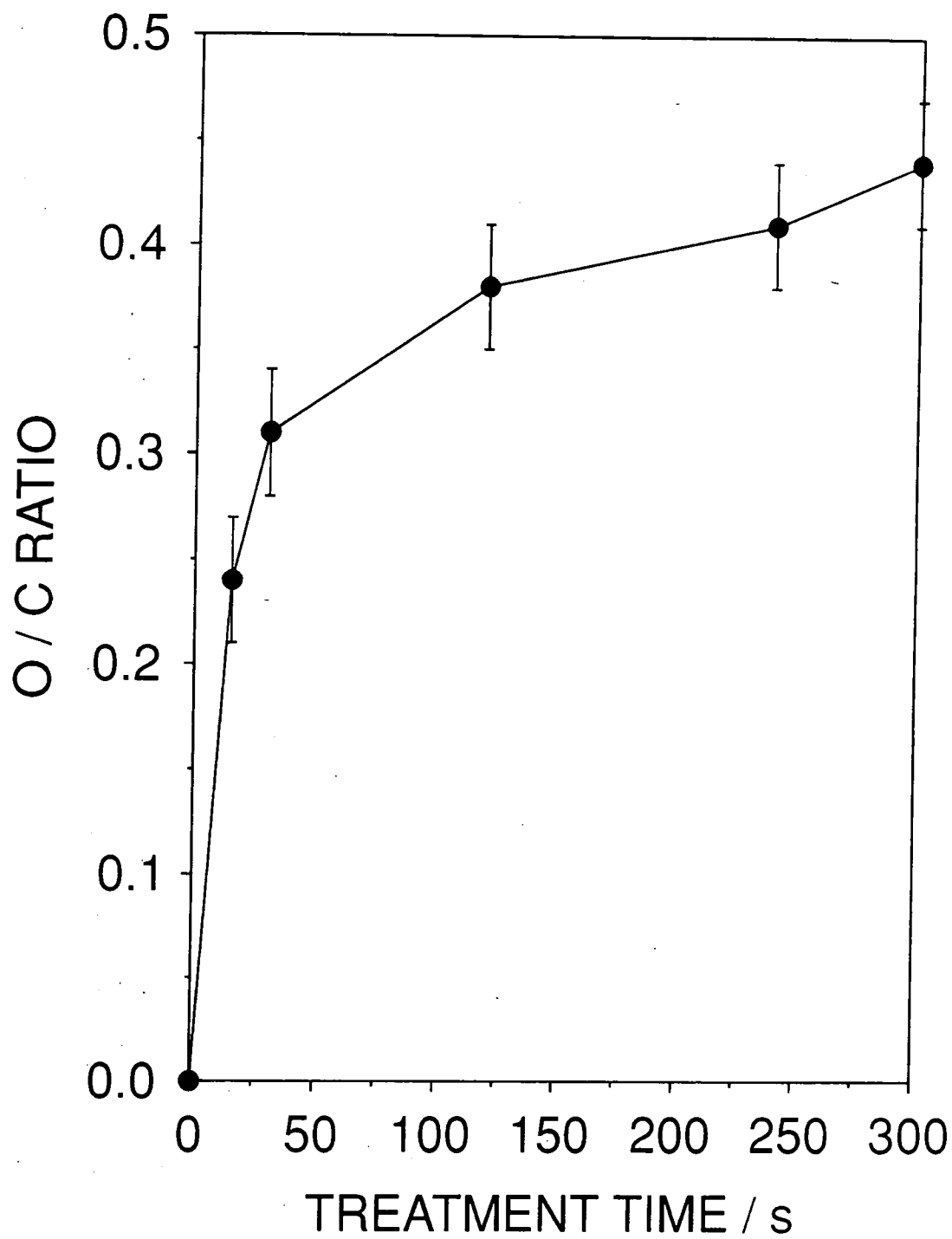Influence of silent discharge treatment time upon O/C ratio of polypropylene.

Figure 2(b):

Influence of silent discharge treatment time upon C(1s) spectra for polypropylene.
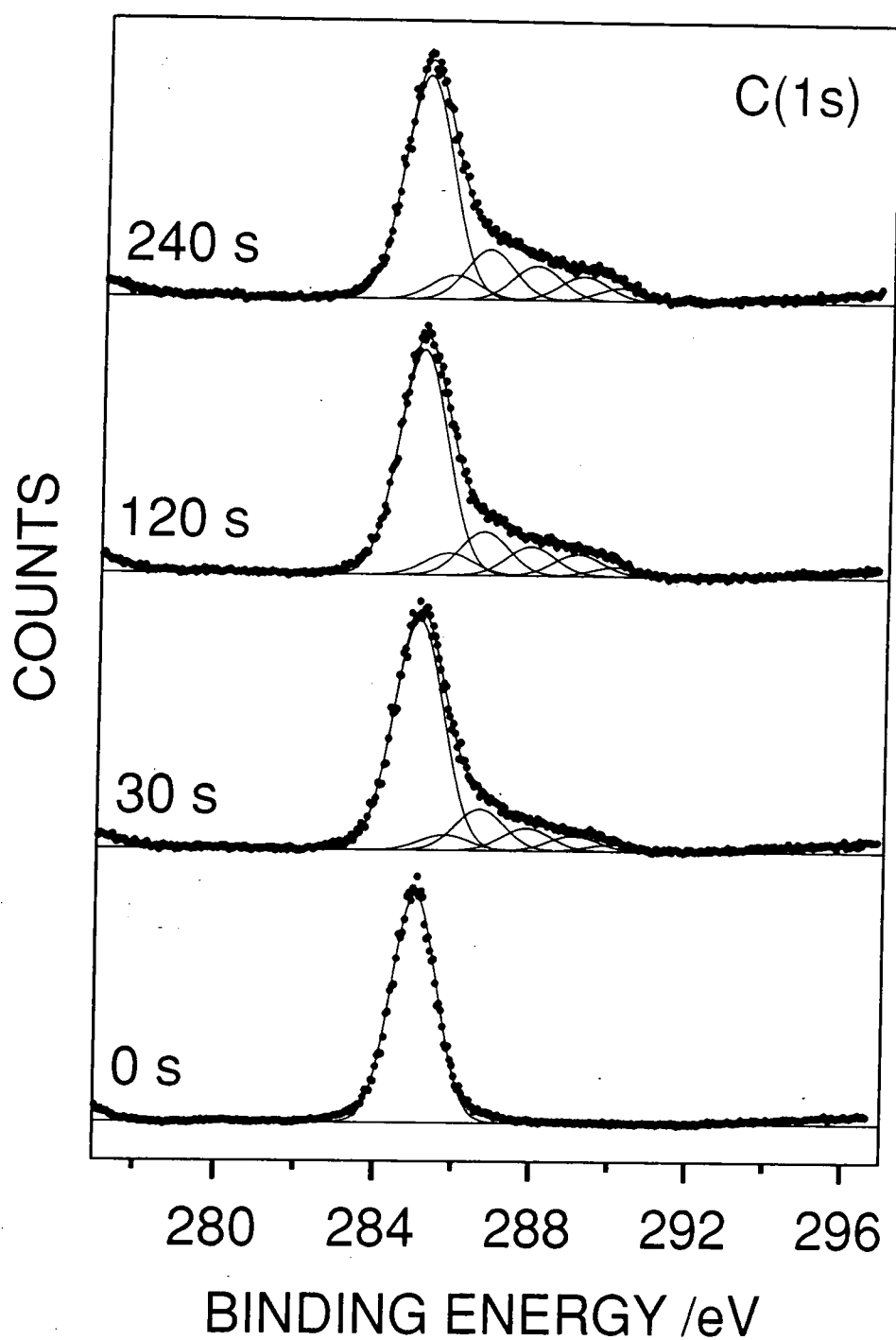
Figure 2(c):

Influence of silent discahrge treatment time upon the relative concentration of oxidised carbon moieties ($\Sigma = 100$ %)
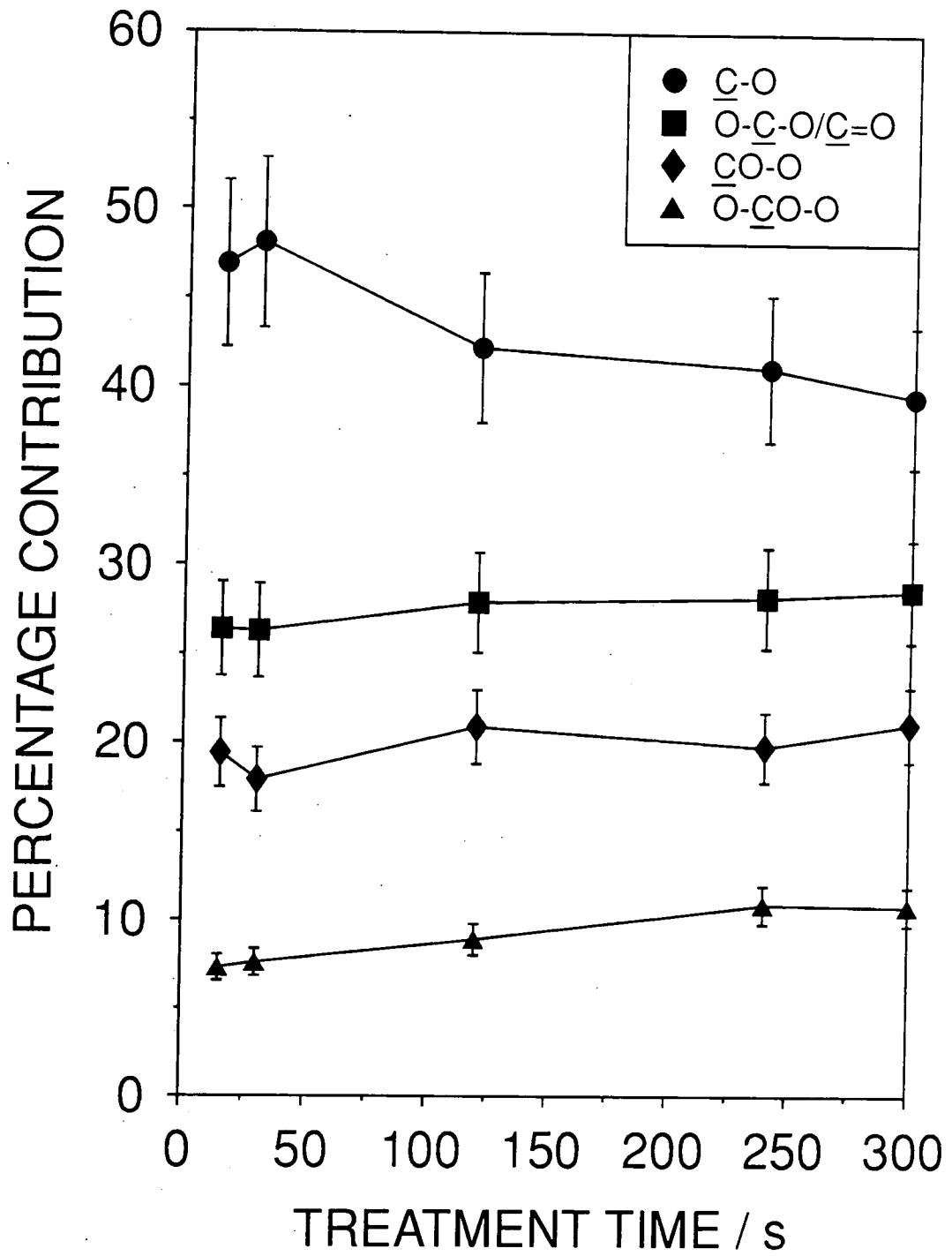
Figure 3:

C(1s) XPS spectra of polypropylene: (a) untreated; (b) 30 s silent discharge treatment; and (c) silent discharge treatment followed by solvent washing.
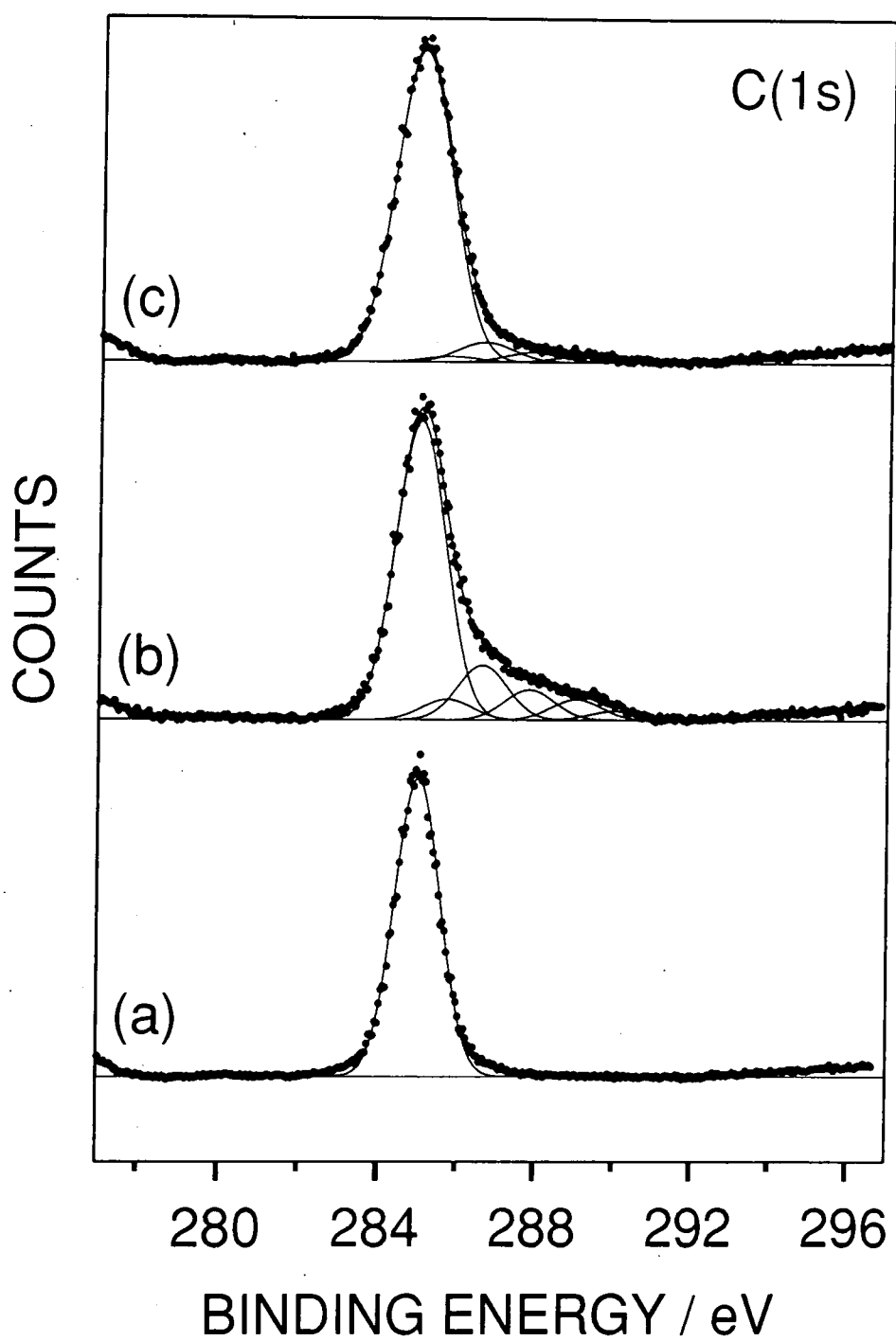
Figure 4(a):

Influence of ageing time upon O/C ratio of polypropylene.
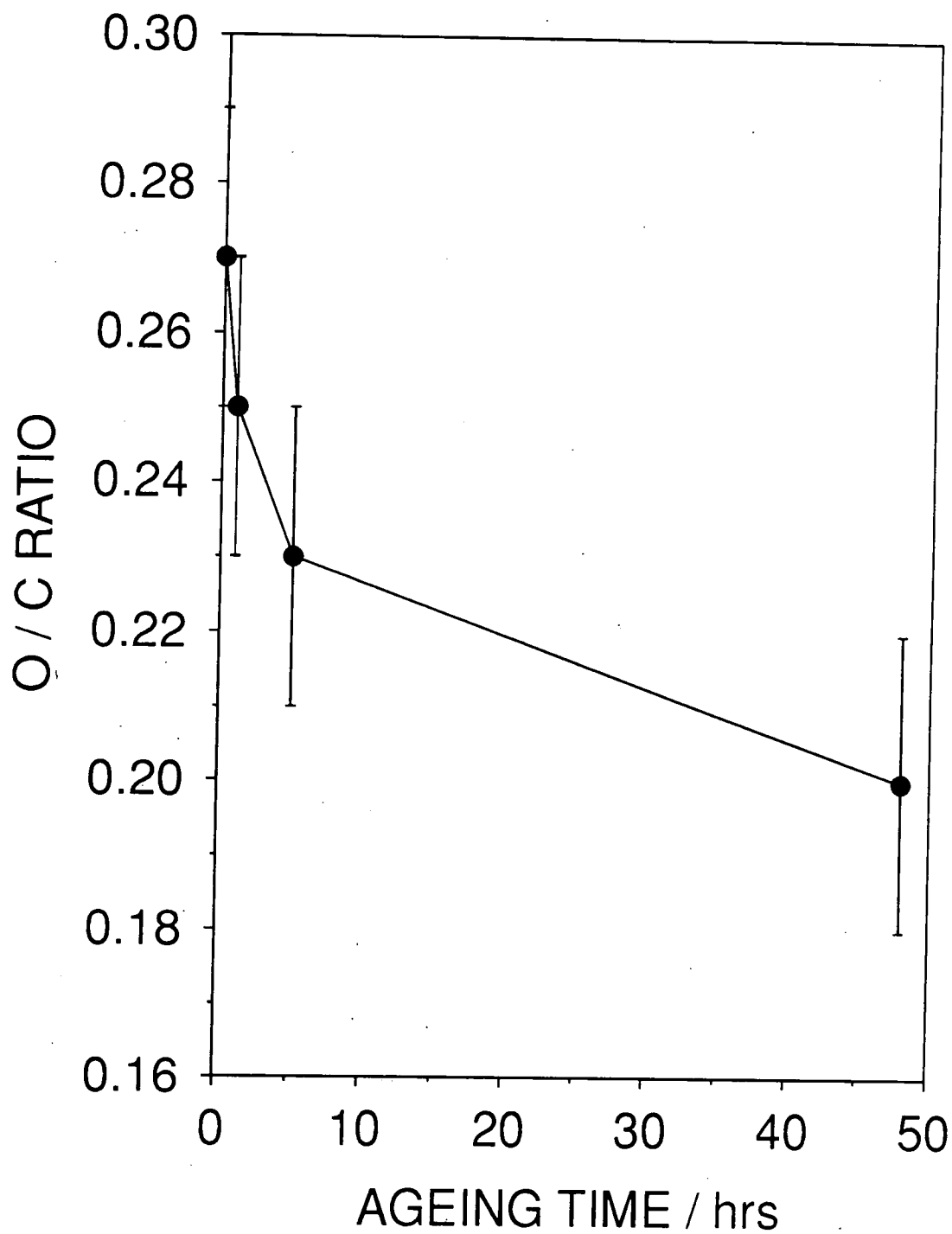
Figure 4(b):

Influence of ageing time upon C(1s) spectra for polypropylene.
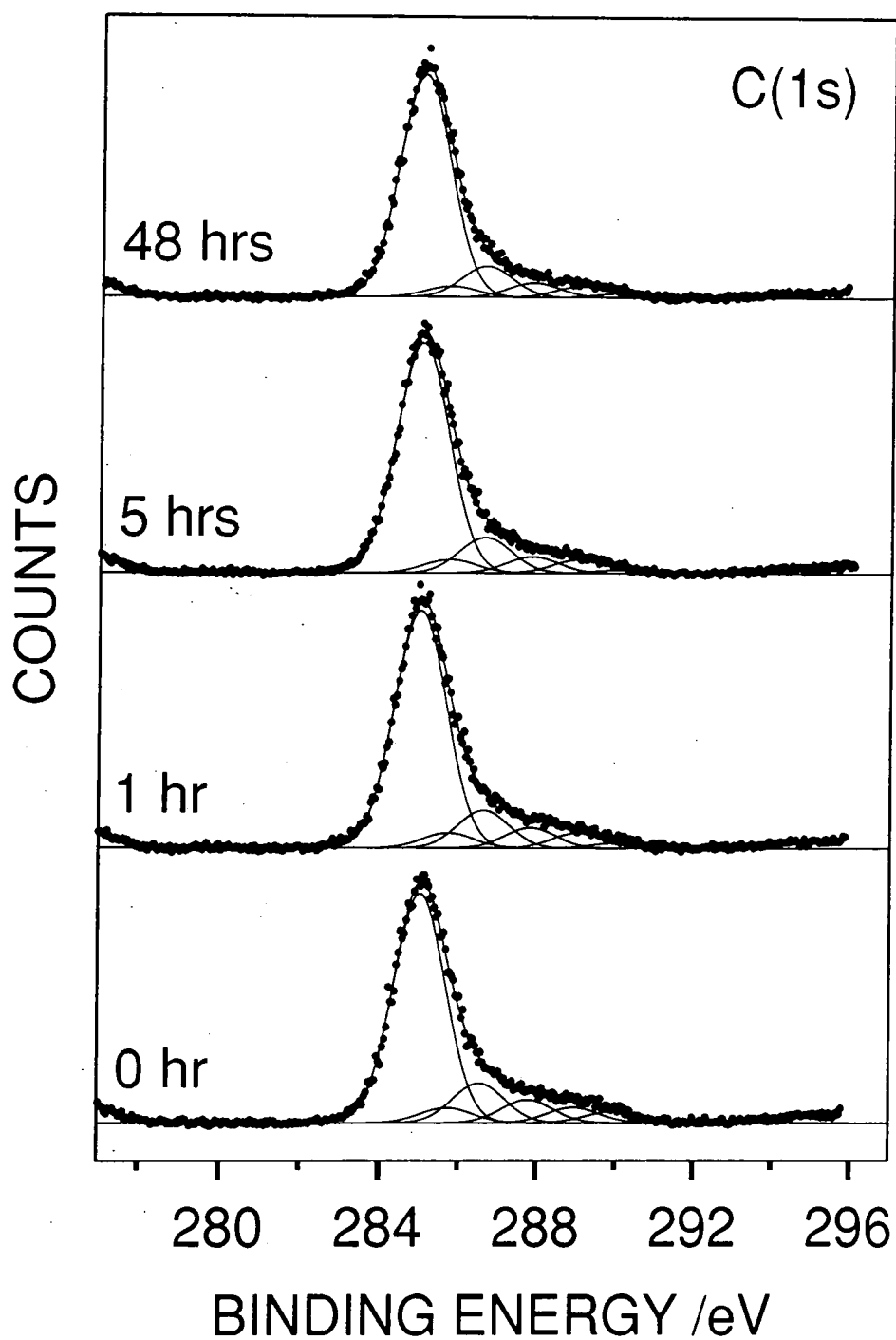
Figure 4(c):

Influence of ageing time upon the relative concentration of oxidised carbon moieties (Σ = 100 %).
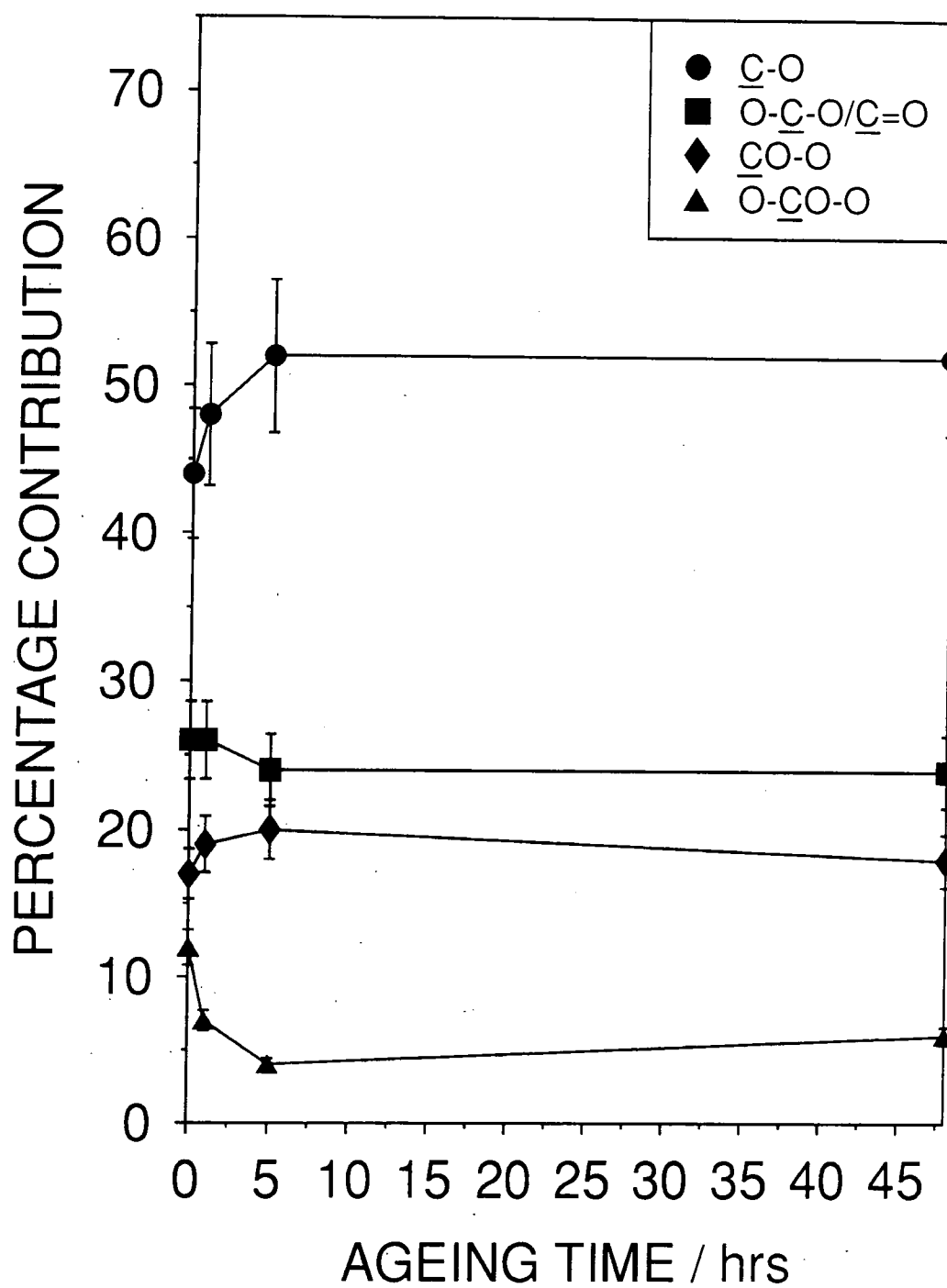
Table 1: The relative peak intensities of the oxidised carbon peaks ($\Sigma = 100\%$) for unwashed and washed 30 s silent discharge treated polypropylene.

Sample	$\underline{C}$-O	O-$\underline{C}$-O / $\underline{C}$=O	$\underline{C}$O-O	-O-$\underline{C}$O-O-
Unwashed	48 ± 3	26 ± 2	18 ± 2	8 ± 1
Washed	53 ± 3	26 ± 2	15 ± 2	6 ± 1

3.3.2 Solution State ^{1}H NMR

Solution state ^{1}H NMR spectra were taken of the species washed off with chloroform from both untreated and silent discharge treated polypropylene, Figure 5. A small amount of residual non-deuterated chloroform is evident in the recorded spectra at 7.3 ppm, this being typical of commercially available deuterated chloroform solvent.[22]

The NMR spectrum of the washed off species from untreated polypropylene consists of two sets of peaks. The first group covers a broad range from 0.8 ppm to 1.3 ppm and corresponds to protons attached to -CH$_3$, -CH$_2$, and -CH groups primarily from washed out atactic polypropylene.[23] This is not too surprising, since during the industrial manufacture of biaxially oriented blown polypropylene film, the majority of polymer is present in the isotactic state with a small amount in the atactic form (98 % isotactic, 2% atactic for the polymer used). Atactic polypropylene produced in this way tends to have a lower molecular weight and does not crystallise (i.e. it is located in the amorphous (more mobile) regions of the film), hence it is much more soluble compared to its isotactic counterpart, i.e. the former can be washed out with chloroform despite being present in very low concentrations. The sharp peak at 1.6 ppm is characteristic of water residue present in the chloroform solvent. The second set of ^{1}H NMR peaks comprises two weak groupings at 6.7 and 7.1 ppm which correspond to protons bonded to vinylic or aromatic carbons.[24] These are most likely to originate from trace amounts of antioxidants added to the polypropylene film during manufacture.[25] The intensity of the antioxidant features is small compared to those from the atactic polypropylene, thereby suggesting that the majority of the washed out species must be atactic polypropylene.

Solution state ^{1}H NMR analysis of the chloroform wash taken from silent discharge treated polypropylene shows that the distribution of peaks in the 0.6 to 1.3 ppm region has changed, this is most likely due to some isotactic polymer containing species also being removed,[26] which leads to an overlap with the previously observed atactic features. The water peak at 1.6 ppm has become much broader as a result of hydrogen bonding between the water and washed off low molecular weight oxidised material (LMWOM). In addition, a broad feature is discernible between 1.8 ppm to 2.4 ppm, this can be attributed to H atoms bonded to an sp^3 carbon centre adjacent to an oxygen atom (i.e. alcohols, ethers, esters, etc.).

Figure 5:

Solution state proton NMR spectra of: (a) washed species from untreated polypropylene:
and (b) washed species from 120 s silent discharge treated polypropylene.
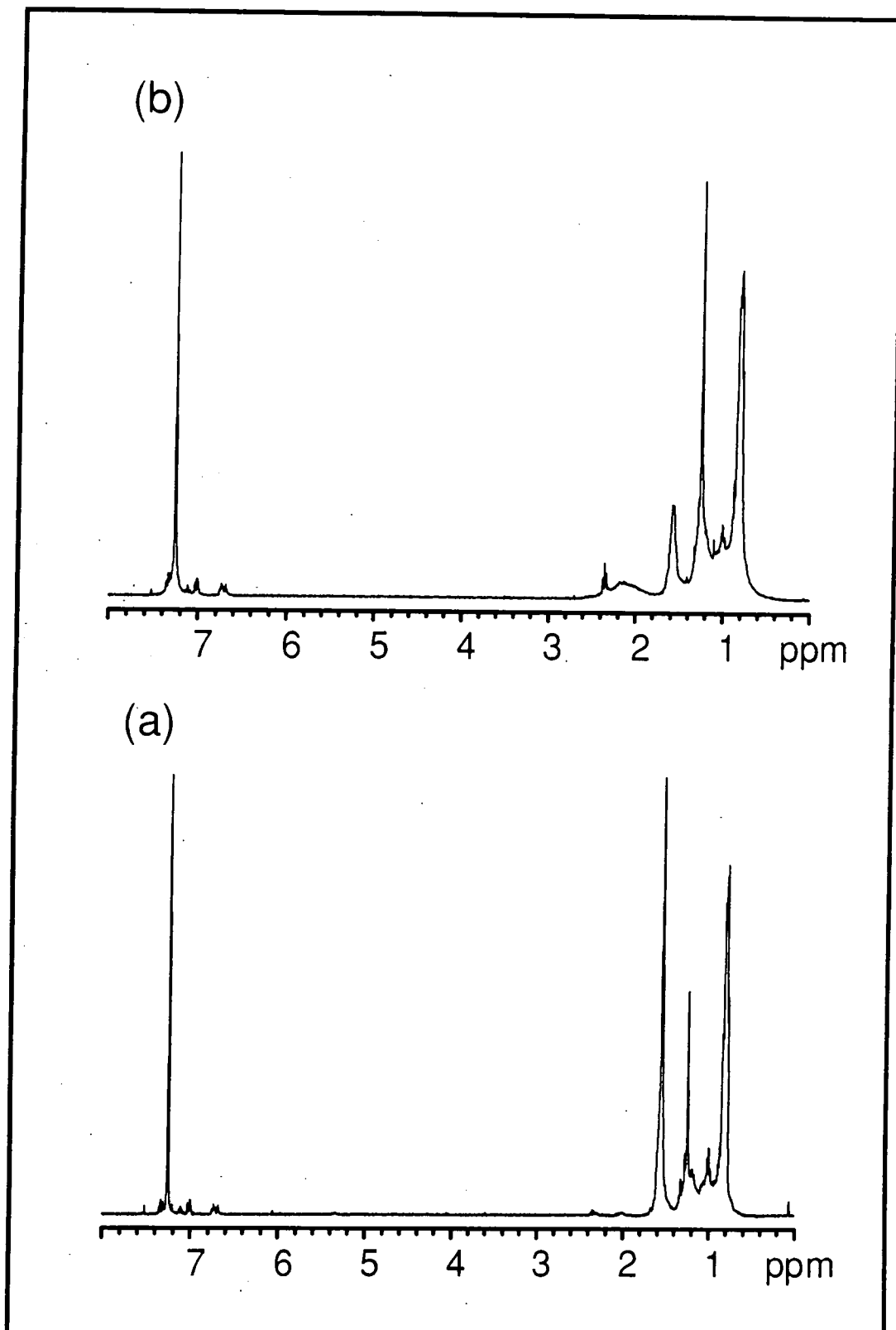
3.3.3 TOF-SIMS

The positive ion survey scan of the treated film, Figure 6, is at first sight relatively unchanged with respect to that expected from the untreated polypropylene.[27] However, closer inspection of the peaks at any nominal mass reveals oxygenated fragments in addition to the original hydrocarbon ($C_xH_y^+$) only peaks. Some examples are shown in Figure 7. The peak at m/z 113 is not a feature of the polypropylene spectrum, consistent with all the components being due to oxygen containing fragment ions. The peak assignments are from exact mass measurement and are within ~ 20 ppm of the calculated masses.

An even more striking change is seen in the negative ion spectrum, Figure 8. The untreated surface gives only C_1^- and C_2^- clusters (m/z 12-14 and 24-26 respectively). The expected atomic peaks due to O^-/OH^- (m/z 16, 17) are accompanied by NO_2^- and NO_3^- (m/z 46, 62) and an extensive series of fragment clusters extending up to nearly m/z 500. These are all ions with the general structure $C_xH_yO_z^-$. Some examples are given in Figure 9 for the mass range m/z < 100. At higher masses the pattern of peaks in the clusters repeating every 14 amu (CH_2) is very similar, Figure 8(b). One representative set is shown in Figure 10. Within this set there are fragments with the generic formulae $C_6O_5H_n^-$, $C_7O_4H_n^-$, $C_8O_3H_n^-$ and possibly $C_5O_6H_n^-$ and $C_9O_2H_n^-$ (weaker components). Because of the greater degree of components overlapping at higher mass the assignment of the weaker components becomes increasingly uncertain. Overall, the SIMS spectra from the treated surface confirm the very high O/C ratio seen in XPS. It is interesting to note that the negative ion spectrum contains unambiguous contributions from CO_3^- and HCO_3^- (m/z 60, 61). This helps to confirm the assignment of the higher binding energy C(1s) component.

All the prominent peaks in the spectra from the extract deposited on silicon corresponded to those from polypropylene the antioxidant Irganox 1076.[27] In contrast to the spectra from the treated polymer surface, $C_xH_yO_2^\pm$ peaks were very weak.

For the submonolayer of the extract on silver, three sets of peaks were observed: those characteristic of the etched silver substrate; those due to cationized Irganox 1076;

and an envelope of peaks between ~m/z 500-1400, Figure 11. Again each cluster pattern repeats at intervals of mass equal to that of CH_2 and the two most prominent components are separated by a mass equal to ^{109}Ag - ^{107}Ag. These peaks can be assigned the generic formula $(CH_2)_nOAg^+$ on the basis of accurate mass measurement (the presence of the antioxidant $[M+Ag]^+$ peaks at m/z 637, 639 was helpful in this respect). The envelope may therefore be due to functionalised low molecular weight material resulting from oxidative chain scission of the polypropylene backbone. The highest mass clusters observed correspond to chains involving up to 100 carbon atoms. Such long hydrocarbon chains functionalised with one oxygen atom are consistent with the observations made by XPS and NMR analysis.

3.3.4 Atomic Force Microscopy

There is a clear difference in topographical appearance between the untreated and silent discharge treated polypropylene surfaces. The fibrillar structure of biaxially oriented polypropylene is lost and replaced by large globular type features (0.5 - 1.0 μm in diameter), these increase in size with longer treatment times, Figure 12. Washing the silent discharge treated polypropylene film in a 50/50 mixture of isopropyl alcohol and cyclohexane causes the disappearance of the globular features, which is consistent with the droplets being soluble. However, the washed samples do not display the biaxial features seen previously for the untreated polymer; instead much smaller globular features are evident with diameters of just a few hundred nanometers.

Ageing studies of the dielectric barrier treated polypropylene surfaces showed a gradual shrinking of the globular material with time, Figure 13.

Figure 6:

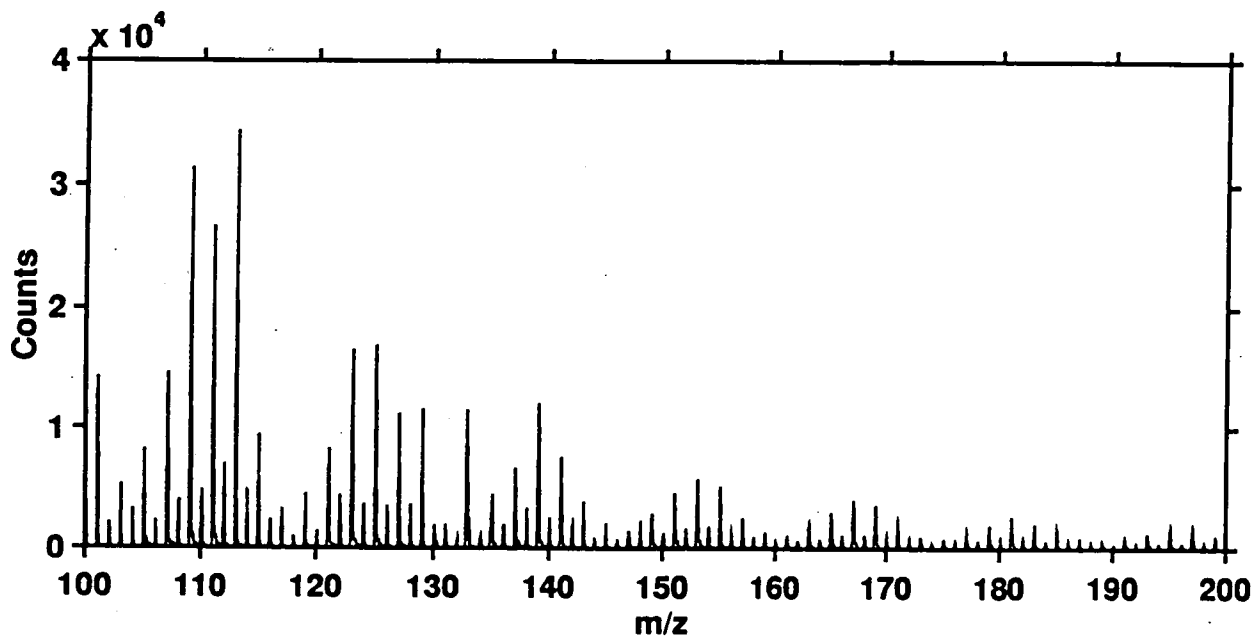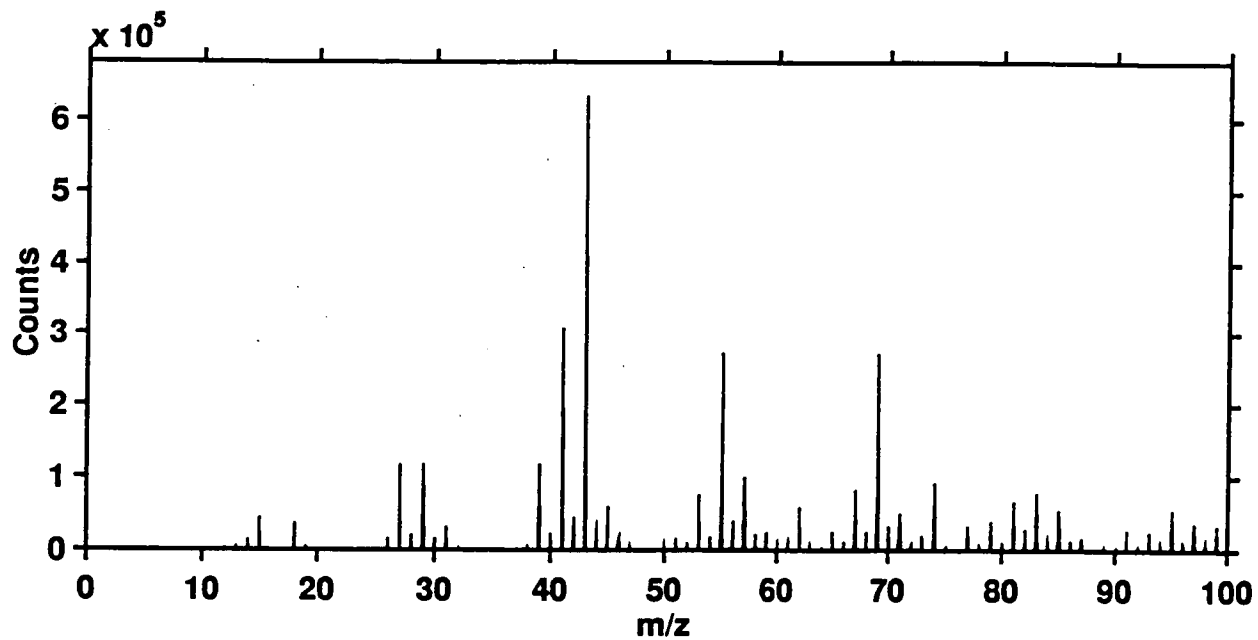Positive TOFSIMS of polypropylene silent discharge treated for 30 s.

Figure 7:

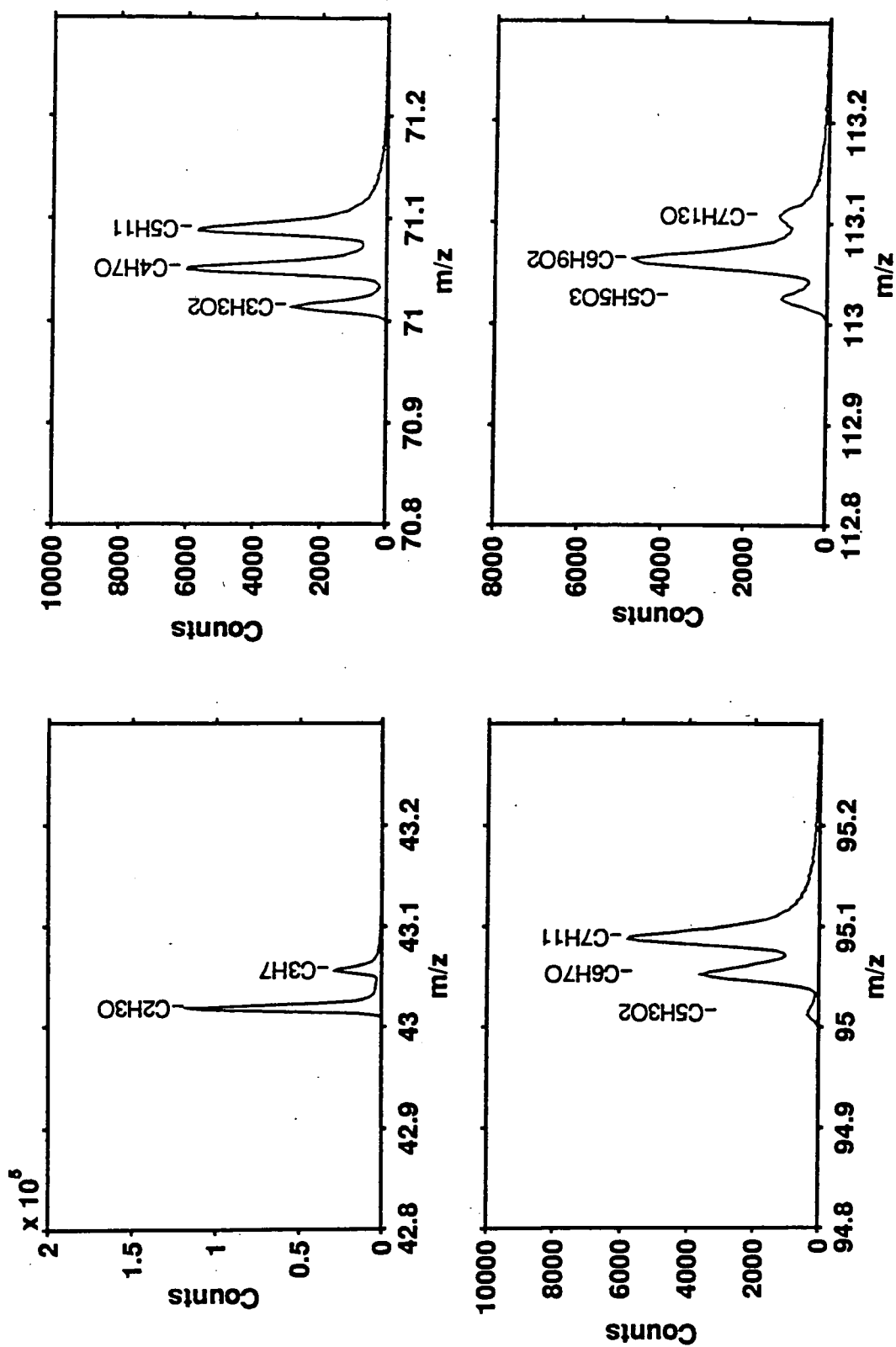Resolved components of selected peaks from Figure 6.

Figure 8(a):

Negative TOFSIMS of polypropylene silent discharge treated for 30 s; m/z 10-200 range.
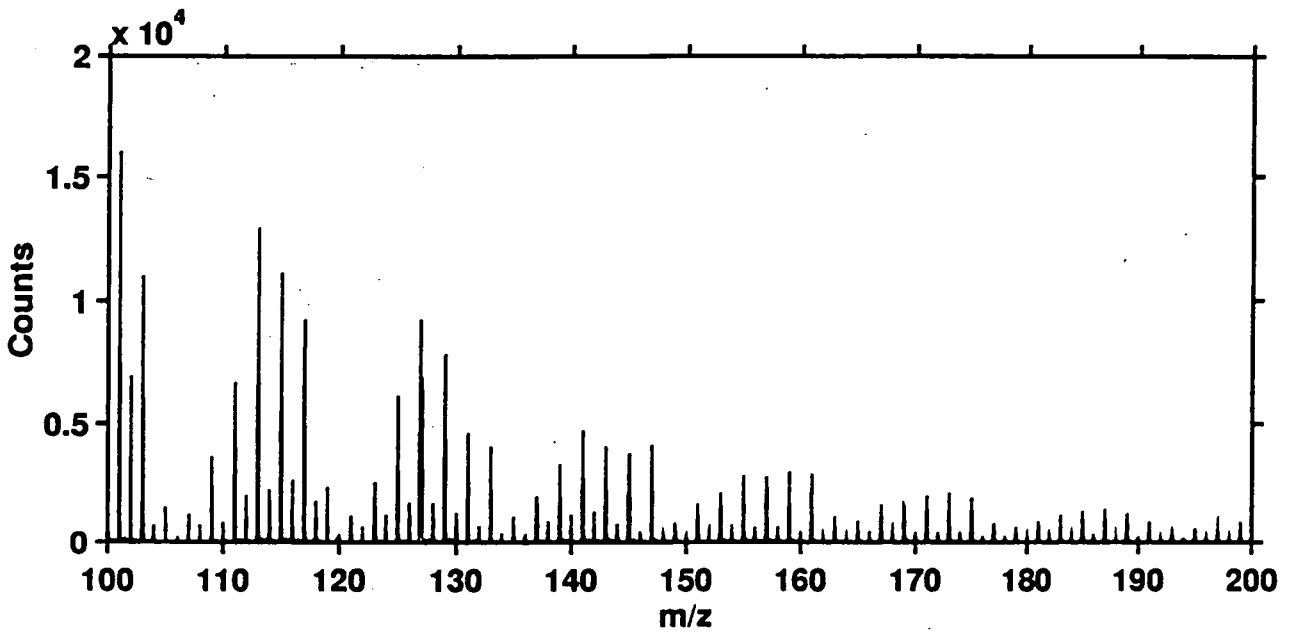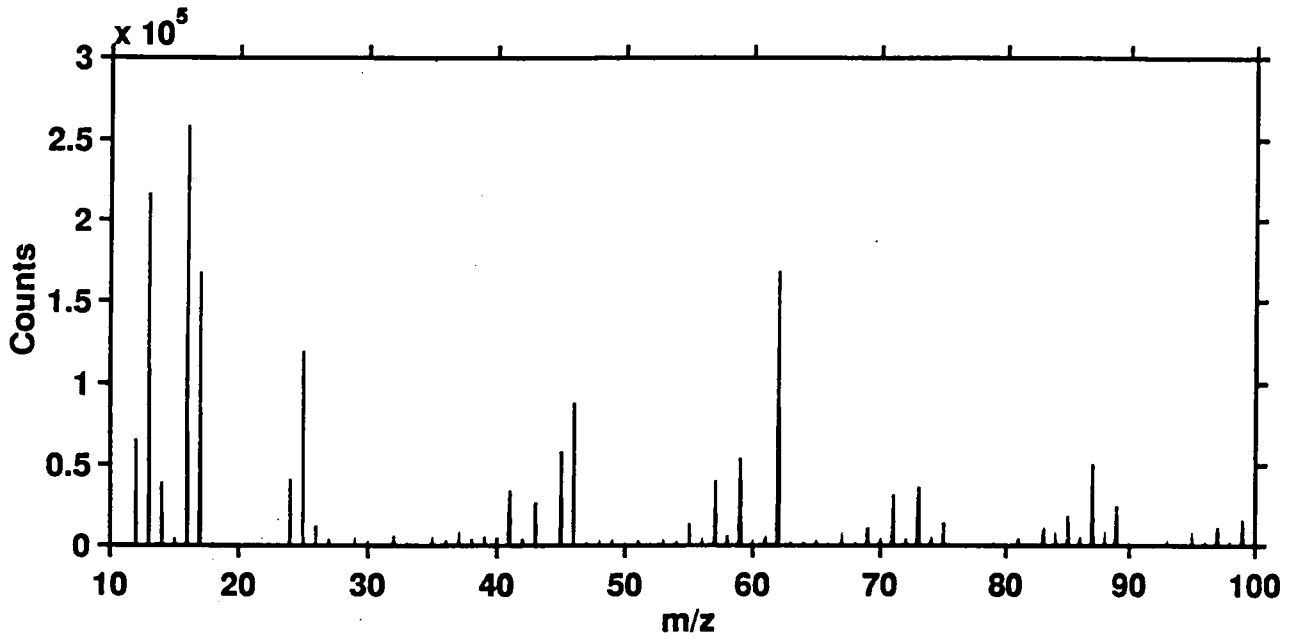
Figure 8(b):

Negative TOFSIMS of polypropylene silent discharge treated for 30:m/z 100-450 range.
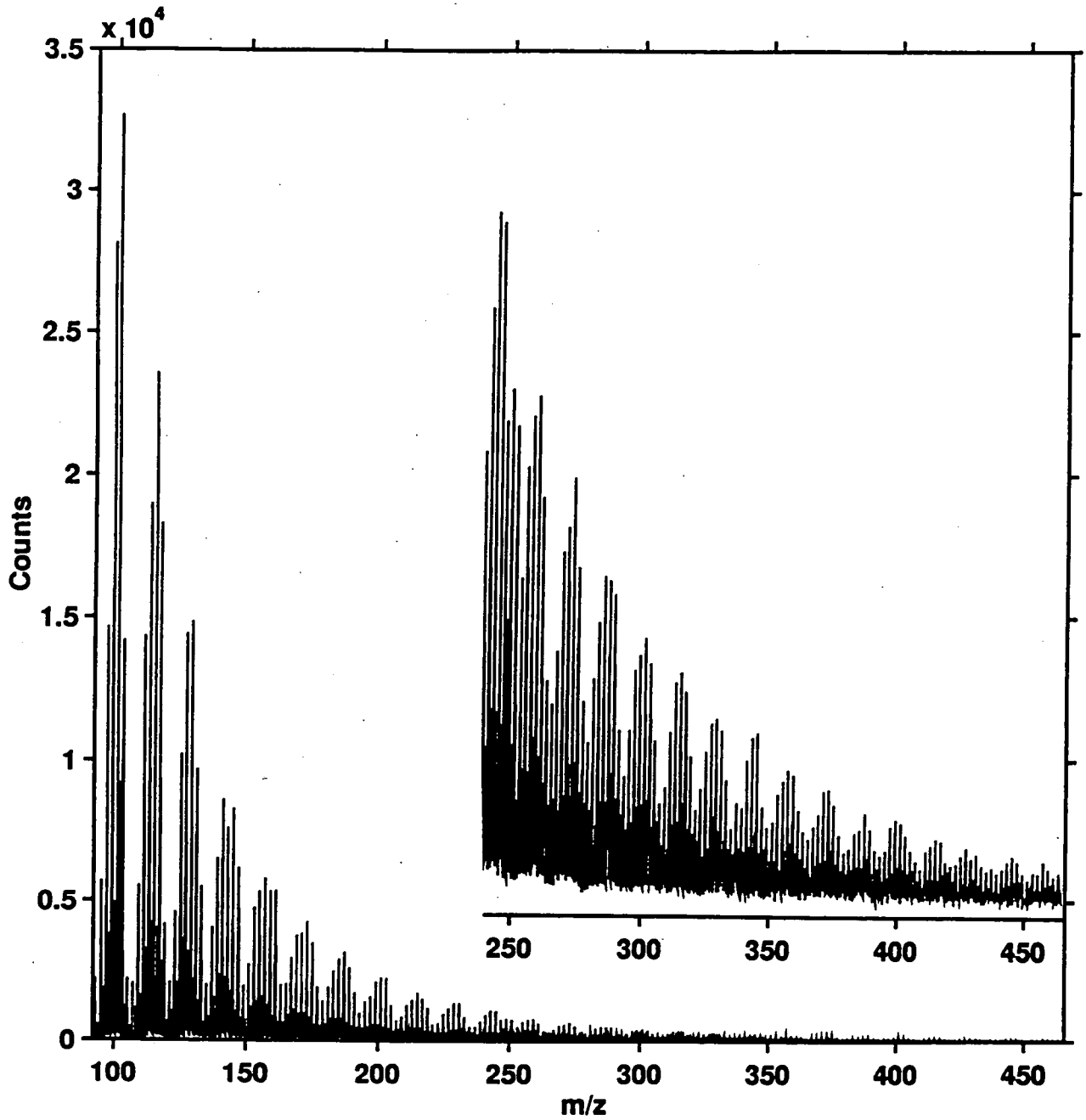
Figure 9:

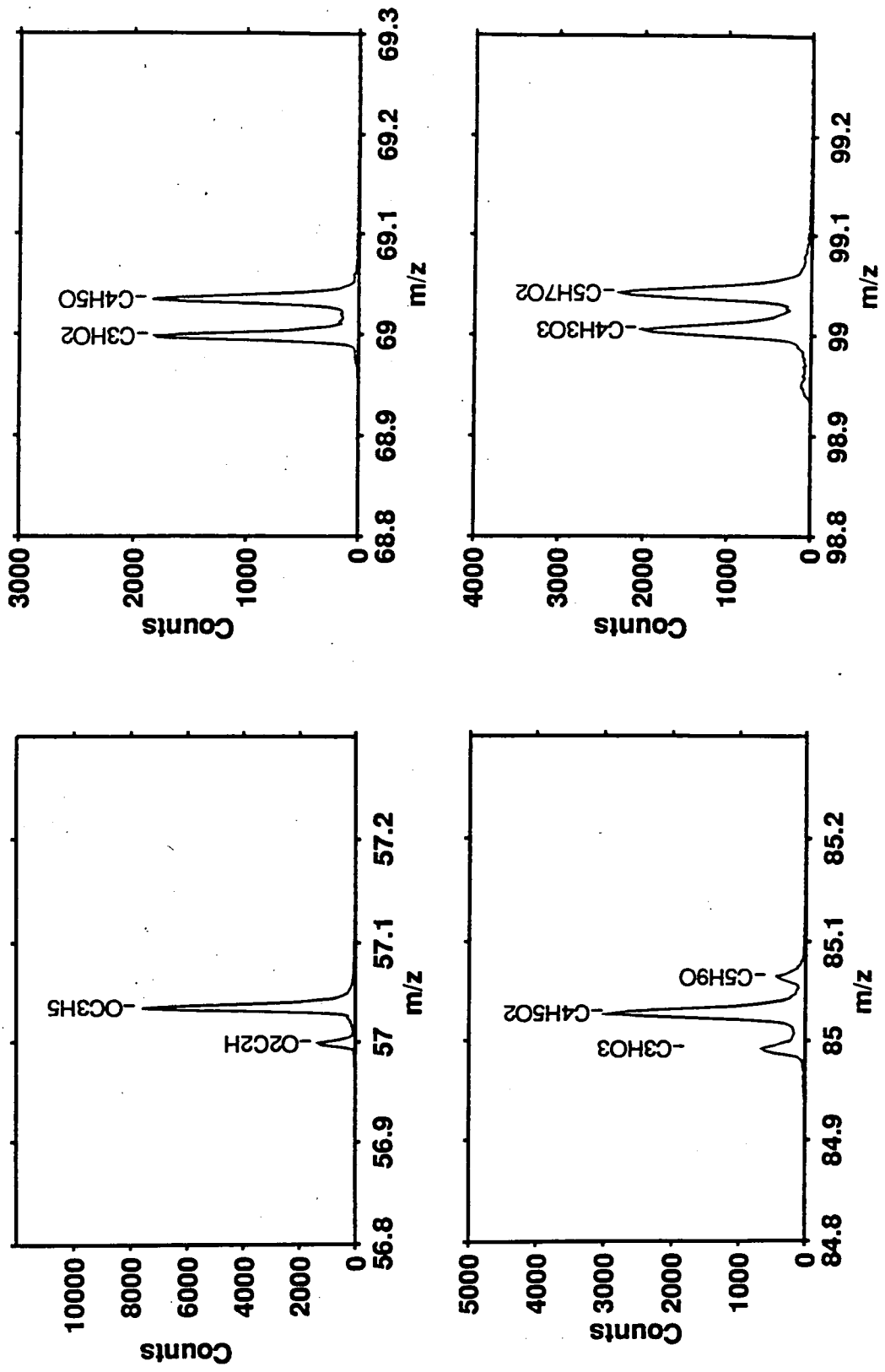Resolved components of selected peaks from Figure 8(a).

Figure 10(a):

Representative details of cluster composition in Figure 8(b); intensity pattern with the cluster centred on m/z 157.
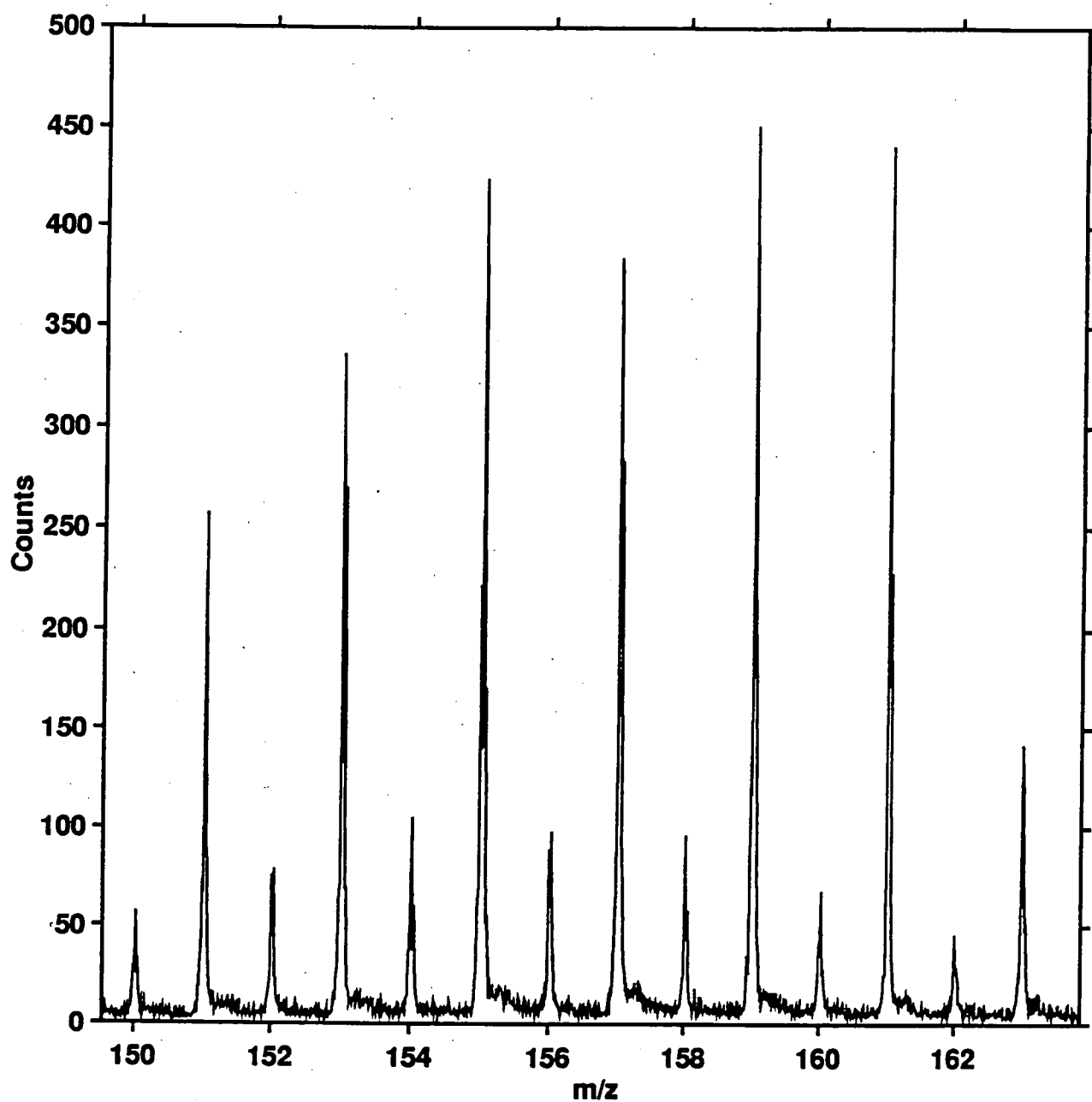
Figure 10(b):

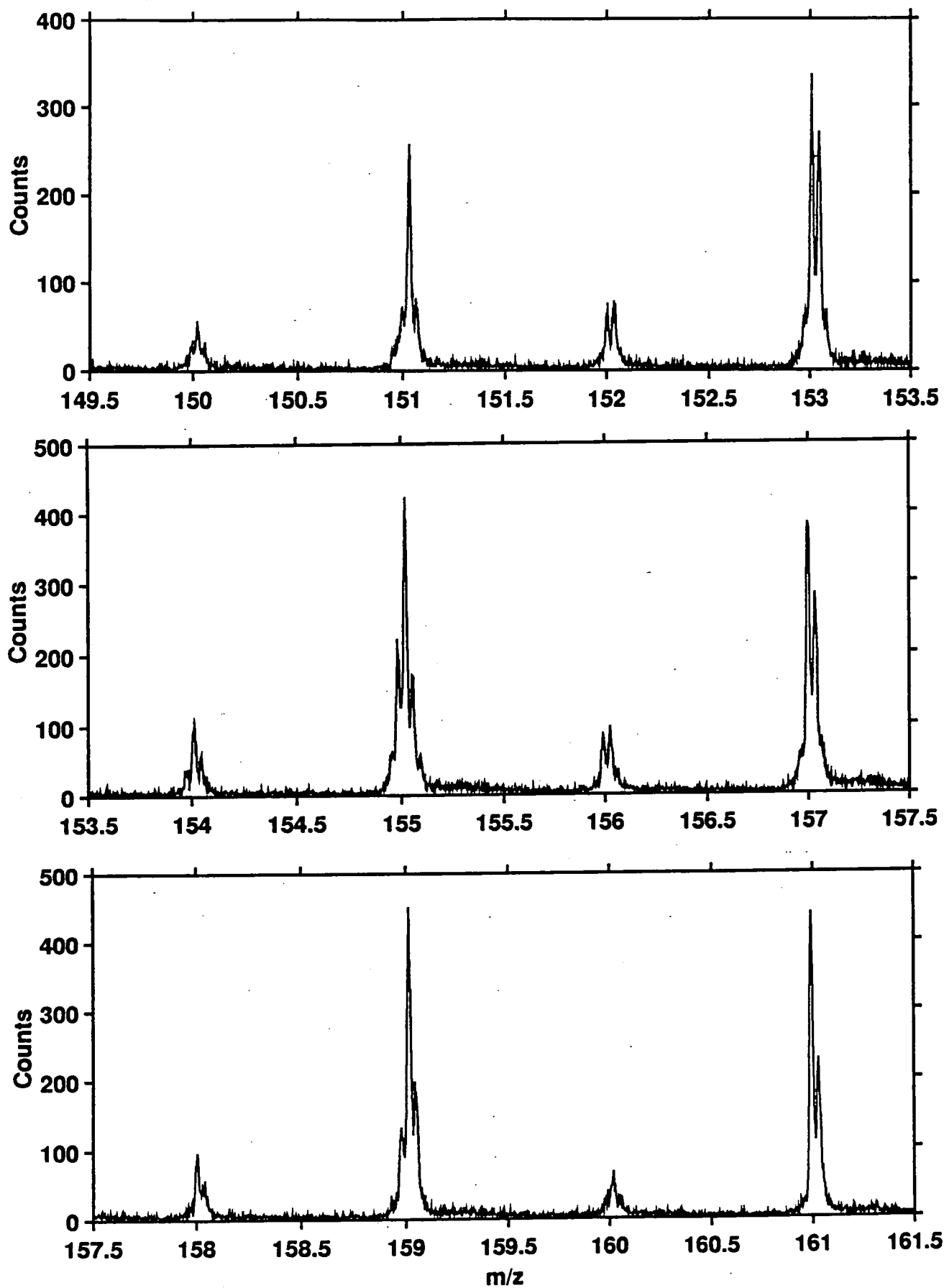Representative details of cluster composition in Figure 8(b): resolved components at each nominal mass.

Figure 11(a):

Partial positive TOFSIMS of chloroform extract deposited as a sub-monlayer on etched silver foil showing the cationized oligomer distribution between m/z 500-1400 (the peak at ~ m/z 1160 has not been assigned).

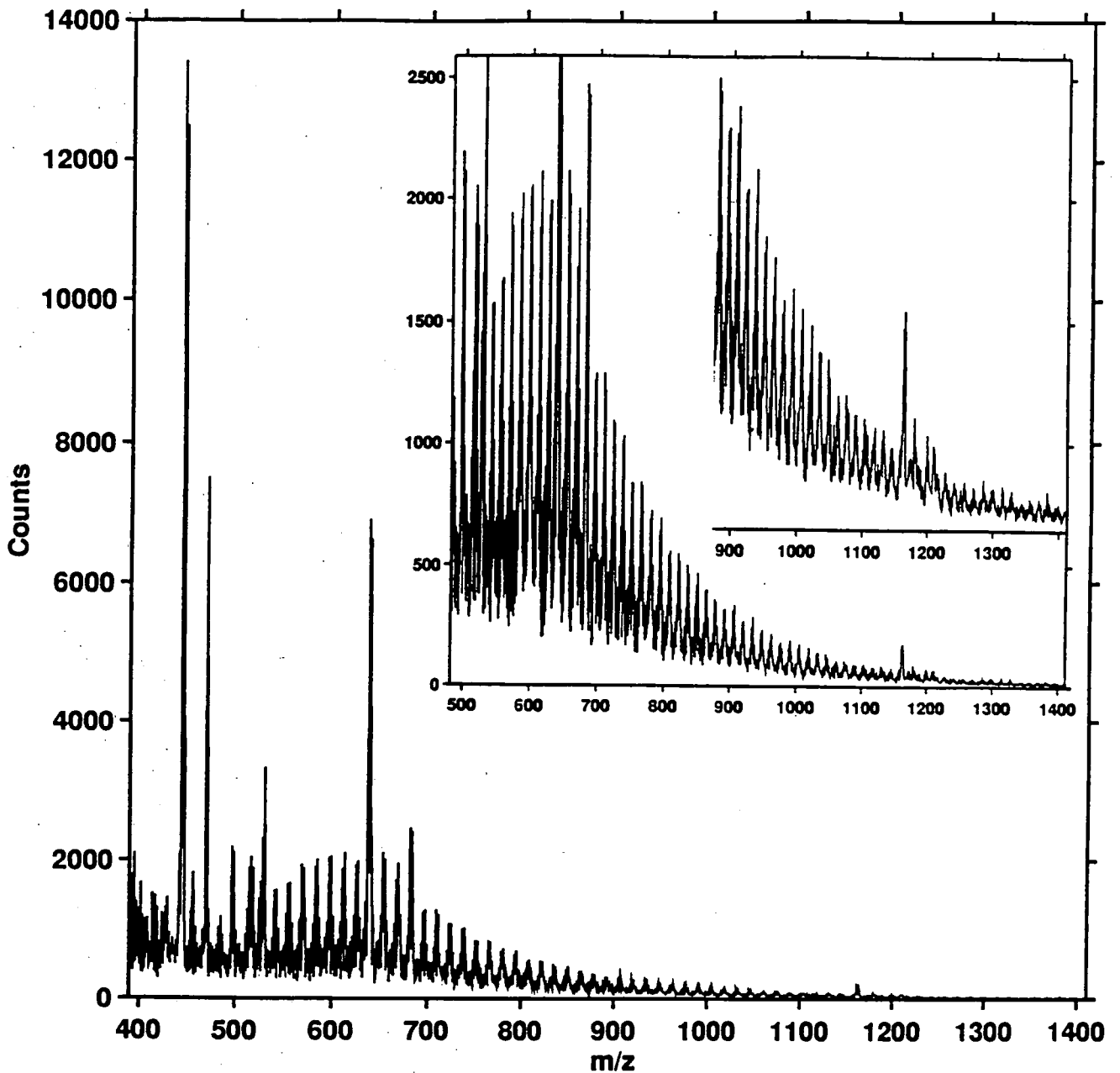Figure 11(b):
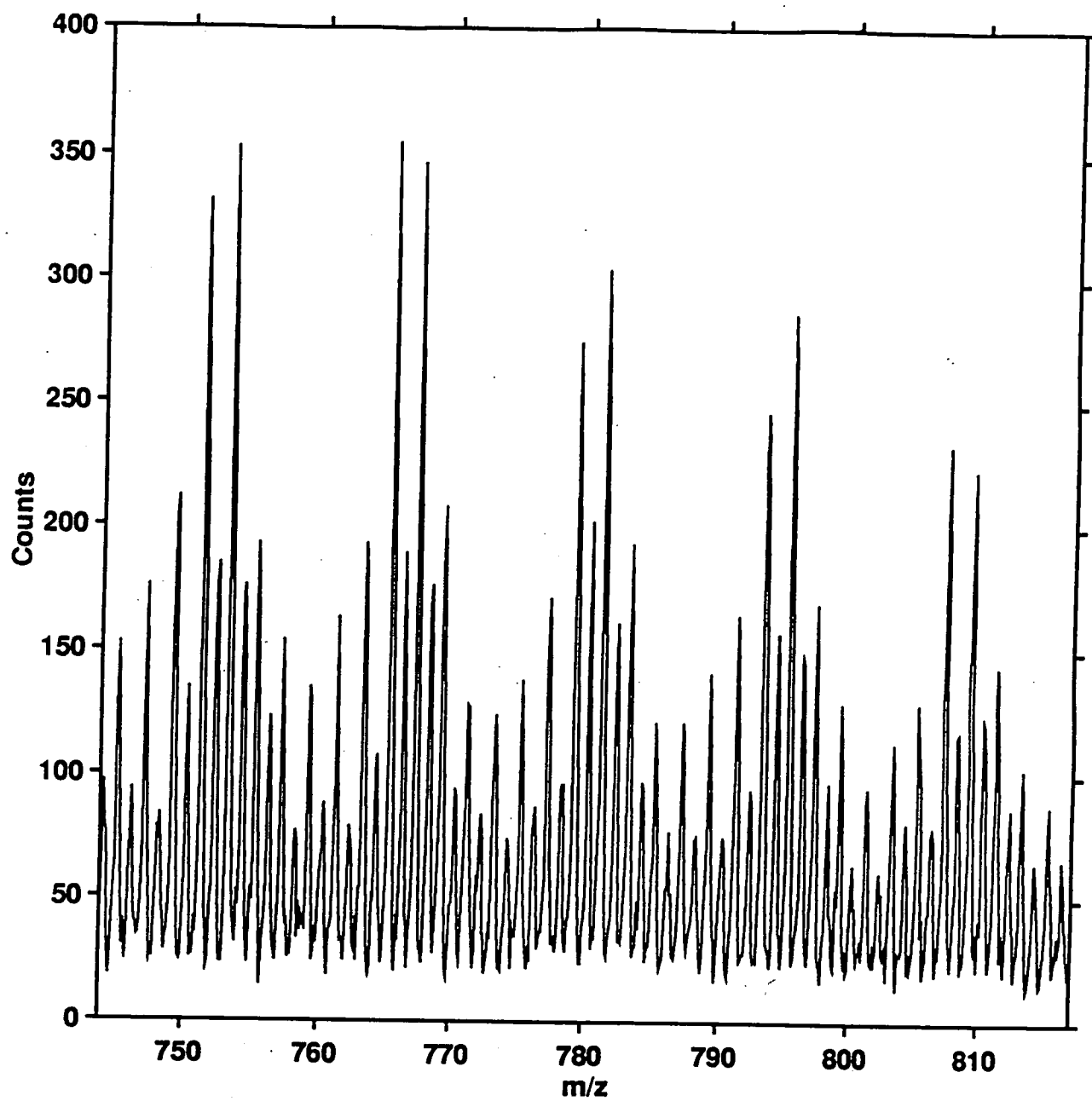
Detail of representative clusters shown in figure 11(a).
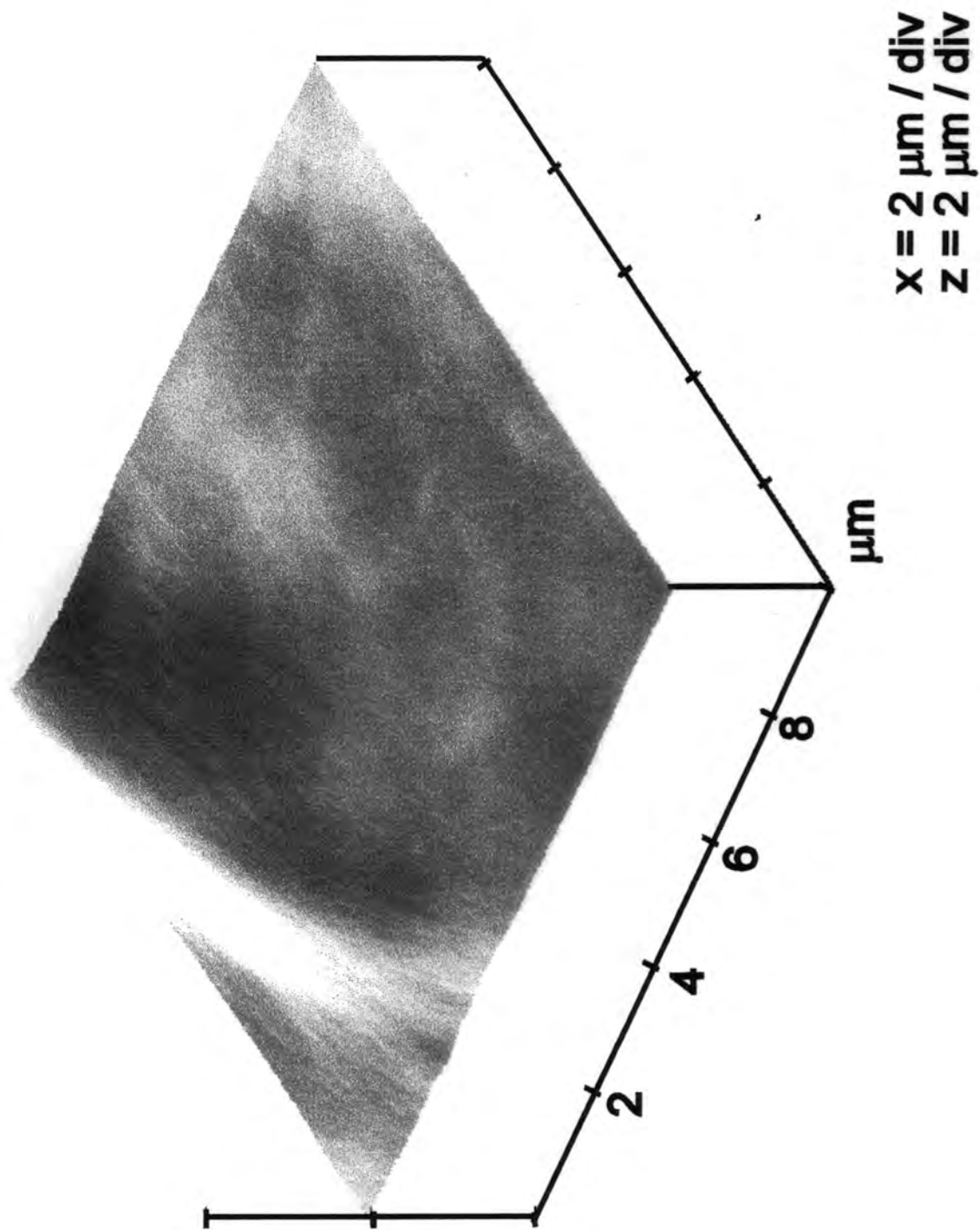
Figure 12(a): AFM image of untreated polypropylene.

x = 2 μm / div
z = 2 μm / div

μm

2 4 6 8

96

Figure 12(b): AFM image of polypropylene silent discharge treated for 30 s.

x = 2 μm / div
z = 2 μm / div

μm
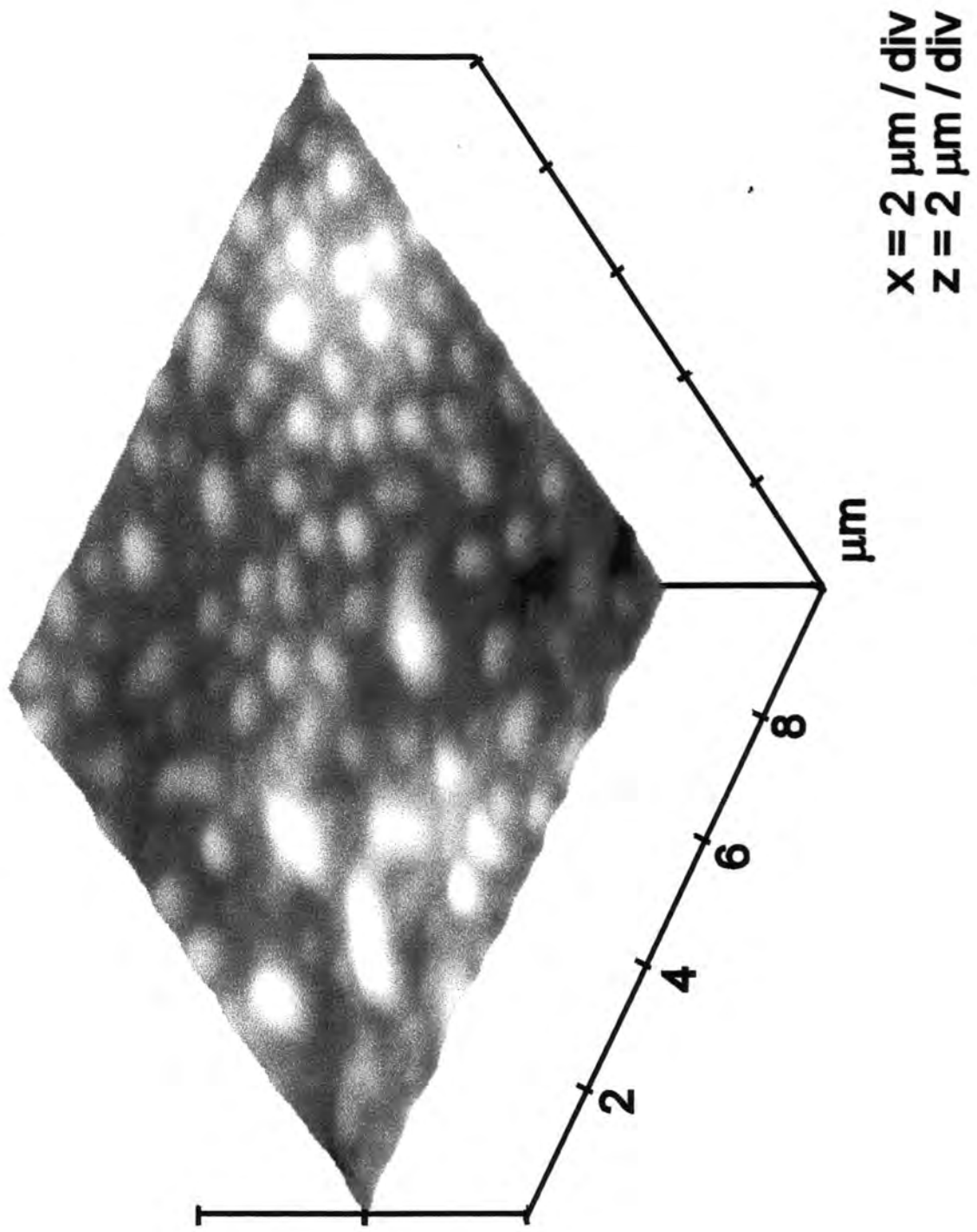
Figure 12(c): AFM image of polypropylene silent discharge treated for 240 s.
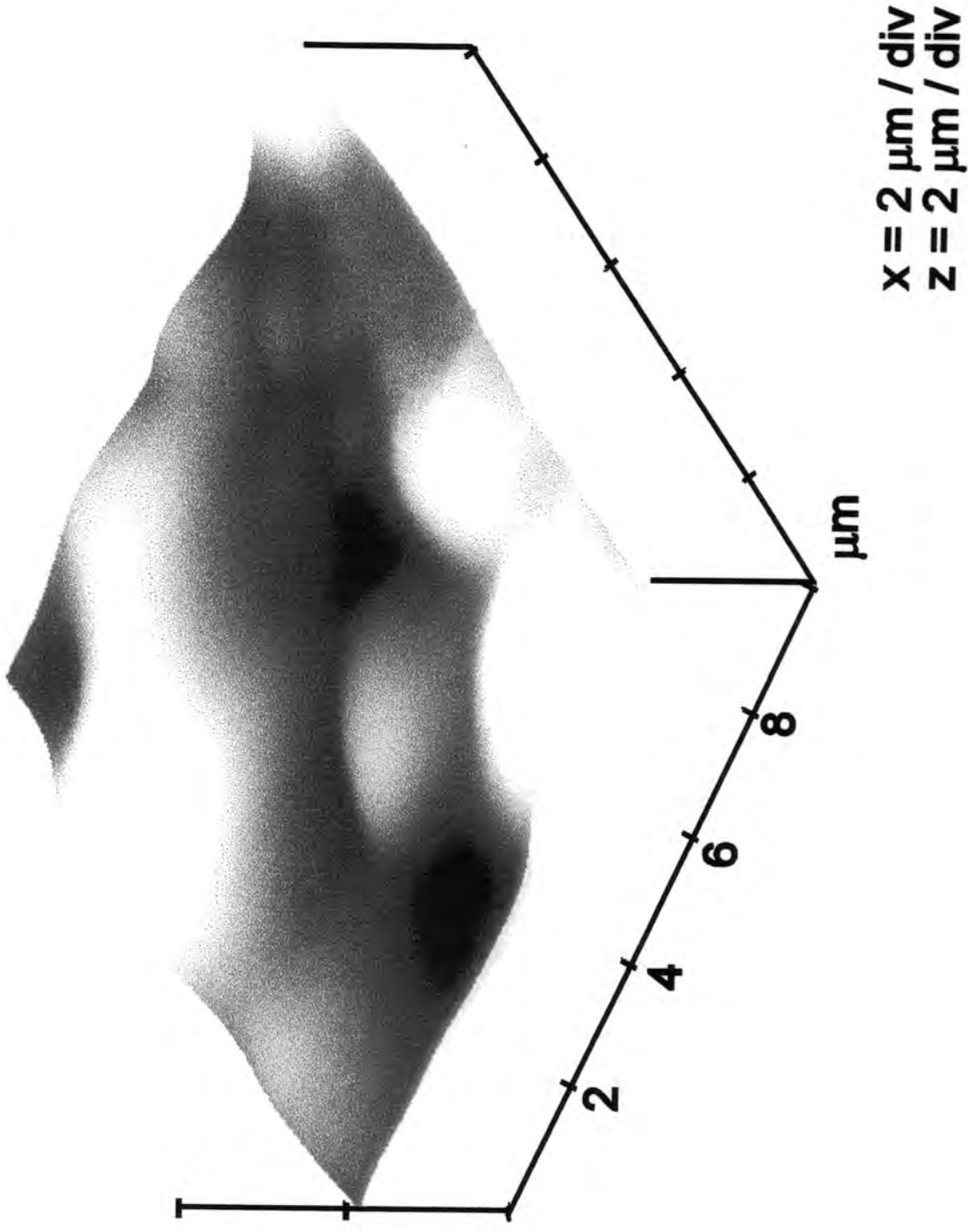
x = 2 μm / div
z = 2 μm / div

μm

Figure 12(d): AFM image of polypropylene silent discharge treated for 240 s then solvent washed.
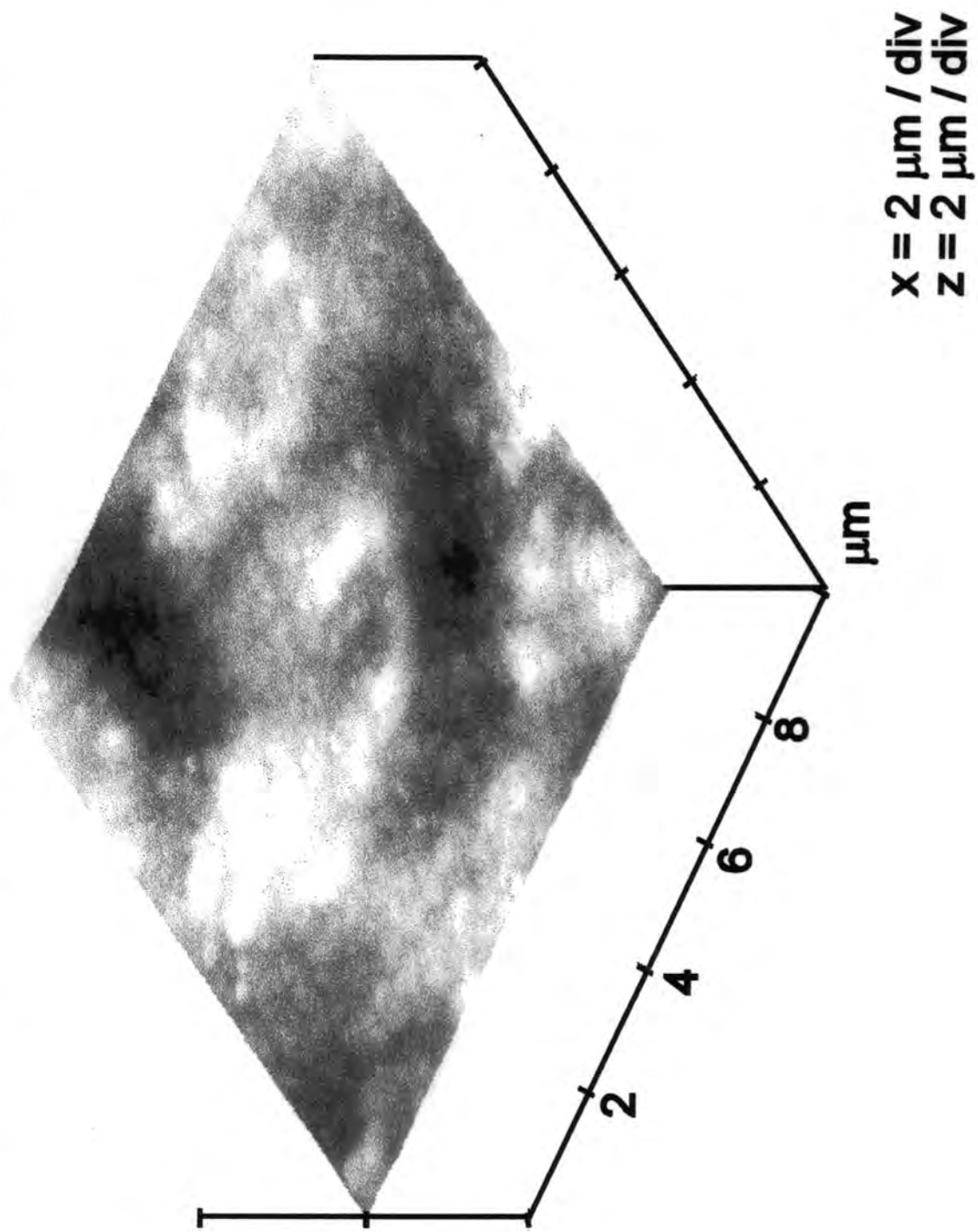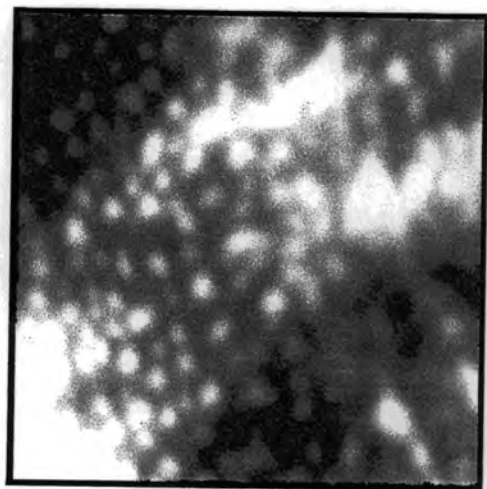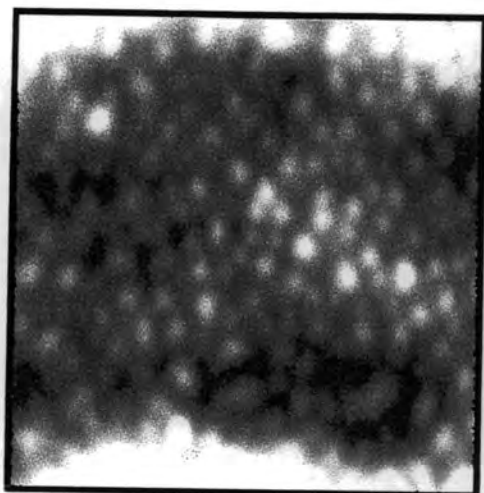

μm

x = 2 μm / div
z = 2 μm / div

Figure 13(a): 10 μm wide AFM images of aged silent discharge treated polypropylene. The vertical scale is 200 nm.
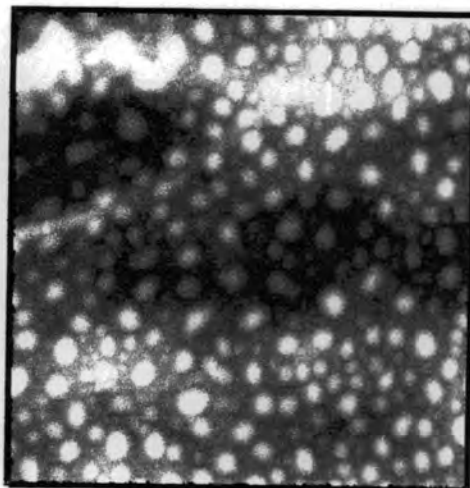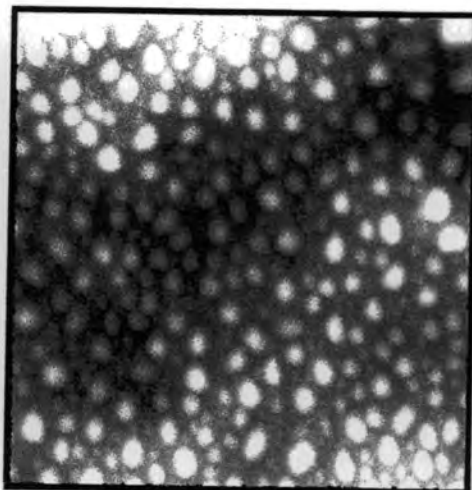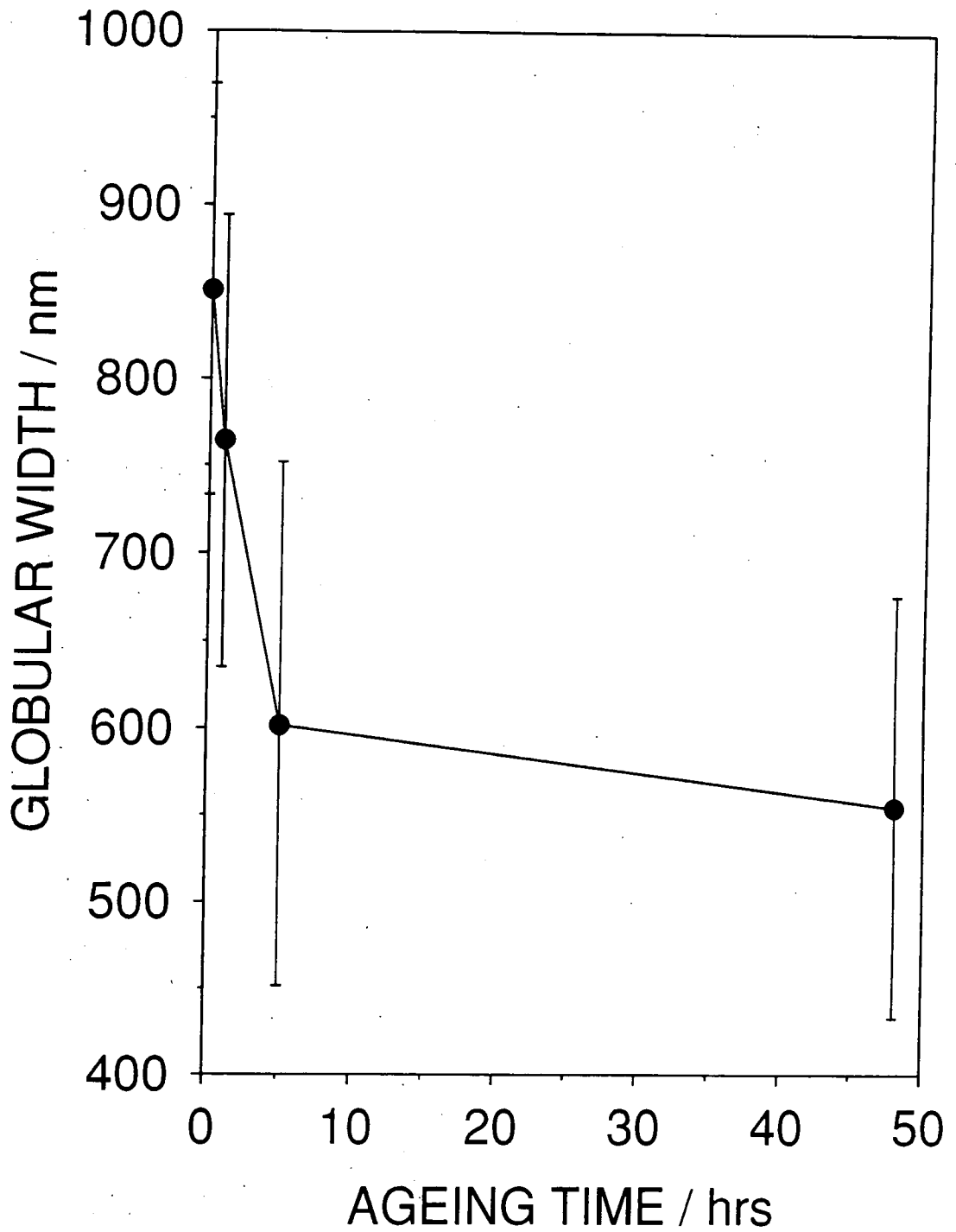
JUST TREATED

AGED 1 HR

AGED 5 HRS

AGED 48 HRS

Figure 13(b):

Variation in average globule size for 30 s silent discharge treated polypropylene as a function of ageing period

3.4 DISCUSSION

Silent discharge treatment is known to initiate polymer oxidation via chain scission, hydrogen abstraction, and oxygen attachment processes, leading to the formation of low molecular weight oxidised material (LMWOM).[19-28] which can be removed by solvent extraction.[29 30] The small amounts of Nox species detected by TOF-SIMS have also been identified on discharge treated surfaces by MIRS[31] and XPS.[28] The globular features observed by AFM can be attributed to the agglomeration of the LMWOM caused by the difference in surface energies between the LMWOM and the untreated polymer, since it is energetically unfavourable for high surface energy substances to interact with low surface energy olefinic polymers.[32] It is important to note that despite a gradual levelling off in the chemical composition of the plasma treated layer, the LMWOM globules continue to expand in size with exposure time, Figures 2 and 6 respectively. These observations can help to rationalise the reported variability in performance of plasma treated polymers for adhesive applications, since over-treatment can lead to excessive LMWOM and the formation of a weak interfacial layer despite the treated surface exhibiting good wettability characteristics.

A variety of explanations have been put forward to account for the ageing of plasma treated polymers, these include: migration of mobile species out of the polymer bulk,[33] rearrangement of the modified polymer,[34] and desorption of the more volatile constituents from the surface. Some or all of these mechanisms may be responsible for the ageing behaviour seen in the surface topography and O/C ratio. Furthermore, surface ageing helps to explain why there can often exist a discrepancy in the measured adhesive strength of a plasma treated surface; clearly the time between plasma treatment and bonding will be critical.

3.5 CONCLUSIONS

Atmospheric dielectric barrier treatment of biaxially oriented polypropylene in air leads to the formation of globular low molecular weight oxidised material (LMWOM). The formation of such globular features can be accounted for in terms of the difference in surface energies between LMWOM and the underlying olefinic polymer substrate. This

102

LMWOM is seen to gradually disappear with time away from the treated polymer surface.

REFERENCES

1 . Wells, R. K. Ph. D. Thesis, University of Durham, 1993.

2 . Brewis, D. M. In *Polymer Science*; Jenkins, A. D. Ed.; North-Holland: Amsterdam, 1972; Volume 2, Chapter 13.

3 . Coopes, I. H.; Griffen, K. J.; *J. Macromol. Sci. Chem.* **1982**, *17*, 217.

4 . Prutton, M.; *Surface Physics*; Clarendon: Oxford, 1983.

5 . Owen, M. J.; Gentle, T. M.; Orbeck, T.; Williams, D. E. In *Polymer Surface Dynamics*; Andrade, J. D. Ed.; Plenum: New York, 1988; Chapter 7.

6 . Garbassi, F.; Morra, M.; Occhiello, E. *Polymer Surfaces: From Physics to Technology*; Wiley: Chichester, 1994.

7 . Siemens, W. *Ann. Phys. Chem.* **1857**, *102*, 66.

8 . Eliasson, B.; Hirth, M.; Kogelschatz, U. *J. Phys. D: Appl. Phys.* **1987**, *20*, 1421.

9 . Eliasson, B.; Kogelschatz, U. *IEEE Trans. Plasma Sci.* **1991**, *19*, 309.

10 . Razumouskii, S. D.; Kefeli, A. A.; Zackov, G. E. *Eur. Polym. J.* **1971**, *7*, 275.

11 . Hudis, M. In *Techniques and Applications of Plasma Chemistry*; Hollahan, J. R.; Bell, A. T. Eds.; Wiley: London, 1974, Chapter 3.

12 . Mayoux, C. J. *IEEE Trans. Elect. Insul.* **1976**, *11*, 139.

13 . Carlsson, D. J.; Wiles, D. M. *Macromolecules* **1969**, *2*, 587.

14 . Sakai, Y.; Umetsa, K.; Migasaka, K. *Polymer* **1993**, *34*, 3362.

15 . Rasburn, J.; Klein, P. G.; Ward, I. M. *J. Polym. Sci., Polym. Phys. Ed.* **1994**, *32*, 1329.

16 . Ershov, Yu. A.; Gak, Yu. V. *Izv. Akad. Nauk SSSR, Ser. Khim.* **1967**, *4*, 778.

17 . Ranby, B.; Rabek, J. F. *Photodegradation, Photo-oxidation and Photostabilization of Polymers*; Wiley: London, 1975.

18 . Briggs, D.; Kendall, C. R.; Blythe, A. R.; Wootton, A. B. *Polymer* **1986**, *27*, 1058.

19 . Strobel, M.; Dunatov, C.; Strobel, J. M.; Lyons, C. S.; Perron, S. J.; Morgen, M. C. *J. Adhesion Sci. Technol.* **1989**, *3*, 321.

20 . Reichlmaier, S.; Hammond, J. S.; Hearn, M. J.; Briggs, D. *Surface and Interface Analysis* **1994**, *21*, 739.

21 . Wells, R. K.; Badyal, J. P. S. *J. Polym. Sci., Polym Chem. Ed.* **1992**, *30*, 2677.

22 . Derome, A. E. *Modern NMR Techniques for Chemistry Research*; Pergamon: Oxford, 1987.

23 . Tonelli, A. E. *NMR Spectroscopy and Polymer Microstructure: The Conformational Connection*; VCH: New York, 1989.

24 . Brown, D. W.; Floyd, A. J.; Sainsbury, M. *Organic Spectroscopy*; Wiley: Chichester, 1988.

25 . Cotton, N. J.; Bartle, K. D.; Clifford, A. A.; Dowle, C. J. *J. Appl. Polym. Sci.* **1993**, *48*, 1607.

26 . Heatley, F.; Zambelli, A. *Macromolecules* **1969**, *2*, 618.

27 . The Wiley Static SIMS Library; Wiley: Chichester, 1996.

28 . Briggs, D.; Kendall, C. R.; Blythe, A. R.; Wootton, A. B. *Polymer* **1983**, *24*, 47.

29 . Xiao, G. Z. *J. Mat. Sci. Letts.* **1995**, *14*, 761.

30 . Lee, S. H. *J. Colloid Interface Sci.* **1995**, *14*, 761.

31 . Blythe, A. R.; Briggs, D.; Kendall, C. R.; Rane, D. G.; Zichy, V. J. I. *Polymer* **1978**, *19*, 1273.

32 . Cherry, B. W. *Polymer Surfaces*; Cambridge University: Cambridge, 1981, p18.

33 . Occhiello, E.; Morra, M.; Cinquina, P.; Garbassi, F. *Polymer* **1992**, *33*, 3007.

34 . Garbassi, F.; Morra, M.; Occhiello, E.; Barino, L.; Scordamaglia, R. *Surface and Interface Analysis* **1989**, *14*, 585.

CHAPTER 4:

STRUCTURE AND OXIDATIVE PLASMA DEGRADATION OF HEXATRIACONTANE CRYSTALS

4.1 INTRODUCTION

In the previous two chapters it has been shown that plasma treatment can be used to alter the chemical and physical properties of polymer substrates. However an understanding at the molecular level of these processes is currently lacking. One of the main reasons for this is that the substrates tend to be poorly defined.[1] An easy way of overcoming this drawback is to use a model polymer surface.[2] For instance, hexatriacontane ($C_{36}H_{74}$) is a straight chain paraffinic molecule which packs into a highly crystalline form[3]. hence it can serve as a good model for high density polyethylene.[2,4,5] Furthermore, its electronic valance structure[6] and ultraviolet absorption characteristics[7] are found to be virtually identical to those of high density polyethylene.

The aim of this chapter is to describe the non-equilibrium oxidative plasma modification of hexatriacontane surfaces. XPS and solution state NMR have been used to follow the chemical changes taking place, whilst atomic force microscopy provides an insight at the molecular level into the extent of heterogeneous degradation across the substrate surface.

4.2. EXPERIMENTAL

4.2.1 Sample Preparation

Hexatriacontane (Aldrich, 98 %) crystals were deposited directly onto a glass slide during re-crystallisation from toluene solution.[5] Optical microscopy showed that the crystals were platelets (20 to 50 µm long), and tended to lie flat on the glass substrate.

4.2.2 Silent Discharge Treatment

Atmospheric pressure air silent discharge treatments were carried out using a home built parallel plate dielectric barrier discharge reactor operating at 3 kHz. 11 kV, with an electrode gap of 3.00 ± 0.05 mm. Silent discharge treatment times were kept short (5 s and 60 s for AFM and XPS / NMR respectively) in order to follow the early stages of oxidative attack at the hexatriacontane crystal surfaces.

4.2.3 Sample Analysis

A Digital Instruments Nanoscope III atomic force microscope was used to examine the topographical nature of the hexatriacontane crystal surfaces prior to and immediately after electrical discharge exposure. Molecular resolution images of the crystal structure were obtained using contact mode AFM. Whilst tapping mode AFM was used to image larger scan areas.

A Kratos ES300 electron spectrometer equipped with a MgKα X-ray source (1253.6 eV) and a concentric hemispherical analyser was used for XPS analysis. Photoemitted electrons were collected at a take-off angle of 30° from the substrate normal, with electron detection in the fixed retard ratio (FRR, 22:1) mode.

Solution state ^{1}H NMR spectroscopy was also used to follow the chemical changes taking place during atmospheric dielectric barrier treatment of hexatriacontane. Both the unmodified and modified crystals were dissolved in deuterated chloroform and analysed using a Varian VXR-400s NMR spectrometer.

4.3 RESULTS

4.3.1 Atomic Force Microscopy

AFM analysis of untreated hexatriacontane crystals shows rhombic platelets with an acute angle of 80 ± 5°; this morphology is typical of paraffinic crystals[3,8,10,11], Figure 1. Molecular resolution AFM image of hexatriacontane is shown in Figure 2(a).

2-D Fourier analysis is a well known method of image analysis.[12,13] If an image contains a repeating function with wavelength λ at an angle θ then the 2-D Fourier transform spectrum will display this function as a single point $1/\lambda$ distance from the origin and at the angle θ.[14] By performing an inverse 2-D Fourier transform of just these periodic functions then a filtered image containing just the functions can be obtained.

2-D Fourier transform analysis of Figure 2(a), Shown in Figure 2(b), shows that these crystals possess a crystal structure with lattice spacings of 0.63 ± 0.05 nm and 0.78 ± 0.05 nm with a lattice angle of 92 ± 5°. These lattice parameters compare well with the values of 0.56 nm and 0.74 nm and an orthorhombic crystal structure obtained by X-ray diffraction for the bulk crystal.[11,15,16] The Fourier filter image of Figure 2(a) is shown in Figure 2(c). An edge dislocation is also discernible in Figures 2(a) and 2(c), where an extra plane of molecules has produced a distortion in the lattice packing.[17]

Oxidative attack is concentrated around the crystal edges during silent discharge treatment of the hexatriacontane crystals to produce a jagged appearance with angles of 80 ± 5°, and 100 ± 5°, Figure 3. Small globular features are also evident.

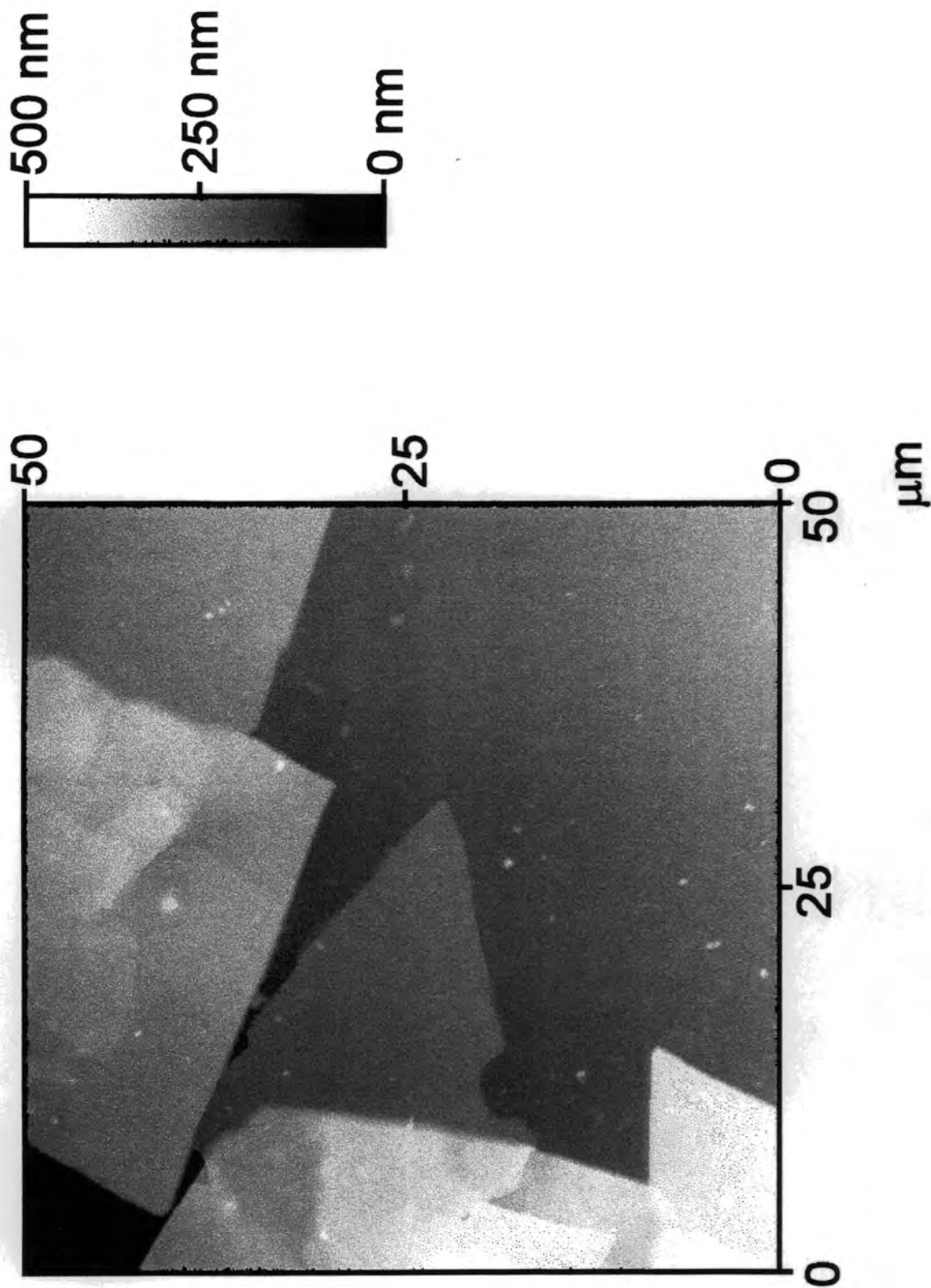Figure 1: Tapping mode AFM image of hexatriacontane platelet crystals.

109

Figure 2(a): Contact mode AFM image at molecular resolution for hexatriacontane.
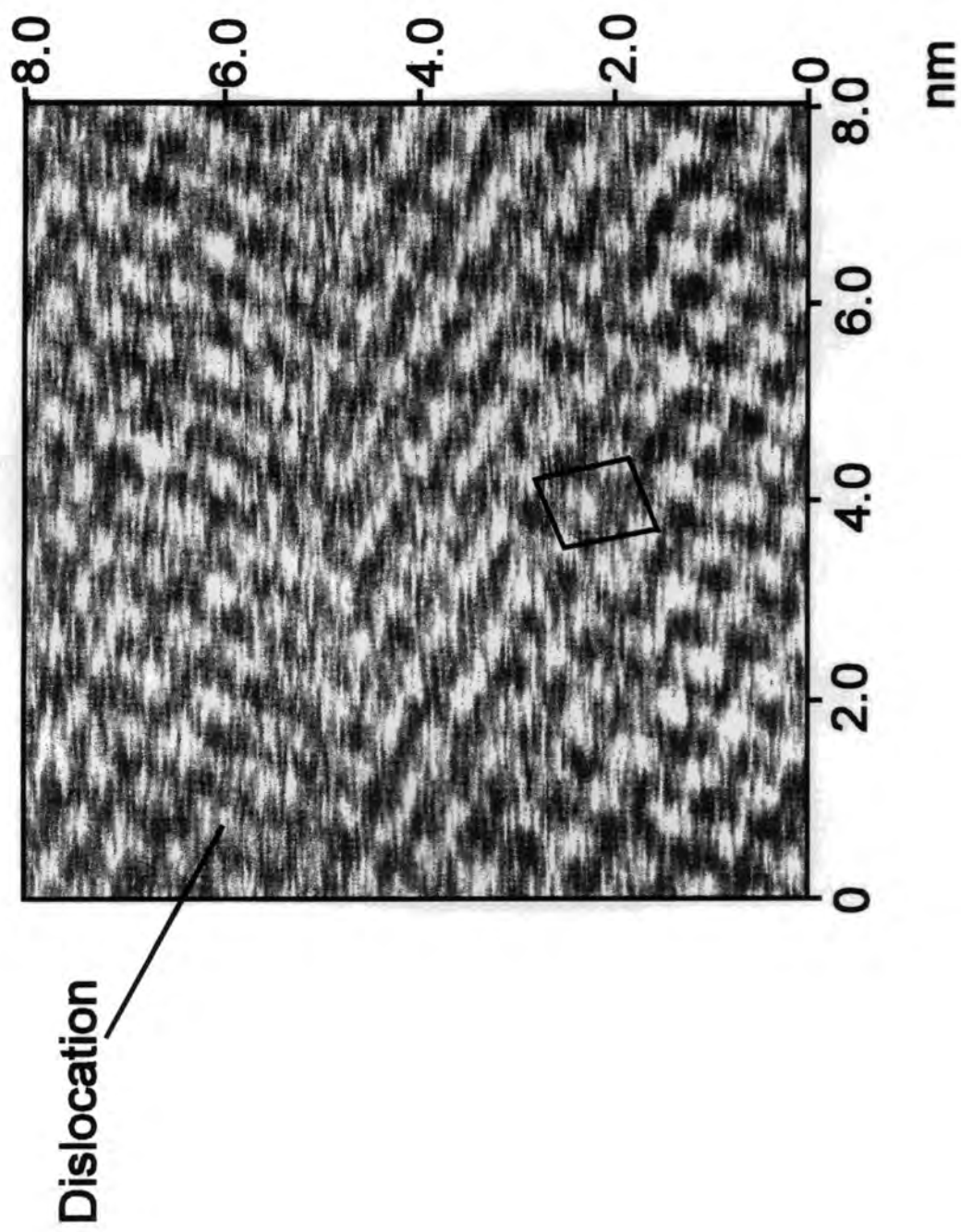
Dislocation

8.0

6.0

4.0

2.0

0

8.0   6.0   4.0   2.0   0

nm

Figure 2(b): 2D Fourier transform of molecular resolution image shown in Figure 2(a).
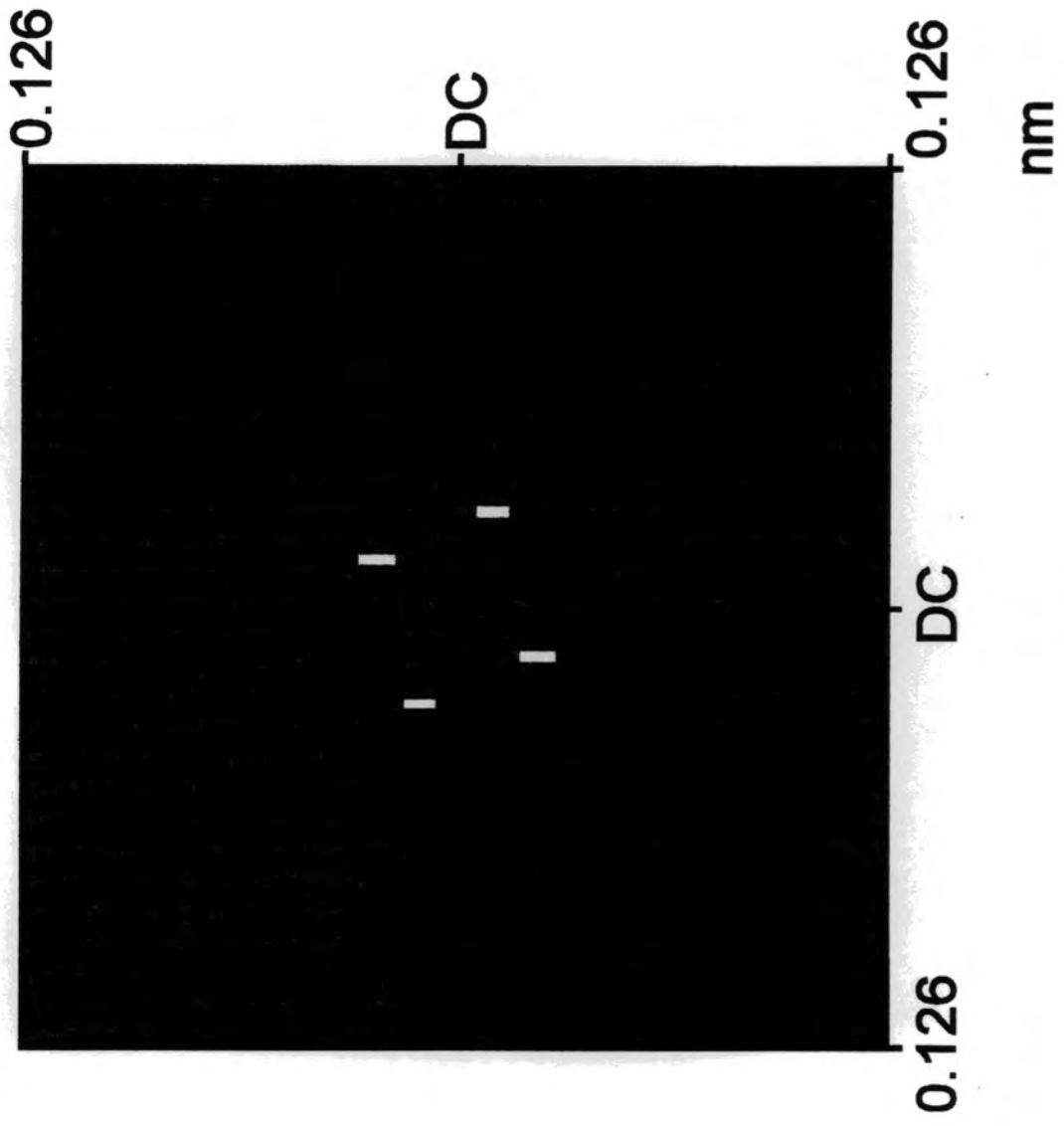
111

Figure 2(c): Fourier filtered image of Figure 2(a).
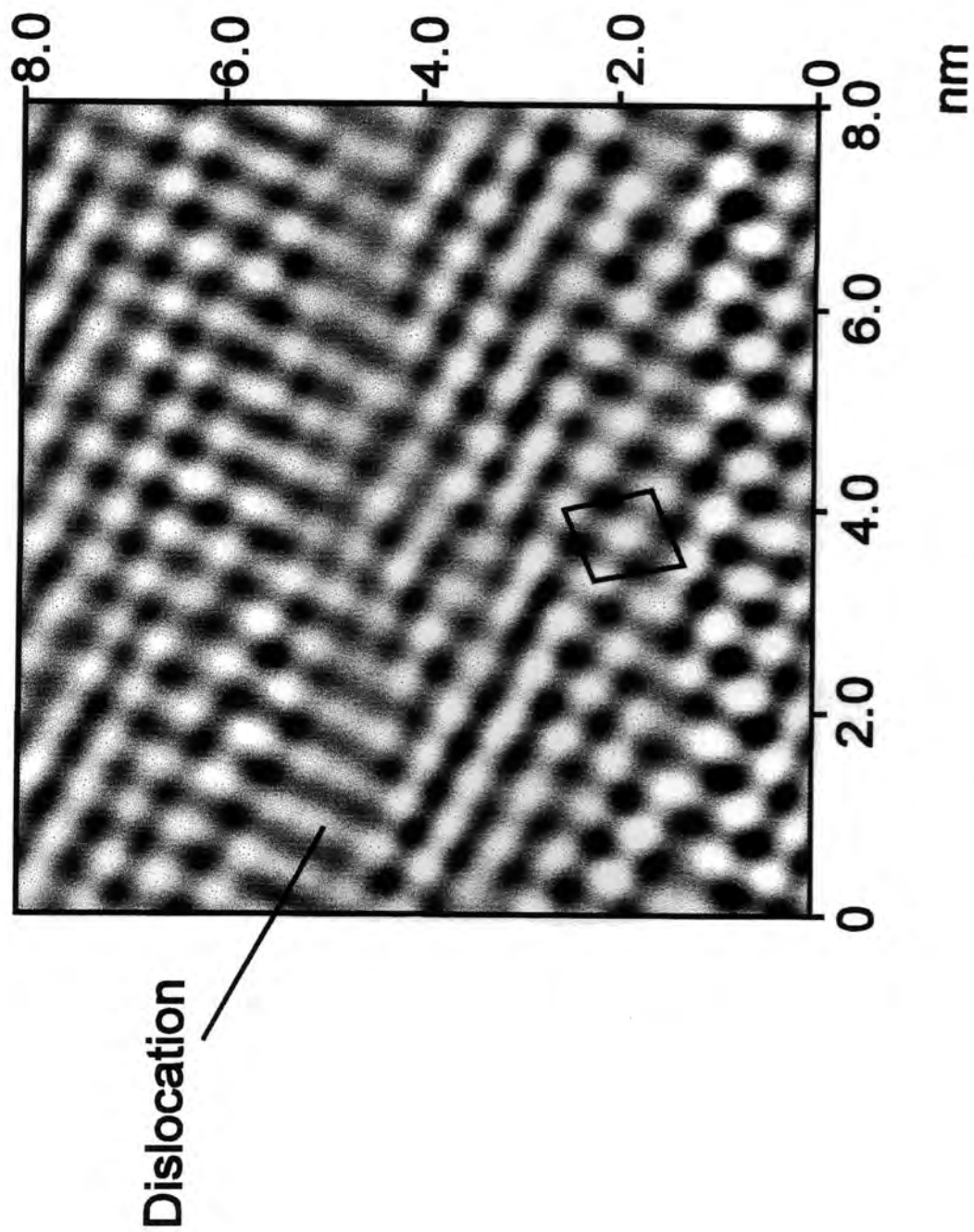
Dislocation

112

Figure 3(a): Tapping mode AFM image of the edge of an untreated hexatriacontane crystal.
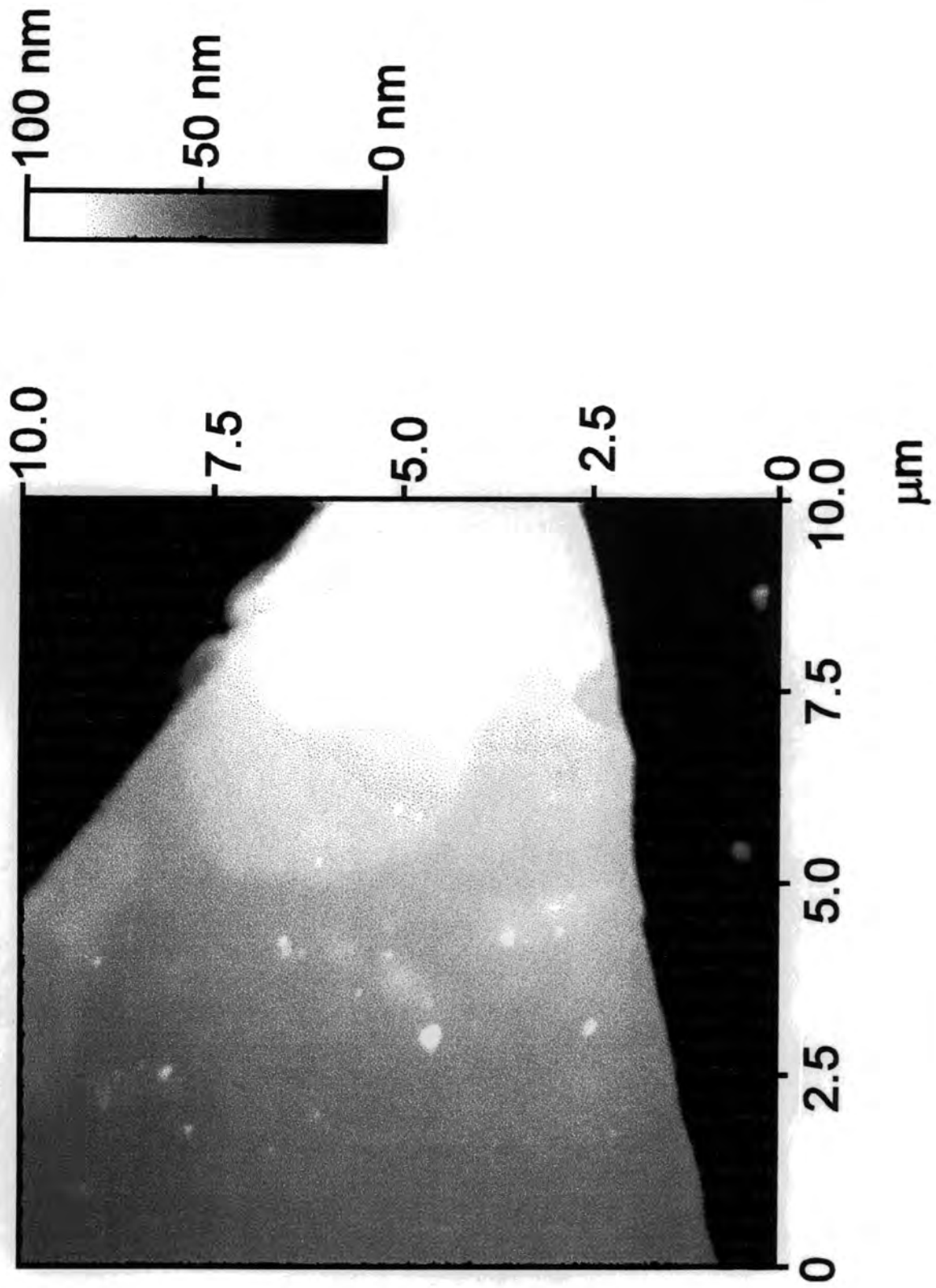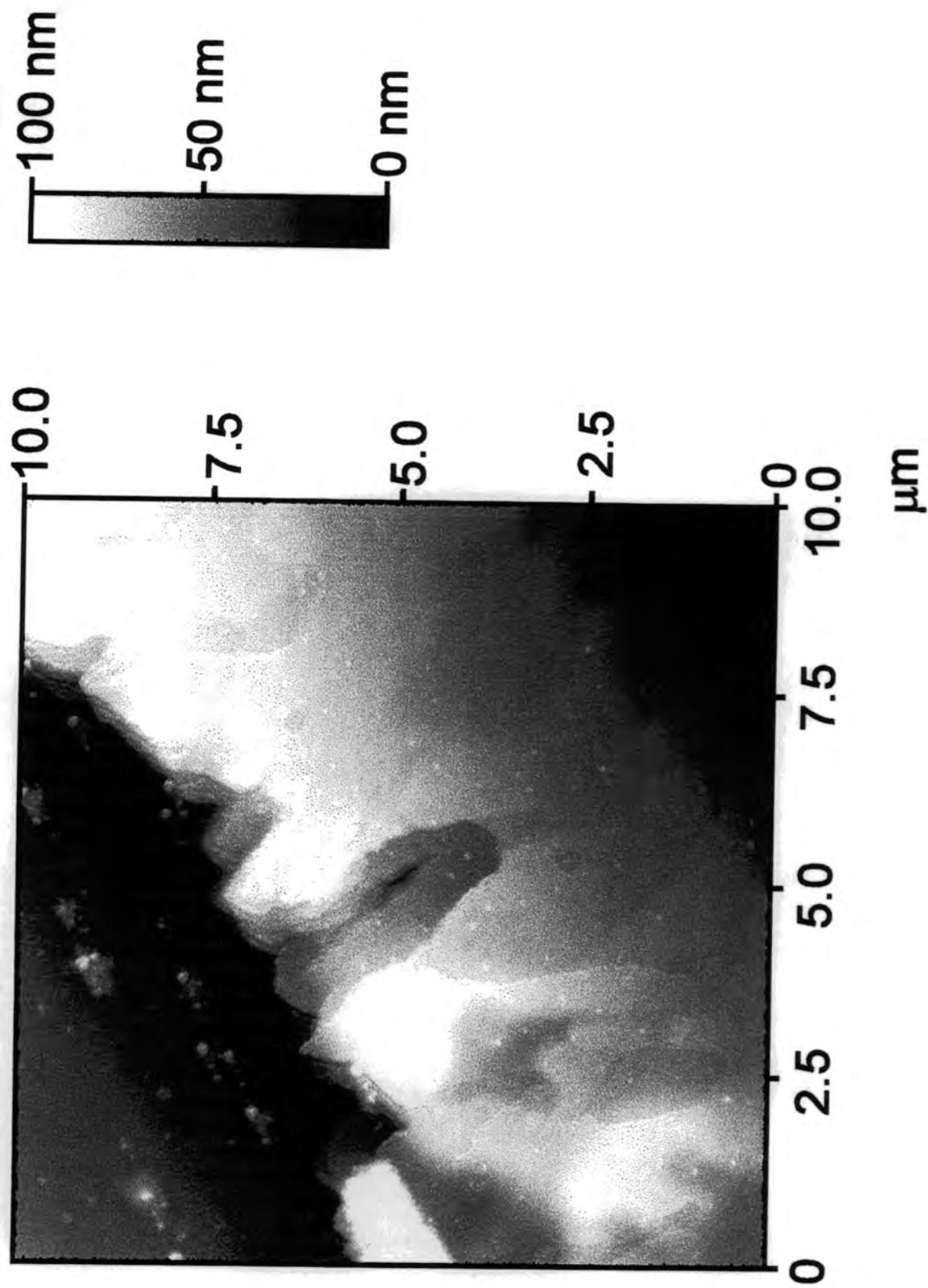
113

Figure 3(b): Tapping mode AFM image of the edges of an silent discharge treated hexatriacontane crystal.

114

4.3.2 X-ray Photoelectron Spectroscopy

The C(1s) spectrum of the untreated hexatriacontane crystals displayed a main peak at 285.0 eV, which corresponds to C_xH_y (i.e. $-CH_2$, and $-CH_3$ groups), Figure 4. Silent discharge treatment resulted in the appearance of various types of oxidised carbon moieties, as described in chapter 2.

4.3.3 NMR Spectroscopy

The proton NMR spectrum of hexatriacontane crystals dissolved in deuterated chloroform shows four peaks, Figure 5(a):[18] 7.5 ppm (non-deuterated chloroform impurity), 1.5 ppm (absorbed water), 1.2 ppm ($-CH_2$ groups along the alkyl chain backbone), and 0.9 ppm ($-CH_3$ groups at the chain ends). The chain length was calculated from the peak area ratios to be 40 ± 4 carbon atoms.

Silent discharge treatment gave rise to three effects in the NMR spectrum, Figure 5(b). Firstly, a general broadening of the CH_2 and CH_3 peaks was evident, this is consistent with an increasing number of different chemical environments. Also average chain length was found to have been shortened to approximately 20 ± 4 carbon atoms. Finally, three new peaks appeared: 5.1 ppm (vinylic carbon - carbon double bonds), 2.0 ppm (CH_2 groups adjacent to carbon-carbon double bonds, and ether groups), and 1.7 ppm (hydrogen atom bonded to a carbon centre which is either adjacent to an ether group or two carbon atoms away from a carbon-carbon double bond). These assignments were confirmed by COSY NMR experiments.

Figure 4:

C(1s) spectra of hexatriacontane crystals: (a) untreated; and (b) following 60 s silent discharge treatment.
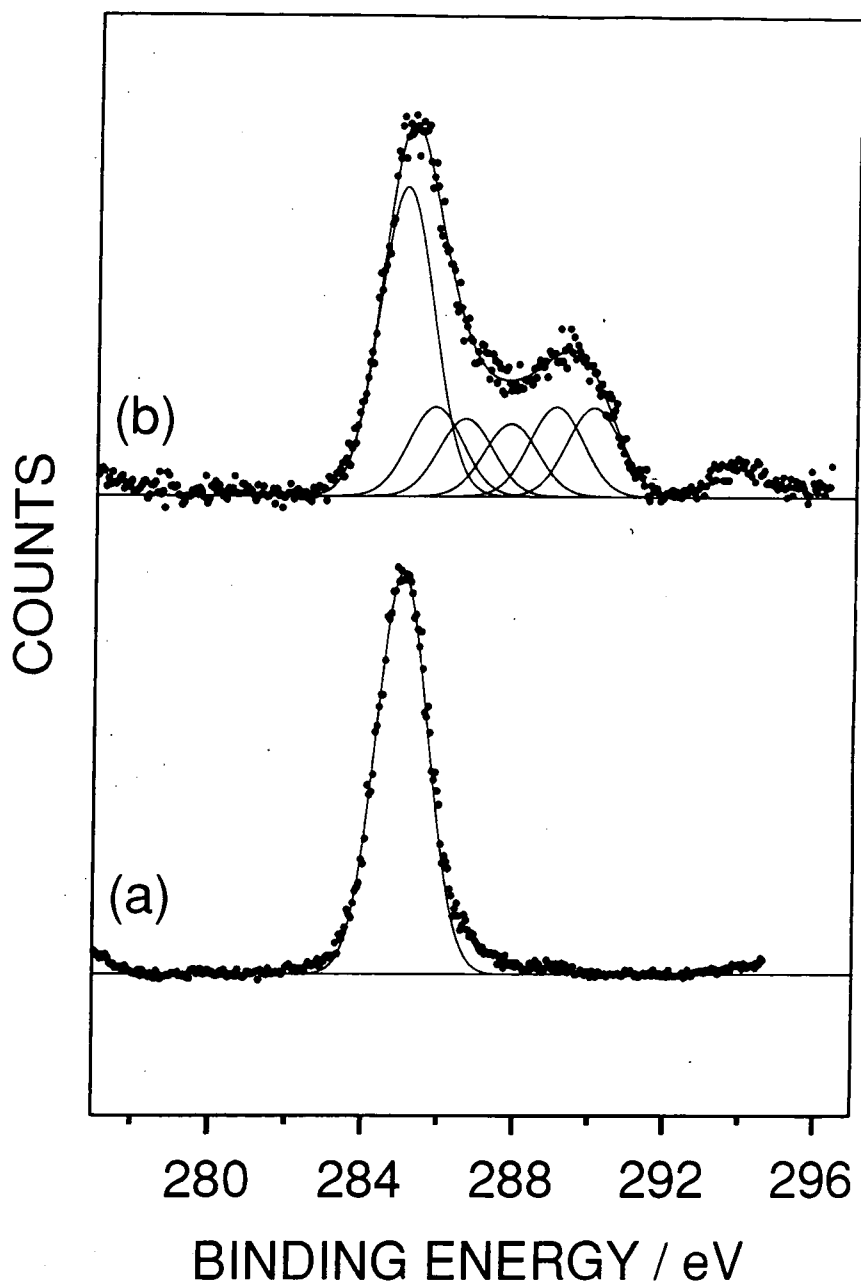
Figure 5:

Solution state proton NMR spectra of hexatriacontane crystals: (a) untreated; and (b) following 60 s silent discharge treatment.
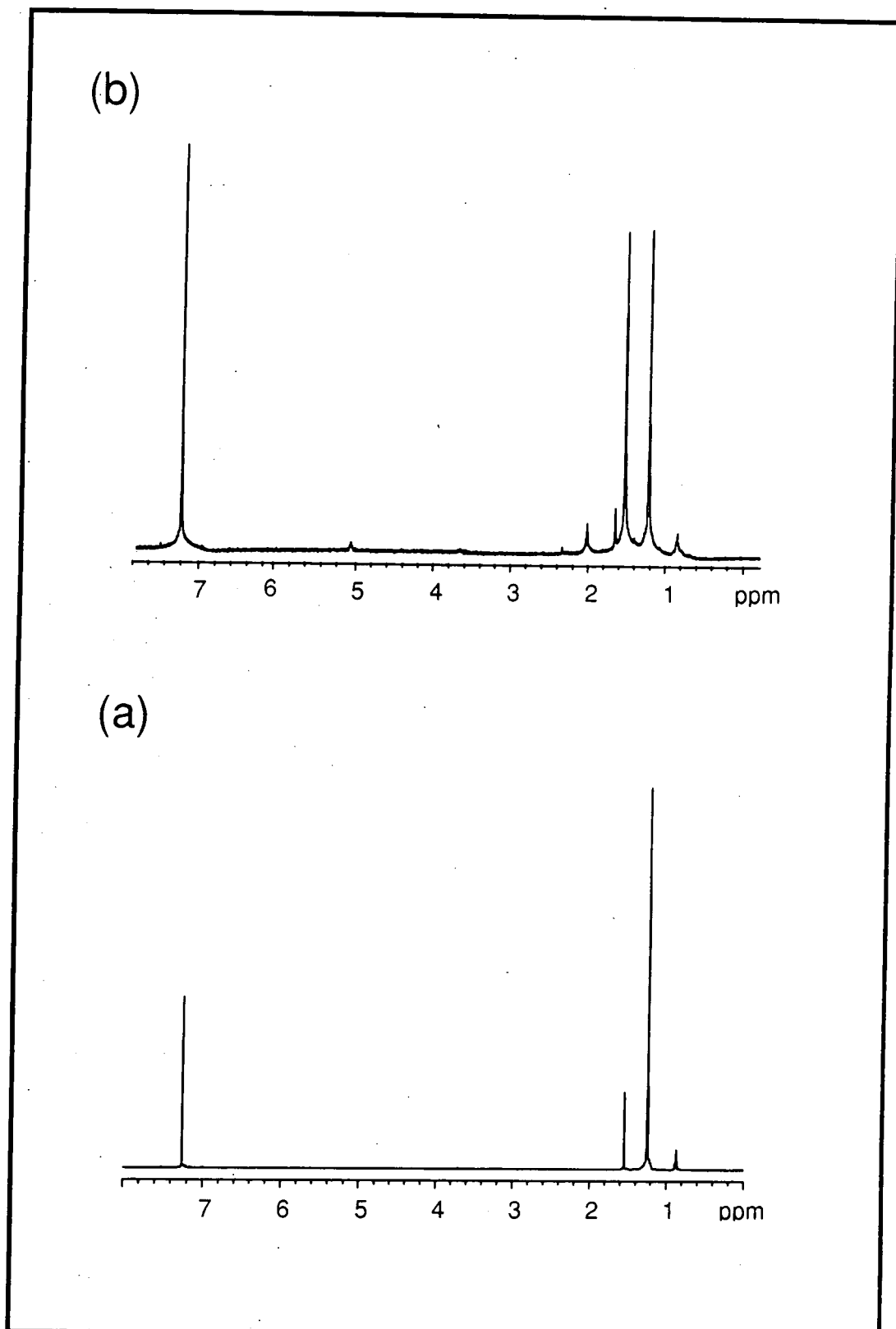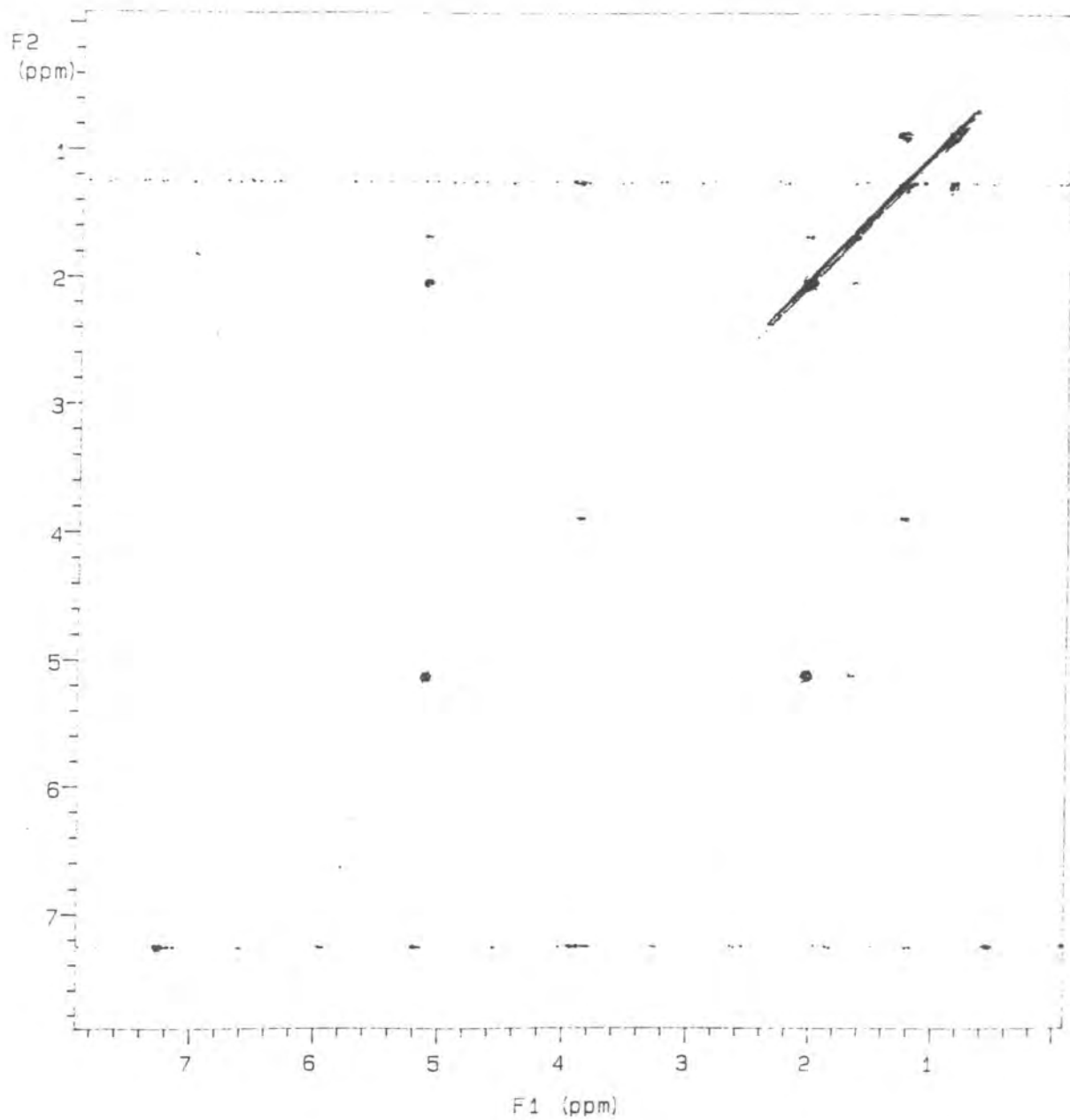
Figure 6:

COSY proton NMR spectrum of hexatriacontane crystals following 60 s silent discharge treatment.

4.4 DISCUSSION

Atomic force microscopy has shown that the surface of hexatriacontane crystals consists of an orthorhombic structure containing lattice spacings of 0.63 nm and 0.78 nm. This corresponds to the (001) surface of hexatriacontane crystals,[11] and therefore means that the hexatriacontane chains are all aligned perpendicular to the crystal surface, with the edges of each crystal exposing alkyl chain backbones.

A variety of species are known to be produced within an atmospheric pressure air dielectric barrier discharge,[19 20] these include: electrons, oxygen atoms, ozone, and ultraviolet radiation. Such a reactive medium can initiate polymer oxidation via chain scission, hydrogen abstraction, and oxygen attachment processes. It has previously been reported that H_2O, CO, CO_2 and H_2 gases are eliminated from the surface during low pressure oxygen plasma treatment of hexatriacontane[5,21,22]. In the present study, AFM analysis has shown that silent discharge treatment leads to a greater rate of degradation around the edges of the hexatriacontane crystals, rather than at the surface. This can be attributed to there being a greater rate of oxidative reaction along the backbone of hexatriacontane molecules than at the methyl end groups which are present on the (001) crystal surfaces. Distinct jagged edges are evident which have a tip angle of comparable magnitude to that associated with the bulk packing of hexatriacontane molecules.[3] Such jagged degradation features are most likely to nucleate from around edge dislocation centres, since these regions already possess a considerable level of lattice instability, Figure 7.

XPS and NMR analysis have shown that hexatriacontane molecules undergo chain oxidation and chain scission[23,24] during silent discharge treatment. This leads to the formation of carbon-carbon double bonds and a variety of oxygenated carbon centres. Hexatriacontane molecules will react with atomic oxygen, ozone, electron streamers, and UV photons from the silent discharge to produce free radical centres along the alkyl backbone. These can subsequently undergo further reaction to form oxidised carbon moieties, or lead to the formation of carbon-carbon double bonds via the disportionation of secondary radical centres[25], or hydrogen abstraction from a free radical chain end.[26].

4.5 CONCLUSIONS

Hexatriacontane crystals have been employed as a model system for high density polyethylene. Atmospheric silent discharge treatment in air is found to lead to localised oxidative degradation around the edges of hexatriacontane crystals and the formation of oxygenated and unsaturated carbon species.

Figure 7: Jagged edge formation during silent discharge treatment of hexatriacontane crystals (where $t_0 < t_1 < t_2 < t_3$).
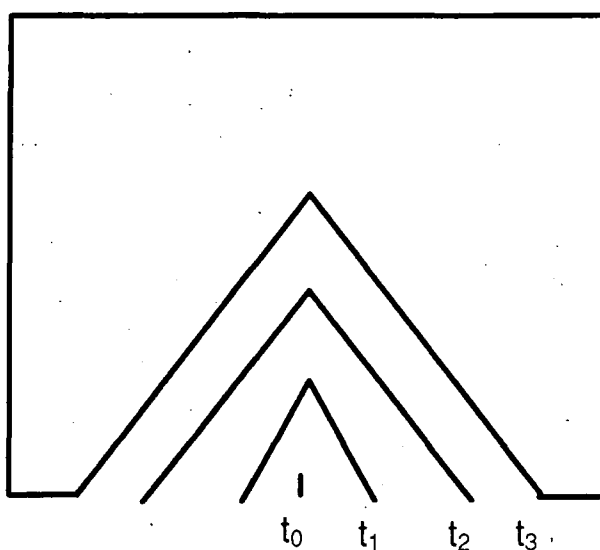
REFERENCES

1 . Andrade, J. D. In *Polymer Surface Dynamics*; Andrade, J. D. Ed.; Plenum: New York; 1988, Chapter 1.

2 . Pomlin-Epaillard, F.; Pomepui, B.; Brosse, J.-C.; *J. Polym. Sci., Polym. Chem. Ed.* **1993**, *31*, 2671.

3 . Simon, B.; Grassi, A.; Boistelle, R. *J. Cryst. Growth.* **1974**, *26*, 77.

4 . Rei Vilar, M.; Schott, M.; Pfluger, P. *J. Chem. Phys.* **92**, *1990*, 5722.

5 . Clouet, F.; Shi, M. K. *J. Appl. Polym. Sci.* **1992**, *46*, 1955.

6 . Pireaus, J. J.; Caudano, R. *Phys. Rev. B* **1977**, *15*, 2242.

7 . George, R. A.; Martin, D. H.; Wilson, E. G. *J. Phys. C* **1972**, *5*, 871.

8 . Carter, P. W.; Ward, M. D. *J. Am. Chem. Soc.* **1993**, *115*, 11521.

9 . Matsushige, K.; Hamano, T.; Horiuchi, T. *J. Cryst. Growth* **1995**, *146*, 641.

10 . Tengrotenhuis, E.; Vandereerden, J. P.; Hoogesteger, F. J.; Jenneskens, L. W. *Chem. Phys. Lett.* **1196**, *250*, 549.

11 . Boistelle, R.; Simon, B.; Pepe, G. *Acta Cryst. B* **1976**, *32*, 1240.

12 . Bramble, S. K.; Jackson, G. R. *J. Forensic Sci.* **1994**, *39*, 920.

13 . Watson, S. K. *Geophysics* **1993**, *58*, 835.

14 . Brigham, E. O. *The Fast Fourier Transform and its applications*; Prentice-Hall: New Jeresy, 1988; Chpater 11.

15 . Stocker, W.; Bar, G.; Kunz, M.; Moller, M.; Magnov, S. N.; Cantow, H. J. *Polym. Bulletin* **1991**, *26*, 215.

16 . Wang, Q. G.; Annis, B.; Wunderlich, B. *J. Polym. Sci., Polym. Phys. Ed.* **1994**, *32*, 2653.

17 . Zemlin, F.; Reuber, E.; Beckmann, E.; Zeitler, E.; Dorest, D. L. *Science* **1985**, *229*, 461.

18 . Derome, A. E. *Modern NMR Techniques for Chemistry Research*; Pergamon: Oxford, 1987.

19 . Eliasson, B.; Hirth, M.; Kogelschatz, U. *J. Phys. D: Appl. Phys.* **1987**, *20*, 1421.

20 . Eliasson, B.; Kogelschatz, U. *IEEE Trans. Plasma Sci.* **1991**, *19*, 309.

21 . Shi, M. K.; Clouet, F. *J. Appl. Polym. Sci.* **1992**, *46*, 2063.

22 . Shi, M. K.; Christoud, J.; Holl, Y.; Clouet, F. *J. Macromolecular Sci - Pure Appl Chem.* **1993**, *A30*, 219.

23 . Strobel, M.; Dunatov, C.; Strobel, J. M.; Lyons, C. S.; Perron, S. J.; Morgon, M. C. *J. Adhesion Sci. Technol.* **1989**, *3*, 321.

24 . Gerenser, L. J. *J. Adhesion Sci. Technol.* **1987**, *1*, 303.

25 . Ranby, B.; Rabek, J. F. *Photodegradation, Photo-oxidation and Photostabilization of Polymers*; Wiley: London; 1975.

26 . Adam, J. H.; Goodrich, J. E. *J. Polym. Sci., Polym. Phys. Ed.* **1979**, *13*, 333.

CHAPTER 5:
NON-EQUILIBRIUM PLASMA TREATMENT OF MISCIBLE
POLYSTYRENE / POLYPHENYLENE OXIDE BLENDS

5.1 INTRODUCTION

Economically it is much cheaper to just mix together two or more existing polymers, rather than having to develop a polymer for each new application. This process is not new.[1-3] For instance, the well known polystyrene / poly(2,6-dimethyl-1,4-phenylene oxide) miscible blend system finds widespread commercial use in the thermoplastics industry.[4-6] The surface characteristics of such polymer blend mixtures need not necessarily be a straightforward weighted average of the values known for the respective components. Indeed, this can offer scope for the tailoring of important surface properties, e.g. thermal behaviour, adhesion, gas barrier, electrical conductivity, etc. In this study, the surface chemistry and topography of polystyrene / polyphenylene oxide miscible blend mixtures is investigated following low pressure glow discharge and atmospheric pressure dielectric barrier discharge non-equilibrium plasma modification. In particular, the issue of whether oxidative plasma treatment of this miscible blend system results in just a straightforward average of the changes seen for the respective parent polymers, or if there exists some unusual physicochemical behaviour at the surface is addressed.
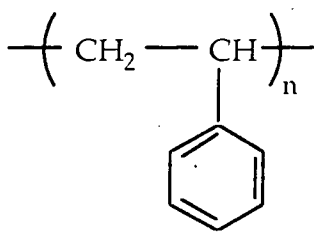
Polystyrene (PS)
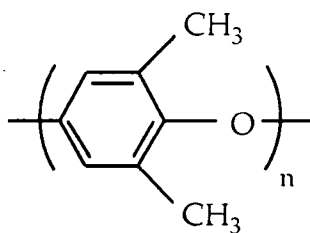
Poly (2,6-dimethyl 1,4-phenylene oxide (PPO)

5.1.1 Factors affecting Polymer - Polymer Miscibility

One of the major drawbacks of blending is the relatively few polymers that can form miscible blends with each other. Miscible polymers are polymers that when blended together form a single phase.

The qualitative thermodynamic argument which limits the miscibility of polymers derives from the contribution of the entropy of mixing (ΔS_{mix}) to the free energy of mixing expression.[7]

$$\Delta G_{mix} = \Delta H_{mix} - T\Delta S_{mix} \qquad (5.1)$$

Where ΔG_{mix} is the free energy of mixing and ΔH_{mix} is the heat of mixing. Generally ΔH_{mix} is positive and although ΔS_{mix} is also generally positive, the entropy contribution is small due to the large molecular weights of the polymers.[8] This means that ΔG_{mix} tends to be positive hence the polymers remain immiscible. Even when ΔG_{mix} is negative, the mixing of the polymers will only occur if the free energy of mixing is lower than the free energy of the individual polymer components.[7] Generally two polymers will remain immisible unless there is a driving force to lower the free energy of mixing.

In order to lower the free energy of mixing ΔH_{mix} has to be reduced. In most cases this is done by specific interactions between the two polymers,[7,9] so that ΔH_{mix} now has two contributions:

$$\Delta H_{mix} = \Delta H_{mix}^{(dis)} + N\Delta H_{mix}^{(sp)} \qquad (5.2)$$

where $\Delta H_{mix}^{(dis)}$ represents the dispersive forces between the two polymers (generally positive) and $\Delta H_{mix}^{(sp)}$ relates to the energy of interaction between the two polymers (generally negative) and N is the number of interactions between the two polymers. Increasing the interactions will reduce the free energy and the miscibility of the polymers will be enhanced. These interactions range from relative week interactions (such as dipole - dipole interactions) to very strong interactions (hydrogen bonding).

5.1.2 Review of the Surface Studies into Polymer Blends

Surface studies of polymer blends originated in the 1980's. In the study of the surface properties of polymer blends often uses conventional surface sensitive techniques, such as XPS, SSIMS and ATR-IR, can be to determine the surface characteristics of polymer blends.

X-ray Photoelectron Spectroscopy (XPS) has been used to determine the surface composition of both immiscible[10,11] and miscible[12] polymer blends produced from both solvent cast[13] and injection moulded[14] methods. Studies of immiscible polymer blends, such as polystyrene / poly (ethylene oxide)[10] and polycarbonate / poly (dimethyl siloxane)[11] blends, have shown that surface enrichment occurs of one component of the polymer blend. This can be accounted for by considering the surface energy of the individual polymers. Any system will act to lower its surface energy. This means, in the case of polymer blends, that surface enrichment of the component with the lowest surface energy will occur, so that the system has an overall lower surface energy. For example, polystyrene segregates in the case of polystyrene / poly (ethylene oxide) blends and poly (dimethyl siloxane) segregates in the case of polycarbonate / poly (dimethyl siloxane) blends. For blends that are in their 'equilibrium' state then the surface should be exclusively occupied by the constituent of lowest surface energy.[12] However rarely is the equilibrium state reached, due to the molecular rearrangements this would entail. XPS studies have also been performed on miscible polymer blends, such as polystyrene / poly (vinyl methyl ether)[12] blends. Again surface enrichment is seen from the component with the lowest surface energy.

However there are limitations in using XPS to study the surface compositions of polymer blends. In order for XPS to be effective there must be an elemental or at least a functional group difference between the two components of the polymer blend. Also the sample depth of XPS is in the order of several nanometers and the surface composition obtain from XPS is an average of the blend composition in this region, and not necessarily just at the surface.

Static secondary ion mass spectrometry (SSIMS) is used in the study of polymer blends.[15] The main advantage of using SSIMS over XPS is that the SSIMS sample

depth is much smaller than for XPS (approximately 1 nm) and can determine the surface composition without an elemental difference between the components of the blend. For example SSIMS has successfully been used to determine the surface composition of PS / deuterated-PS blends by detecting $C_7H_7^+$ and $C_7D_7^+$ ions.[16] However SSIMS cannot be used directly to determine the surface composition because the intensity of a SSIMS peak is dependant, to several orders of magnitude, on several factors. There are three main factors in contributing to the SSIMS peak intensity.[17] The first is the chemical bonding and environment that a ion-fragment originates from and the second is instrument specific artefacts. The SSIMS spectrometer is usually tuned before a sample can be analysed, which normally involves maximising a specific peak and there is no guarantee that the maximised signal is the global maximum. The finial problem involves sample charging, which is usually overcome by flooding the sample with electrons. However, different components of a blend may have different levels of charging. The second and third contributions can be overcome by using a time of flight spectrometer (TOF) and a self compensating sample charge, respectively. The first problem, is more difficult to solve. A common way of overcoming this problem is to use relative peak intensities (RPI). Recently the surface compositions of polycarbonate/polystyrene (PC/PS) blends were investigated using both XPS and TOF-SSIMS using the RPI method and the results were found to be comparable.[17] SSIMS can also give spatial information on polymer blends. Imaging SSIMS gives the spatial information from a specific ion, and can be used to obtain the surface blend morphology[18].

Another technique that is often used in the surface studies of polymers is attenuated total reflectance Fourier transform infra red spectroscopy (ATR-FTIR). However ATR-FTIR has had a limited role in the study of the surface composition of polymer blends. ATR-FTIR effectiveness is limited by its rather large sample depth (of the order several μm) and that the intensity of the peaks and the sample depth are both dependant on the wavelength of the peak. It is then difficult to obtain definite quantitative information from ATR-FTIR.

5.2 EXPERIMENTAL

5.2.1 Sample Preparation

Thin films of polystyrene (Aldrich; M_w = 280,000) / polyphenylene oxide (Aldrich; M_w = 244,000) polymer blends were prepared by spin coating from a 5% w/v chloroform solution onto glass slides. All blend compositions are quoted in terms of percentage weight. Visual examination indicated that the films were completely transparent, with no clouding, irrespective of the blend composition; this can be taken as being consistent with a single phase polymer blend, since any phase separation should lead to light scattering.[19]

5.2.2 Non-equilibrium Plasma Treatment

Low pressure oxygen glow discharge modification of the polymer blend films was carried out in a cylindrical electrodeless reactor, as described in chapter 2. The experimental procedure is the same as chapter 2 and will not be repeated here. Plasma treatments were carried out at 10 W power for 60 s in all cases. This was found to result in a limiting level of surface modification.

Atmospheric silent discharge air plasma treatments were carried out for a duration of 120 s using a home built parallel plate dielectric barrier discharge reactor operating at 3 kHz, 11 kV, with an electrode gap of 3.00 ± 0.05 mm as described in chapter 3.

Subsequent washing experiments of both types of plasma treated blend films were carried out using a 50 / 50 isopropanol / cyclohexane polar / non-polar solvent mixture (neither polystyrene nor polyphenylene oxide are soluble in either of these solvents at room temperature).[20]

5.2.3 Sample Analysis

A Kratos ES300 electron spectrometer equipped with a MgKα source (1253.6 eV) and a concentric hemispherical analyser was used for XPS surface analysis of the

polymer blend surfaces before and following plasma treatment. The ES 300 electron spectroscope is described in chapter 2.

A Digital Instruments Nanoscope III atomic force microscope was used to examine the topographical nature of the polymer blend surfaces prior to and immediately following electrical discharge exposure. All of the AFM images were acquired in air using the Tapping mode, and are presented as unfiltered data. RMS roughness values were obtained from unfiltered images.

5.3 RESULTS

5.3.1 X-ray Photoelectron Spectroscopy

Only carbon and oxygen XPS lines were evident for untreated, low pressure oxygen plasma treated, and atmospheric silent discharge treated polymer blends. The C(1s) XPS spectrum for each blend mixture was peak fitted as described in chapter 2. Except that an additional peak at 291.6 eV with a different FWHM, was fitted. This peak corresponded to the π - π^* shake-up satellite associated with phenyl ring centres.[21] Clean polystyrene exhibited a main peak at a C(1s) binding energy of 285.0 eV along with a π - π^* transition satellite. The O/C ratio for untreated polyphenylene oxide was measured to be 0.14 ± 0.02, this in good agreement with the theoretical value of 0.13 expected from the parent polymer repeat unit. A linear variation in O/C ratio was found for the blend mixtures with increasing polyphenylene oxide concentration, Figure 1. This was accompanied by a corresponding change in shape of the C(1s) envelope. Figure 2.

Low pressure oxygen plasma treatment of all the polymer blend mixtures resulted in oxygen incorporation at the surface, Figure 1. If one takes into account the oxygen present beforehand due to polyphenylene oxide, then both of the parent polymers appear to be oxidised to a similar extent. The O/C ratio varies in approximately a linear fashion with increasing polyphenylene oxide concentration, this is indicative of no preferential oxidation or etching of either blend component. C(1s) peak fitted XPS spectra of plasma treated blend mixtures are shown in Figure 3(a). Washing of these glow discharge modified polystyrene / polyphenylene oxide blends in a cyclohexane / isopropanol solvent mixture resulted in a decrease in the amount of oxygen present at the surface. Figures 1

and 3(b). This suggests that low pressure oxygen plasma treatment generates low molecular weight oxidised material (LMWOM) which can be washed off. Interestingly, the trend seen in the O/C ratio during low pressure oxygen plasma treatment is reversed on solvent washing, with polystyrene retaining a greater proportion of its incorporated oxygen species compared to polyphenylene oxide.

Atmospheric silent discharge treatment of the miscible blend mixtures also exhibits a linear rise in the O/C ratio with increasing polyphenylene oxide concentration. However the rate of change with blend composition is markedly greater compared to the untreated and low pressure oxygen plasma treated polymer blends, Figure 1. C(1s) peak fitted XPS spectra for silent discharge treated polymer blend mixtures reflect this linear variation, Figure 4(a). Solvent washing of the silent discharge treated polystyrene / polyphenylene oxide blends removed a significant amount of modified polymeric material, Figures 1 and 4(b). In this case the trend in O/C ratio did follow the behaviour for the unwashed case, although it is clearly evident that modified polyphenylene oxide material is more readily removed in comparison to oxygenated polystyrene. Contrary to low pressure oxygen plasma treatment, washing of atmospheric dielectric barrier discharge treated blend surfaces did not completely remove the oxidised polyphenylene oxide species.

Figure 1:

Variation in the O/C XPS ratio for the various treatments (the unshaded symbols correspond to solvent washing).
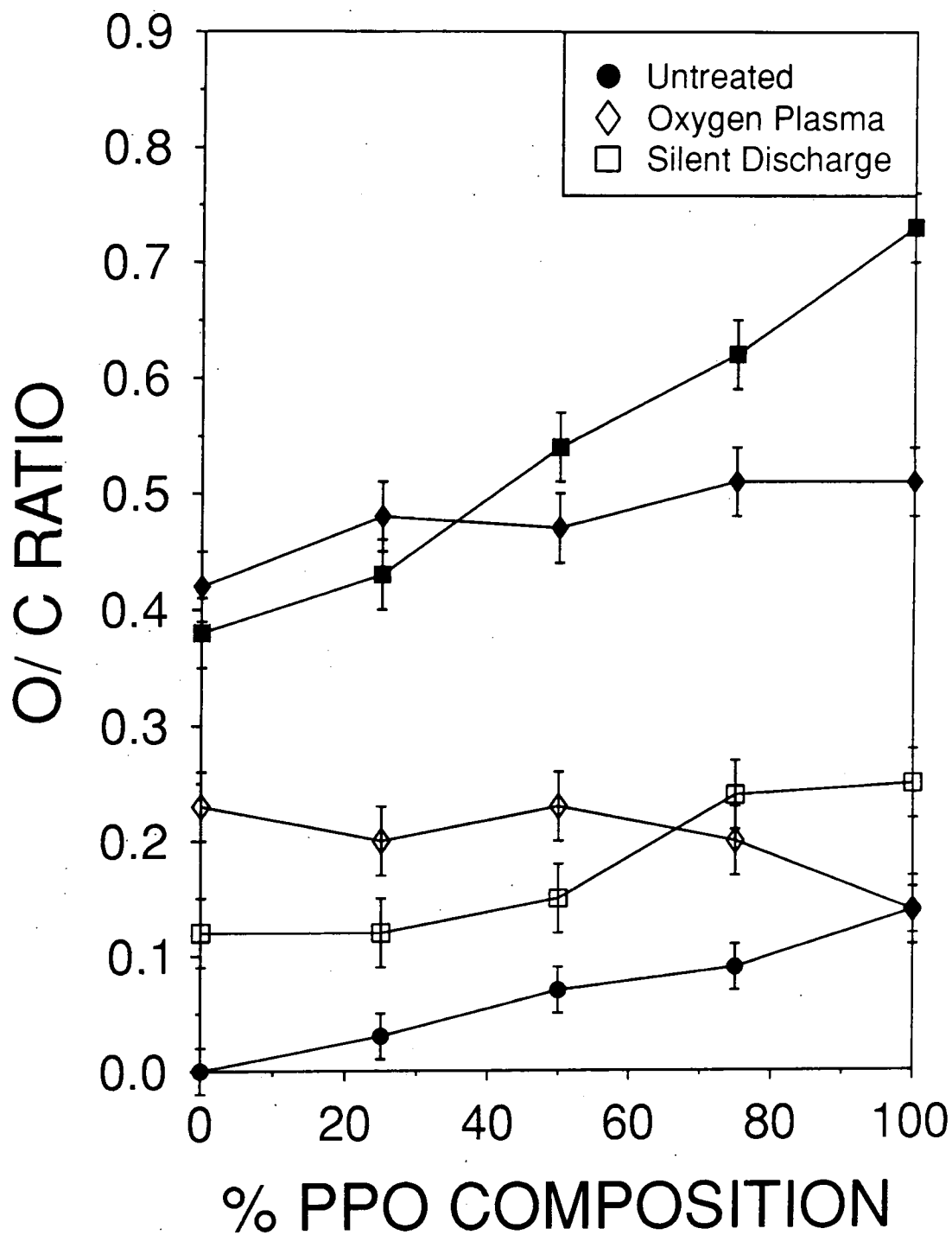
Figure 2:

C(1s) peak fitted spectra for untreated polystyrene / polyphenylene oxide blend mixtures with increasing polyphenylene oxide content.
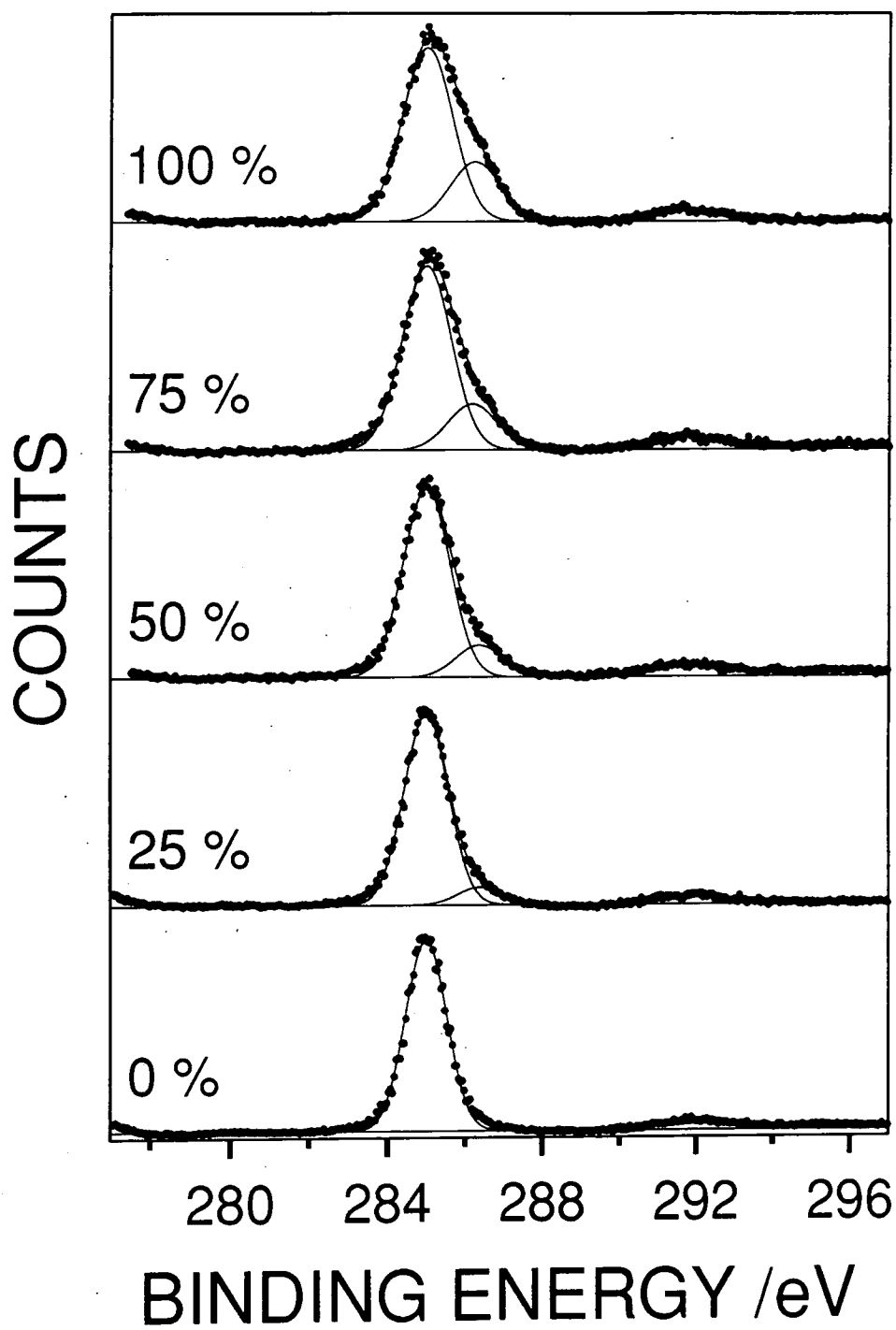
Figure 3(a):

C(1s) XPS peak fitted spectra for low pressure oxygen plasma treated PS/PPO polymer blends with increasing polyphenylene oxide content.
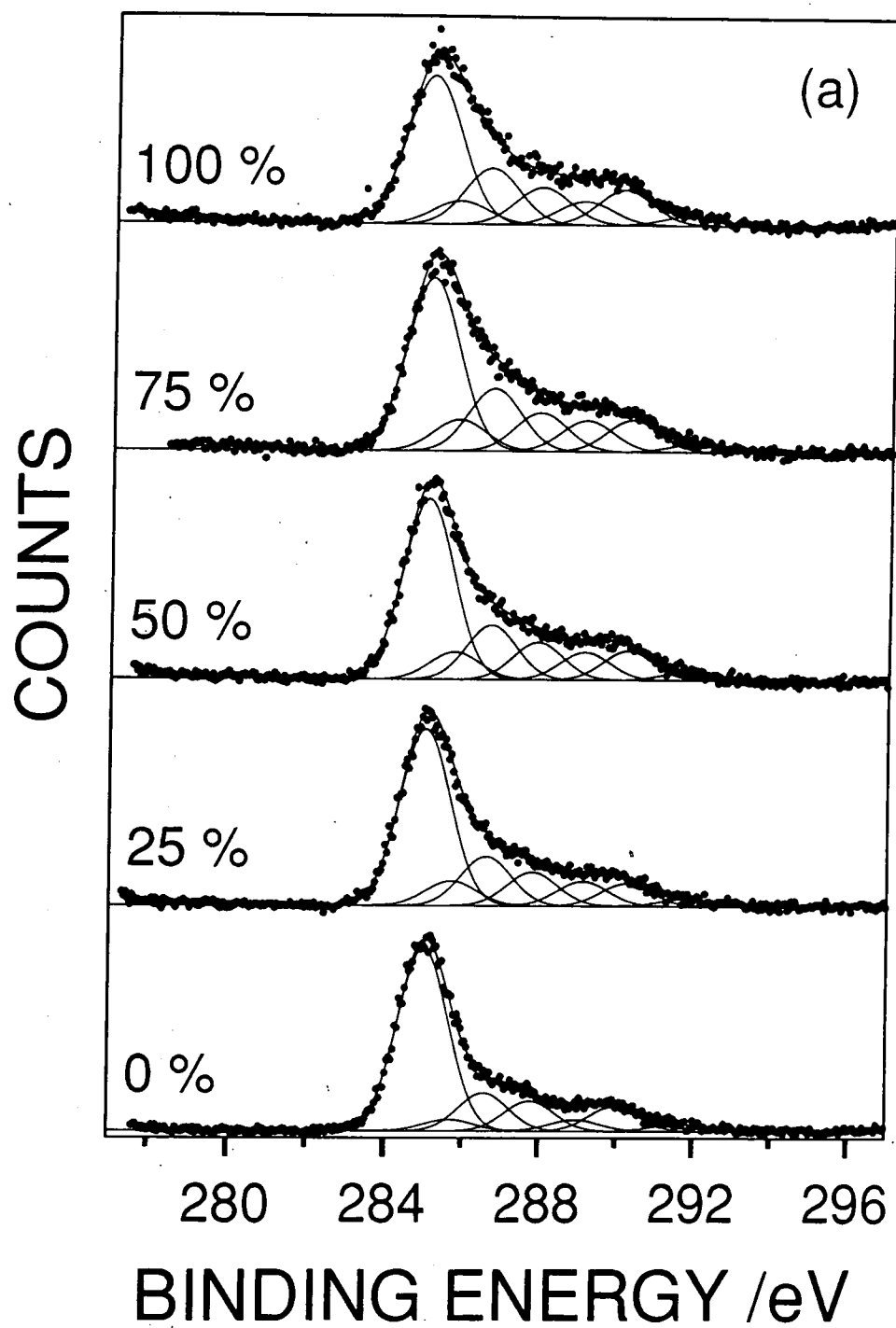
Figure 3(b):

C(1s) XPS peak fitted spectra for low pressure oxygen plasma treated PS/PPO polymer blends followed by solvent washing, with increasing polyphenylene oxide content.
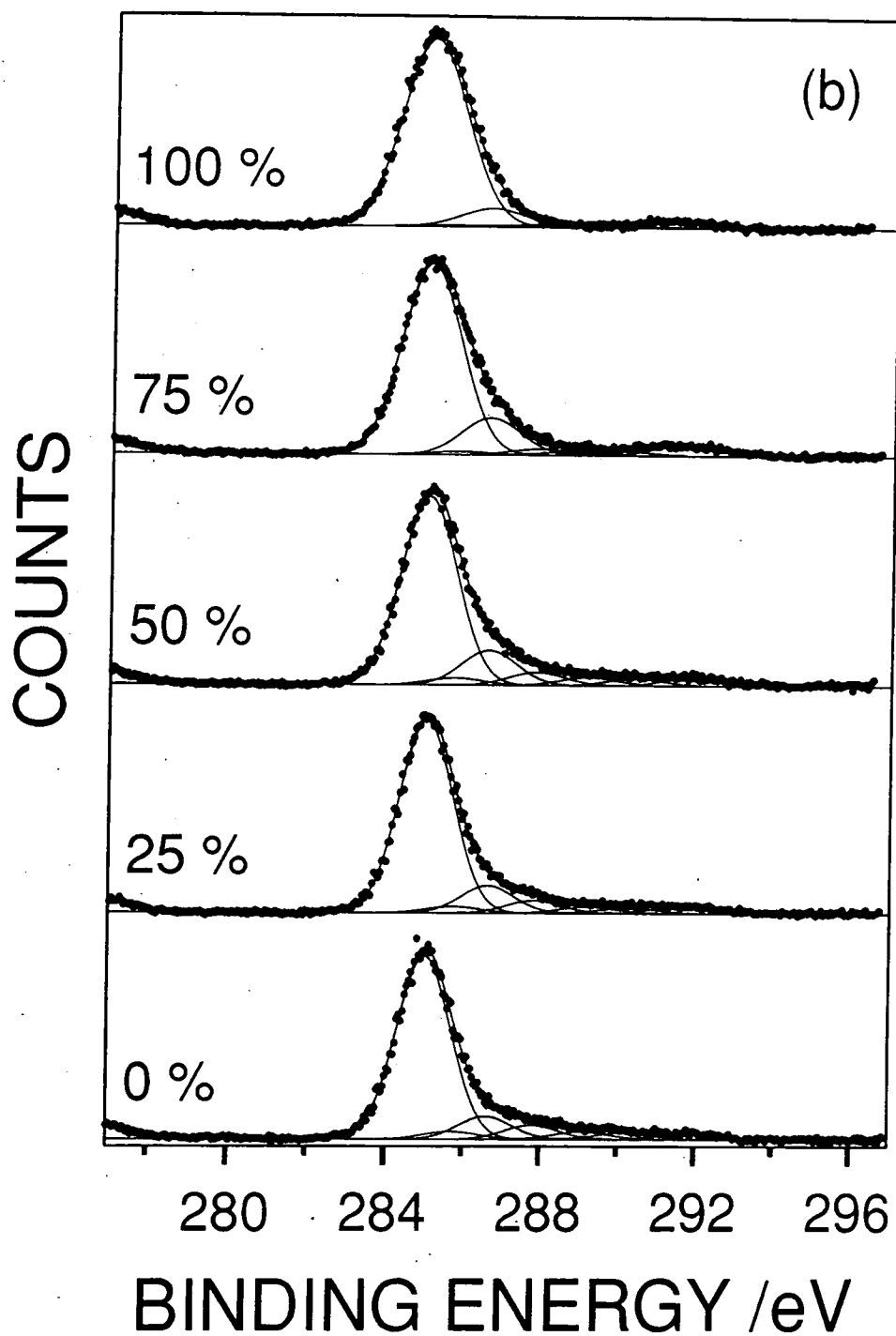
Figure 4(a):

C(1s) XPS peak fitted spectra for atmospheric pressure silent discharge treated PS/PPO
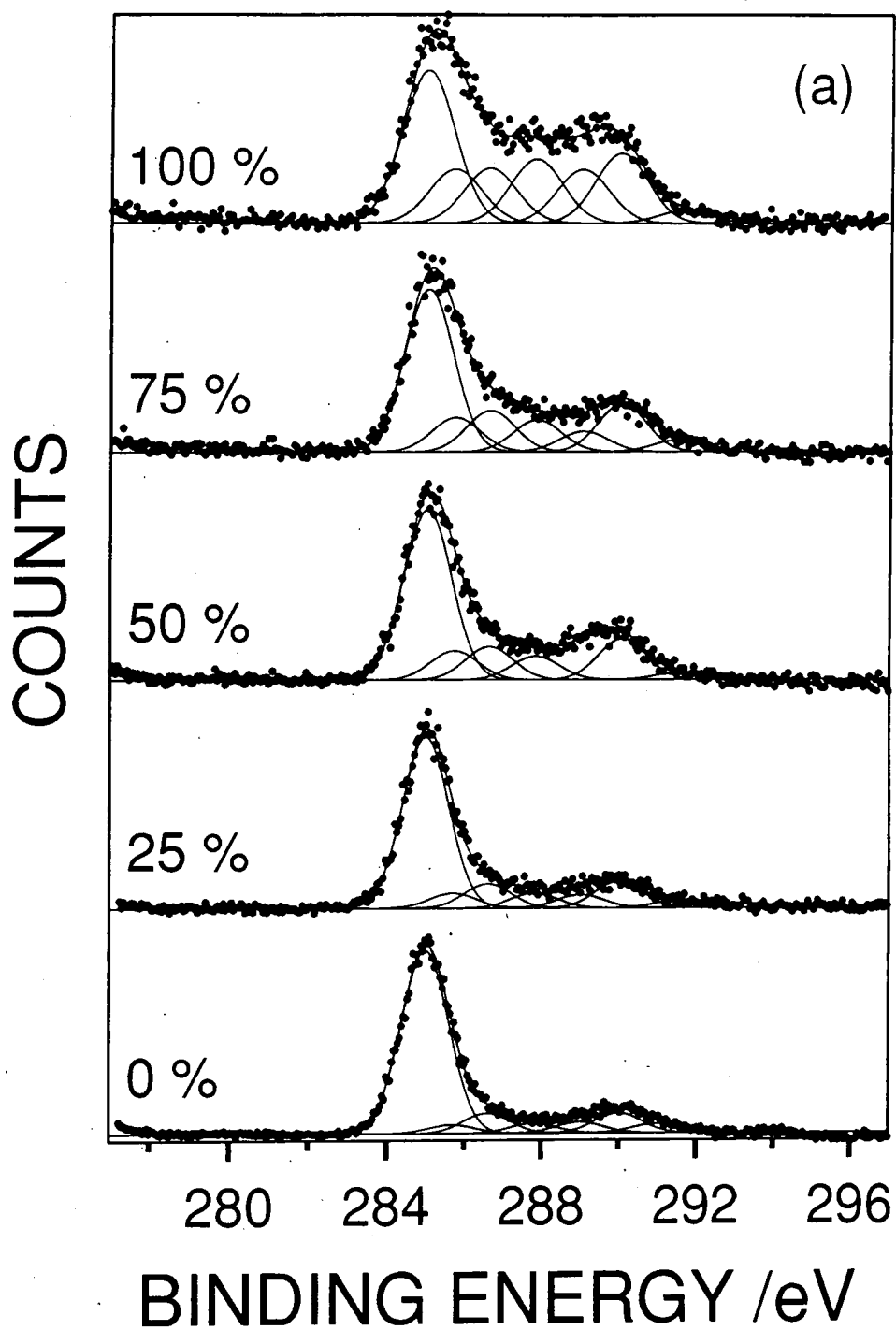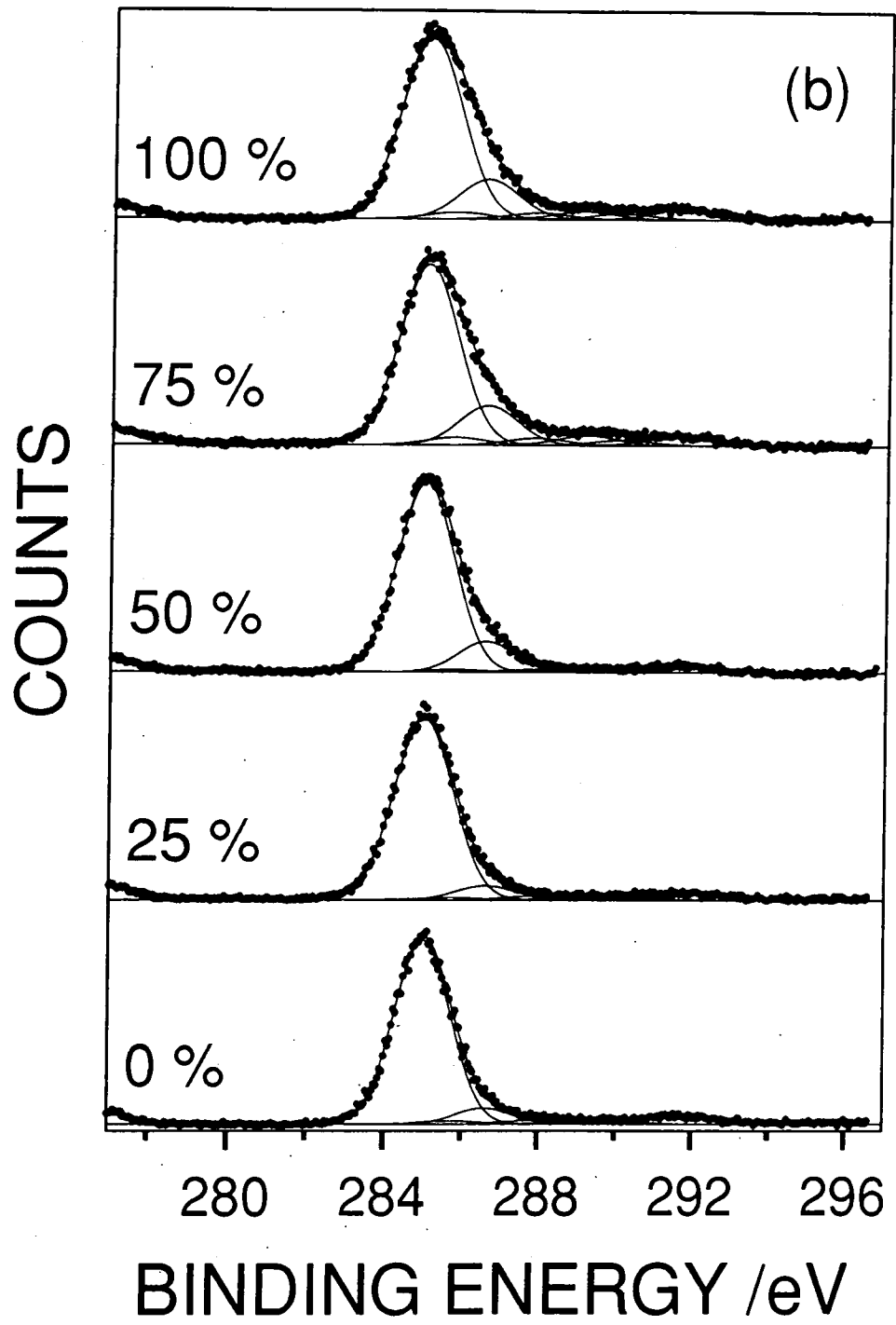polymer blends with increasing polyphenylene oxide content.

Figure 4(b):

C(1s) XPS peak fitted spectra for atmospheric pressure silent discharge treated PS/PPO polymer blends followed by solvent washing, with increasing polyphenylene oxide content.

5.3.2 Atomic Force Microscopy

Polystyrene exhibits a fine granular surface structure, whilst polyphenylene oxide appears to be coarser in texture. Figure 5 and Table 1. Therefore the surface morphology of spin coated films is influenced by the polymer itself as well as by the preparation technique. AFM micrographs of the polystyrene / polyphenylene oxide blends taken on a 10 mm scale showed no evidence of any phase separation occurring at the surface. Increasing the polyphenylene oxide concentration in the blend mixtures leads to the gradual collapse of the fine granular polystyrene morphology.

Low pressure oxygen plasma treatment resulted in the formation of globular features which increased in size with polyphenylene oxide content. Figure 6. This was accompanied by a loss of the original blend surface texture, Table 1. Solvent washing of the low pressure plasma treated polymer blend surfaces resulted in an increase in surface roughness Figure 6 and Table 1. Atmospheric silent discharge treatment of polyphenylene oxide and polystyrene also produced globular features, Figure 7. The average globular feature size being much greater for polyphenylene oxide than for polystyrene. Washing of the silent discharge treated polymer blend surfaces removed the large globular features to leave behind a smoother surface (this is contrary to what was observed during low pressure oxygen glow discharge modification), Figure 7 and Table 1.

Table 1: Summary of RMS surface roughness measurements.

Composition / % PPO	Untreated / nm	Low Pressure Plasma Treated / nm		Atmospheric Silent Discharge Treated / nm	
		Unwashed	Washed	Unwashed	Washed
0	0.26	0.56	0.74	3.2	2.9
25	0.22	0.35	0.51	5.2	0.81
50	0.21	0.32	0.71	5.0	1.1
75	0.20	0.37	0.87	5.2	0.76
100	0.34	0.61	0.20	14.3	0.51

Figure 5(a): AFM image of untreated polystyrene.

x = 0.2 μm / div
z = 20 nm / div

μm

0.2   0.4   0.6   0.8

137
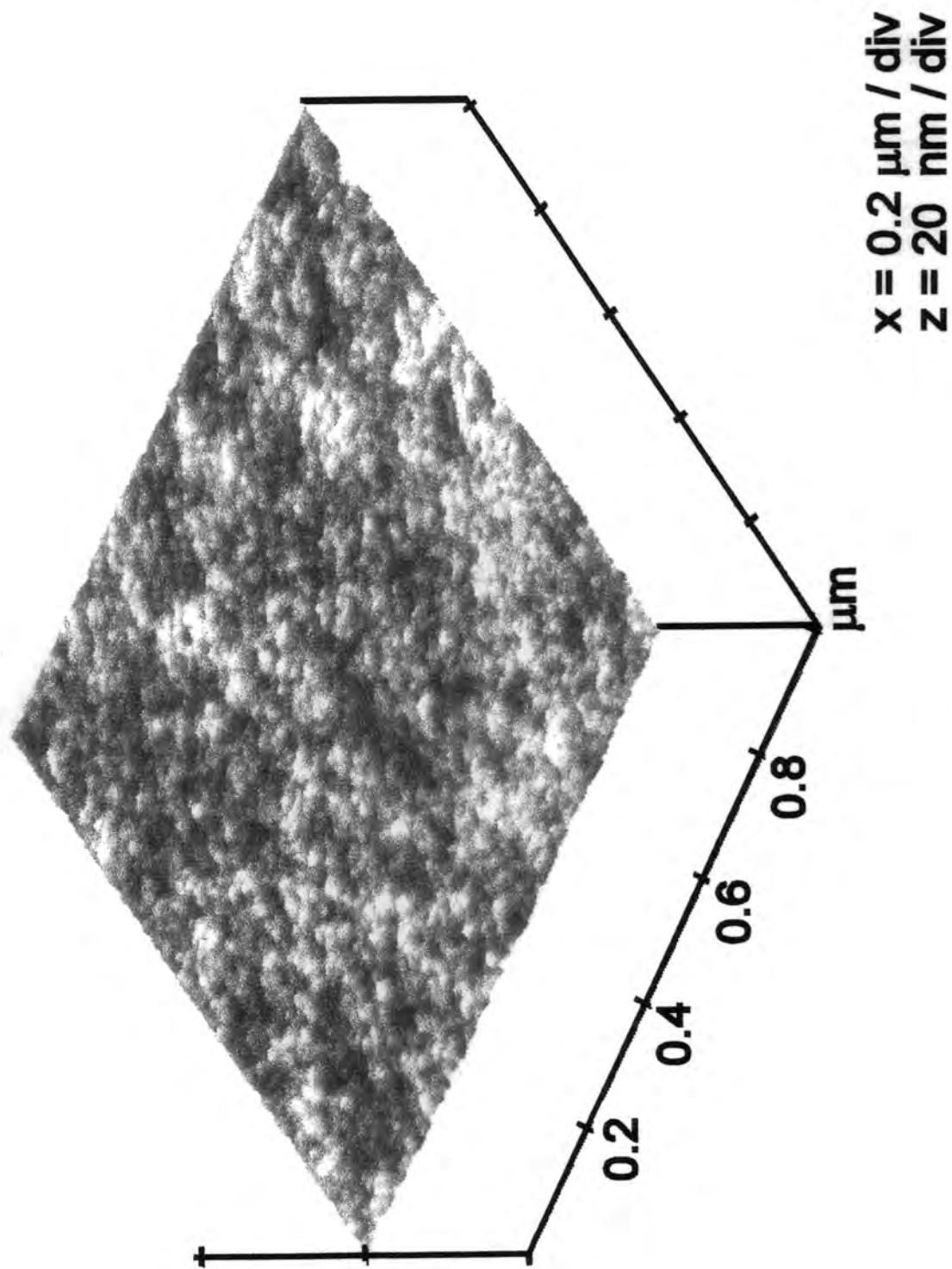
Figure 5(b): AFM image of untreated 50/50 PPO/PS blend.

x = 0.2 μm / div
z = 20 nm / div
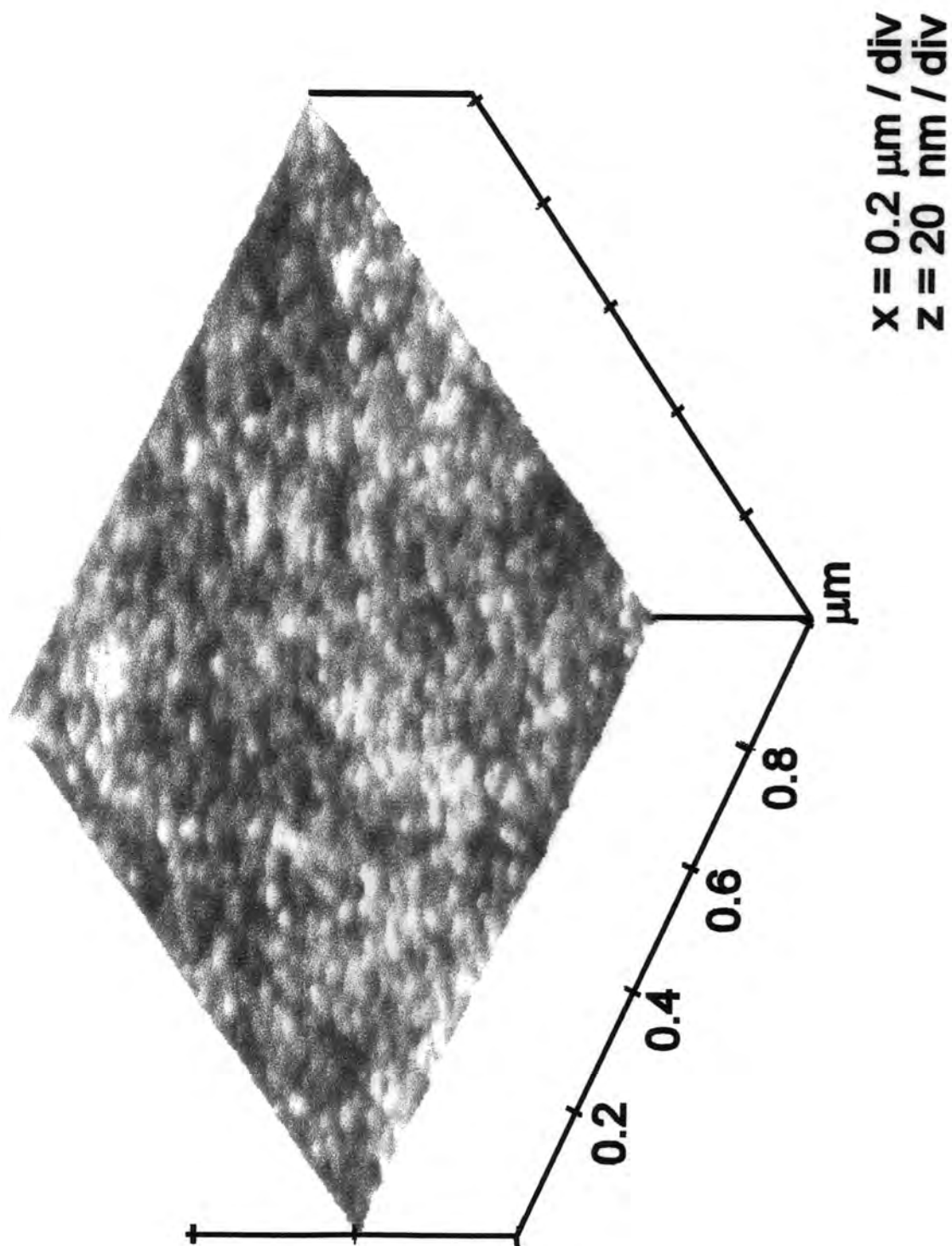
Figure 5(c): AFM image of untreated pure poly phenylene oxide.

x = 0.2 µm / div
z = 20 nm / div

0.2 0.4 0.6 0.8

µm

139
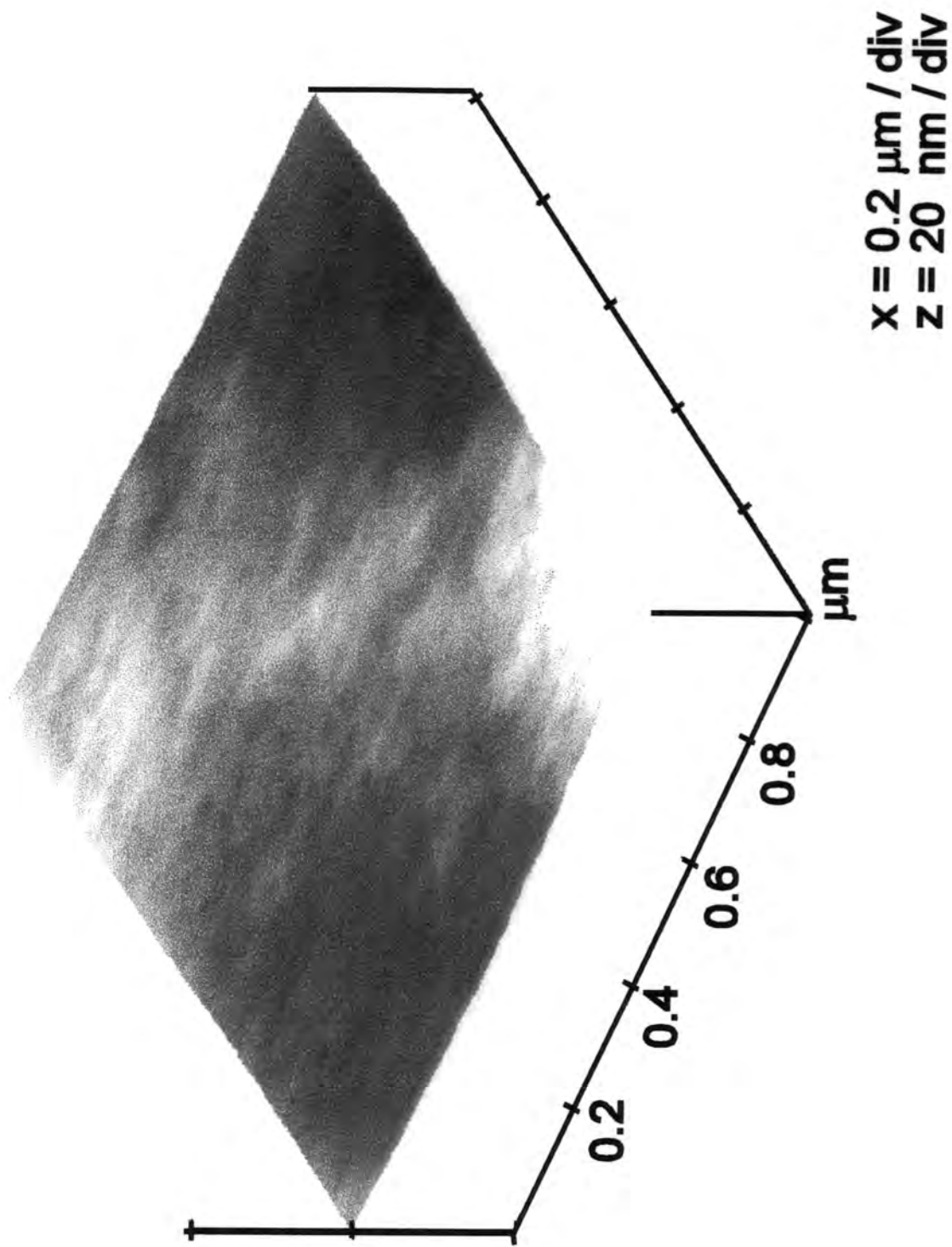
Figure 6(a): AFM image of oxygen plasma treated polystyrene.

x = 0.2 μm / div
z = 20 nm / div
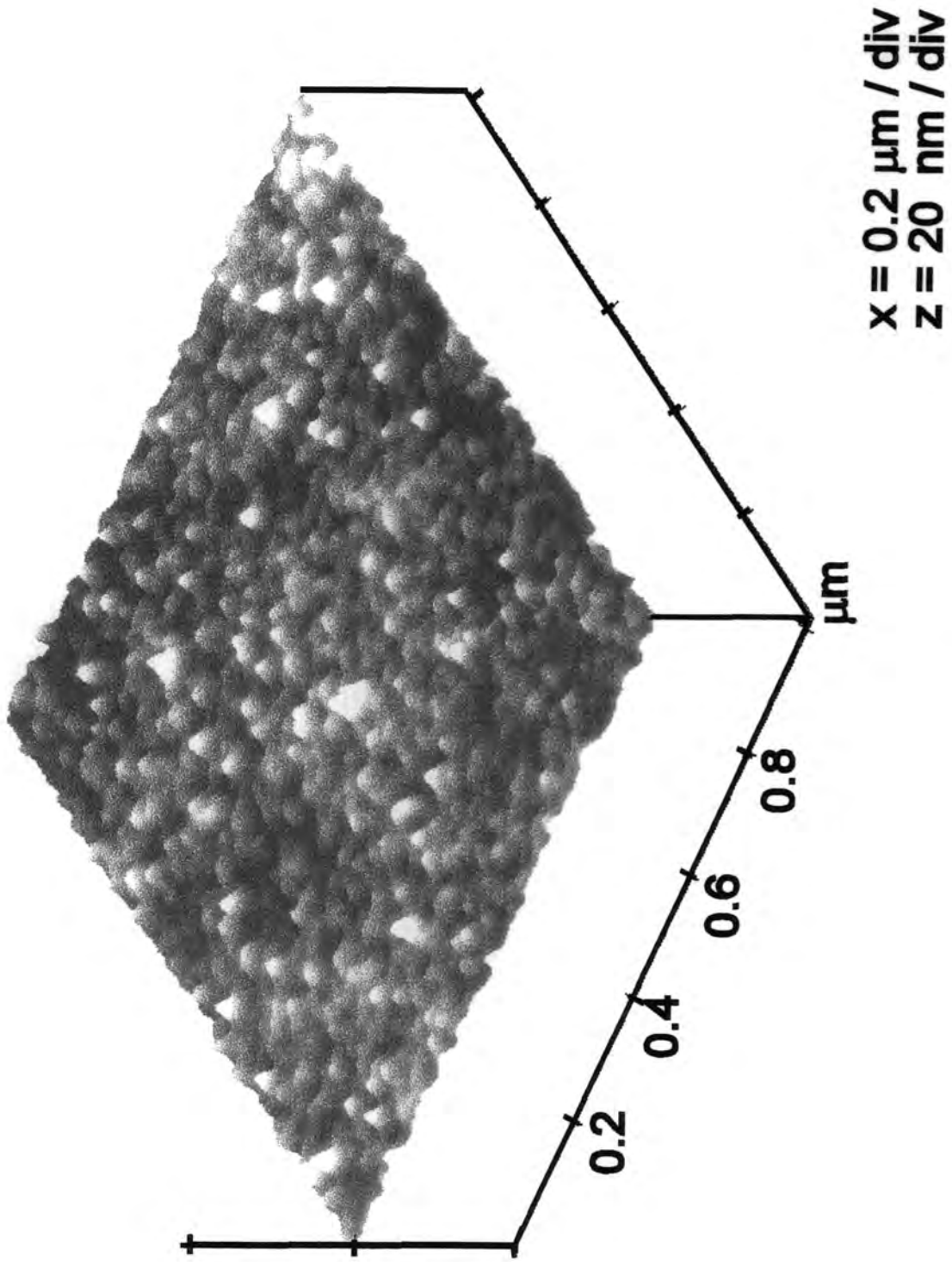
Figure 6(b): AFM image of oxygen plasma treated 50/50 PPO/PS blend.

x = 0.2 μm / div
z = 20 nm / div

μm

0.2 0.4 0.6 0.8
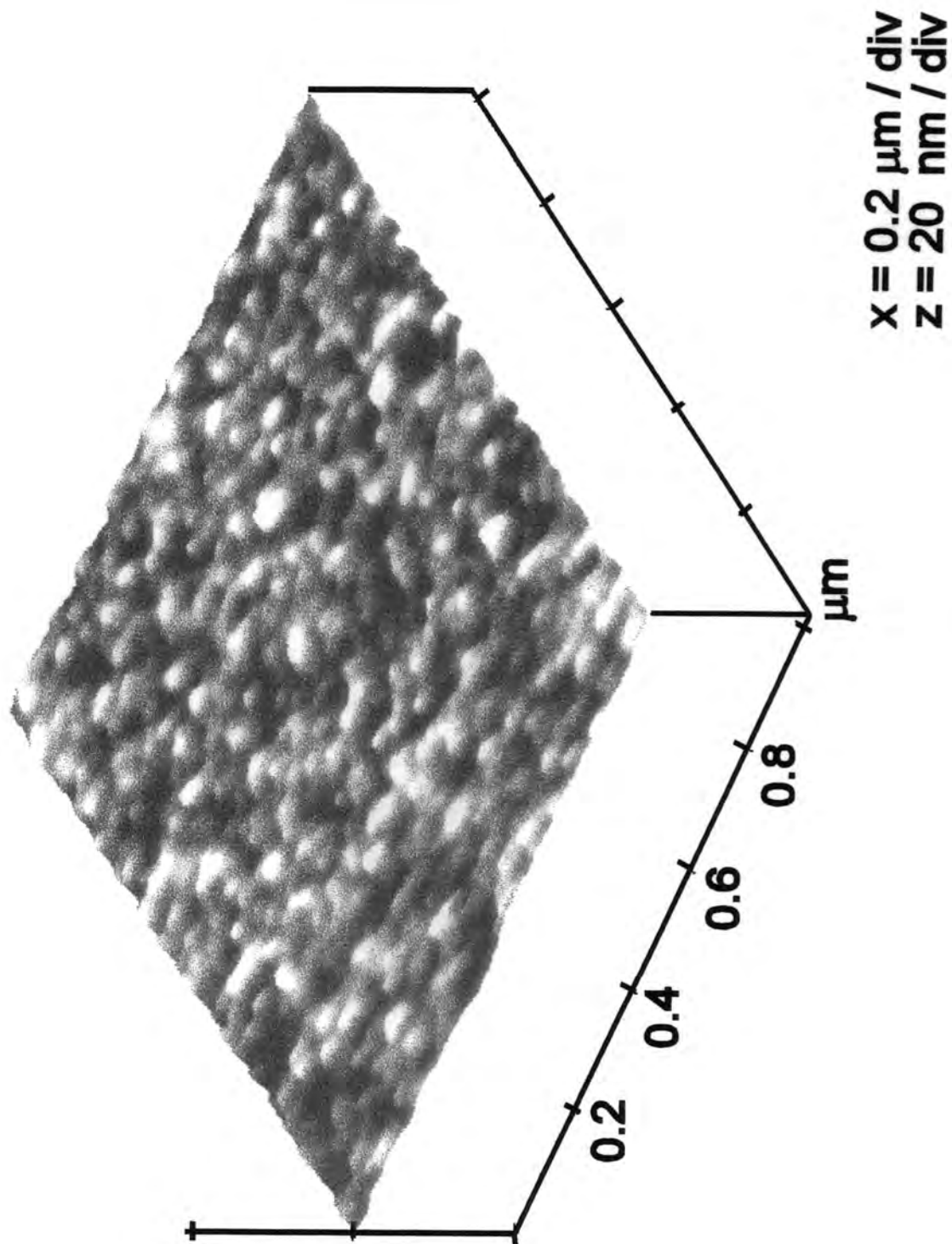
Figure 6(c): AFM image of oxygen plasma treated pure polyphenylene oxide.

x = 0.2 μm / div
z = 20 nm / div
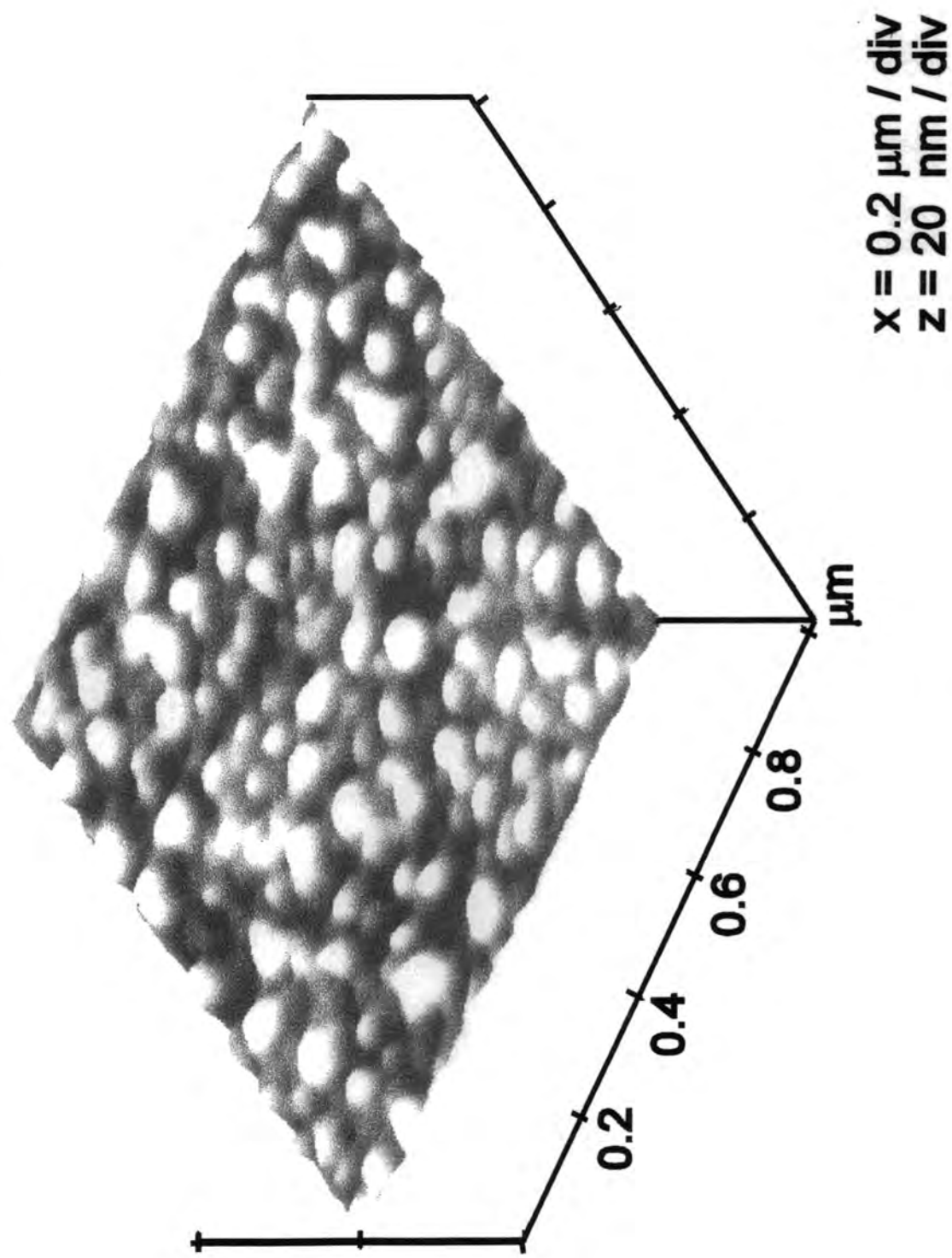
Figure 6(d) AFM image of oxygen plasma treated 50/50 PPO/PS blend followed by solvent washing.

x = 0.2 μm / div
z = 20 nm / div

143
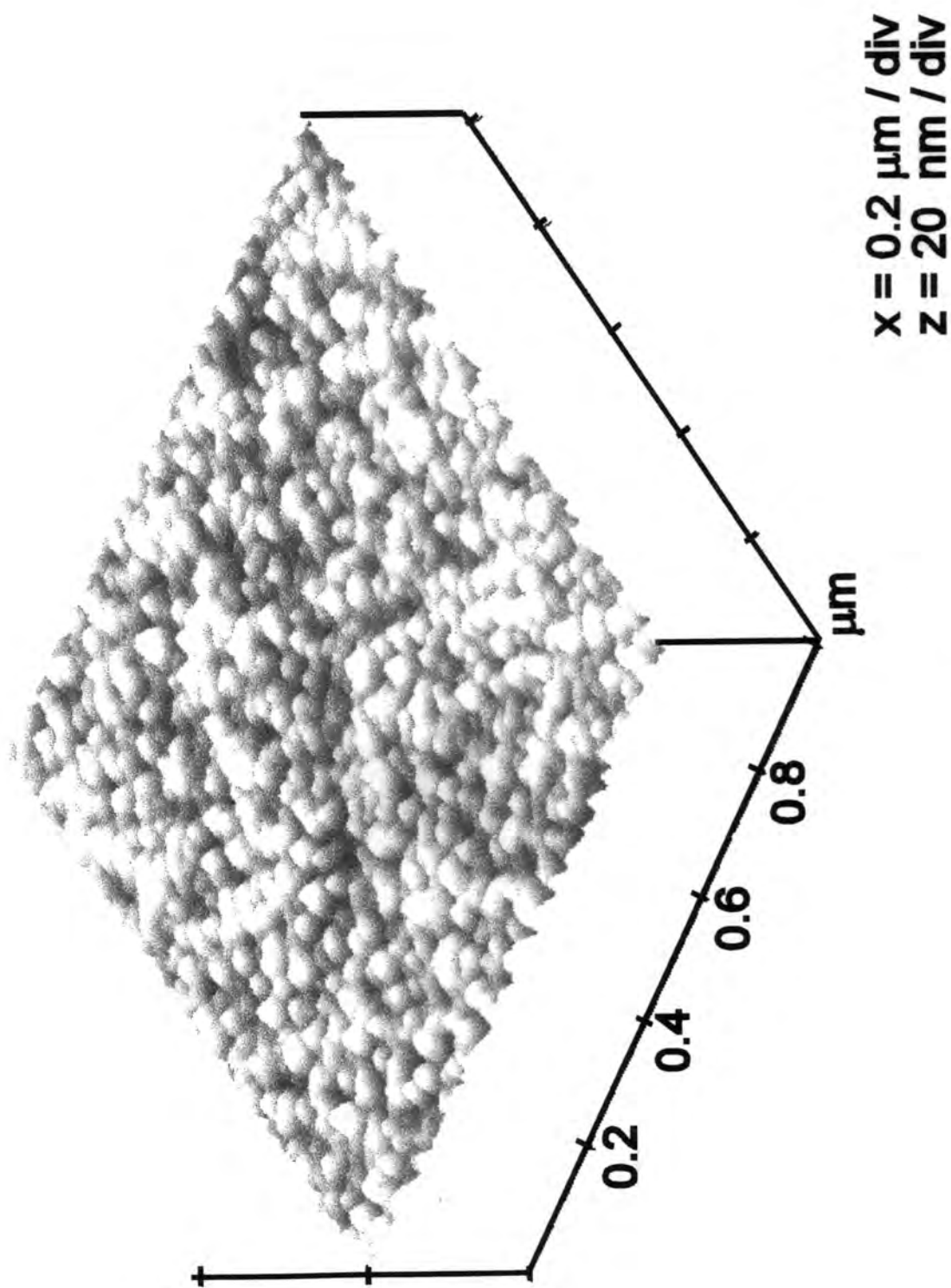
Figure 7(a): AFM image of silent discharge treated polystyrene.

x = 0.2 μm / div
z = 0.2 μm / div

μm

0.2   0.4   0.6   0.8

144
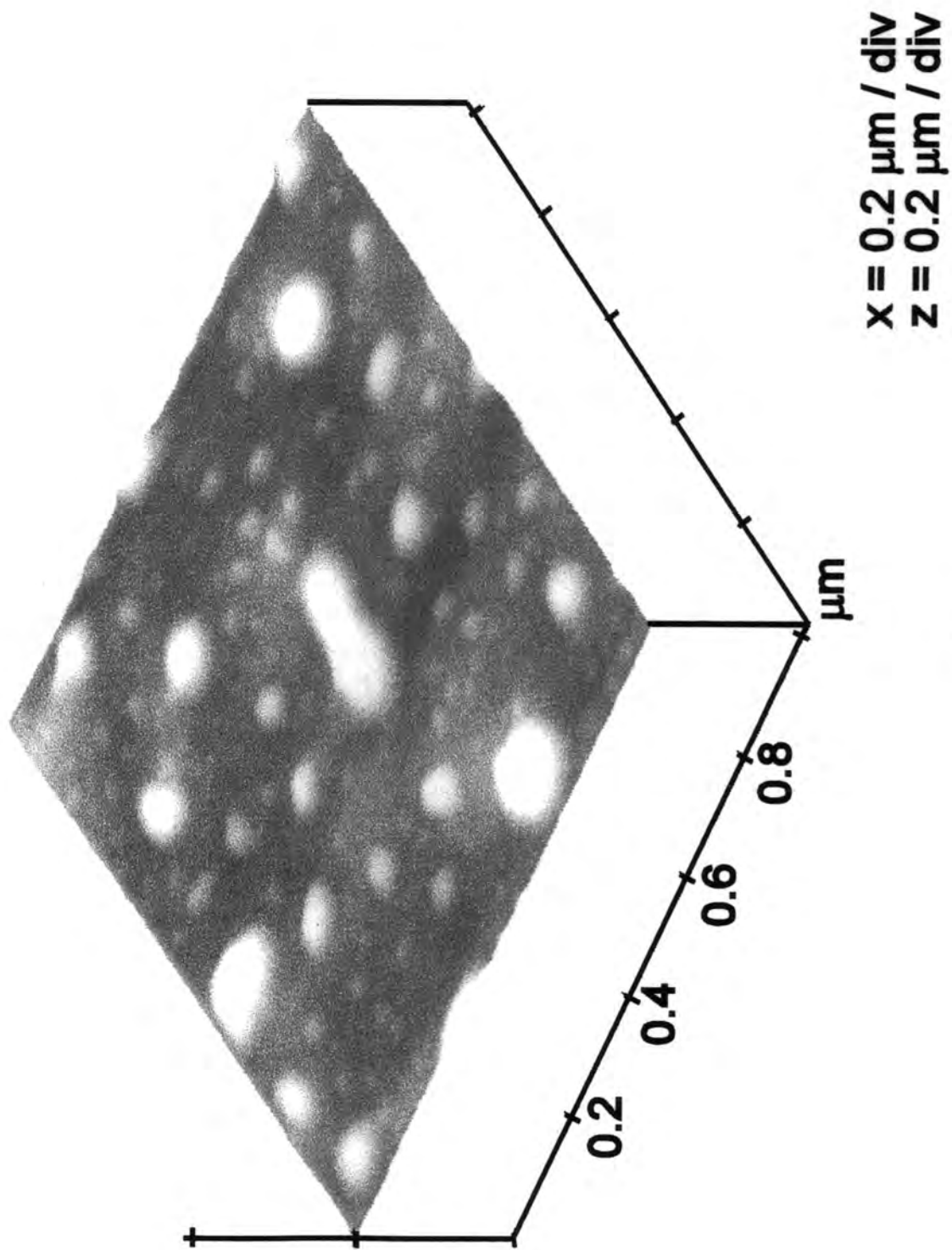
Figure 7(b): AFM image of silent discharge treated 50/50 PPO/PS blend.

x = 0.2 μm / div
z = 0.2 μm / div

μm

0.2 0.4 0.6 0.8

145
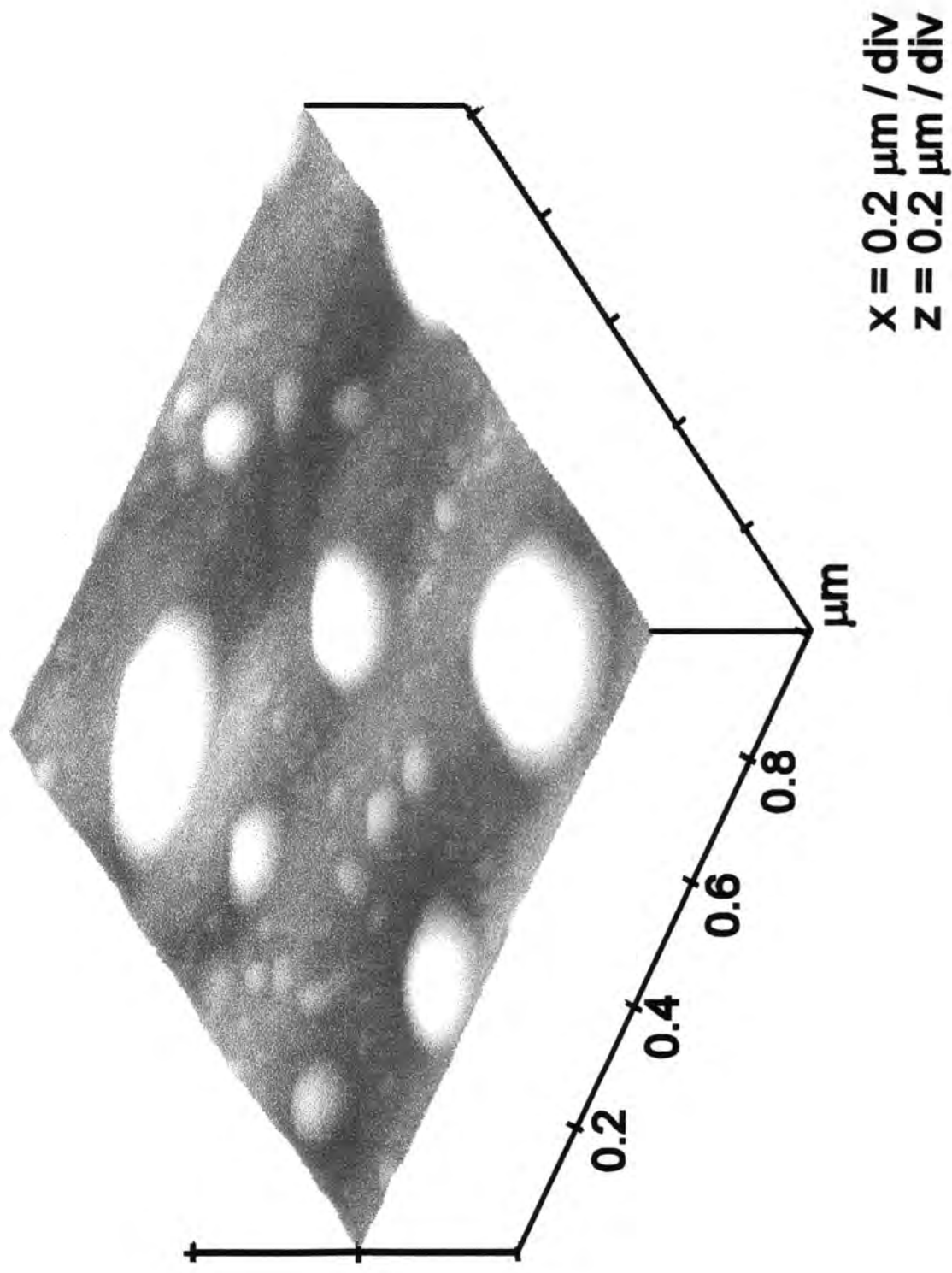
Figure 7(c): AFM image of silent discharge treated pure polyphenylene oxide.

x = 0.2 μm / div
z = 0.2 μm / div

146
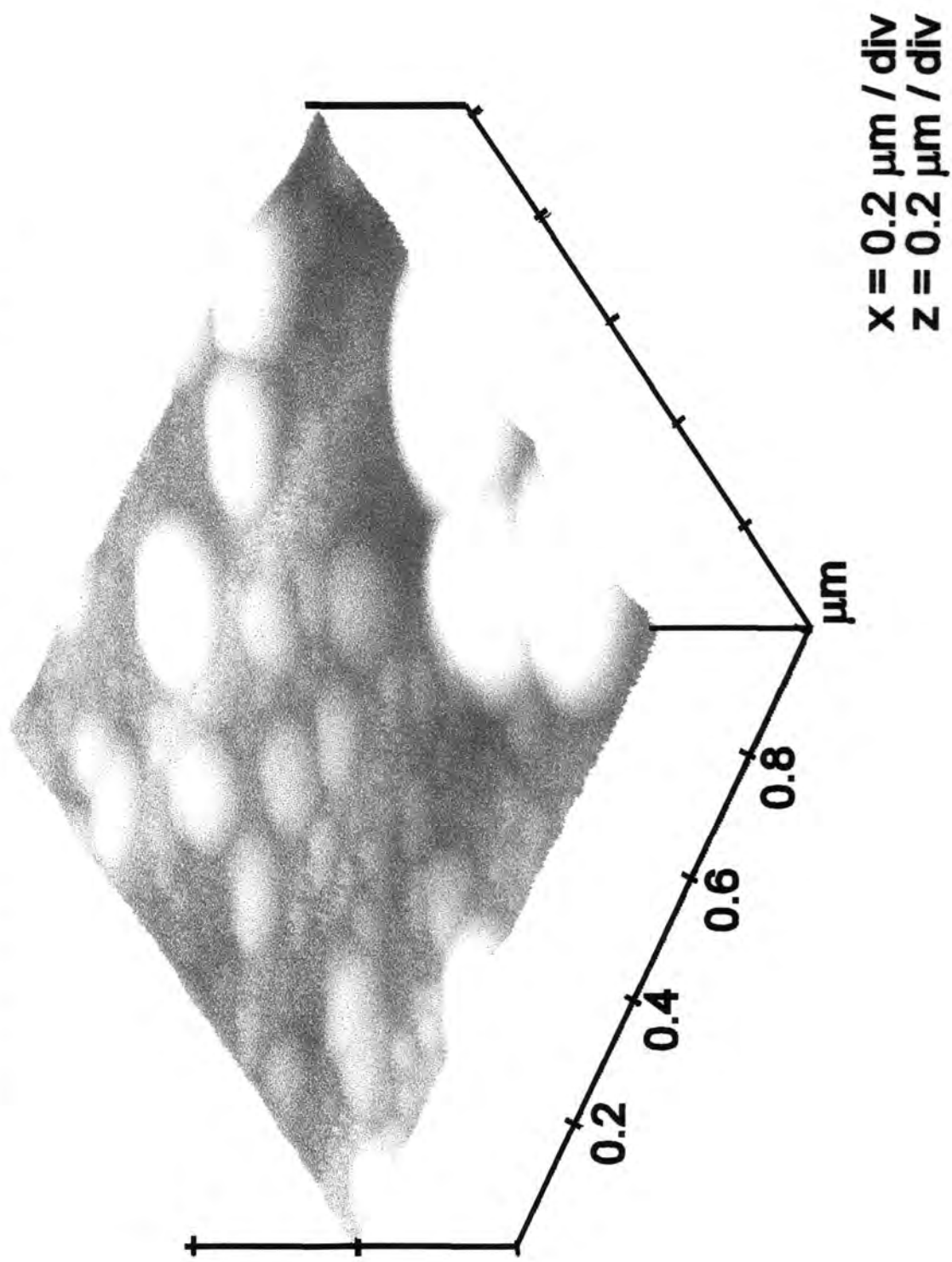
Figure 7(d) AFM image of silent discharge treated 50/50 PPO/PS blend followed by solvent washing.

x = 0.2 μm / div
z = 0.2 μm / div

147
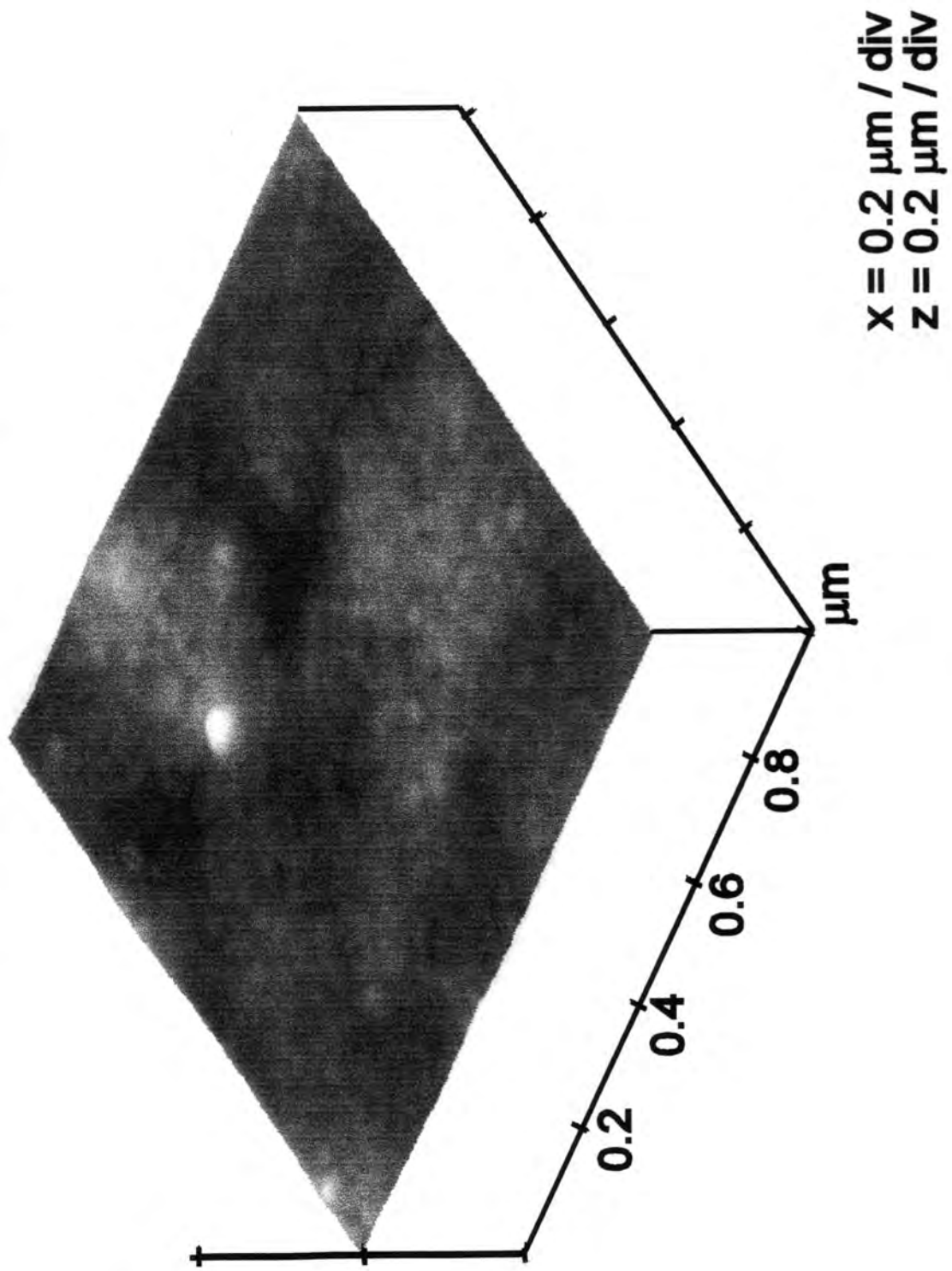
5.4 DISCUSSION

Miscibility over the entire composition range for polystyrene / polyphenylene oxide blends has been known for a long time and widely investigated using a variety of techniques (e.g. glass transition temperature,[22] neutron scattering studies.[23]). Infrared[24] and ultraviolet[25] spectroscopic studies have shown that this high miscibility arises from strong interactions between the phenyl rings contained in polyphenylene oxide and polystyrene. Pure polystyrene or blends with a high polystyrene content tend to be brittle. However blends with a polyphenylene oxide content of greater than 30% are ductile glasses.[26] This variation in mechanical properties has been attributed to the intermolecular disruption of stacks of polystyrene polymer chains by polyphenylene oxide.[27] These interactions can be used to account for the observed disappearance of the parent polystyrene granular surface morphology upon blending with polyphenylene oxide.

Typically, for a polymer blend one would expect surface enrichment of the component with the lowest surface energy.[28] Polystyrene and polyphenylene oxide have surface energies of 33 dynes cm^{-1} and 41 dynes cm^{-1} respectively[29,30]. Therefore surface enrichment of polystyrene would be expected in the case of polystyrene / polyphenylene oxide blend mixtures. The observed linear variation in polyphenylene oxide content at the surface with blend composition suggests that no surface segregation of either component of the polymer blend is occurring within the XPS sampling depth (2 nm). The lack of surface enrichment might be due to phenyl ring interactions between the two polymer constituents hindering the migration of polystyrene towards the surface[25] combined with molecular entanglements.[31] Alternatively, fast evaporation of the chloroform solvent during spin coating may be preventing the blend from reaching thermodynamic equilibrium.[28]

For both parent polymers, electrical discharge treatment results in the formation of C-O, O-C-O, C=O, O-C=O, and O-CO-O functionalities at the surface and chain scission as discussed in chapter 2 and 3. Attenuation of the π-π^* shake-up satellite during plasma modification is indicative of the phenyl centres being attacked during treatment.[32-34] Solvent washing experiments have shown that there is a greater loss of oxygenated material from electrical discharge treated polyphenylene oxide - rich blend

mixtures. This can be attributed to polyphenylene oxide being more susceptible towards chain scission as a consequence of its phenyl ring being located within the polymer backbone rather than being pendant (as is the case for polystyrene): aromatic pendant groups promote stability of the polymer backbone by enhancing radiationless deactivation.[35] Also the polar C-O bond along the polyphenylene oxide backbone will be susceptible to nucleophilic attack by plasma generated oxygen species. In the case of atmospheric silent discharge treatment, UV radiation of lower energy is generated. This can lead to less chain scission within the subsurface region, and helps to explain why some of the oxygenated functionalities remain in tact during solvent washing of the silent discharge treated polyphenylene oxide - rich blends but not for the oxygen plasma treated blends which is contrary to the normal polymeric behaviour. In the case of solvent rinsing of low pressure oxygen plasma modified polystyrene - rich mixtures, the low molecular weight polyphenylene oxide fraction is preferentially removed.

The greater oxygen content present in the low molecular weight oxidised material makes it incompatible with the underlying untreated polymer due to a large difference in their respective surface energies; this leads to the formation of globules at the surface.[36 37] It can be seen from the AFM micrographs, that even a small amount of polystyrene attenuates the amount of low molecular weight oxidised material being produced. Although silent discharge modification causes a greater perturbation of the surface topography,[38] this is not found to be the case following solvent washing of the respective treated surfaces, Table 1; an increase in roughness is found for low pressure plasma modification of the polymer blend surfaces, whilst the converse was noted for silent discharge treatment.

5.5 CONCLUSIONS

No significant surface enrichment within the XPS sampling depth is found for either parent component of polystyrene / polyphenylene oxide blends. The surface topography belonging to each parent polymer is destroyed upon mixing due to the disruption of phenyl ring stacks present in polystyrene by interpenetrating polyphenylene oxide chains. Atmospheric dielectric barrier treatment of the polymer blends leads to a larger amount of low molecular weight oxidised globular material being produced in comparison to low pressure oxygen plasma modification. These oxidised moieties can be

149

partially washed off by a solvent, which leads to a change in both the chemical composition and topography at the surface. From the point of view of incorporating oxygen into the surface (which is not associated with low molecular weight oxidised material), low pressure oxygen plasma treatment is better suited for polystyrene - rich compositions, whereas silent discharge modification is more appropriate for polyphenylene oxide - rich blends.

REFERENCES

1 . Olabisi, O.; Robeson, L. M.; Shaw, M. T. *Polymer - Polymer Misisciblity*; Academic: New York; 1979.

2 . Borggreve, R. J. M.; Gaymans, R. J.; Schuijer, J.; Ingen Houssz, J. F. *Polymer* **1987**, *28*, 1489.

3 . Clark, M. B.; Burchart, C. A.; Garadella, J. A. *Macromolecules* **1991**, *24*, 799.

4 . Prest, W. M.; Porter, R. S. *J. Polym. Sci., A-2.* **1972**, *10*, 1639.

5 . Shultz, A. R.; McCullough, C. R. *J. Polym. Sci., A-2.* **1972**, *10*, 307.

6 . deAraujo, M. A.; Stadler, R.; Cantow, H.-J. *Polymer* **1988**, *29*, 2235.

7 . Paul, D. R. In *Polymer Blends*; Paul, D. R.; Newman, S., Eds.; Academic: New York, 1978; Vol. 1, Chapter 1.

8 . Billmeyer, F. W. *Textbook of Polymer Science*; Wiley: New York, 1962.

9 . Coleman, M. M.; Serman, C. J.; Bhagwagar, D. E.; Painter, P. C. *Polymer* **1990**, *31*, 1187.

10 . Thomas, H. R.; O'Malley, J. J. *Macromolecules* **1981**, *14*, 1316.

11 . Schmitt, R. L.; Gardella, J. A.; Salvati, L. *Macromolecules* **1986**, *19*, 648.

12 . Bhatia, Q. S.; Pan, D. H.; Koberstein, J. T. *Macromolecules* **1988**, *21*, 2166.

13 . Angulo-Sanchez, J. L.; Short, R. D. *Polymer* **1995**, *36*, 1559.

14 . Bhatia, Q. S.; Burrell, M. C.; Chera, J. J. *J. Appl. Poym. Sci.* **1992**, *46*, 1915.

15 . Occhiello, E.; Garbassi, F. *Macromol. Symp.* **1994**, *78*, 131.

16 . Zhao, X.; Zhao, W.; Sokolov, J.; Rafailovich, M. H.; Schwarz, S. A.; Wilkens, B. J.; Jones, R. A. L.; Kramer, E. J. *Macromolecules* **1991**, *24*, 5991.

17 . Thompson, P. M. *Anal. Chem.* **1991**, *63*, 2447.

18 . Simko, S. J.; Bryan, S. R.; Griffis, D. P.; Murrey, R. W.; Linton, R. W. *Anal. Chem.* **1985**, *17*, 1986.

19 . Krause, S. In *Polymer Blends*; Paul, D. R.; Newman, S., Eds.; Academic: New York, 1978; Vol. 1, Chapter 2.

20 . Fuchs, O. In *Polymer Handbook*; Brandrup, J.; Immergut, E.H. Eds.; Wiley: New York, 1989; 3rd ed, p379.

21 . Clark, D.T.; Dilks, A. *J. Polym. Sci., Polym. Chem. Ed.* **1977**, *15*, 15.

22 . Stoelting, J.; Karasz, F. E.; MacKnight, W. J. *J. Polym. Eng. Sci.* **1970**, *16*, 133.

23 . Maconnachie, A.; Kambour, R. P.; Bopp, R. C. *Polymer* **1984**, *25*, 357.

24 . Lefebvre, D.; Jasse, B.; Monnerie, L. *Polymer* **1981**, *22*, 1616.

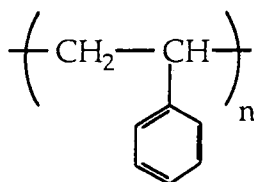25 . Wellinghoff, S. T.; Koenig, J. L.; Baer, E. *J. Polym. Sci., Polym. Phys. Ed.* **1977**, *15*, 1913.

26 . Wellinghoff, S. J.; Baer, E. *J. Appl. Polym. Sci.* **1978**, *22*, 2025.

27 . Mitchell, G. R.; Windle, A. H. *J. Polym. Sci., Polym. Phys. Ed.* **1985**, *23*, 1967.

28 . Bhatia, Q. S.; Pan, D. H.; Koberstein, J. T. *Macromolecules* **1988**, *21*, 2166.

29 . Toyama, M.; Ito, T.; Moriguchi, H. *J. Appl. Polym. Sci.* **1970**, *14*, 2039.

30 . Lee, L.-H. In *Advances in Chemicals 87*; Gould R. F., Ed.; American Chemical Society: Washington, DC, 1968.

31 . Donald, A. M.; Kramer, E. J.; *Polymer* **1982**, *23*, 461.

32 . Razumouskii, S. D.; Kefeli, A. A.; Zackov, G. E. *Eur. Polym. J.* **1971**, *7*, 275.

33 . Occhiello, E.; Morra, M.; Cinquina, P.; Garbassi, F. *Polymer* **1992**, *33*, 3007.

34 . Clark, D. T.; Dilks, A. *J. Polym. Sci., Polym. Chem. Ed.* **1979**, *17*, 957.

35 . Taylor, G. N.; Wolf, T. M. *Polym. Eng. Sci.* **1980**, *20*, 1087.

36 . Overney, R. M.; Luthi, R. Haefke, H.; Frommer, J.; Meyer, E.; Guntherodt, H.-J.; Hild, S.; Fuhrmann, J. *Appl. Surface Sci.* **1993**, *64*, 197.

37 . Greenwood, O. D.; Hopkins, J.; Badyal, J. P. S. *Macromolecules* submitted.

38 . Greenwood, O. D.; Boyd, R. D.; Hopkins, J.; Badyal, J. P. S. *J. Adhesion. Sci. Technol.* **1995**, *9*, 311.

CHAPTER 6:

OXYGEN GLOW DISCHARGE AND SILENT DISCHARGE TREATMENT OF IMMISCIBLE POLYSTYRENE / POLYCARBONATE POLYMER BLEND SURFACES
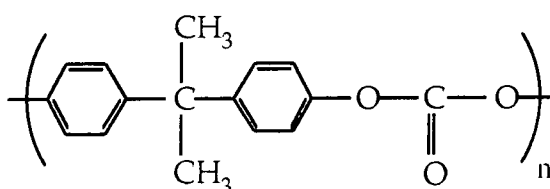
6.1 INTRODUCTION

Many different types of immiscible polymer blend are used in industry.[1] In such systems, phase separation occurs within the bulk of the blends, whilst the surface can be enriched by one of the constituent polymers (for a review of the surface studies into polymer blends see chapter 5). Quite often polymer blend surfaces require plasma activation prior to bonding.[2] Understanding the phase morphology is of critical importance in the study of immiscible polymer blends. Both the mechanical[3-5] and thermal[6,7] properties of a polymer blend depend on its phase morphology. It its then important to study both the surface chemical properties and phase morphology at the surface for both untreated and treated polymer blends.

This chapter describes how XPS and AFM were used to study the surfaces of immiscible polystyrene / polycarbonate blend mixtures[8] before and after low pressure oxygen plasma and atmospheric silent discharge treatment. XPS is used to track the variation in surface chemical composition, whilst AFM has helped to identify the respective constituent phases.

$$\left(CH_2 - \underset{\underset{\bigcirc}{|}}{CH}\right)_n$$

Polystyrene (PS)

$$\left(\bigcirc - \underset{\underset{CH_3}{\overset{CH_3}{|}}}{C} - \bigcirc - O - \underset{\overset{\|}{O}}{C} - O\right)_n$$

Bisphenol-A Polycarbonate (PC).

6.1.1 Morphological Studies of Polymer Blends

The major techniques that have been used in order to elucidate the phase morphology of immiscible polymer blends are optical microscopy, electron microscopy and scanning probe microscopy.

Optical microscopy has been used to investigate polymer blends,[9] but is limited by its poor resolution, and the need for a large refractive index between the phases of the polymer blend in order to obtain phase contrast. In the case of polymer blends that transmit visible light, optical microscopy becomes a bulk technique.

Electron microscopic techniques such as scanning electron microscopy (SEM) and transmission electron microscopy (TEM) have been widely used to determine a polymer blends morphology.[9] TEM is not often used in polymer blend work due to the difficulties in obtaining a thin enough sample in order to perform the analysis. SEM is the most widely used technique in the study of polymer blends. However SEM cannot be used directly in order to determine the phase morphology due to the fact that the yield of secondary electrons used to obtain the image are independent of surface composition, and phase contrast is not achieved. The are several ways of obtaining contrast between phases using SEM. One of the most common is the selective etching of a specific component of a polymer blend.[10] This can be achieved by selective oxidation, electron beam irradiation or by using a solvent.[11] However this technique suffers from the need to find a suitable etching agent which can easily introduce artefacts at the surface, modifying the phase morphology. Another method that is commonly used is the selective staining of the blend surface.[12,13] If one phase of a polymer blend is stained with a heavy metal compound, then the phase morphology can be determined by imaging with the primary or backscattered electrons emitted from the surface. The yield of primary electrons emitted from a surface is determined by the average atomic number of the sample area being scanned. Staining a sample changes its chemistry, which again may modify its phase morphology, such as causing phase separation.[14] Backscattered electrons are emitted from deeper within a sample than secondary electrons, causing images obtained from backscattered electrons to have a lower resolution.

The invention in 1986 of the Atomic Force Microscope (AFM) by Binning[15] has presented a completely new technique for the investigation of the morphology of polymer blends.[16-18] The AFM, although insensitive to variations in surface composition is very sensitive to any topographical variations, much more so than the SEM. AFM can be used directly to determine the phase morphology if there is any height variation. Alternatively variations in the AFM technique can be used to determine the phase morphology such as frictional force microscopy (FFM),[19] force modulation AFM,[20] Chemical sensing AFM,[21] and phase modulation AFM.[22]

6.2 EXPERIMENTAL

6.2.1 Sample Preparation

Thin films of polystyrene (Aldrich, Mw = 280 000) / polybisphenolcarbonate (General Electric, Mw = 40 000) blends were prepared by spin coating from a 5% w/v chloroform solution onto glass slides. Blend compositions are given as bulk weight percent. Immiscible blends generally tend to be cloudy due to the presence of phase boundaries which scatter light,[23] however the polystyrene / polycarbonate blend mixtures were almost transparent in appearance because of the constituent polymers having almost identical refractive indices.[24]

6.2.2 Non-equilibrium Plasma Treatment

Low pressure oxygen glow discharge treatments were carried out in a cylindrical electrodeless reactor. The reactor and experimental procedure is described in chapter 2. Plasma treatments were carried out at 10 W for 60 s in all cases. This was found to result in a limiting level of surface modification.

Atmospheric silent discharge air plasma treatments were carried out for a duration of 120 s using a home built parallel plate dielectric barrier discharge reactor operating at 3 kHz, 11 kV, with an electrode gap of 3.00 ± 0.05 mm, as described in chapter 3.

Subsequent washing experiments of the treated blend films were carried out using a 50 / 50 isopropanol / cyclohexane polar / non-polar solvent mixture (neither polystyrene nor polycarbonate are soluble in either of these solvents at room temperature).[25]

6.2.3 Sample Analysis

A Kratos ES300 electron spectrometer equipped with a MgKα source (1253.6 eV) and a concentric hemispherical analyser was used for XPS surface analysis of the polymer blend surfaces before and following plasma treatment, as described in chapter 2.

A Digital Instruments Nanoscope III atomic force microscope was used to examine the topographical nature of the polymer blend surfaces prior to and immediately following electrical discharge exposure. All of the AFM images were acquired in air, and are presented as unfiltered data. Topographical analysis comprised a combination of tapping mode AFM and phase modulation AFM, both of which are described in chapter 1.

6.3 RESULTS

6.3.1 X-ray Photoelectron Spectroscopy

XPS wide-scan spectra were taken to check for the absence of any surface-active inorganic additives. C(1s) spectra of each blend mixture was peakfitted as described in chapter 2 and 5. The C(1s) envelope for untreated polystyrene can be assigned to a hydrocarbon component, $-\underline{C}_xH_y-$ at 285.0 eV, and a $\pi-\pi^*$ shake-up satellite feature at 291.7 ± 0.1 eV, which accounts for approximately 5.3 ± 0.2 % of the total C(1s) peak area, Figure 1. The experimentally measured O/C ratio for polycarbonate was found to be 0.21 ± 0.02, which is consistent with the theoretically expected value of 0.19; $-\underline{C}_xH_y$ (285.0 eV), $\underline{C}$-O (286.6 eV), and O-$\underline{C}$O-O (290.4 eV) environments were evident in the C(1s) region together with a $\pi-\pi^*$ shake-up satellite at 291.8 eV.

The variation in the measured O/C ratio with polymer blend composition was found to be non-linear, Figure 2. Virtually no O(1s) signal was detected from the surface

156

up to a concentration of approximately 50% polycarbonate: beyond this value, the O/C ratio increased rapidly prior to eventually plateauing off at the value associated with pure polycarbonate. The C(1s) spectra show a corresponding rise in intensity of the C-O (286.6 eV) and O-CO-O (290.4 eV) peaks with increasing bulk polycarbonate content, Figure 1.

Both polystyrene and polycarbonate appear to undergo similar levels of oxidation for both oxygen plasma and silent discharge, with the polycarbonate being oxidised to a slightly greater extent, Figure 1. Silent discharge treatment produces more of the highly oxidised material than oxygen plasma treatment, Figure 1 and Table 1. The variation in O/C ratio with blend composition followed the same trend as seen previously for the untreated polymer blend mixtures, Figure 2. Solvent washing of these oxygen plasma and silent discharge treated polystyrene / polycarbonate blend surfaces showed a reduction in the O/C ratio. From these results it can be concluded that soluble low molecular weight oxidised material (LMWOM) is generated during plasma treatment.[26,27] Silent discharge produces significantly more LMWOM as washing of silent discharge treated surfaces removes more oxidised material than washing of plasma treated surfaces, Table 1.

Table 1: O/C ratios and relative peak intensities of the oxidised carbon peaks (Σ = 100 %) for untreated and treated 75./ 25 polycarbonate / polystyrene blend.

|	O/C ratio	Relative oxidised peak intensity.			
		C-O	C=O/ O-C-O	CO-O	O-CO-O
Untreated	0.18 ± 0.02	71 ± 5	0	0	29 ± 3
Plasma treated	0.52 ± 0.03	38 ± 3	27 ± 3	15 ± 2	20 ± 2
Plasma treated washed	0.30 ± 0.03	54 ± 4	21 ± 2	7 ± 1	19 ± 2
Silent discharge treated	0.51 ± 0.03	34 ± 3	20 ± 2	15 ± 2	31 ± 3
Silent discharge treated washed.	0.18 ± 0.02	67 ± 5	8 ± 1	5 ± 1	20 ± 2

158

Figure 1(a):

C(1s) peak fitted spectra of untreated polystyrene / polycarbonate blend surfaces as a function of polycarbonate loading.
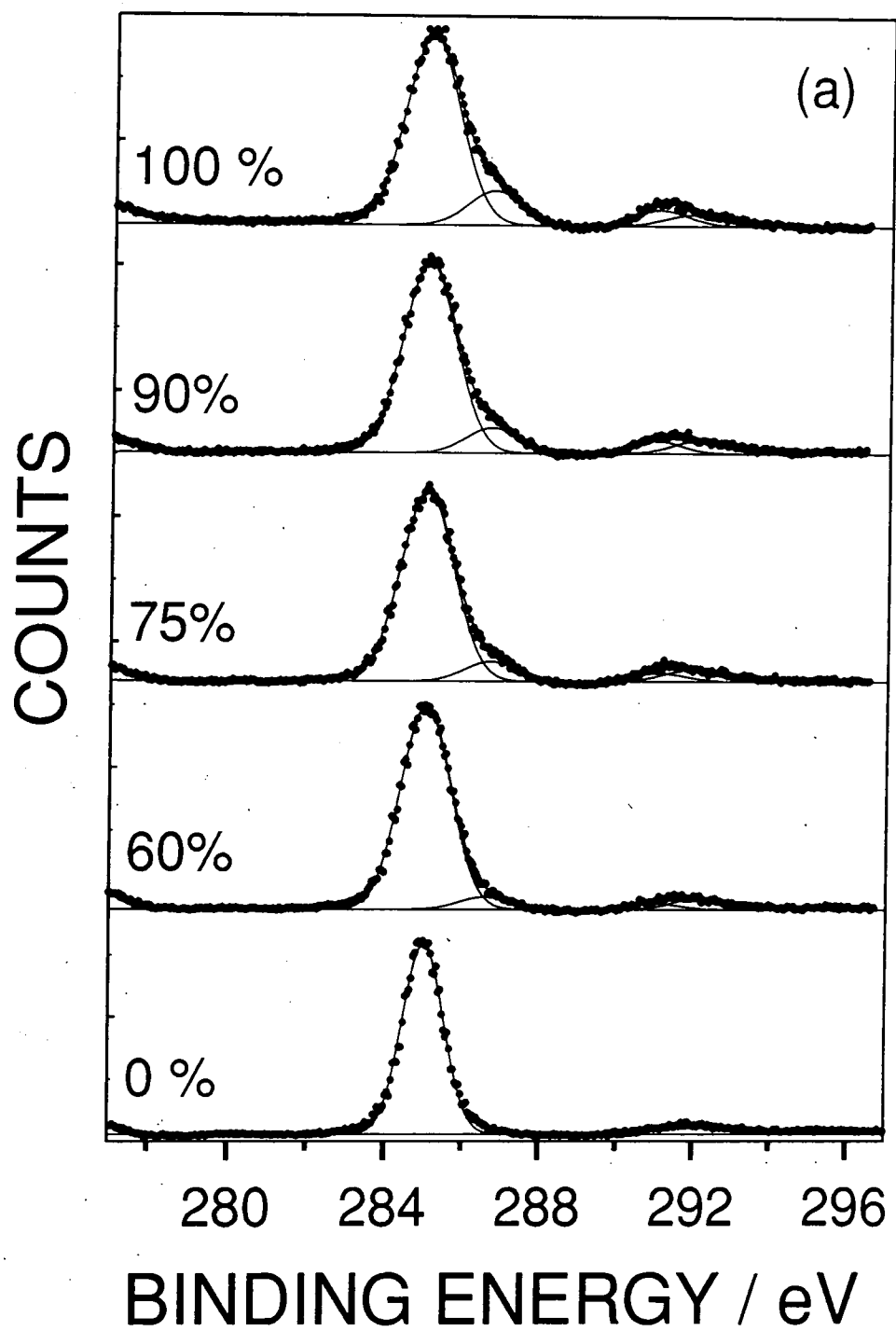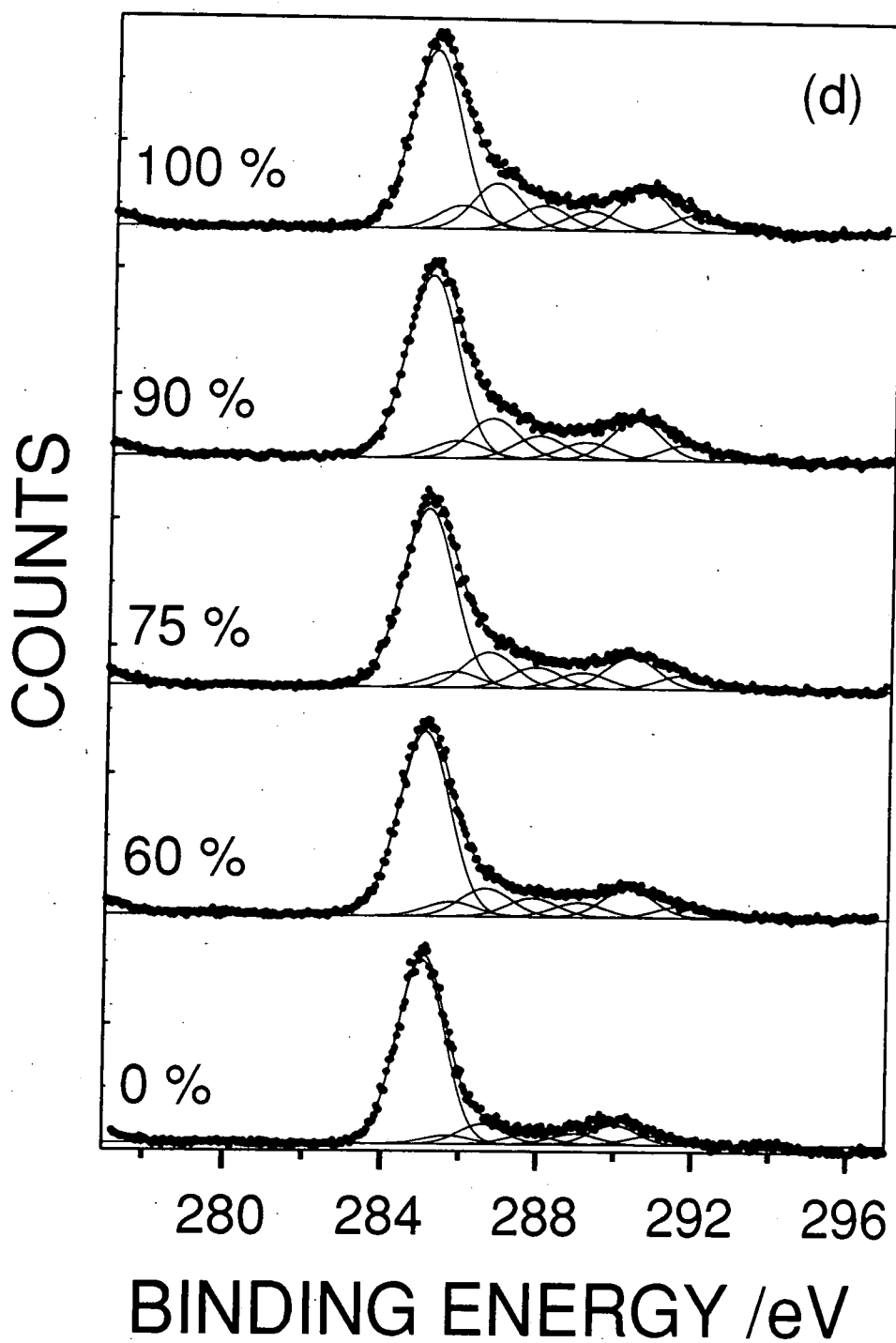
Figure 1(b):

C(1s) peak fitted spectra of oxygen plasma treated polystyrene / polycarbonate blend surfaces as a function of polycarbonate loading.
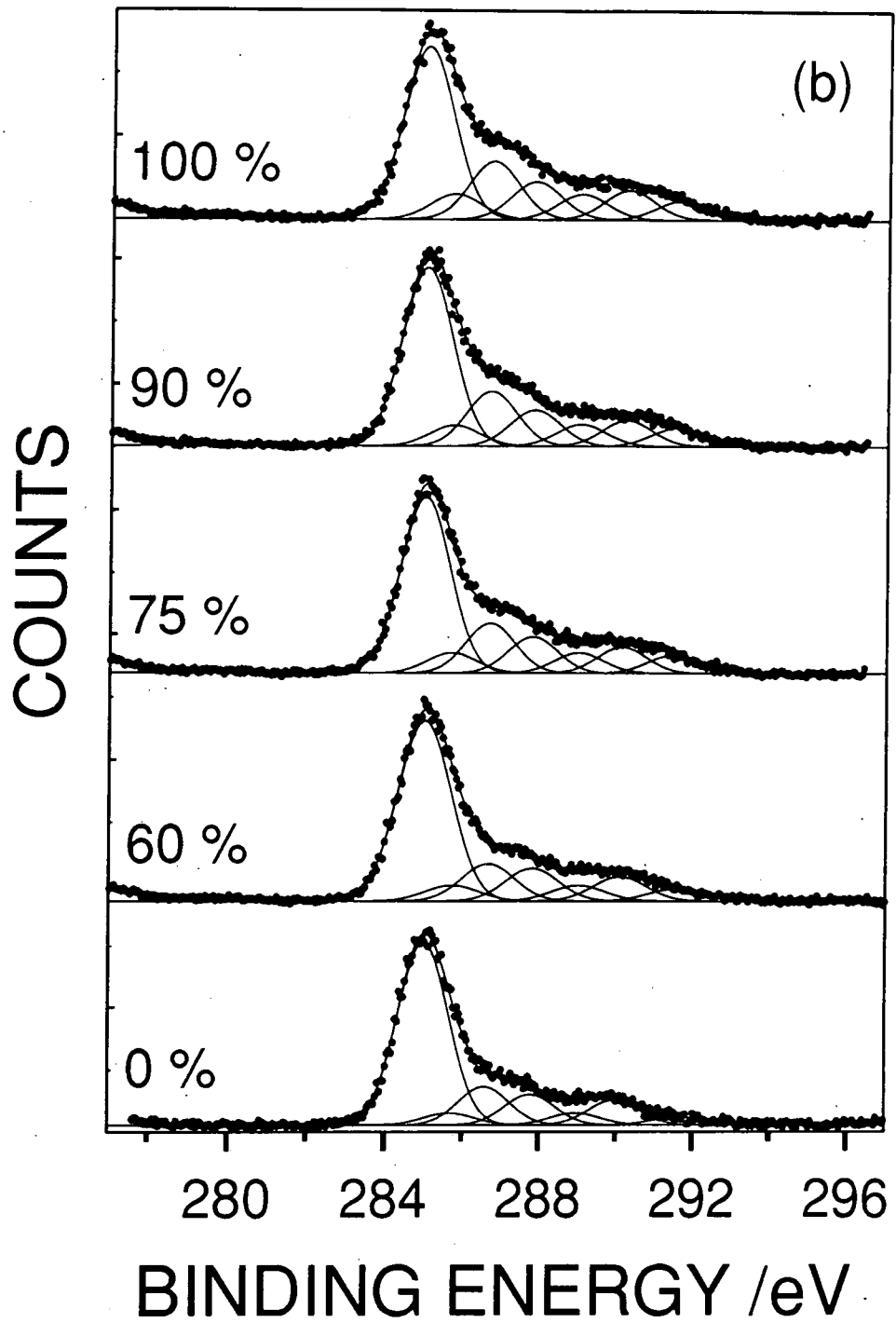
Figure 1(c):

C(1s) peak fitted spectra of 25/75 polystyrene / polycarbonate polymer blend (i) untreated; (ii) oxygen plasma treated; (iii) oxygen plasma treated polystyrene / polycarbonate blend surfaces followed by solvent washing.
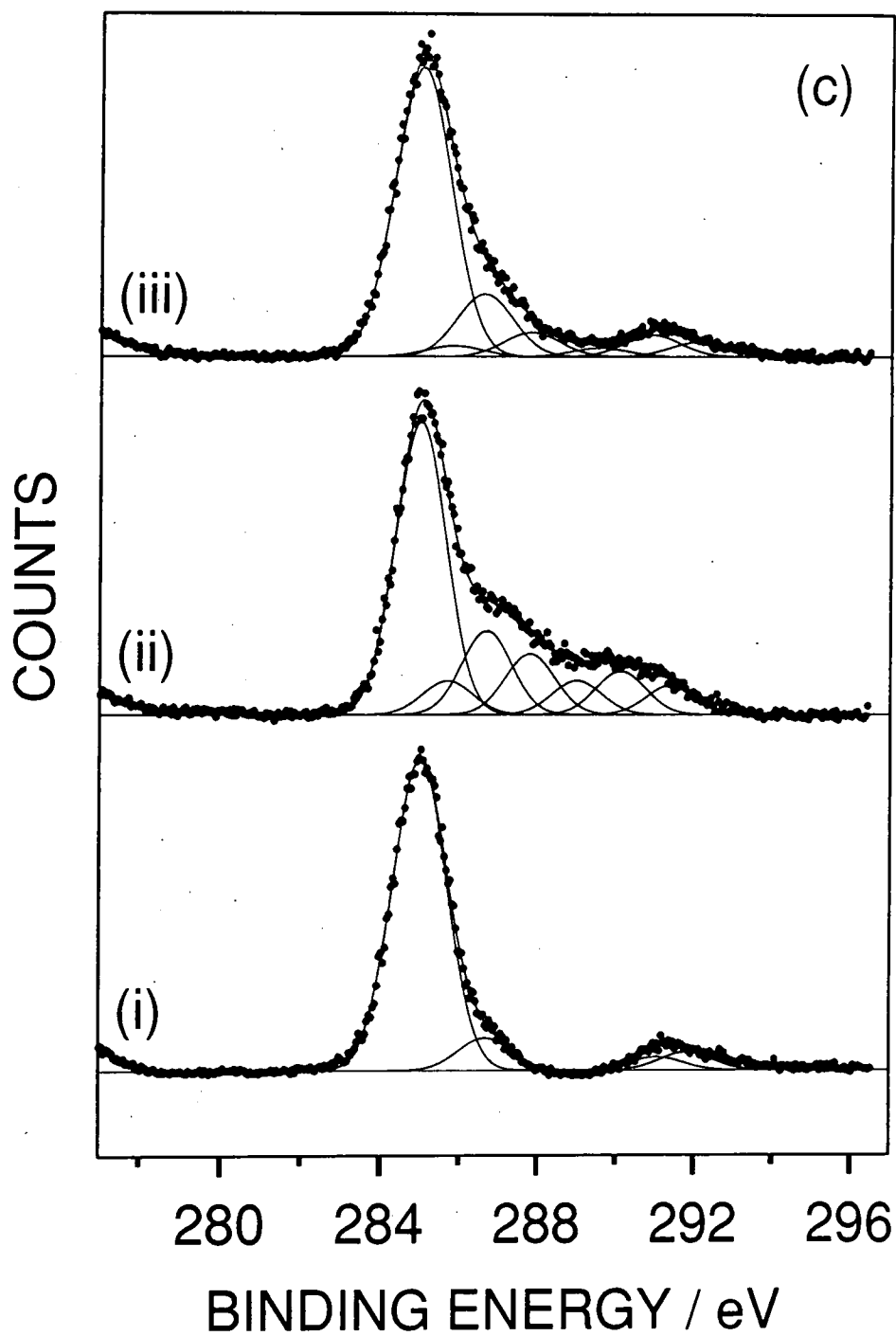
Figure 1(d):

C(1s) peak fitted spectra of silent discharge treated polystyrene / polycarbonate blend surfaces as a function of polycarbonate loading.

Figure 1(e):

C(1s) peak fitted spectra of oxygen plasma treated polystyrene / polycarbonate blend surfaces followed by solvent washing as a function of polycarbonate loading.
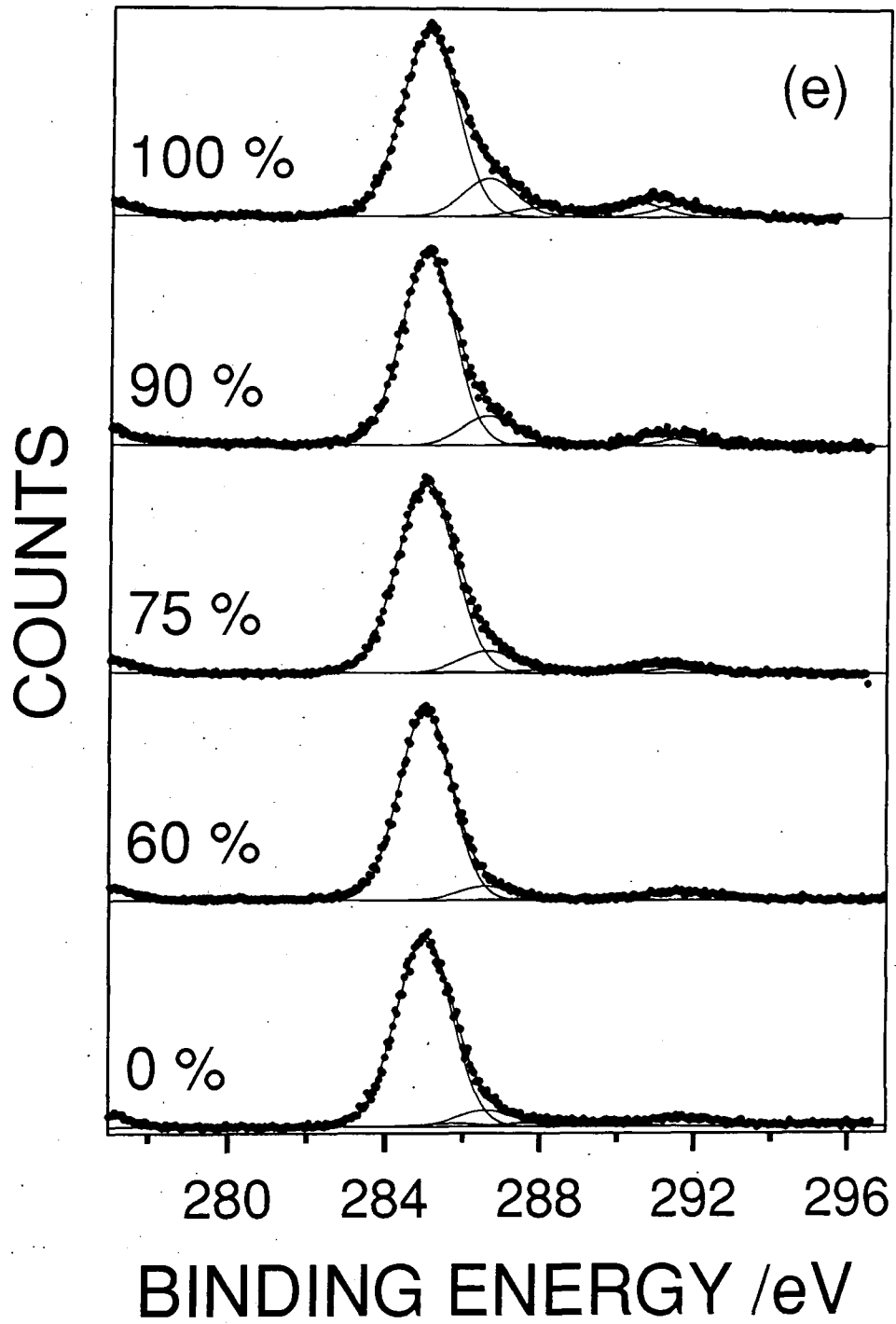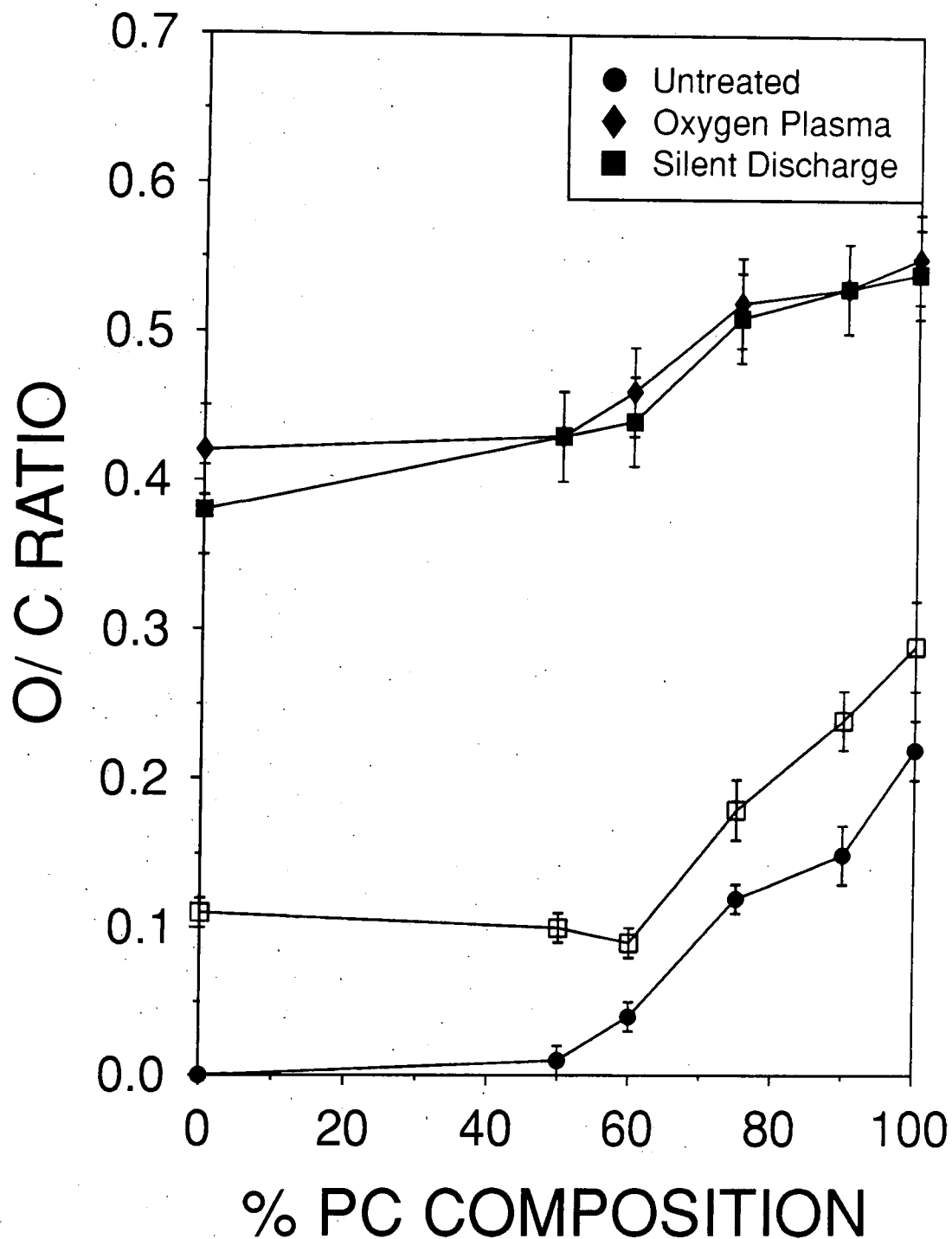
Figure 2:
Variation in the O/C ratios for the polystyrene / polycarbonate blend surfaces: untreated;
silent discharge treated; and silent discharge treatment followed by solvent washing
(unshaded squares).

6.3.2 Atomic Force Microscopy

AFM was used in both tapping and phase modulation modes. Tapping mode AFM analysis of the untreated polymer blend surfaces revealed a two phase system, Figure 3. The different constituents of the blend were shown up more clearly by using Phase Modulation AFM, Figures 3-4; two types of feature are evident: a localised continuous phase (polycarbonate) containing submicron circular nodules (polystyrene), and an extended continuous phase (polystyrene),[28] The latter component completely swamps the surface at polystyrene loadings of greater than 40%, Figure 4.

Oxygen plasma treatment of the parent polymers had negligible effect on the surface topography on the 10 μm scale, Figure 5. Oxygen plasma modified blend surfaces show evidence of raised areas on the localised continuous polycarbonate / polystyrene region, ranging in width from 2 μm to 100nm. Indentations are seen on the extended polystyrene phase after washing. This corresponds to an inherent difference in etching rates between the two constituent polymers.[29] Washing of the plasma treated surface in a 50/50 isopropanol / cyclohexane polar / non-polar solvent mixture does not significantly affect the surface topography, Figure 6.

Silent discharge treatment of pure polystyrene film produced smaller globular features compared to polycarbonate, Figure 7. These differences were also evident for the silent discharge modified blend surfaces (thereby aiding in the assignment of the respective blend components). Washing these plasma treated surfaces removed the low molecular weight oxidised material to leave behind terraces at different heights, Figure 8. This topography is similar to the oxygen plasma treated surface's which again is caused by an inherent difference in etching rates between the parent polymers.

165

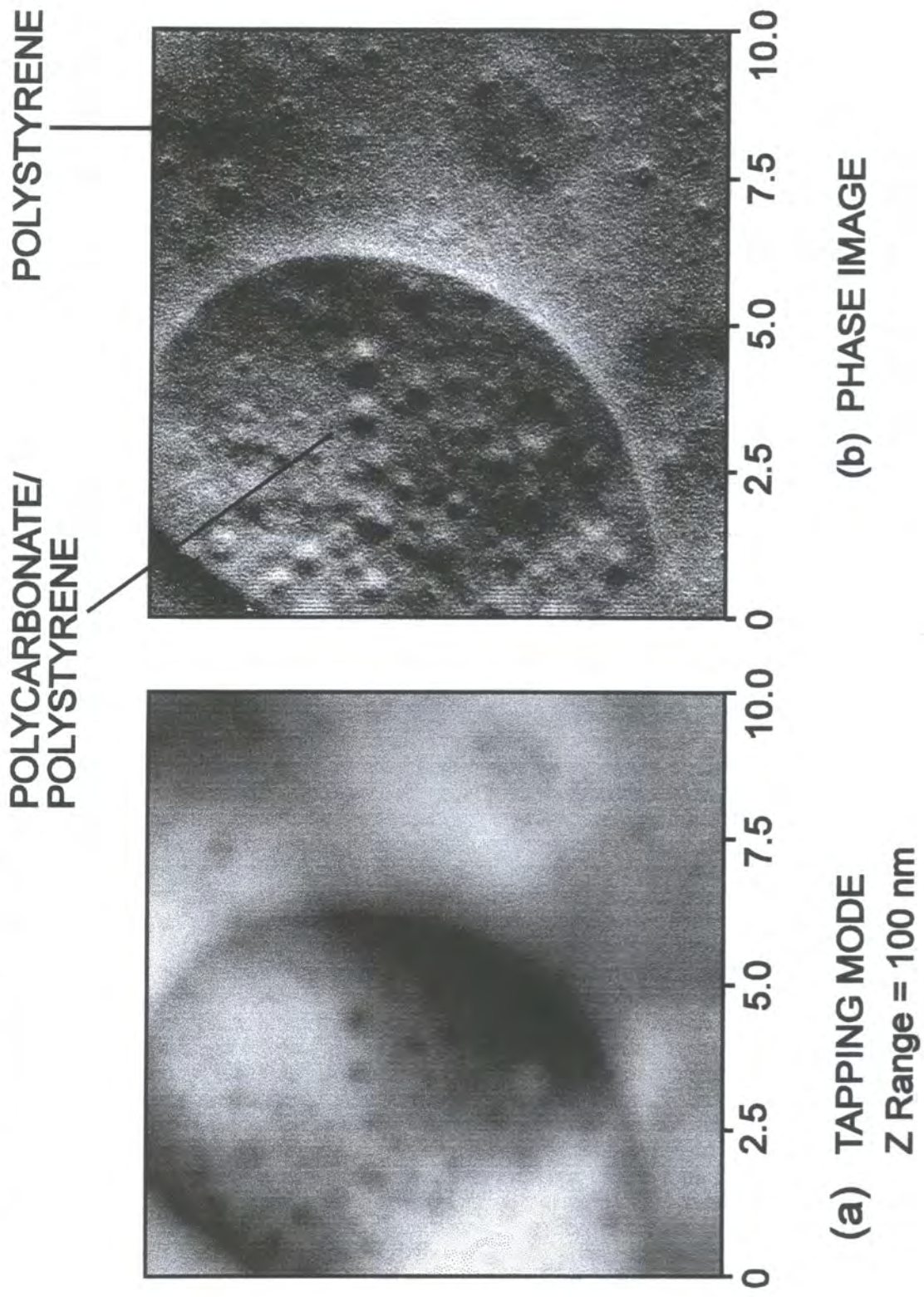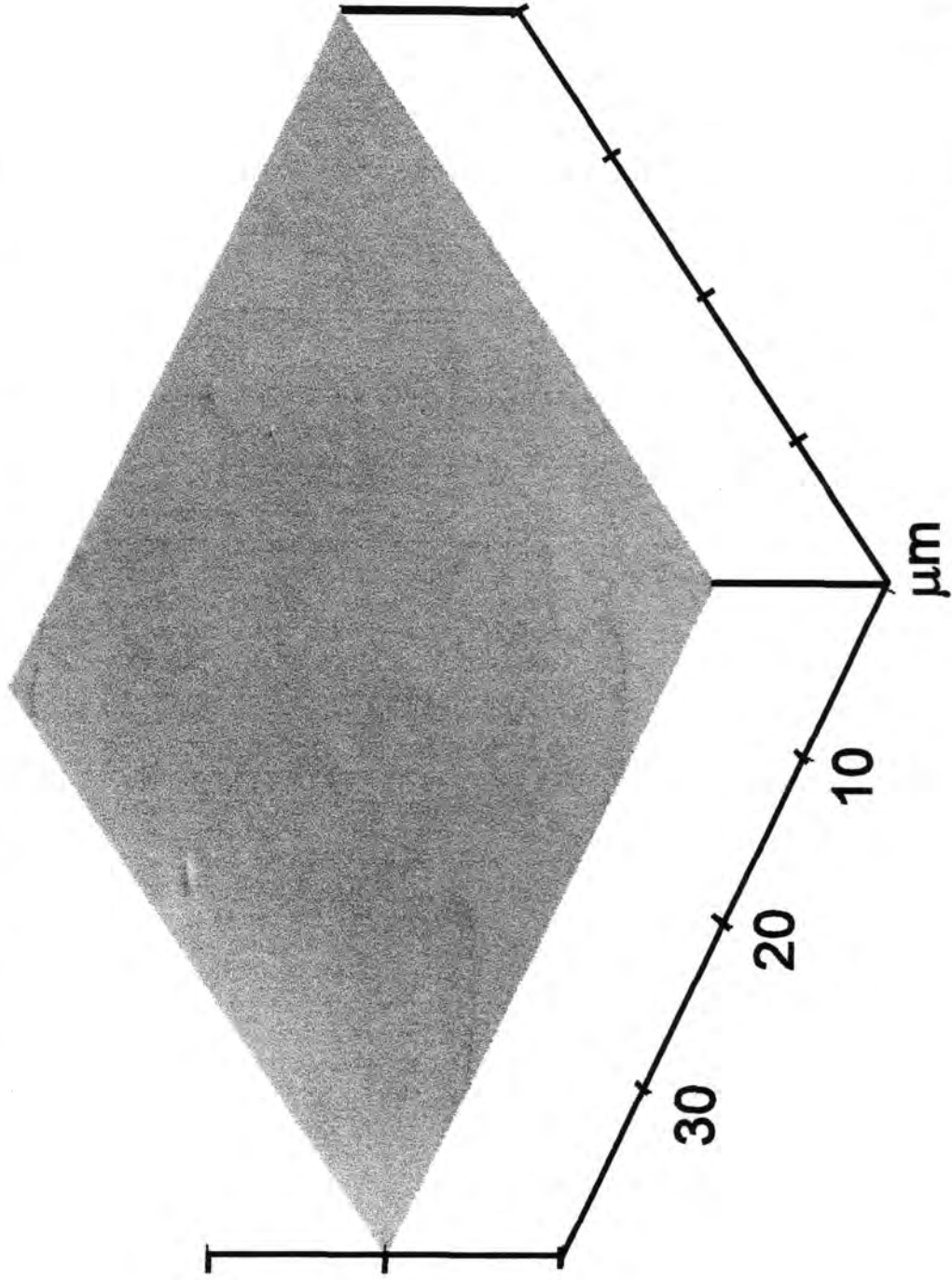Figure 3: 10 µm AFM images of a 60/40 PC/PS blend surface: (a) tapping mode; and (b) phase modulation mode.

POLYSTYRENE

POLYCARBONATE/
POLYSTYRENE

(b) PHASE IMAGE

(a) TAPPING MODE
Z Range = 100 nm

Figure 4(a): 40 μm phase modulation mode AFM image of pure polystyrene.

x = 10 μm / div

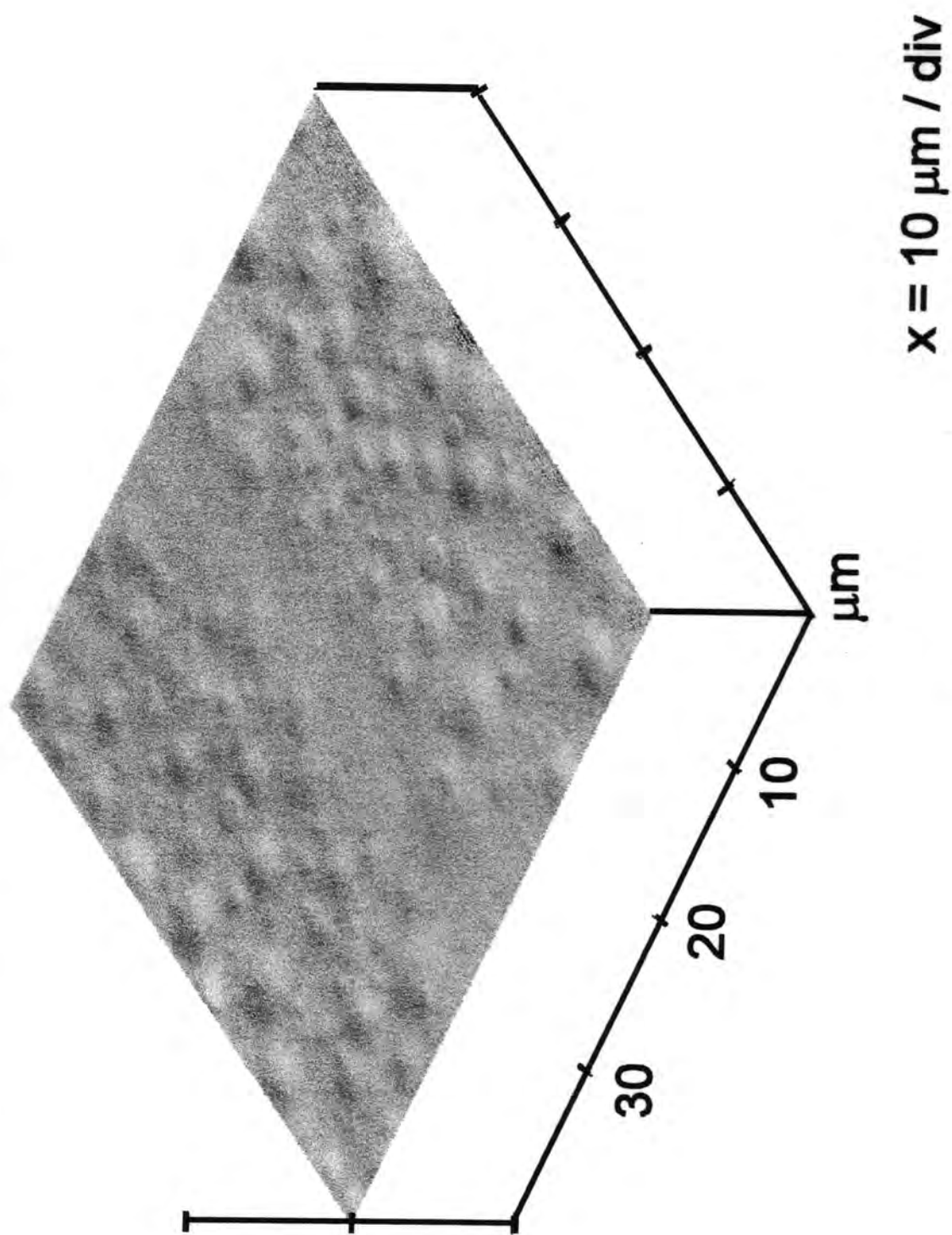Figure 4(b): 40 μm phase modulation mode AFM image of 25/75 PC/PS polymer blend.

μm

30 20 10

x = 10 μm / div

Figure 4(c): 40 μm phase modulation mode AFM image of 50/50 PC/PS polymer blend.

x = 10 μm / div

μm

10

20

30
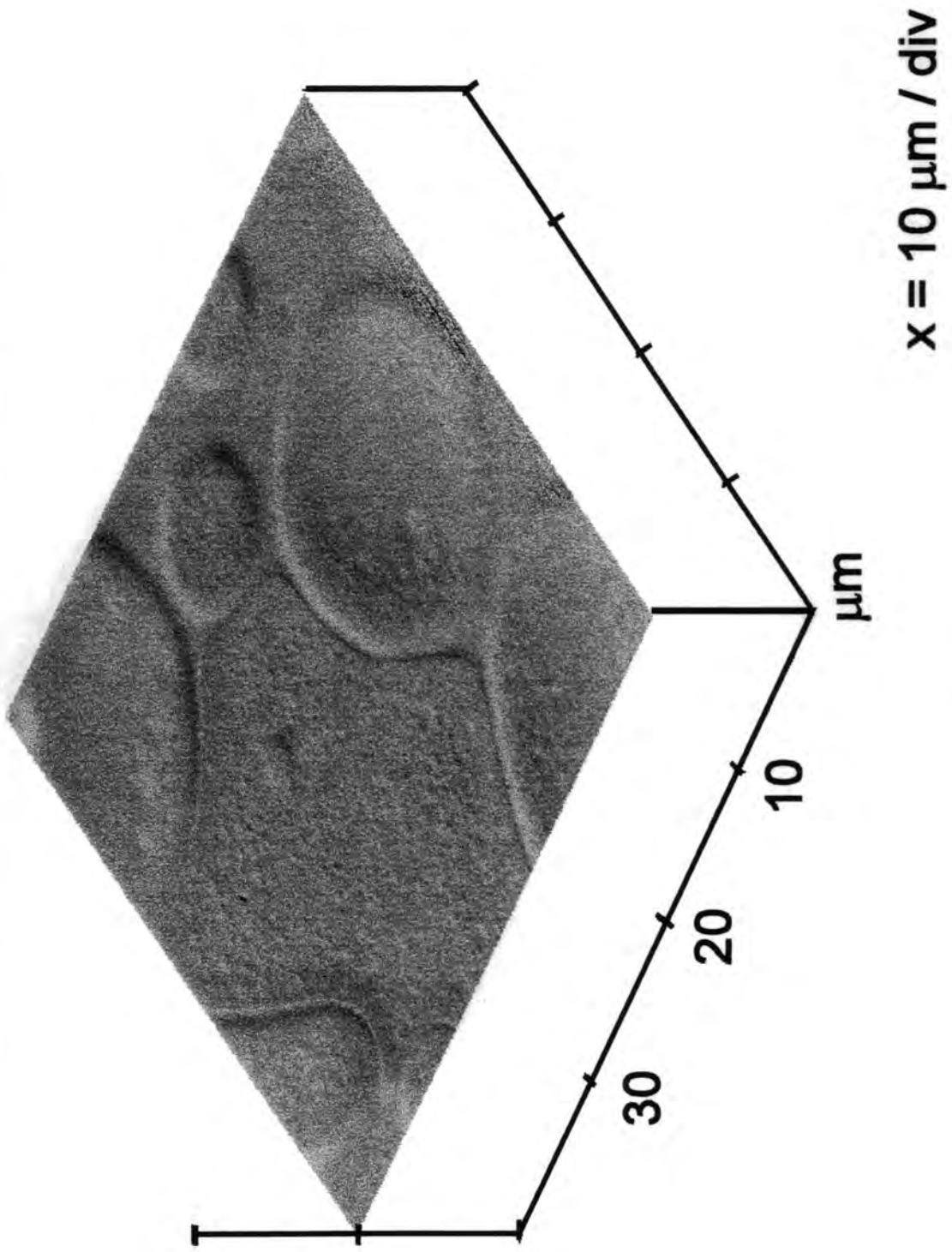
Figure 4(d): 40 μm phase modulation mode AFM image of 60/40 PC/PS polymer blend.

x = 10 μm / div

μm

10

20

30

170
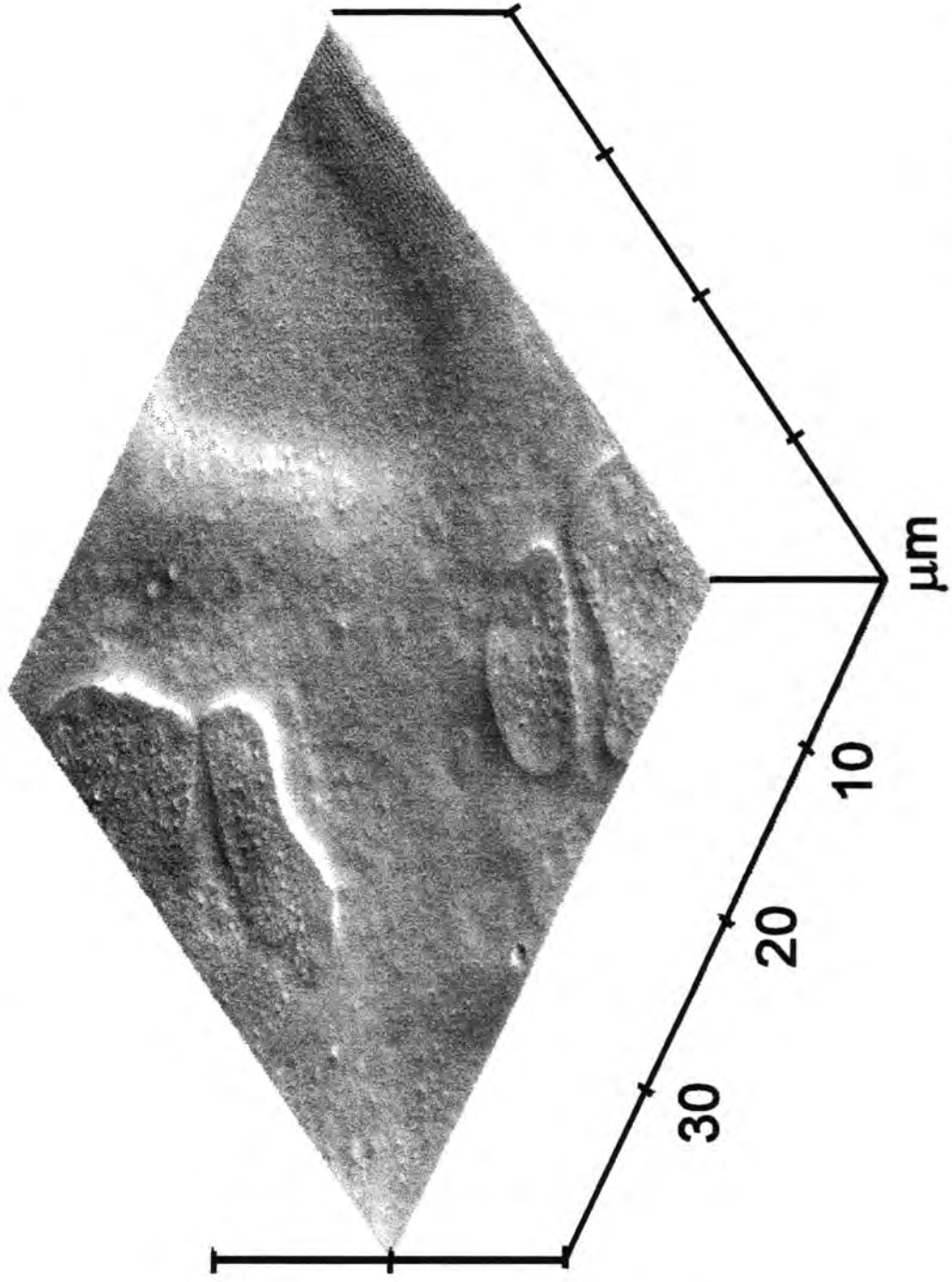
Figure 4(e): 40 μm phase modulation mode AFM image of 75/25 PC/PS polymer blend.

x = 10 μm / div

μm

10

20

30

171
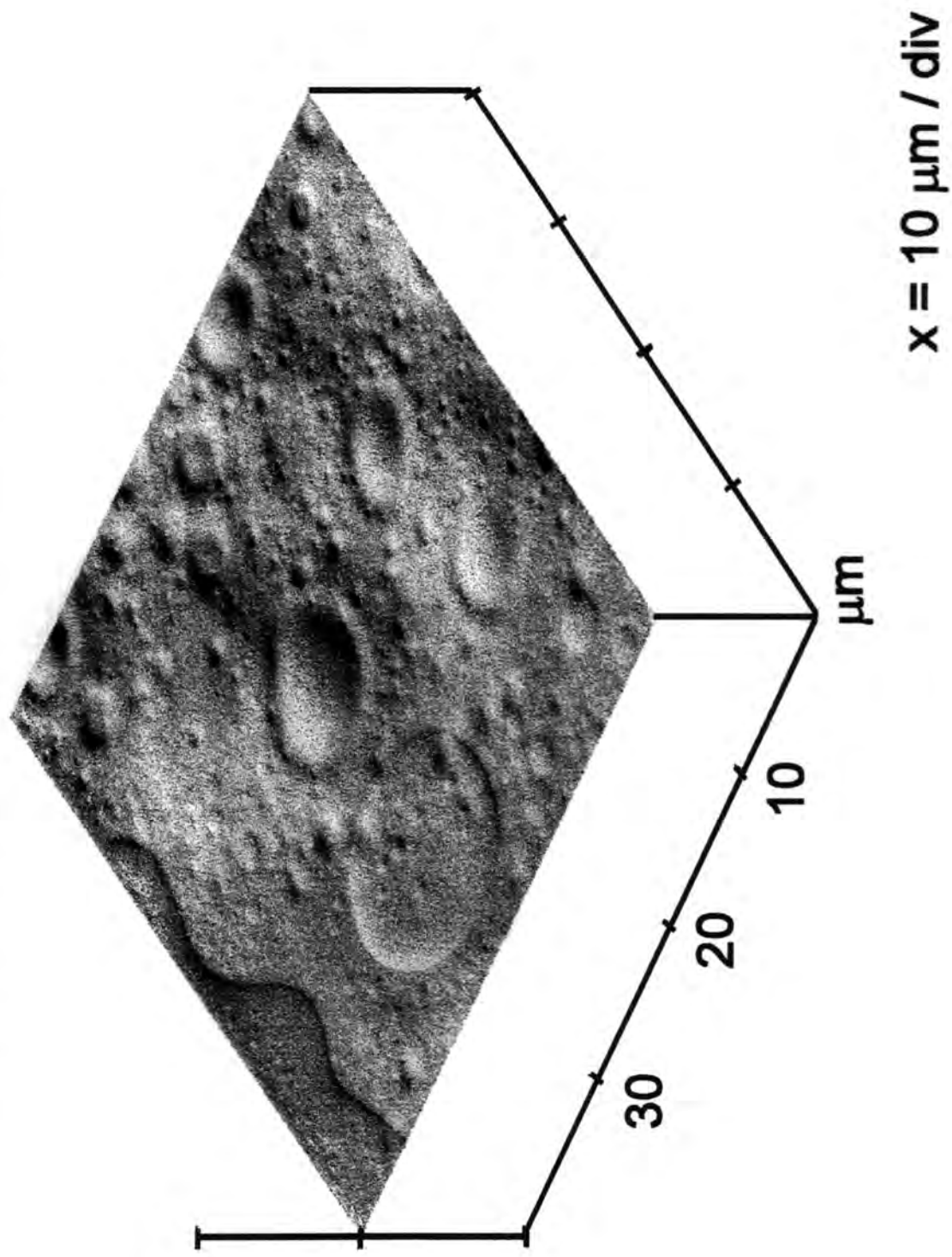
Figure 4(f): 40 µm phase modulation mode AFM image of 90/10 PC/PS polymer blend.

x = 10 µm / div

µm

10

20

30
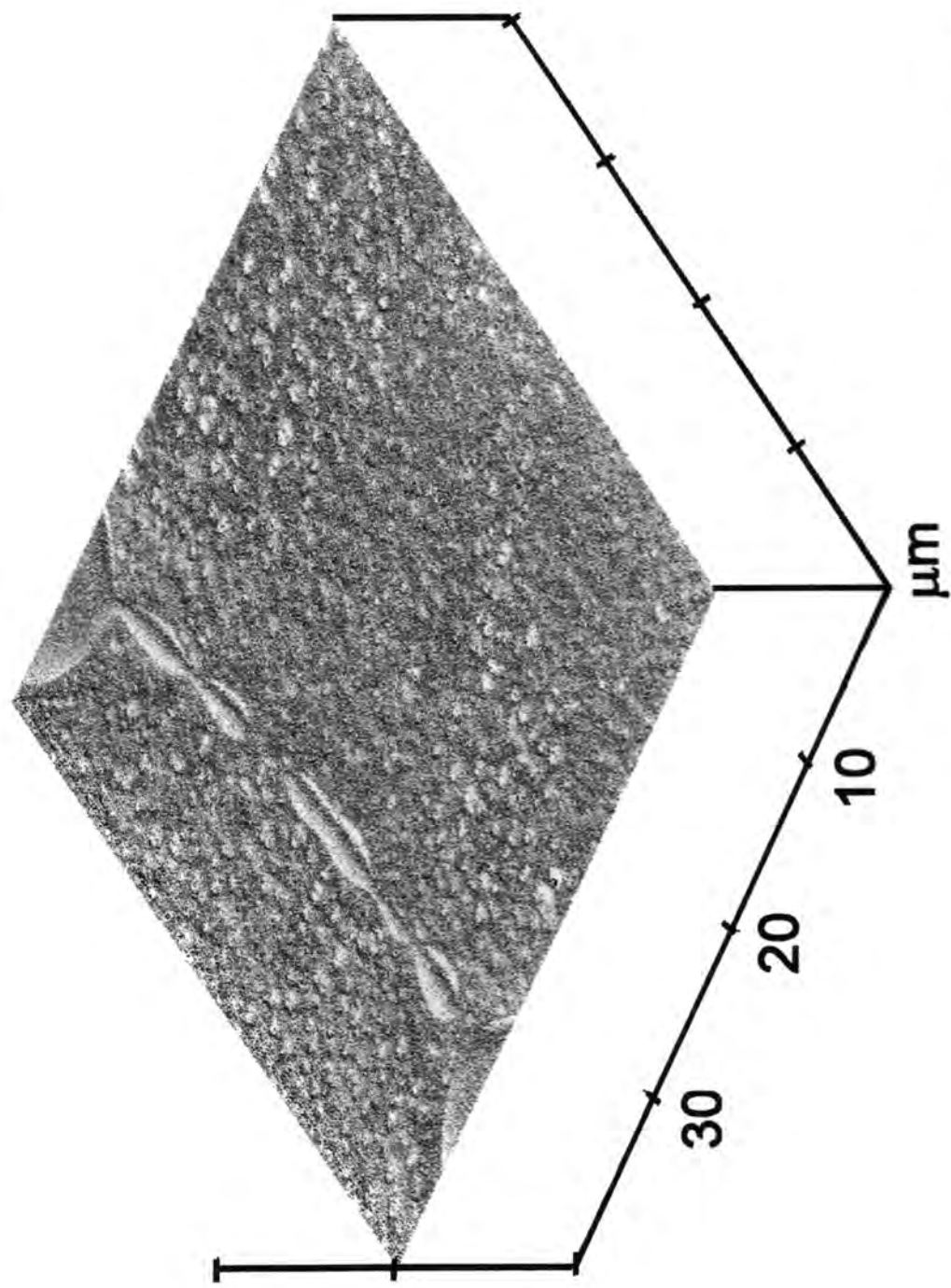
Figure 4(g): 40 μm phase modulation mode AFM image of pure polycarbonate.
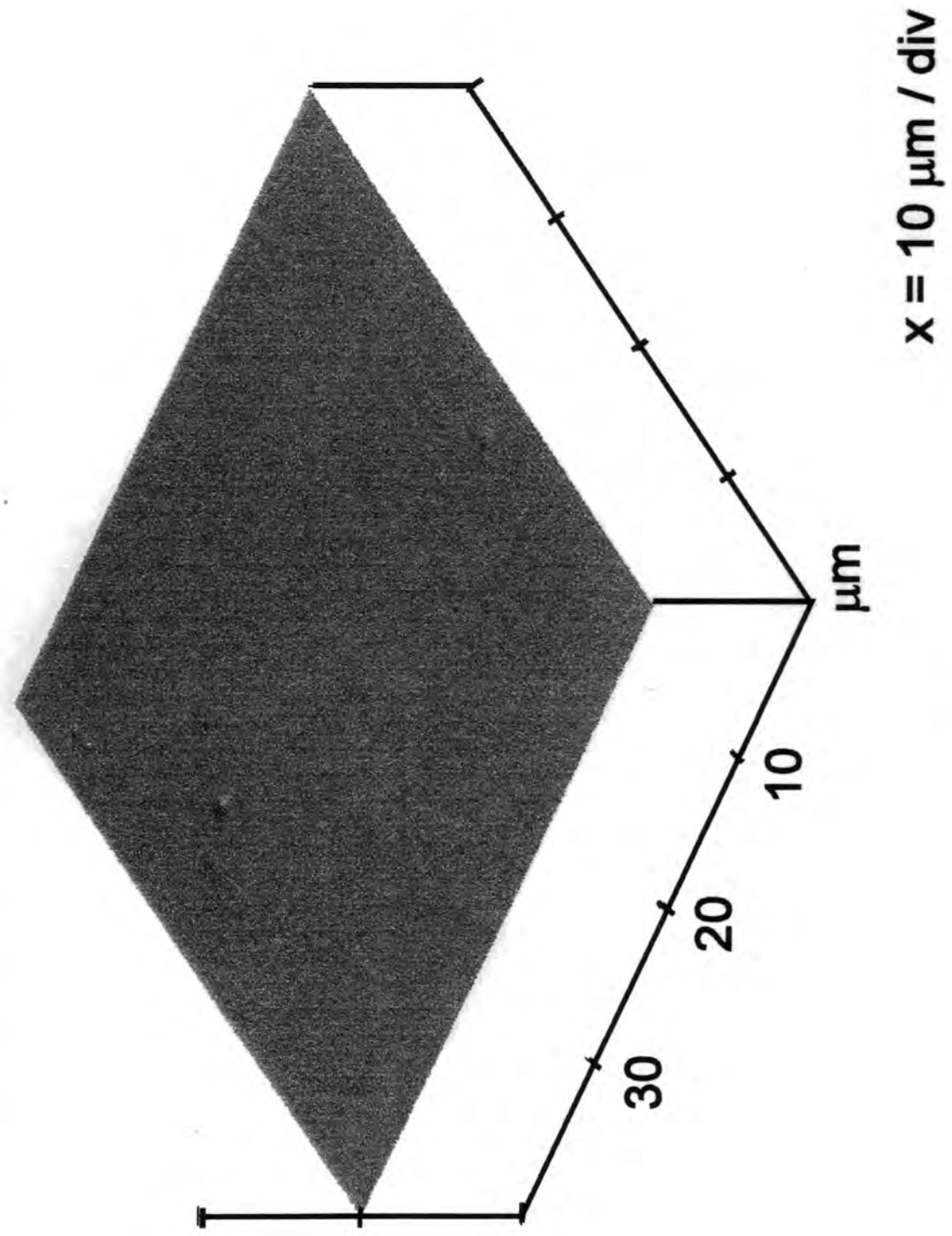
μm

10

20

30

x = 10 μm / div

Figure 5(a): 10 μm tapping mode AFM image of oxygen plasma treated pure polystyrene.

x = 2 μm / div
z = 2 μm / div

μm

2   4   6   8

174
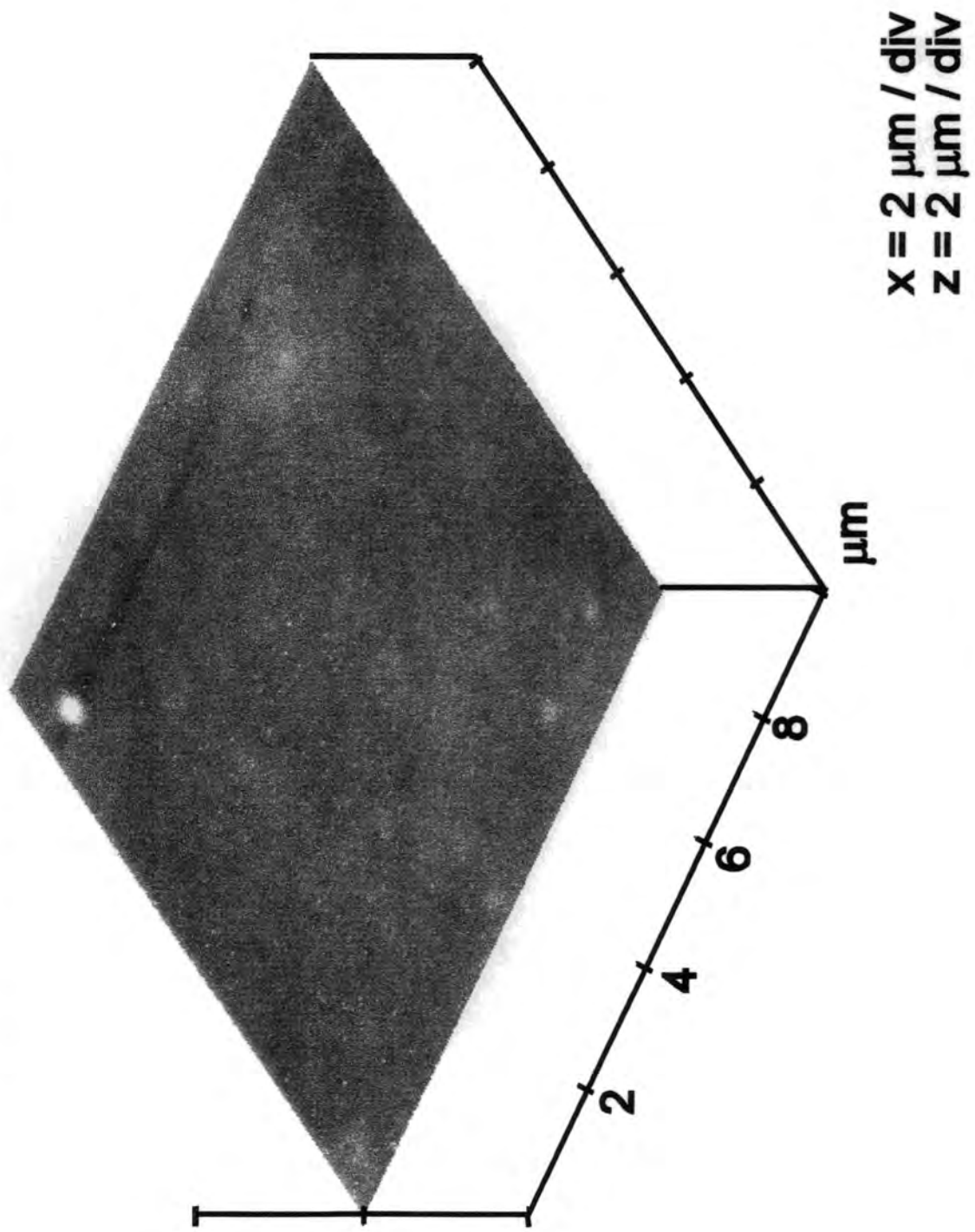
Figure 5(b): 10 μm tapping mode AFM image of oxygen plasma treated 60/40 PC/PS polymer blend.
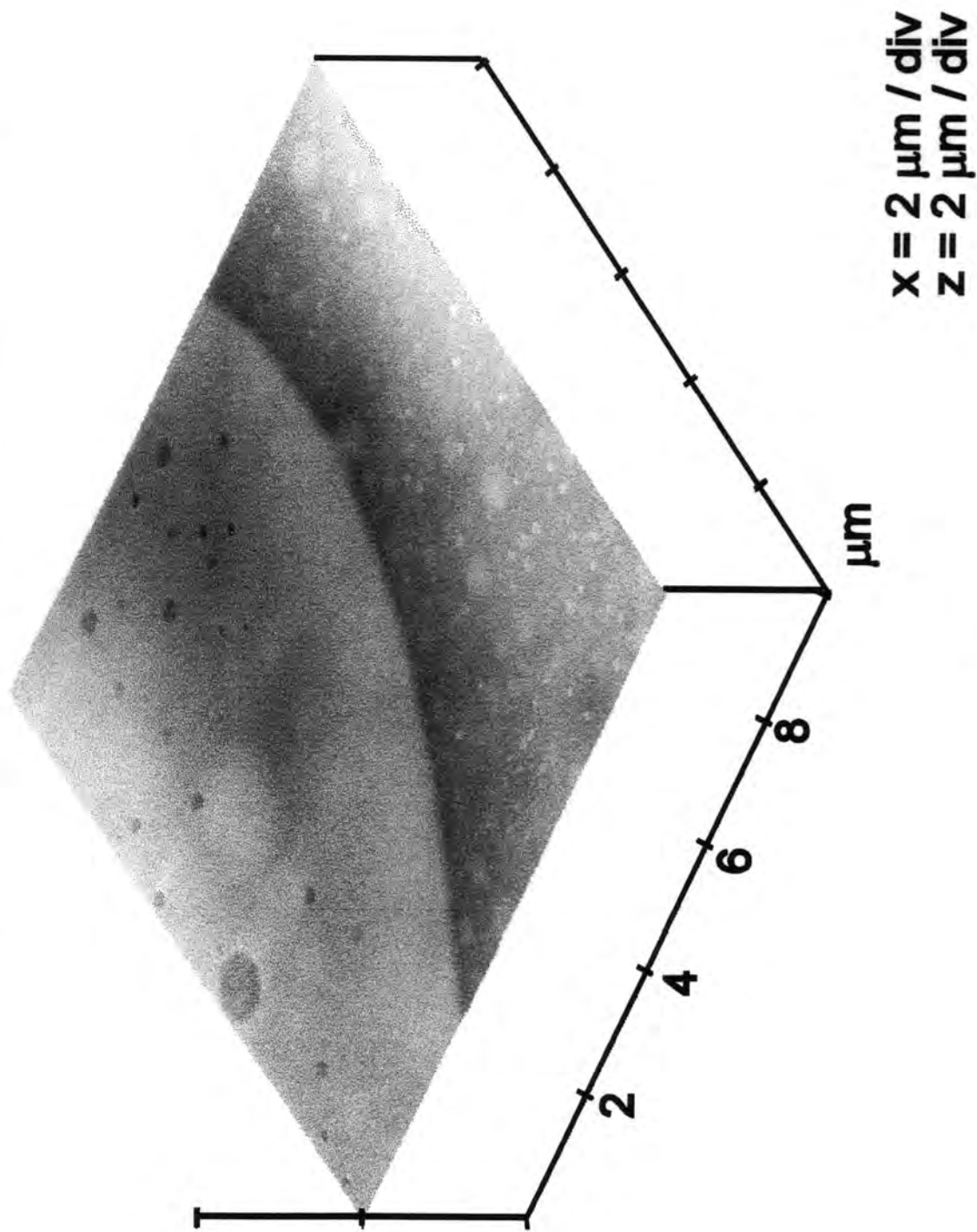
x = 2 μm / div
z = 2 μm / div

μm

2   4   6   8

Figure 5(c): 10 μm tapping mode AFM image of oxygen plasma treated 75/25 PC/PS polymer blend.

x = 2 μm / div
z = 2 μm / div

μm

2   4   6   8

176
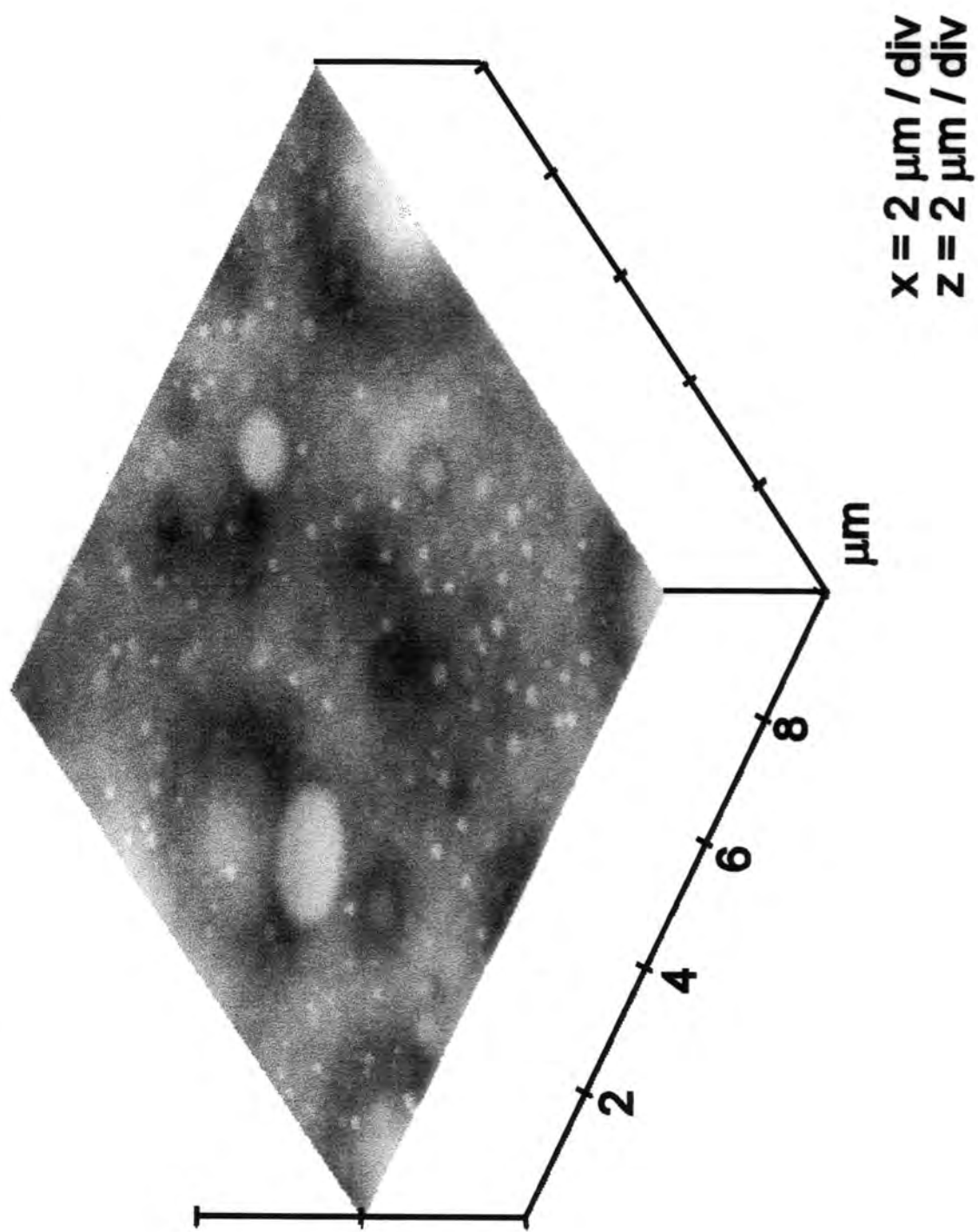
Figure 5(d): 10 μm tapping mode AFM image of oxygen plasma treated 90/10 PC/PS polymer blend.

x = 2 μm / div
z = 2 μm / div

μm

2   4   6   8

177

Figure 5(e): 10 μm tapping mode AFM image of oxygen plasma treated pure polycarbonate.

x = 2 μm / div
z = 2 μm / div

μm

178

Figure 6: 10 μm tapping mode AFM image of oxygen plasma treated 75/25 PC/PS polymer blend followed by solvent washing.

x = 2 μm / div
z = 2 μm / div

μm

2 4 6 8

Figure 7(a): 10 μm tapping mode AFM image of silent discharge treated pure polystyrene.

x = 2 μm / div
z = 2 μm / div

μm

2 4 6 8

Figure 7(b): 10 μm tapping mode AFM image of silent discharge treated 60/40 PC/PS polymer blend.

μm

8   6   4   2

x = 2 μm / div
z = 2 μm / div

Figure 7(c): 10 μm tapping mode AFM image of silent discharge treated 75/25 PC/PS polymer blend.

x = 2 μm / div
z = 2 μm / div

μm

2 4 6 8

Figure 7(d): 10 μm tapping mode AFM image of silent discharge treated 90/10 PC/PS polymer blend.

x = 2 μm / div
z = 2 μm / div

μm

2 4 6 8

Figure 7(e): 10 μm tapping mode AFM image of silent discharge treated pure polycarbonate.

x = 2 μm / div
z = 2 μm / div

μm

184

Figure 8(a): 10 μm tapping mode AFM image of silent discharge treated pure polystyrene followed by solvent washing.

x = 2 μm / div
z = 2 μm / div

μm

2   4   6   8

185

Figure 8(b): 10 μm tapping mode AFM image of silent discharge treated 60/40 PC/PS polymer blend followed by solvent washing.

x = 2 μm / div
z = 2 μm / div

μm

2 4 6 8

Figure 8(c): 10 μm tapping mode AFM image of silent discharge treated 75/25 PC/PS polymer blend followed by solvent washing.

x = 2 μm / div
z = 2 μm / div

μm

2 4 6 8

Figure 8(d): 10 μm tapping mode AFM image of silent discharge treated 90/10 PC/PS polymer blend, followed by solvent washing.

x = 2 μm / div
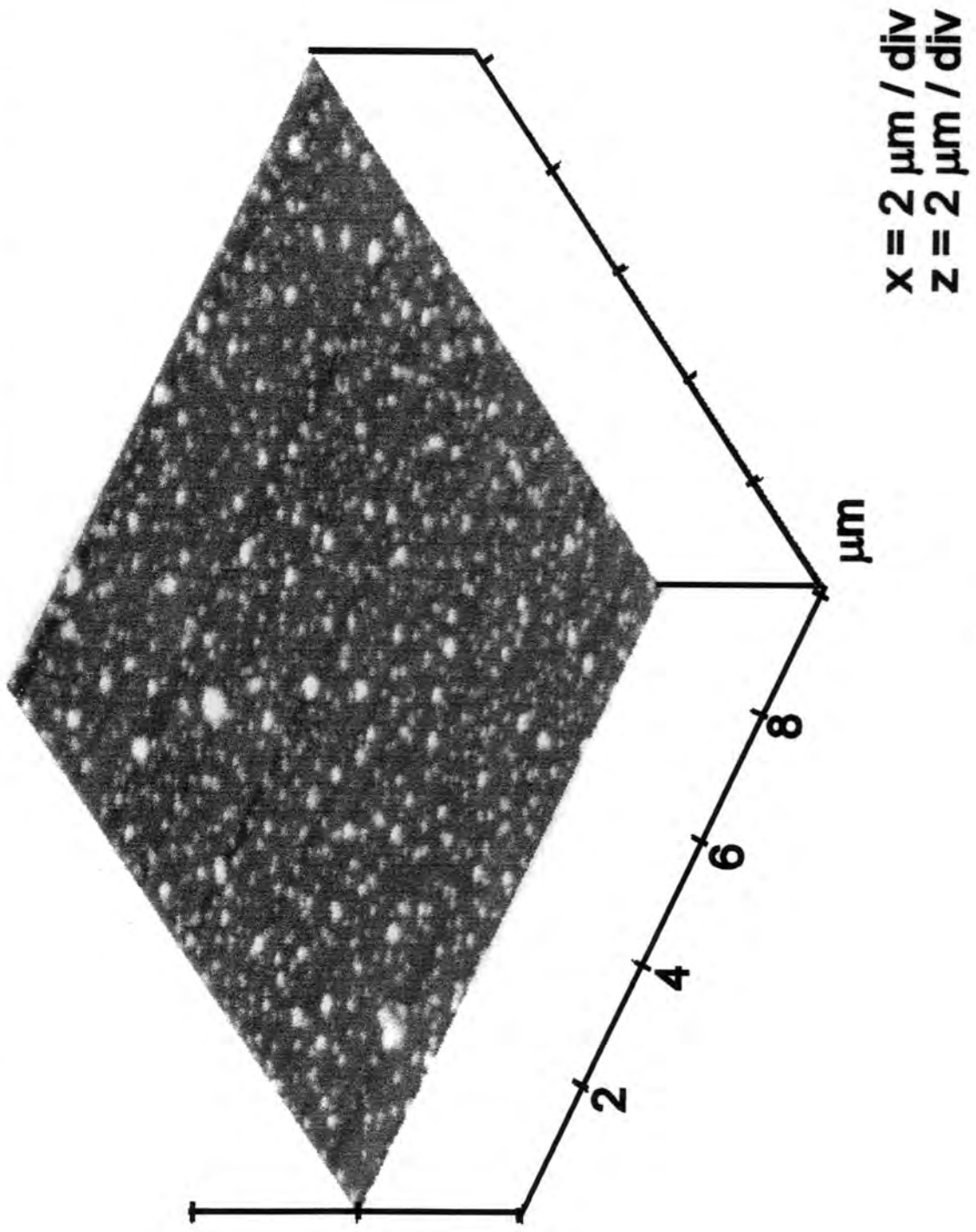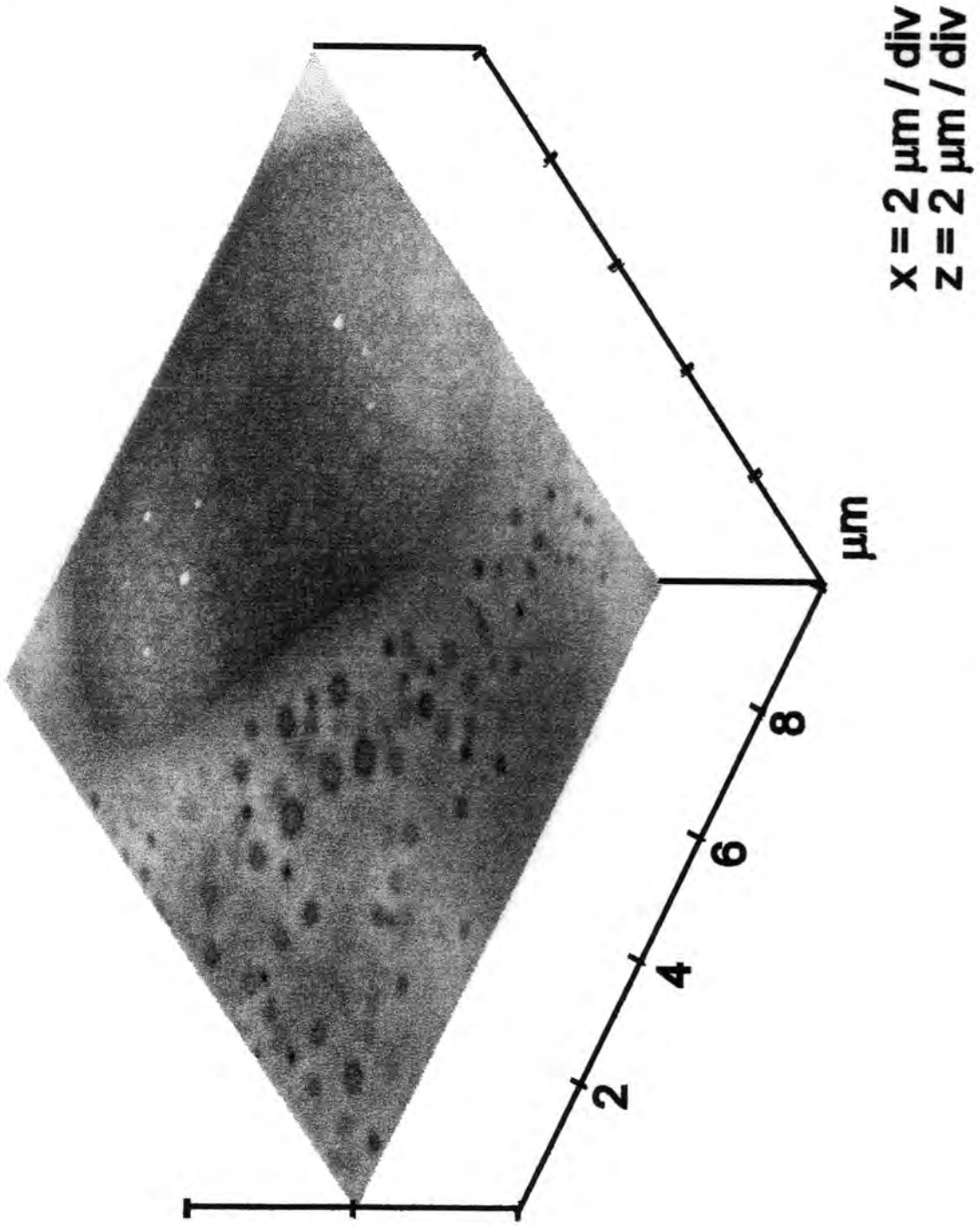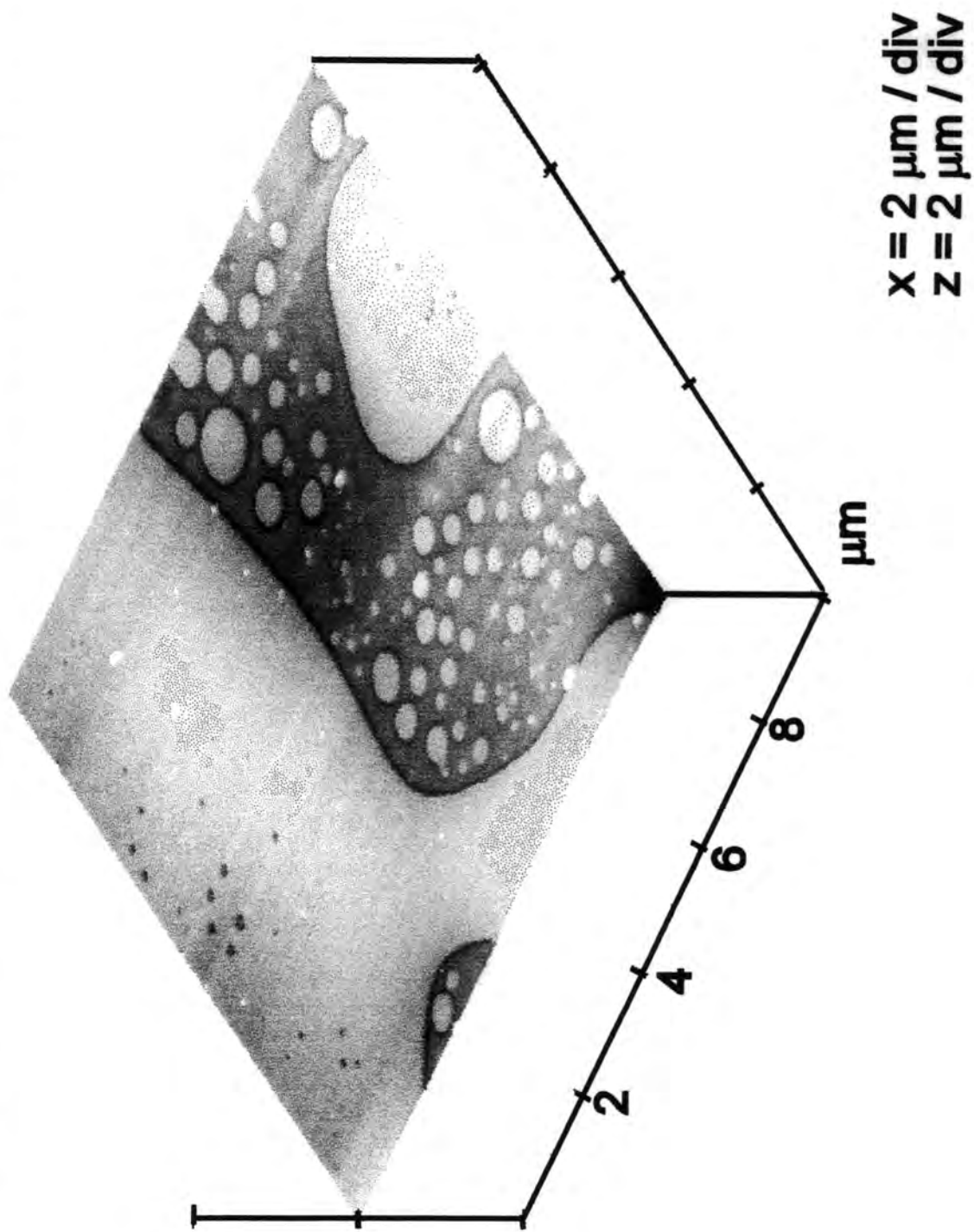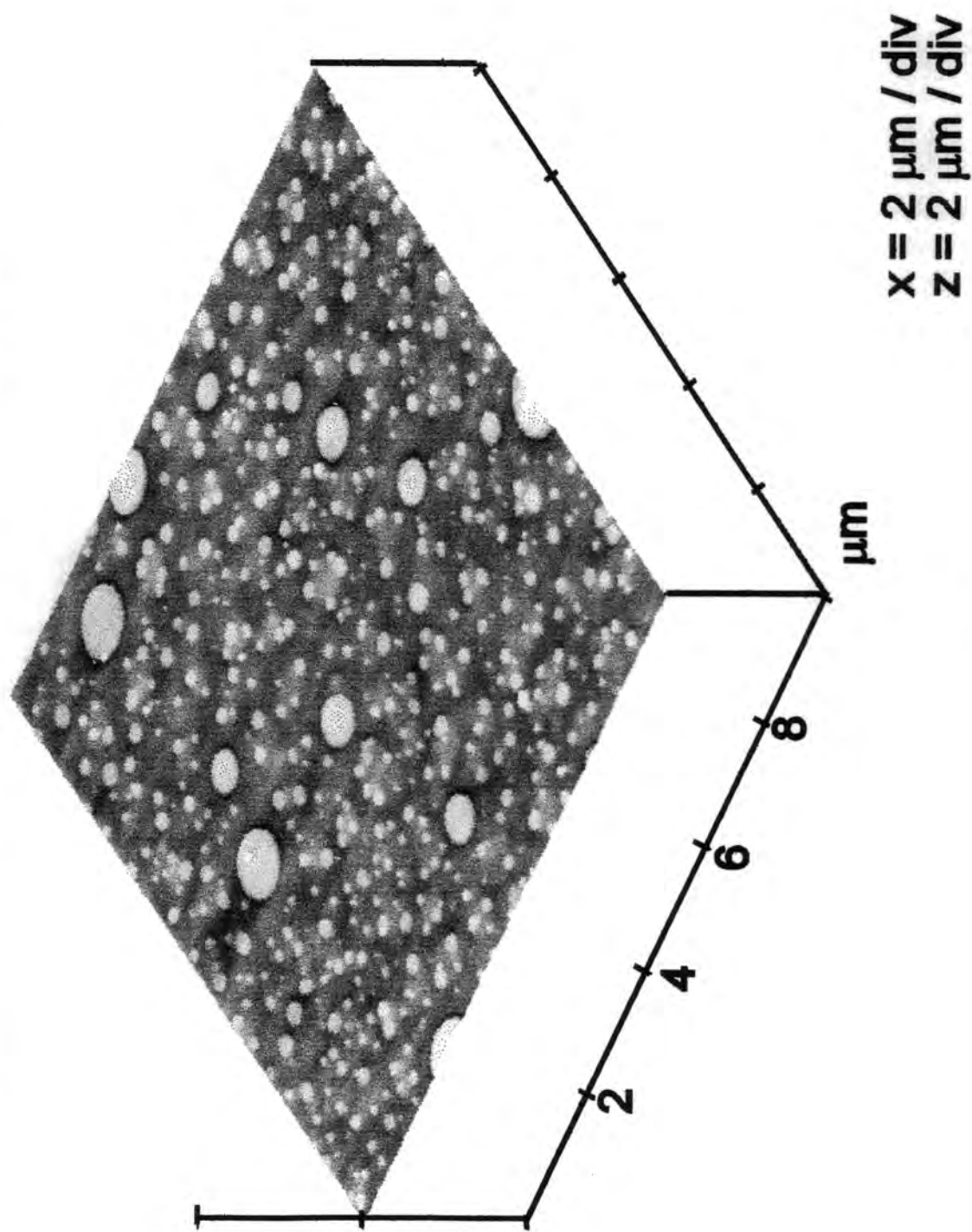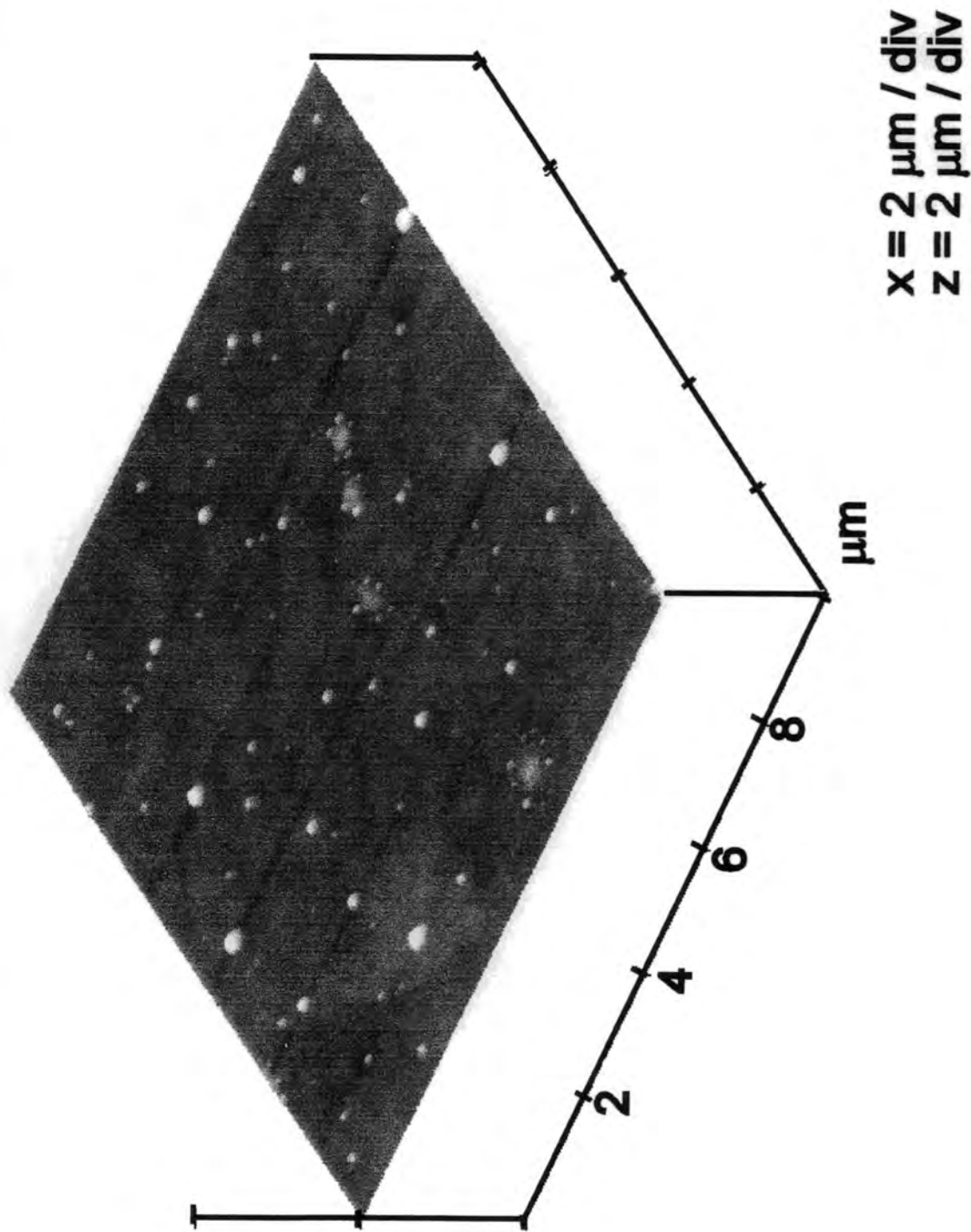z = 2 μm / div

μm

2 4 6 8

Figure 8(e): 10 μm tapping mode AFM image of silent discharge treated pure polycarbonate, followed by solvent washing.

x = 2 μm / div
z = 2 μm / div

μm

2   4   6   8

189

6.4 DISCUSSION

XPS samples over a large area, and therefore effectively yields an average compositional value of the surface. XPS analysis of the polystyrene / polycarbonate polymer blend mixtures exhibits the classical behaviour of an immiscible blend system: a non-linear variation in the O/C ratio with blend composition is observed, which can be attributed to surface enrichment by polystyrene as a result of its lower surface energy (33 dyn cm^{-1})[30] compared to polycarbonate(45 dyn cm^{-1}).[31]

Tapping mode and phase modulation AFM analysis of the untreated polymer blend surfaces showed that polystyrene tends to form a layer on top of the blend at low concentrations of polycarbonate. The underlying blend mixture consists of small circular polystyrene phases embedded within a continuous polycarbonate phase.[8,28] The polymer blend constituent with the higher surface energy is normally expected to be raised to a higher topography.[32] This is consistent with the host polycarbonate matrix appearing higher within the localised blend mixture regions, Figure 3.

Oxygen glow discharge and silent discharge plasmas produce a variety of reactive species which bombard an underlying polymer substrate and lead to the formation of low molecular weight oxidised material (LMWOM), which exists as globules on the surface (see chapters 2 and 3). A difference in wetting behaviour between the LMWOM and the underlying polystyrene / polycarbonate regions helps to identify the respective blend phases. Such oxidative plasma treatment of polymer blend surfaces can lead to preferential etching of one constituent[33,34] as well as chemical modification.[2] The mass rate loss of polycarbonate is twice that of polystyrene during oxidative electrical discharge treatment.[29] This can clearly be seen by AFM analysis of the oxygen plasma treated and the solvent washed silent discharge treated polymer blend surfaces, Figures 5 and 8. The fact silent discharge treated surfaces have to be washed to reveal the phase morphology shows that more LMWOM is generated for silent discharge treated surfaces and that the LMWOM is mobile during its formation. This mobility arises from either the difference in the surface energy or local melting effects occurring on the polymer surface during the silent discharge treatment.[35]

6.5 CONCLUSIONS

Surface enrichment of the polystyrene phase is found to occur for polystyrene / polycarbonate blend mixtures. This is accompanied by polycarbonate forming a continuous bulk phase containing embedded regions of polystyrene. Oxygen plasma and silent discharge treatment of these polymer blend surfaces produces low molecular weight oxidised material, which can be washed off by solvent, to leave behind the polystyrene component raised at a higher topography as a result of polycarbonate having undergone a greater level of degradation during plasma treatment.

REFERENCES

1 . Paul, D. R. In *Polymer Blends*; Paul, D. R.; Newman, S. Eds.; Academic; San Diego. 1987; Volume1, Chapter 1.

2 . Vargo, T. G.; Hook. D. J.; Gardella, J. A.; Eberhardt, M. A.; Meyer. A. E.; Baier. R. E. *J. Polym. Sci., Polym. Chem. Ed.* **1991**, *29*, 535.

3 . Paul, D. R.; Barlow, J. W. In *Multiphase Polymers*; Cooper, S. L.; Estes. G. M. Advances in Chemstry Series 176; American Chemical Society: Washington, D. C., 1979; Chapter 17.

4 . Partridge, I. K. In *Multicomponent Polymer Systems*; Miles, I. S.; Rostami, S. Eds.; Longman: Essex, 1992; Chapter 5.

5 . Borggreve, R. J. M.; Gaymans, R. J.; Schuijer, J.; Ingen Housz, J. F. *Polymer* **1987**, *28*, 1489.

6 . Kresge, E. N. In *Polymer Blends*; Paul, D. R.; Newman, S. Eds.; Academic; San Diego, 1987; Volume 2, Chapter 20.

7 . Utracki, L. A.; Vu-Khanh, T.; In *Multicomponent Polymer Systems*; Miles, I. S.; Rostami, S. Eds.; Longman: Essex, 1992; Chapter 7.

8 . Groeninckx, G.; Chandra, S.; Berghmans, H.; Smets, G. In *Multiphase Polymers*; Cooper, S. L.; Estes, G. M. Eds.; Advances in Chemstry Series 176; American Chemical Society: Washington, D. C., 1979; Chapter 18.

9 . Sawyer, L. C.; Grubb, D. T. *Polymer Microscopy*; Chapmann and Hall: London. 1987.

10 . Dong, L.; Greco, R.; Orsello, G. *Polymer.* **1993**, *34*, 1375.

11 . Mao, L. J.; Zhang, Z. P.; Ying, S. K. *Polym. Comm.* **1991**, *32*, 242.

12 . Goizueta, G.; Chiba, T.; Inoue, T. *Polymer*. **1992**, *33*, 886.

13 . Goizueta, G.; Chiba, T.; Inoue, T. *Polymer*. **1993**, *34*, 253.

14 . Olabisi, O.; Robeson, L. M.; Shaw, M.T. *Polymer - Polymer Misicibility*; Academic: New York, 1979.

15 . Binning, G.; Quate, C. F.; Gerber, C. *Phys. Rev. Lett.* **1986**, *56*, 930.

16 . Motomatsu, M.; Nie, H-Y.; Mizutani, W.; Tokumoto, H. *Jpn. J. Appl. Phys., Part 1* **1994**, *33*, 3775

17 . Nick, L.; Lippitz, A.; Unger, W.; Kindermann, A.; Fuhrmann, J. *Langmuir* **1995**, *11*, 1912.

18 . Viville, P.; Thoelen, O.; Beauvois, S.; Lazzaroni, R.; Lambin, G.; Bredas, J. L.; Kolev, K.; Laude, L. *Appl. Surface. Sci.* **1995**, *86*, 411.

19 . Overnay, R. M.; Meyer, E.; Frommer, D.; Brodbeck, D.; Luthi, R.; Howdt, L.; Guntherodt, H.-J.; Fujihira, M.; Taano, H.; Gotoh, Y. *Nature* **1992**, *359*, 133.

20 . Baselt, D. R.; Baldeschwieler, J. D. *J. Appl. Phys.* **1994**, *76*, 33.

21 . Frisbie, C. D.; Rozsnyai, L. F.; Noy, A.; Wrighton, M. S.; Lieber, C. M. *Science* **1994**, *265*, 2071.

22 . Babcock, K. L.; Prater, C. B. *Phase Imaging: Beyond Topography*; Technical Support Note, Digital Instruments: California; 1995.

23 . Krause, S. In *Polymer Blends*; Paul, D. R.; Newman, S., Ed.; Academic: San Diego, 1978; Vol. 1, Chapter 2.

24 . Mobae, A.; Mckay, R. A.; Schaefer, J. *Macrmolecules* **1992**, *25*, 4084.

25 . Fuchs, O. In *Polymer Handbook*; Brandrup, J.; Immergut, E.H. Eds.; Wiley: New York, 1989; 3rd ed., p379.

26 . Strobel, M.; Dunatov, C.; Strobel, J. M.; Lyons, C. S.; Perron, S. J.; Morgen, M. C. *J. Adhesion. Sci. Techol.* **1989**, *3*, 321.

27 . Briggs, D.; Kendall, C. R.; Blythe, A. R.; Wootton, A. B. *Polymer* **1983**, *24*, 47.

28 . Cheng, T. W.; Keskkula, H.; Paul, D. R. *J. Appl. Polym. Sci.* **1992**, *45*, 1245.

29 . Hansen, R. H.; Pascale, J. V.; deBenedictis, P. T.; Rentzepis. P. M. *J. Polym. Sci. A* **1965**, *3*, 2205.

30 . Toyama, M.; Ito, T.; Moriguchi, H. *J. Appl. Polym. Sci.* **1970**, *14*, 2039.

31 . Lee, L. H. in *Adhesion of High Polymers IV: Relationships Between Surface Wetting and Bulk Properties of High Polymers*; Gould, R. F., Ed.; Advances in Chemsitry Series 87; American Chemical Society: Washington, DC, 1968; p 106.

32 . Motomatsu, M.; Nie, H-Y.; Mizutani, W.; Tokumoto, H. *Jpn. J. Appl. Phys., Part 1* **1994**, *33*, 3775

33 . Takamatsu, S.; Kobayashi, T.; Komoto, T.; Sugiura, M.; Ohara, K. *Polymer* **1994**, *35*, 3598.

34 . Kushida, M.; Imaizumi, Y.; Harada, K.; Ueno, N.; Sugita, K. *Jpn. J. Appl. Phys.* **1995**, *34*, 4234.

35 . Overney, R. M.; Luthi, R.; Haefke, H.: Frommer. J.: Meyer. E.: Guntherodt. H.-J.: Hild, S.; Fuhrmann, J. *Appl. Surface Sci.* **1993**, *64*, 197.

CHAPTER 7:

ATOMIC FORCE MICROSCOPY INVESTIGATION INTO

SINGLE CRYSTALS OF POLY (DIMETHYL SILANE).

7.1 INTRODUCTION

Polymer single crystals have been known to be grown from dilute solutions since 1953.[1] They all have the same general appearance of thin lamellae with the lateral dimensions of microns and a thickness of the order of nanometers.[2,3] In the crystal the polymer chains are almost vertical to the lamellor surface. Since the end to end distance of a fully extended polymer chain is several hundred nanometers long[4] then the only way the polymer chain can be incorporated into the polymer crystal is by chain folding.[4,5] There are two main models for chain folding; a random (switch board) model and a regular adjacent folding model.[6] Experimental evidence from neutron scattering[7] and infra-red[8] spectroscopies has shown that chain folding occurs in a polymer single crystal via the latter model, as shown in Figure 1. There is a considerable body of evidence[9] that points to the existence of an "amorphous layer" associated with the chain folds of the polymer,[9] physically absorbed polymer material,[9] or surface defects.[10]

The morphology of single crystals has been extensively studied using electron microscopy[11,12] and atomic force microscopy.[3,13,14] Recently there has been a great interest in molecular resolution of highly crystalline polymers.[15-18] Molecular resolution of single crystals has been hampered by the small size of the carbon atoms and the presence of the amorphous layer. Here we investigate the morphology and crystal structure of poly (dimethyl silane) grown from solution, using atomic force microscopy. Poly (dimethyl silane) is a highly crystalline polymer which adopts an all-trans arrangement in the solid[19] which crystallises with large lattice parameters due to silicon's large size compared to carbon's.

Figure 1: Chain folds in a polymer single crystal

Polymer Chains
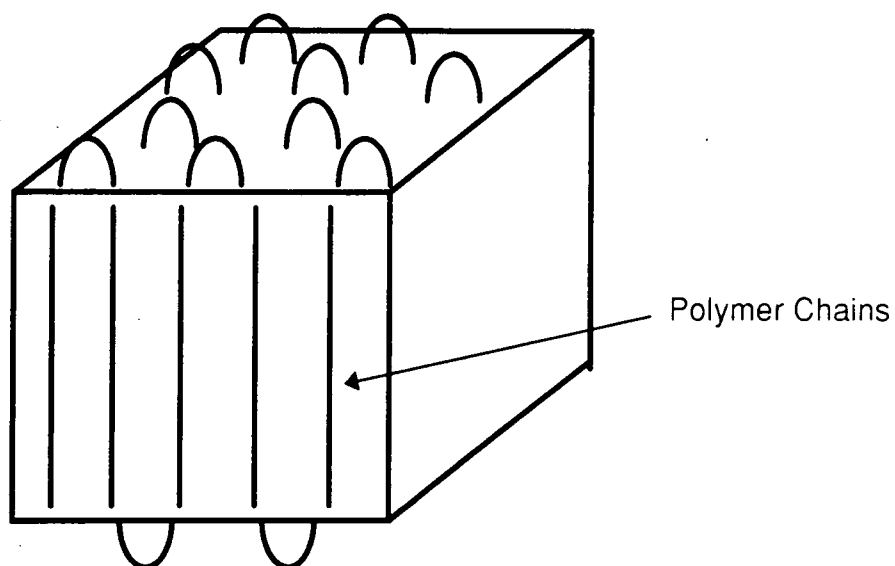
7.2 EXPERIMENTAL

7.2.1 Preparation of Poly (dimethyl silane) Single Crystals

A very dilute (0.001 % w/v) solution of poly (dimethyl silane) (ABCR) in toluene was prepared. This solution was heated to 100 °C for 30 minutes and then allowed to slowly cool to room temperature. Drops of the suspension were deposited onto freshly cleaved mica and the solvent was allowed to evaporated before AFM analysis.

7.2.2 Atomic Force Microscopy

All AFM images were taken using the contact mode of a Digital Instruments Nanoscope III microscope. Cantilevers and tips were fabricated from silicon nitride. 200 μm long cantilevers were used with a spring constant of 0.06 Nm^{-1}. Micron scale images were obtained by using the 100 μm J-scanner and molecular resolution images were obtained with the 1 μm A-scanner.

7.3 RESULTS AND DISCUSSION

A 2 micron wide scan of a of a crystal of poly (dimethyl silane), Figure 2, shows a orthorhombic platelet structure. The thickness of the crystallite is of the order of 5 nm. This agrees with previous thickness measurements of single crystal poly (dimethyl silane) studied using electron microscopy.[20] Molecular scale resolution images of poly (dimethyl silane), Figure 3, shows rows of rod likes species. The length of the Si-Si bonds in the polymer backbone of poly (dimethyl silane) is 0.4 nm.[19] The separation of the rod like features seen in in figure 3 is of the order of a micron and do not correspond to the polymer repeat units. It is more likely that these rod-like features correspond to chain folds at the single crystal surface, Figure 1. If this is so then this would correspond to a monoclinic crystal structure with lattice parameters of 0.80 ± 0.05 nm and 1.24 ± 0.05 nm with a lattice angle of $95° \pm 5°$ (shown in Figure 3). This is consistent with the monoclinic unit cell having a = 1.218 nm, b = 0.800 nm, c = 0.388 nm and $\gamma = 91°$ with interchain lattice spacings of 0.608 nm as determined by x-ray diffraction.[19]

Figure 2: Contact mode AFM image of a poly (dimethyl silane) single crystal.
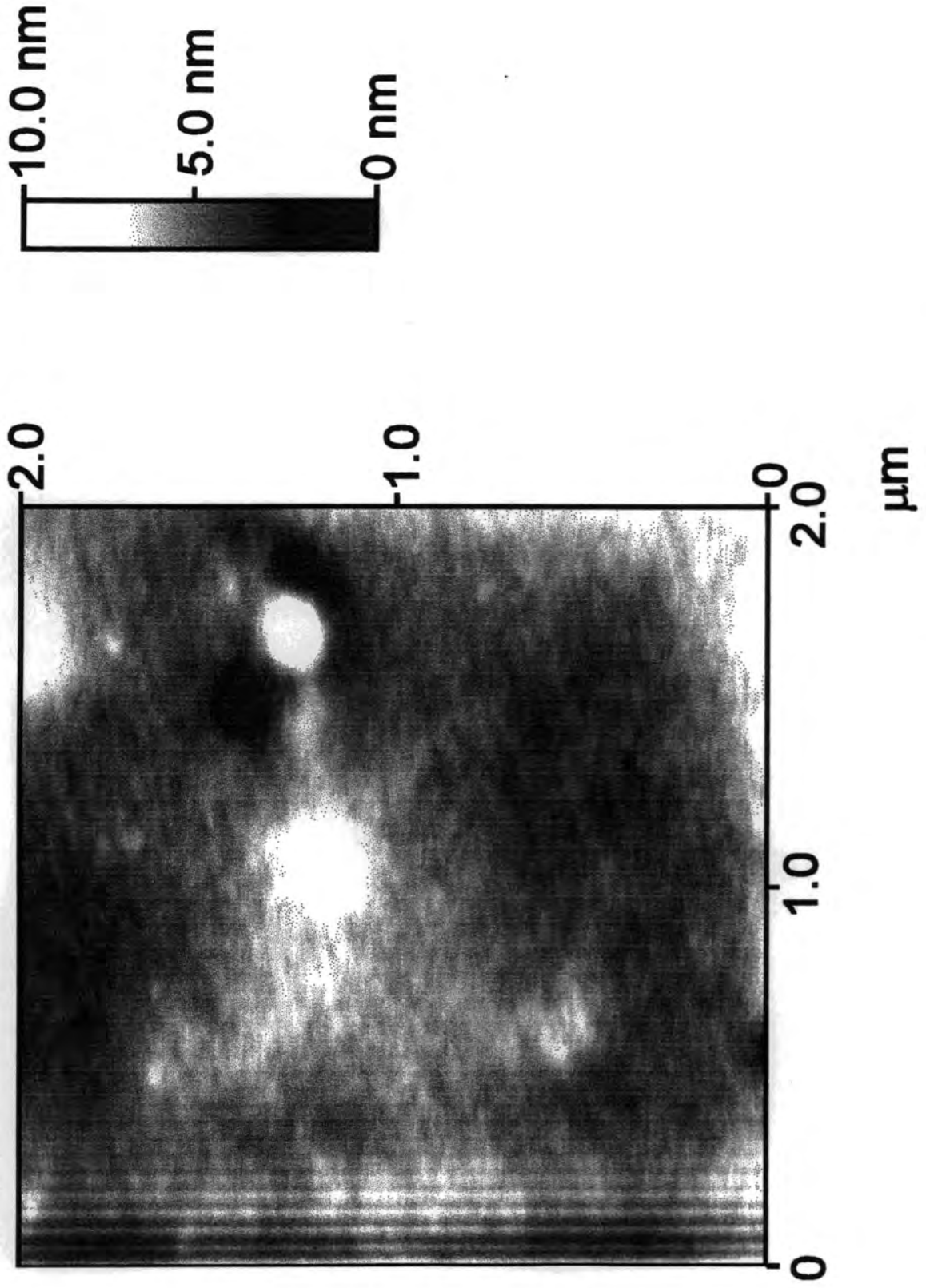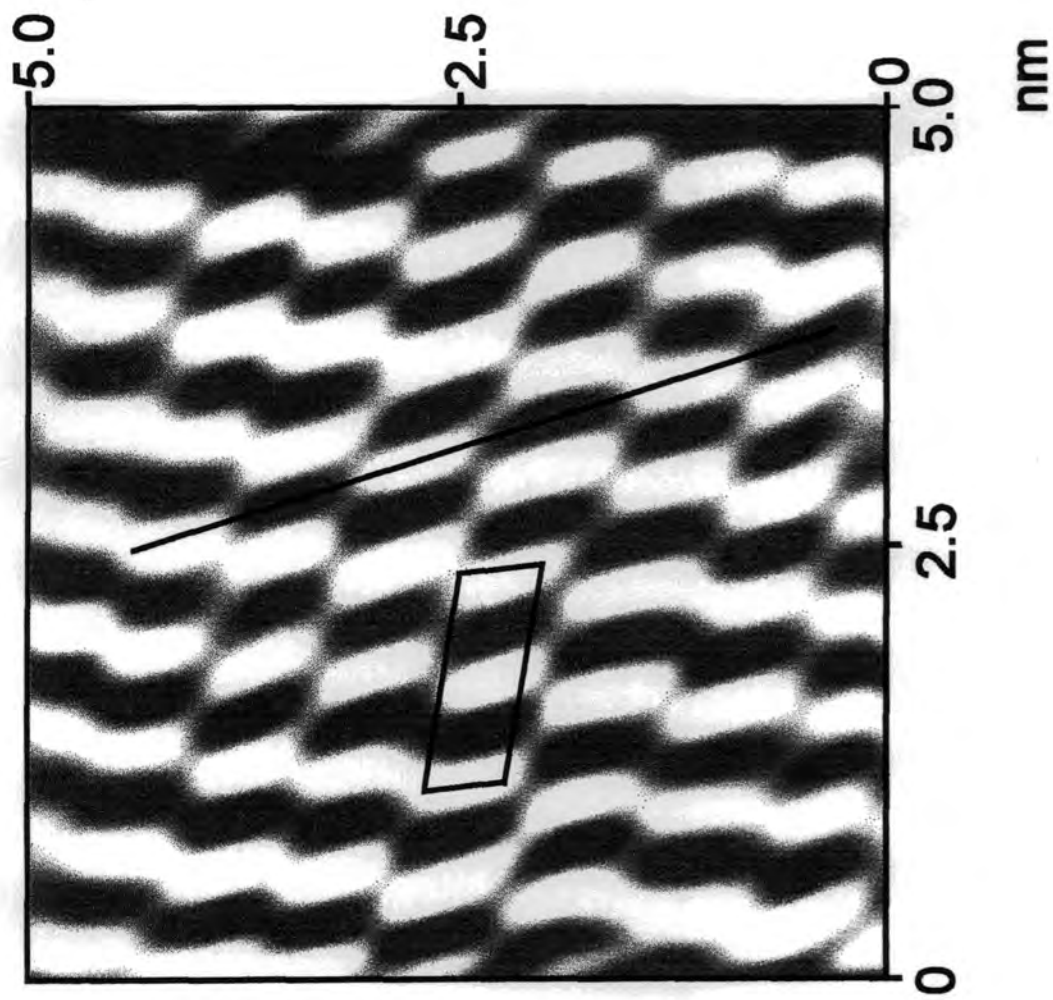
199

Figure 3: Molecular resolution AFM image of a poly (dimethyl silane) single crystal surface.

7.4 CONCLUSIONS

Atomic force microscopy has been used to determine the morphology of polymer (poly (dimethyl silane)) single crystals and to visualise the chain folding occurring at the surface of a single crystal.

REFERENCES

1 . Schlesinger, W.; Leeper, H. M. *J. Polym. Sci.* **1953**, *11*, 203.

2 . Billmeyer, F. W. *Textbook of Polymer Science*; Wiley: New York, 1962.

3 . Nakagawa, Y.; Hayashi, H.; Takahagi, T.; Soeda, F.; Ishitani,A.; Toda,A.: Miyaji, H. *Jpn. J. Appl. Phys.* **1994**, *33*, 3771.

4 . Billingham, N. C.; Jenkins, A. D. In *Polymer Science*; Jenkins, A. D., Ed.: North-Holland: Amsterdam, 1973; Vol 1, Chapter 2.

5 . Keller, A. *Philos. Mag.* **1957**, *2*, 1171.

6 . Frank, F. C. *Faraday Discuss. Chem. Soc.* **1979**, *68*, 7.

7 . Sadler, D. M. In *Structure of Crystalline Polymers*; Hall, I. H., Ed.; Elsevier Applied Science: London, 1984; Chapter 4.

8 . Krimm, S.; Cheam, T. C. *Faraday Discuss. Chem. Soc.* **1979**, *68*, 244.

9 . Hoffman, J. D.; Davis, G. T. In *Polymer Surfaces*; Clark, D. T.; Feast, W. J., Eds.: Wiley: Chichester, 1978; Chapter 13.

10 . Sharples, A. In *Polymer Science*; Jenkins, A. D., Ed.; North-Holland: Amsterdam, 1973; Vol 1, Chapter 4.

11 . Tsuji, M.; Isoda, S.; Ohara, M.; Kawaguchi, A.; Katayama, K *Polymer* **1982**, *23*, 1568.

12 . Isoda, S.; Tsuji, M.; Ohara, M.; Kawaguchi, A.; Katayama, K. *Polymer* **1984**, *24*, 1155.

13 . Vancso, G. J.; Nisman, R.; Snetivy, D.; Schohnerr, H.; Smith, P.; Ng, C.; Yang, H. F. *Colloids and Surfaces A* **1994**, *87*, 263.

14 . Miles, M. J.; Jandt, K. D.; McMaster, T. J.; Willamson, R. L. *Colloids and Surfaces A* **1994**, *87*, 235.

15 . Stockler, W.; Bickmann, B.; Magonov, S. N.; Cantow, H.; Lotz, B.; Wittmann, J. C.; Moller, M. *Ultramicroscopy* **1992**, *42*, 1141.

16 . Snetivy, D.; Vancso, G. J.; Rutledge, G. . *Macromolecules* **1992**, *25*, 7037.

17 . Snetivy, D.; Vancso, G. J. *Polymer* **1994**, *35*, 461.

18 . Jandt, K. D.; Buhk, M.; Miles, M. J.; Petermann, J. *Polymer* **1994**, *35*, 2458.

19 . Lovinger, A. J.; Padden, F. J.; Davis, D. D. *Macromolecules* **1991**, *24*, 132.

20 . Lovinger, A. J.; Padden, F. J.; Davis, D. D. *Polymer* **1991**, *32*, 3086.

CHAPTER 8:

CONCLUSIONS

This thesis has studied both the chemical and physical effects of non-equilibrium plasma treatment on the surface properties of polymers and polymer composites. The effects of two non-equilibrium plasmas have been studied. A low pressure oxygen glow discharge plasma and an atmospheric silent discharge plasma.

Both oxygen plasma and silent discharge plasma treatments of selected polymers (polypropylene, polystyrene, polyphenylene oxide and polycarbonate) produce low molecular weight oxidised material (LMWOM) at the surface. This LMWOM tends to conglomerate into globular features at the surface due to the large difference in surface energies between the LMWOM and the polymer. The globular features generated are ten times larger for silent discharge treatment than for oxygen plasma treatment. This effect is probably caused by ablation from the plasma treated surface or local melting effects at the silent discharge treated surface. It hase been found that care must be taken not to over treat the polymer surface as this will produce a layer of oxidized material which will not adhere well to the untreated polymer beneath it.

Plasma treatment of a model polymer surface (hexatriacontane) has shown that plasma attacks the side of a polymer crystal rather than the top, which is more directly exposed to the plasma. Plasma attack also appears to be initiated at defect sites in the crystal. This effect is accounted for by the greater mobility and the lower lattice energy of polymer chains at the edge of the crystal and at defect sites. Chemical compositional analysis of silent discharge treated hexatriacontane shows the formation, as well as LMWOM, of carbon-carbon double bonds during silent discharge treatment.

Surface analysis of a miscible (polystyrene / polyphenylene oxide) blend shows that significant interpenetration of the polymers occurs leading to molecular entanglements which destroy the original surface structure of the parent polymers. Oxygen plasma treatment produces significantly more LMWOM on poly phenylene oxide treatment than for polystyrene treatment, however the level of oxidation is the same. For silent discharge treatment the level of oxidation and the amount of LMWOM

are directly related to each other, for both polymers. For the oxidation of blend surfaces then oxygen plasma treatment is better suited for polystyrene rich surfaces and silent discharge treatment is more appropriate for poly phenylene oxide rich surfaces.

The phase morphology of an immisible polymer (polystyrene / polycarbonate) blend was determined using the recently invented phase imaging - atomic force microscopy. Oxygen plasma treatment of the blend surfaces reveals the phase morphology from the different etching rates of the parent polymers. Silent discharge treatment produces a layer of LMWOM, which has to be washed off to reveal the phase morphology.

In summary this thesis has shown that for the oxidative modification of polymers by non-equilibrium plasmas, the reaction conditions have to be matched to the polymer system. If the oxidative conditions are too weak then the oxidation will not significantly affect the polymer surface properties. If the oxidative conditions are too strong then this will lead to a oxidised surface layer that is weakly bound to the polymer. Control of reaction pathways by using selective plasma conditions has been demonstrated. Oxygen plasma treatment of poly phenylene oxide causes rapid chain scission of the polymer, whilst silent discharge treatment causes excessive oxidation.

APPENDIX:

UNIVERSITY OF DURHAM - BOARD OF STUDIES IN CHEMISTRY COLLOQUIA, LECTURES AND SEMINARS FROM INVITED SPEAKERS

1993

October 4   Prof. F.J. Feher, University of California

Bridging the Gap Between Surfaces and Solution with Sessilquioxanes

October 27   Dr. R.A.L. Jones, Cavendish Laboratory

Perambulating Polymers

November 10 Prof. M.N.R. Ashfold, University of Bristol

High Resolution Photofragment Translational Spectroscopy: A New Way to Watch Photodissociation

November 17 Dr. A. Parker, Rutherford Appleton Laboratory

Applications of Time Resolved Resonance Raman Spectroscopy to Chemical and Biochemical Problems

1994

January 26   Prof. J. Evans, University of Southampton

Shining Light on Catalysts

February 2   Dr. A. Masters, University of Manchester

Modelling Water Without Using Pair Potentials

February 16 Prof. K.H. Theobald, University of Delaware

February 23   Prof. P.M. Maitlis, University of Sheffield

Across the Border: From Homogeneous to Heterogeneous Catalysis

October 19   Prof. N. Bartlett, University of California

Some Aspects of Ag(II) and Ag(III) Chemistry

November 23 Dr. J.M. Williams, University of Loughborough

New Approaches to Asymmetric Catalysis

December 7   Prof. D. Briggs, ICI and University of Durham

Surface Mass Spectrometry

1995

January 18   Dr. G. Rumbles, Imperial College

Real or Imaginary Third Order Non-Linear Optical Materials

March 1   Dr. M. Rosseinsky, Oxford University

Fullerene Intercalation Chemistry

April 26   Dr. M. Schroder, University of Edinburgh

Redox-active Macrocyclic Complexes: Rings, Stacks and Liquid Crystals

May 3   Prof. E.W. Randall, Queen Mary and Westfield College

New Perspectives in NMR Imaging

October 11   Prof. P. Lugar, University of Berlin

Low Temperature Crystallography

November 17 Prof. D. Bergbreiter, Texas A&M

Design of Smart Catalysts, Substrates and Surfaces from Simple Polymers

November 22 Prof. I. Soutar, Lancaster University

A Water of Glass? Luminescence Studies of Water Soluble Polymers

1996

January 10   Dr. B. Henderson, Waikato University

Electrospray Mass Spectrometry-A New Sporting Technique

January 17   Prof. J.W. Emsley, Southampton University

Liquid Crystals: More Than Meets the Eye

January 31   Dr. G. Penfold, ?

Soft Soap and Surfaces

March 6   Dr. R. Whitby, University of Southampton

New Approaches to Chiral Catalysts: Induction of Planar and Metal Centred Asymmetry

March 12   Prof. V. Balzani, University of Bologna

Supramolecular Photochemistry

Conference Attended

August 20th - 25th 1995   12th International Symposium on Plasma Chemistry, University of Minnesota, USA.

Examined Lecture Courses

General Laboratory Techniques (Dr. Hampshire)

Spectroscopies (Dr. Halliday)

Electron Microscopy (Dr. Durose)

The Physical Chemistry of Polymer Science (Prof. R. W. Richards)